The Thesis Committee for Scott Thomas Gabel
Certifies that this is the approved version of the following thesis:

Generation, Stability, and Transport of Nanoparticle-Stabilized Oil-in-Water Emulsions in Porous Media

APPROVED BY

SUPERVISING COMMITTEE:

Supervisor:
_____

Steven L. Bryant

Co-Supervisor:
_____

Chun Huh

Generation, Stability, and Transport of Nanoparticle-Stabilized Oil-in-Water Emulsions in Porous Media

by

Scott Thomas Gabel, B.S.Chem.E.

Thesis

Presented to the Faculty of the Graduate School of

The University of Texas at Austin

in Partial Fulfillment

of the Requirements

for the Degree of

Master of Science in Engineering

The University of Texas at Austin

May 2014

Dedication

To God, my parents, my family, and my friends.

Acknowledgements

Abstract

Generation, Stability, and Transport of Nanoparticle-Stabilized Oil-in-Water Emulsions in Porous Media

Scott Thomas Gabel, M.S.E.

The University of Texas at Austin, 2014

Supervisors: Steven L. Bryant, Chun Huh

The ability of nanoparticles to stabilize oil/water emulsions provides many interesting opportunities for the petroleum industry. Emulsions can be used as a displacing fluid for enhanced oil recovery to improve sweep efficiencies. Emulsions can be used to improve conformance control by effectively blocking thief zones in reservoirs with a high degree of heterogeneity. As shown in this thesis emulsions can be used to deliver fluids that contact and mobilize residual oil. It is imperative to understand emulsion behavior in porous media for design purposes in enhanced or improved oil recovery processes involving emulsions.

Nanoparticle-stabilized oil-in-water emulsions were continuously generated by co-injecting aqueous nanoparticle dispersion and oil through a beadpack. There exists a critical shear rate below which a stable emulsion will not be generated. The critical shear rate increased with decreasing bead size. Above the critical shear rate, the droplet size of the generated emulsion was a function of shear rate and decreased with increasing shear rate. The stable emulsions were characterized by their droplet size and rheology. The emulsion viscosity was highly dependent upon droplet size and not the bulk oil

viscosity in the emulsion. The emulsions were highly shear thinning and emulsions with smaller droplets were more viscous than emulsions with larger droplets.

Highly stable emulsions that were generated by co-injection were collected, separated from excess phase(s) and injected into beadpacks. In most experiments the injected emulsion coalesced into the bulk fluids. Whether the bulk fluids generated a new emulsion in the bead pack depended on the shear rate, bead size, and initial saturation of the beadpack. Different beadpack experiments showed the transition from one flow regime to a second flow regime as the slow movement of a coalescence/regeneration front propagated through the beadpack.

Coreflood experiments confirmed the mechanisms hypothesized for the beadpack emulsion injection experiments. When a stable emulsion was injected the effluent emulsion rheology and droplet size were altered solely as a result of being forced through sandstone cores, not because of fluids contacted within the core. The shear rate controlled whether the emulsion coalesced and produced no effluent emulsion, regenerated into an emulsion with larger droplets, or regenerated into an emulsion with smaller droplets.

Oil recovery experiments showed that nanoparticle-stabilized oil-in-water emulsion increased the recovery of oil compared to a waterflood for cores with immobile and mobile oil. The mechanism is the coalesced oil droplets form a flowing phase that is miscible with oil present in the core and thus achieves a much more efficient displacement. The possible continuous generation and coalescence of droplets may have increased the apparent viscosity, improving the sweep efficiency of the emulsion injection.

A novel oil recovery mechanism was shown in imbibition experiments where nanoparticle dispersion was used to displace oil. Large shear rates coupled with the

affinity for nanoparticles at the oil water interface enabled residual oil to be mobilized, or for residual oil blobs to spawn smaller droplets that are stabilized by the nanoparticles and thus can be transported with the dispersion through the core.

Table of Contents

List of Tables

List of Figures

Chapter 1

Introduction

Oil/water emulsions stabilized by silica nanoparticles have vast potential in many different petroleum applications. The majority of the emulsions that are used in the petroleum industry are stabilized with surfactants. Surfactant adsorption onto reservoir rocks limits the potential for long term propagation of surfactants in reservoirs. Solid particles can be used to stabilize emulsions and have several advantages compared to surfactant stabilized emulsions. Emulsions stabilized with solid particles are common throughout in the food and pharmaceutical but are rarely used in the petroleum industry. Emulsions stabilized with colloidal size solid particles have little use in the petroleum industry because colloidal particles are in the micron size range. This causes the solid particles to become trapped in rock pores making it impossible for long range transport in reservoirs.

Nanoparticles offer many new opportunities in the petroleum industry. Nanoparticles are two orders of magnitude smaller than colloidal particles. This allows them to flow through rock pores with little to no retention. Because nanoparticles are solid, they can withstand harsh reservoir conditions. High viscosity emulsions can be generated with silica nanoparticles. Viscous emulsions could be used to manage mobility control in high viscosity oil reservoirs. Emulsions could provide an efficient, piston-like displacement of heavy oils. Viscous emulsions could also be used to improve conformance control by plugging highly permeable formations. Emulsions could be used to deliver recovery enhancing chemicals. For example, an emulsion could be

used to deliver a viscosity reducing oil solvent to heavier oils. For nanoparticle stabilized emulsions to become widely used in oil field applications, a better understanding of emulsion generation, stability, and flow behavior is necessary. The work in this thesis will investigate the generation, stability, and flow behavior of nanoparticle stabilized emulsions in porous media.

1.1 THESIS OUTLINE

There are six chapters in this thesis. The first chapter is an introduction into emulsions and their potential applications in the petroleum industry. The second chapter is a literature review of relevant work related to the research presented in this thesis. In the third, fourth, and fifth chapters the experimental materials/procedures will be outlined, including results and discussion. The third chapter will investigate emulsion generation by co-injection through a beadpack, including critical shear rate experiments and emulsion characterization. In the fourth chapter emulsion injection experiments were performed in the beadpack to investigate emulsion flow and stability through porous media. In the fifth chapter a number of coreflood experiments were performed to build upon the beadpack experiments. Residual oil recovery experiments and emulsion dilution experiments are also presented in the fifth chapter. The fifth chapter will also investigate the difference between direct emulsion injection and co-injection of oil and nanoparticle dispersion. The sixth chapter will discuss the conclusions drawn from this research as well as recommendations for future research work.

Chapter 2

Literature Review

2.1 NANOPARTICLE-STABILIZED "PICKERING" EMULSIONS

An emulsion is a mixture of two normally immiscible fluids. When oil and water are mixed small droplets will form but will eventually coalesce due to favorable energy conditions. The addition of an emulsifying agent can cause the droplets to remain intact creating a stable emulsion. Surfactants are the most common emulsifying agent and typically work to reduce the interfacial tension between the two immiscible fluids. Pickering (1907) determined that solid, colloidal size particles could stabilize emulsions without the use of surfactants by adsorption at the oil-water interface. Emulsions that are stabilized with solid particles, since known as Pickering emulsions, have shown exceptional stability.

When solid particles adsorb at the interface between oil and water they form a rigid barrier. This protective barrier keeps the droplets from coalescing and creates emulsions that are very stable over long periods of time. For spherical particles, the contact angle θ the particle makes with the interface dictates whether the emulsion created is water-in-oil or oil-in-water. Hydrophilic particles have a contact angle < 90° measured in the aqueous phase so a larger portion of the particle resides in the water phase. This creates a bending around the oil droplets creating oil-in-water emulsions. Conversely, hydrophobic particles have a contact angle > 90° so a larger portion of the particle will reside in the oil phase. This creates bending around water droplets forming water-in-oil emulsions. Figure 2.1 shows the curvature of the oil/water interface in relation to the spherical particles contact angle (Binks 2002).

3
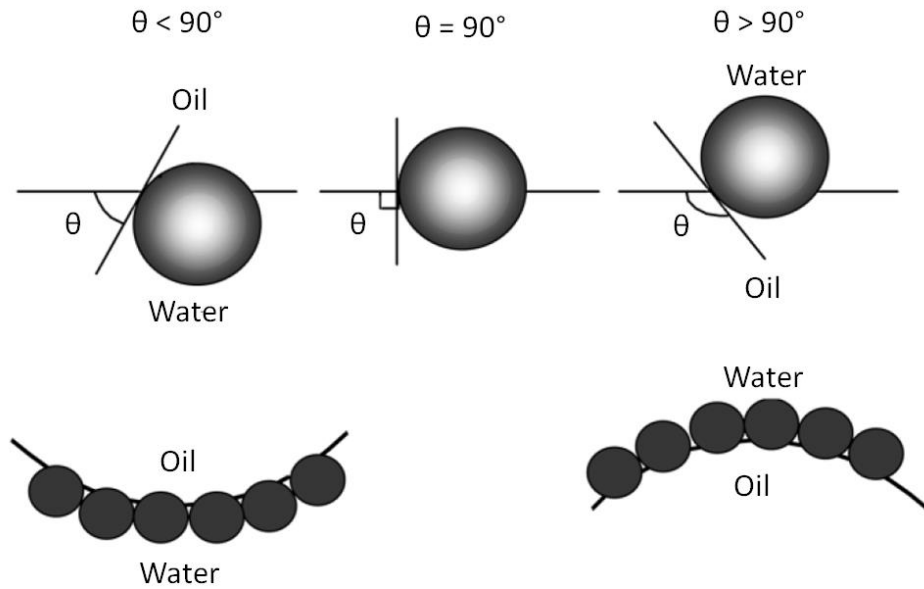
Figure 2.1: The contact angle at oil-water dictates internal emulsion structure (Binks 2002).

Particle size, shape, wettability, and coating all affect emulsion stability. In order to create a stable emulsion a significant amount of energy is required to adsorb and hold the particles at the oil-water interface. The adsorption energy, E, required to adsorb and hold a particle at the oil-water interface is determined from the following equation:

$$E = \pi r^2 \gamma_{ow}(1 \pm cos\theta)^2$$

where r is the radius of the particle, γ_{ow} is the interfacial tension, and θ is the contact angle of the particle at the interface as measured through the aqueous phase. At 25°C the interfacial tension between mineral oil and water is approximately 0.049 J/m^2 (Stan et. al 2009). Figure 2.2 plots the adsorption energy needed adsorb a spherical particle

4

(Nyacol DP 9711) at the mineral oil-water interface at 25°C versus contact angle. It is apparent from Figure 2.2 that adsorption energy is highly dependent upon contact angle. For contact angles between 60°-120° it takes a large amount of energy (a few thousand kT) to adsorb and hold the particles at the interface. Consequently, the adsorption of the particles at the interface is more or less irreversible causing very stable emulsions. In contrast most surfactant molecules require very little energy to detach particles from the interface, several kT, so they may not be as effective emulsion stabilizers (Aveyard et al. 2003).
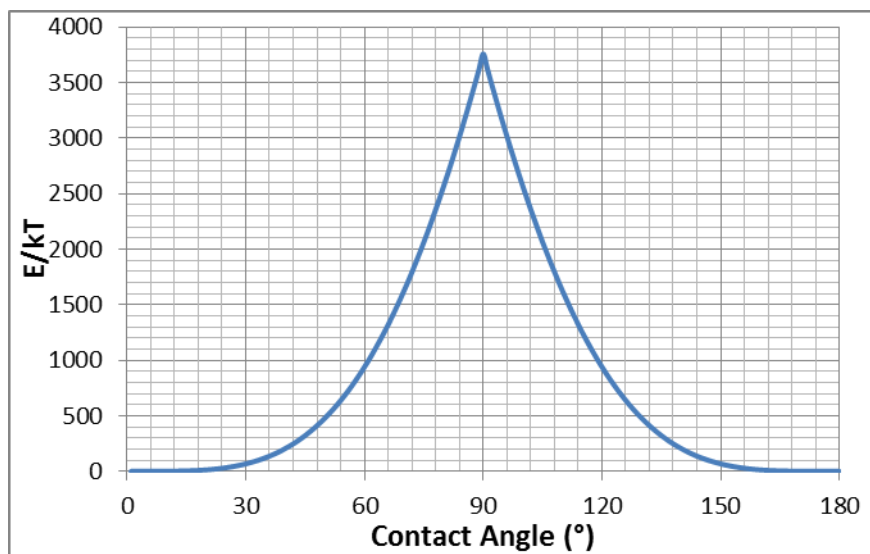
Figure 2.2: Adsorption /desorption energy as a function of contact angle for particles with $r=10$ nm at the water/mineral oil interface at 25°C.

Nanoparticles have several other potential advantages over surfactants, which are used to lower the oil-water interfacial tension. Surfactant adsorption onto reservoir rocks, especially carbonate rocks, create chemical oil recovery problems. Because

5

surfactants adsorb onto the surface of rocks, surfactant chemical solutions can lose their effectiveness as they travel through porous media. This creates long-term transport problems, causing the recovery process to become inefficient and uneconomical (Zhou et al. 2012). Nanoparticles have shown the ability to travel through porous media with little to no retention due to their small size (Caldelas 2010).

Nanoparticles can be engineered out of different materials to give them certain functional properties. For example, paramagnetic nanoparticles made of iron oxide have shown the ability to locally heat when paired with an induced magnetic field (Davidson 2012). Surface modifications to nanoparticles can give them catalytic or reactive properties (Zhang et al. 2009). Nanoparticles surfaces can be modified with surfactants as well giving them other potentially useful properties. Figure 2.3 is a schematic of a surface coated nanoparticle.
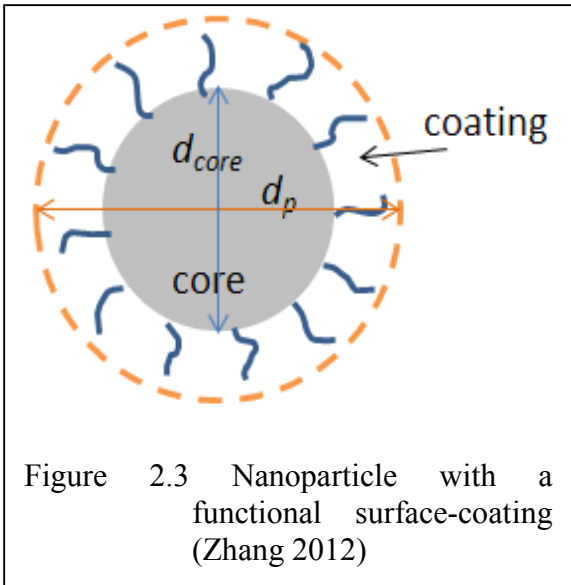
Figure 2.3 Nanoparticle with a functional surface-coating (Zhang 2012)

One advantage of using nanoparticles to generate emulsions is that dispersions with a small weight percent of nanoparticles have shown the ability to stabilize emulsions. Zhang (2009) showed that nanoparticle dispersions as low as 0.5 wt% nanoparticles could stabilize an emulsion for several months. Zhang et al. (2009) generated stable emulsions in sandstone and cement fractures by co-injecting dodecane and nanoparticle dispersions as low as 1 wt%. Aveyard et al. (2003) created stable

toluene-in-water emulsions with 0.5 wt% hydrophilic silica nanoparticles. Similarly, 0.05 wt% silica nanoparticle dispersions have shown the ability to stabilize CO_2 foams by co-injection in a bead pack (Espinosa 2011). Hariz (2012) used 1 wt % nanoparticle dispersions to stabilize foams in fractured and un-fractured sandstone cores.

Zhang (2009) investigated the stability of nanoparticle stabilized emulsions over a wide range of experimental conditions including changes in volume ratio, salinity, nanoparticle concentration, and wettability of the nanoparticles. Stable emulsions were generated over a wide range of conditions when the nanoparticle concentration was greater than 0.5 wt%. Binks et al. (2007) showed that adjusting the pH of the aqueous phase can increase emulsion stability by altering the charge of nanoparticles and those particles with zero charge generate the most stable emulsions.

2.2 NANOPARTICLE STABILIZED EMULSION/FOAM STABILITY IN POROUS MEDIA

Roberts (2011) determined it was possible to stabilize emulsions by co-injecting dodecane and nanoparticle dispersion through both sandstone and cement fractures. He concluded there was a critical shear rate of 8,000 s^{-1} above which a stable emulsion will form in a fracture by co-injection. Below 8,000 s^{-1}, stable emulsion did not form from co-injection through a fracture. Roberts also performed displacement experiments in fractures where nanoparticle dispersion displaced dodecane and conversely, displaced nanoparticle dispersion by dodecane injection. In these displacement experiments stable emulsion did not form even though the shear rate exceeded the reported critical shear rate required for stable emulsion generation in a fracture by co-injection.

Chung (2013) determined that emulsion formed in-situ during drainage experiments where n-octane displaced nanoparticle dispersion. Although stable

7

emulsion was not present in the effluent, the evidence of emulsion generation was from the fact that the effective mobility was reduced by a factor of two. These in-situ emulsions were produced at shear rates of approximately 85 s^{-1}. The shear rate that produced the in-situ emulsions for Chung were approximately two orders of magnitude lower than the shear rates required for emulsion generation in a fracture reported by Roberts.

CO$_2$-in-water foams were stabilized with PEG-coated silica nanoparticles in Boise sandstone cores by co-injection in work done by Hariz (2012). The critical shear rate found for these experiments ranged from 460 s^{-1} to 1,145 s^{-1}. Hariz also performed co-injection experiments with CO_2 and nanoparticle dispersions through cement fractures where stable foams were generated at shear rates as low as 3,360 s^{-1}.

Espinosa (2011) was able to stabilize CO$_2$-in-water foams using nanoparticles in 180 μm beadpacks at ambient temperatures at a shear rate of 1430 s^{-1}. He speculated that the critical shear rate at ambient temperature was lower than the 1430 s^{-1} although experiments were not performed at lower shear rates. At a temperature of 75 °C the critical shear rate for CO2 foam generation was 2,500 to 3,000 s^{-1}. At a temperature of 90 °C the critical shear rate for foam generation was about 4,000 s^{-1}.

2.3 IMPROVED MOBILITY CONTROL WITH EMULSIONS

Limitations on improving oil recovery have long been a problem in the petroleum industry. The most common types of fluids used to displace oil are brine and CO_2. Often these fluids have lower viscosities than the oil they are displacing. This leads to unfavorable mobility ratios and can cause viscous fingering resulting in poor sweep efficiencies.

The mobility ratio for immiscible displacement is defined as the ratio of mobility between the displacing fluid and displaced fluid. The equation for the mobility ratio, M of water displacing oil is shown below where, λ, is the mobility of each fluid, k_r, is the relative permeability, and μ is fluid viscosity.

$$M = \frac{displacing\ fluid\ mobility}{displaced\ fluid\ mobility} = \frac{\lambda_{water}}{\lambda_{oil}} = \frac{k_{r_{water}} * \mu_{oil}}{k_{r_{oil}} * \mu_{water}}$$

Many reservoirs have heavier oils with viscosities ranging from 50 to 5,000 cP which are still mobile. After primary recovery, waterflooding is typically used as an economically viable form of secondary recovery. Due to unfavorable mobility ratios (M>>1) majority of the oil in high viscosity oil reservoirs is bypassed. Emulsions can be used to increase water viscosity, decreasing mobility ratios resulting in a more efficient oil recovery.

Viscous oil recovery with solid stabilized emulsions was a recovery method conceived by J.R. Bragg (Bragg 1999). The idea was to use water-in-oil emulsions stabilized by solid particles to displace viscous oil. A fully stable water-in-oil emulsion would provide a piston-like, miscible displacement. A field test of solid stabilized emulsions in the Celtic field proved to be successful with significant improved oil recovery (Kaminsky et al. 2010). The emulsion, stabilized with mineral fines, was used to displace a 4000 cP oil was approximately 40% oil and 60% brine. The emulsion was generated using a specially designed in line mixer. The Celtic pilot proved that solid stabilized emulsions could be generated and injected through a reservoir for a long period of time (approximately 3 years) while maintaining moderate stability at the field scale.

Rocha de Farias et al. (2012) showed that injecting surfactant stabilized crude oil-in-water emulsions increased recovery of crude oil compared to brine injection in sandpack experiments. They generated the emulsion by injecting a surfactant solution and crude oil through a filter with a controlled mesh size. Moradi et al. (2012) showed that surfactant stabilized crude oil-in-water could effectively increase oil recovery in corefloods of Berea sandstone cores. They generated emulsions using an Ultra Turrax T 25 basic high speed homogenizer. In their corefloods, they observed an oscillatory pressure behavior during emulsion injection which they attributed to a blockage-release mechanism. The mechanism asserts there is an increase in curvature at the droplet tip when droplets are trapped in pore throats, which are smaller than the droplets. This causes an increase in capillary pressure at the front edge of a droplet. The increase in capillary pressure causes an increase in the pressure of the driving flow. As the droplet is forced through the pore throat pressure relaxation occurs, lowering the pressure drop. They asserted that as emulsion was continually injected this mechanism was repeated over and over causing the oscillatory pressure response (Moradi et al. 2012). Similar pressure responses were seen in this thesis.

For emulsions to be used at the field scale, emulsions need to be generated with cheap and readily available oils. Fu and Mamora (2010) generated stable emulsions with used engine oil which is abundant with over a billion gallons used per year in the U.S. The soot contained in used engine oil provides the solid particles needed to stabilize emulsions. They emulsified different types of used engine oils with brine using a high shear mixer at 5,000 RPM.

10

2.4 IMPROVED CONFORMANCE CONTROL WITH EMULSIONS

Poor sweep efficiencies are a common problem in crude oil reservoirs with a high degree of heterogeneity. Brine preferentially travels through portions of the reservoir with the highest permeability, leaving bypassed layers of the reservoir. These high permeability layers, often called thief zones, cause the brine to bypass other portions of the reservoir leaving recoverable oil in the reservoir. Plugging materials such as cement, gels, polymer solutions, and other materials are commonly used to block these thief zones, diverting flow in the near wellbore region. These solutions are often successful in the near well bore region but are limited in their ability because of the difficulty in placing them far from the wellbore. Emulsions can be used to plug the high permeability thief zones in the near wellbore region and deeper into the formation.

McAuliffe (1973) showed that oil-in-water emulsions could effectively reduce water permeability in sandstone cores. In his experimental worked he proved that emulsions would preferentially travel through the higher permeability layers, where they would become trapped after injection. In follow up waterfloods the emulsions effectively diverted water flow. Romero et al. (1996) showed that emulsions could be used to effectively reduce water permeabilites in consolidated, consolidated-fractured, and non-consolidated porous media. The reduction in water permeability from the emulsions was higher than 85% in some cases. Zeidani et al. (2007) showed that heavy oil-in-water emulsions, generated with a Brinkham homogenizer at 5,000 rpm, could effectively block a porous medium. They observed that the blocked region could withstand high pressures and that larger droplets may resist higher pressures.

2.5 OTHER POTENTIAL EMULSION APPLICATIONS

Leaky gas wells are a serious problem in the petroleum industry. In Canada alone, thousands of gas wells have leaks causing gas to release into the environment (Zeidani 2006). Not only is this a loss of natural resources but it also contributes harmful greenhouse gases to the atmosphere and can potentially pollute groundwater supplies. The most common remediation for leaky gas wells is cement squeezing. Cement squeezing is an expensive process that is time consuming and can still be ineffective after several squeezing attempts. Emulsions could be injected near the well bore region to block the flow of gas and water from the reservoir. After the emulsion is placed, the casing is filled with brine lowering the pressure gradient across the emulsion which allows the emulsion to block the gas. Zeidani et al. (2006) showed that oil-in-water emulsions could be used to effectively block porous medium. They also showed that emulsions made with heavier oils were better blocking agents because they can withstand higher pressures due to the combination of capillary and viscous forces.

Emulsions can also be used to effectively remediate contaminated soils and ground water aquifers. Lee et al. (2007) investigated the remediation of subsurface dense non-aqueous phase liquids (DNAPL) using emulsions generated with biodegradable vegetable oils. Their results showed that high solubility contaminants could be efficiently removed with vegetable oil emulsion. Kwon et al. (2006) showed that silicone oil in water emulsions could be used to treat chlorinated solvents in soil columns.

Chapter 3

Emulsion Generation by Co-Injection

The method of emulsion generation in the majority of the work previously reviewed was through high shear mixing or high frequency vibrations with closed (batch) systems. Using these methods of emulsification can limit the amount of emulsion generated and the physical properties of the emulsions. Large quantities of uniform emulsions need to be easily and continuously generated for emulsions to be injected at the field scale. To study emulsions behavior in porous media it is useful to have a fast and repeatable method to generate stable emulsions. The method proposed and investigated here is continuous generation by co-injecting an aqueous nanoparticle dispersion and organic phase through a beadpack. This chapter presents experiments on this process in detail. The emulsions generated in this chapter are stabilized through the shearing of the two phases as they pass through pores.

3.1 MATERIALS AND EXPERIMENTAL METHODS

In this section the materials and methods used to generate stable emulsions will be discussed. Large volumes of uniform emulsions were generated by co-injecting an organic phase and nanoparticle dispersion through a beadpack.

3.1.1 Materials Used

Nanoparticle Dispersions

Several different nanoparticles were tested for their ability to generate stable emulsions. The primary nanoparticle dispersion used was Nyacol DP9711. This

13

dispersion was purchased from Nyacol Nano Technologies. The nanoparticles are coated colloidal silica with an average diameter of approximately 20 nm. The coating is a trade secret of Nyacol Nano Technologies. The sample provided to us was 30 wt% silica dispersed in tap water. Nissan Chemical provided many different types of silica nanoparticle dispersions. Several of these samples were tested for their ability to stabilize emulsions.

The primary dispersion used in this study was a 3 wt% NaCl and 2 wt% DP9711 nanoparticle dispersion. De-ionized (DI) water was used to dilute the original dispersion provided by Nyacol. The DI water had a resisitivy of 18.2 MΩ-cm and was prepared using a Thermo Scientific Barnstead E-Pure system. The sodium chloride (NaCl) was purchased from Fisher Scientific and is 99% pure. One important step in dispersion preparation is that the DI water was added to the stock nanoparticle dispersion before adding the sodium chloride (NaCl). When NaCl is added to the stock nanoparticle dispersion before diluting the dispersion the nanoparticles can agglomerate because of the reduction of electrostatic forces.

Organic Phases

Different types of oils were used to generate emulsions. Stable oil-in-water emulsions were generated using light mineral oil, n-octane, and dodecane. All three of these oils were purchased from Fisher Scientific. Table 3.1 shows the viscosity and density for the fluids commonly used throughout this thesis

	Nanoparticle Dispersion	Dodecane	n-Octane	Light Mineral Oil
μ (cP)	1.06	1.34	0.54	40
ρ (g/cm^3)	1.03	0.781	0.703	0.861
σ (mN/m)	N/A	52	51	50

Table 3.1: Relevant properties of fluids used to generate emulsions. Nanoparticle dispersion is 2 wt% Nyacol DP9711, 3 wt% NaCl. Interfacial tension is for the oil/water interface.

Beadpack and Beads

A high pressure column from HiP (High Pressure Equipment Company) was filled with different size beads. The inner diameter of the column is 0.44 cm and its length is 15.24 cm. All of the beads were glass and spherical in shape. Five different bead sizes were used: 180 μm, 275 μm, 500 μm, 1000 μm, and 3000 μm in diameter. Pieces of mesh were put in the end caps of the column to hold the beads in place and keep them from flowing out of the beadpack. When the column is filled with one of the two smaller bead sizes, injected fluids pass primarily through pores between beads. The irregular gaps between the tube walls and the small beads are a small fraction of the pores. When the column is filled with 1000 um beads, the number of gaps is comparable to the number of pores, and when filled with 3000 um beads, the injected fluids pass almost exclusively through gaps. The size of the gaps is proportional to the bead size, so correlations between emulsion behavior and shear rate or the size of pore throats/gaps can still be examined.

15

3.1.2 Beadpack Co-injection Set-Up

The co-injection apparatus was designed with intentions of generating stable oil-in-water emulsions. The set-up was designed to allow for an aqueous nanoparticle dispersion and organic phase to flow simultaneously through a beadpack. Figure 3.1 shows a schematic of the co-injection system. The system was modified several different times but all experiments involved the aqueous and organic phases meeting at a tee positioned just upstream of the beadpack. From the tee, the two phases would enter the beadpack in alternating slugs.
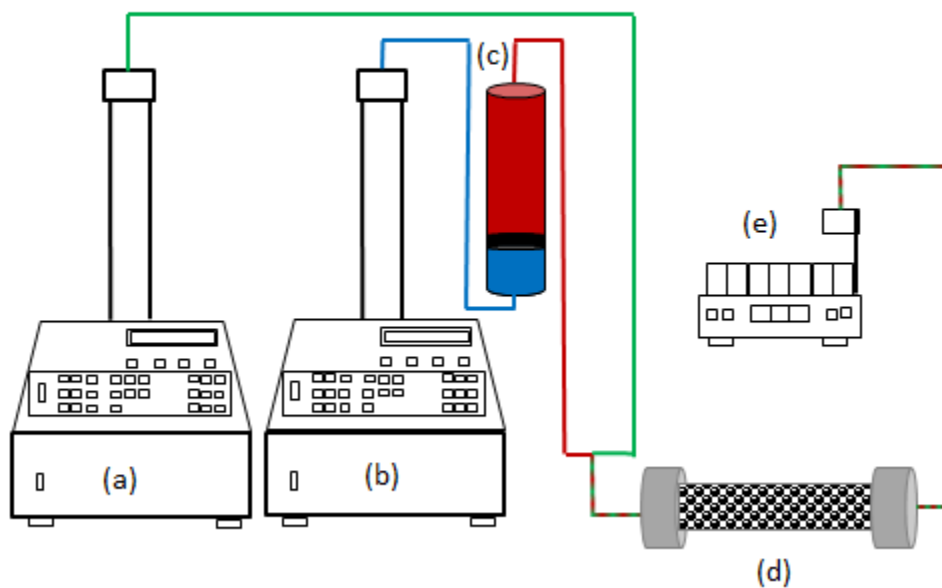
Figure 3.1:   Schematic of co-injection set-up: (a) syringe pump for organic phase, (b) syringe pump for displacing nanoparticle dispersion, (c) accumulator (contains nanoparticle dispersion), (d) beadpack, (e) fraction collector/container. A pressure gauge was not used in this setup.

Pumps

Two pumps were always used in the co-injection system.   In Figure 3.1 the two pumps shown are both D-Series Model 1000 Teledyne ISCO (Lincoln, NE) syringe pumps.   These pumps are capable of pumping up to 408 mL/min and have a maximum operating pressure of 2000 psi.   The organic phase was loaded into one of the pumps while the other was loaded with drive water which would displace the nanoparticle dispersion from the accumulator.   Prior to acquiring a second Teledyne ISCO pump, a dual piston pump was used as the second pump.   The dual piston pump is a Series 1500 HPLC from Lab Alliance (State College, PA) which is capable of pumping fluids up to 12 mL/min and a maximum operating pressure of 6000 psi.

Accumulator

A 400 mL accumulator was incorporated in the system to avoid loading the nanoparticle dispersion directly into the pumps.   Inside the accumulator is a movable piston.   The piston was moved to the bottom of the accumulator. Next, the accumulator was filled with nanoparticle dispersion.   The pump would then inject a drive fluid displacing the piston and in turn the nanoparticle dispersion to the beadpack.

3.1.3 Co-Injection Experimental Procedure

1. Open bead pack to fill with beads
    a. Use vise grip to open bead pack
    b. Flush out remaining beads from previous experiments with water
    c. Insert mesh into bead pack end caps (if mesh is already present then the mesh does not need to be replaced)

d. Put one end cap on the bead pack and position beadpack vertical so open end is facing upward

e. Fill bead pack with beads and put other end cap on the bead pack

2. Load one syringe pump with the organic phase

3. Load second pump with drive water

4. Load the accumulator with the nanoparticle dispersion

5. Attach flow lines except for the last line going into the beadpack

6. Begin injecting fluids to displace any dead volume before attaching lines to beadpack

7. Once any air or fluid in dead volume is removed attach the line to the beadpack

8. Begin co-injecting the two fluids through the beadpack

9. Collect the effluent

3.1.4 Critical Shear Rate Experimental Procedure

The critical shear rate for generating emulsion in the beadpack was investigated. The Nyacol DP 9711 dispersion was co-injected with mineral oil at different flow rates at a 1:1 ratio in the bead pack. These experiments were performed in the HiP bead pack with various bead sizes: 180 microns, 275 microns, 500 microns, 1000 microns, and 3000 microns. The experimental procedure for the critical shear rate experiments is outlined below. It is very similar to the procedure outlined in 3.1.3.

1. Fill beadpack with desired size beads (procedure discussed in 3.1.3)

2. Load one syringe pump with organic phase (mineral oil used for critical shear rate experiments)

3. Load second syringe pump with drive water

4. Load accumulator with nanoparticle dispersion

5. Attach flow lines except for the last line going into the beadpack

6. Beginning at a low flow rate (1 mL/min) inject mineral oil and nanoparticle dispersion at a 1:1 phase ratio to displace any dead volume before attaching lines to beadpack

7. Attach lines to beadpack

8. Collect effluent to see if a stable emulsion formed

9. Incrementally increase the flow rates while still injecting at a 1:1 phase ratio

10. Allow the pressures on the pumps to reach a steady state and let at least 10 pore volumes pass through the beadpack to ensure that new emulsion is collected was formed at the new flow rate

11. Collect newly formed emulsion

12. Repeat steps 8-11 for increasing flow rates for a certain bead size

3.2 DATA ANALYSIS

3.2.1 Permeability of the Bead Pack

The permeability, k, of the bead pack used for emulsion generation and emulsion injection experiments was estimated by the following equation:

$$k = \frac{1}{72\tau} \frac{\phi^3 D_p^2}{(1 - \phi)^2}$$

where τ is the tortuosity, ϕ is the porosity, and D_p is bead diameter. A tortuosity of 25/12 was used because it was experimentally the best fit for tortuosity for randomLy packed spheres (Lake 1989). The porosity was assumed to be 0.36, the minimum bulk porosity for a dense, disordered packing of uniform-sized spheres (Zhang et al. 2006).

3.2.2 Shear Rate in the Beadpack

The shear rate, $\dot{\gamma}_{eq}$, was estimated in the beadpack and core from the following equation (Lake 1989):

$$\dot{\gamma}_{eq} = 4v\left(\frac{\phi}{8k}\right)^{\frac{1}{2}} = \frac{4q}{A\sqrt{8k\phi}}$$

where $v = q/A/\phi$ is the interstitial velocity (cm/s), q is the volumetric flow rate (cm^3/s), A is the cross-sectional area (cm^2), k is the permeability (cm^2), and ϕ is the porosity (dimensionless). This equation treats the pore throats in the beadpack as an equivalent bundle of capillary tubes through which a single phase flows; this idealization is useful in predicting the rheological properties of non-Newtonian fluids flowing in porous media (Lake 1989).

3.2.3 Emulsion Droplet Size

After generating a stable emulsion the average droplet size was measured. Microscopic images of the emulsion were captured using a Nikon Labophot-Pol microscope with digital output and a Nikon Digital Sight DS-Fi1 camera. The microscope was attached to a PC with a program called Nikon NIS-Elements imaging software. This program allows the user to capture images with the microscope.

A small amount of emulsion was transferred from the bulk emulsion to a glass slide by a pipette. The emulsion was spread very thinly on the glass slide so enough light could pass through the emulsion to get a clear image of the droplets. If the layer of the emulsion is too thick light will not pass through the emulsion and an image will not be seen with the microscope. All images were taken while viewing the emulsion with a magnification aperture of 40x which was capable of viewing droplets in the size range of

1-100 microns. Once the images were taken using the microscope a program called ImageJ (a public domain image processing program) was used to calculate the average droplet sizes.

In some cases, to determine a more representative average droplet size of a generated emulsion several different images of the same emulsion were captured with the microscope setup. This is particularly important when measuring emulsions with very large droplets that may have only three to four droplets in a captured image. For the larger droplet emulsions at least twenty different droplets were used in the determination of average droplet size. For the smaller droplet emulsions this was not an issue because a representative sample of emulsion droplets could be captured with one image.

3.2.4 Measuring Emulsion Rheology

An AR-G2 magnetic bearing rheometer from TA Instruments (New Castle, DE) was used to measure the rheology of many of the emulsion generated in this thesis. The AR-G2 rheometer was used to generate plots of viscosity versus shear rate for different emulsions. A detailed description of the procedure used to measure the rheology using this rheometer is given in the Appendix.

3.3   RESULTS

This chapter will present the results for emulsion generation. Fourteen different nanoparticle dispersions were used in an attempt to generate stable emulsion by co-injection through a beadpack. Critical shear rate experiments were also performed using the Nyacol DP 9711 nanoparticle dispersion discussed in Section 3.1.1.

3.3.1 Emulsion Generation with Different Nanoparticle Dispersions

Different nanoparticle dispersions were tested for their ability to stabilize mineral oil-in-water emulsions by co-injecting them through the HiP beadpack with mineral oil. All of these tests were performed with 180 micron beads.   The nanoparticle dispersion and mineral oil were co-injected at a 1:1 phase ratio.   Each phase was flowing at a flow rate of 12 mL/min, for a total flow rate of 24 mL/min. This corresponds to a shear rate of 12,500 s^{-1}.   All tests were conducted at ambient temperature (21 °C) and outlet pressure of 1 atm.

Table 3.2 summarizes the results for co-injection.   Only three nanoparticle dispersions were able to create extremely stable emulsions: DP9711, IPA-ST, and EOR-25.   The emulsions stabilized with these three dispersions were stable for months when stored at ambient conditions.   The other nanoparticles created very weak emulsions that ultimately coalesced back into two separate phases within an hour after they were generated, or no emulsion at all.

Nanoparticle Type	Nanoparticle Weight %	NaCl Weight %	Stable Emulsion Produced
DP-9711	2	3	Yes
IPA-ST	3	2	Yes
EOR - 25	5	1	Yes
EOR - 25	1	1	Coalesced within 24 hours
EOR - 80	1	3	Coalesced within 24 hours
Nexsil 20	2	1	No
SnowTex - N	3	1	No
SnowTex - AK	2	0	No
SnowTex - AK	2	1	No
SnowTex - O	3	1	No
SnowTex - C	2	1	No
SnowTex - 30 -LH	3	1	No
SnowTex - PS - S	2	1	No

Table 3.2 The properties of the nanoparticle dispersions used to generate stable oil-in-water emulsions with mineral oil by co-injection.   Listed is the nanoparticle type, nanoparticle wt%, NaCl wt%, and whether they generated an emulsion when co-injected at a 1:1 phase ratio with mineral oil with a total flow rate of 24 mL/min through a 180 micron beadpack ($\dot{\gamma}_{eq}$=12,500 s^{-1}).

3.3.1.1 Zeta potential of nanoparticle dispersions

Zeta potential is used to quantify the stability of colloidal dispersions. Zeta potential is useful in characterizing the stability of nanoparticle dispersions because electrostatic repulsion is dependent upon zeta potential. Electrostatic repulsion keeps the nanoparticles from aggregating. Higher zeta potential corresponds to high electrostatic repulsion and in turn a very stable dispersion. Conversely, lower zeta potentials are associated with lower electrostatic repulsion and less stable dispersions. The hypothesis was that the nanoparticles in stable dispersions with lower zeta potential would have more affinity to adhere to the oil-water interface than nanoparticles in very

stable dispersions with higher zeta potentials. The zeta potential was measured with a Beckman Coulter (Brea, California) Delsa Nano C Particle Analyzer.   The zeta potential was measured for the nanoparticle dispersions without NaCl as a reference. The reference dispersions without NaCl had the same weight percent nanoparticles as the dispersions used to generate emulsion in the co-injection setup, Table 3.2 above. Table 3.3 shows the zeta potential for the nanoparticle dispersions used to generate emulsions and the reference nanoparticle dispersions.   In all cases, the addition of NaCl lowered the zeta potential of the dispersions.   Two dispersions, IPA-ST and Nyacol DP9711, that made stable emulsion with NaCl also made stable emulsion with their reference solutions. However, the EOR-25 nanoparticle dispersion that made stable emulsion with NaCl did not make stable emulsion with its reference solution.   Zeta potential did not appear to have a strong correlation in the nanoparticle dispersion's ability to stabilize an emulsion. Five different dispersions with zeta potentials of -1.3, -3.5, -13.8, -24.9, and -29.4 mV were able to stabilize emulsions using the co-injection setup.   Other dispersions with a large range of zeta potentials (between 28.7 and -32.1mV) were unable to generate stable emulsion using the co-injection setup, see Table 3.3 for specific zeta potential values. It is possible that zeta potential affects the ability of a nanoparticle dispersion to stabilize an emulsion but other factors including nanoparticle size, coating, concentration, wettability, and salinity all affect the ability of a dispersion to stabilize an emulsion.

Nanoparticle Type	Nanoparticle Dispersion with NaCl		Zeta Potential	Nanoparticle Dispersion without NaCl	Zeta Potential
	Nanoparticle wt%	NaCl wt%	mV	Nanoparticle wt%	mV
DP - 9711	2	3	-3.5	2	-29.4
EOR - 25	5	1	-13.8	5	-32.1
EOR - 25	1	1	-13.7	1	-19.9
EOR - 80	1	3	-5.8	1	-22.7
IPA-ST	3	2	-1.3	3	-24.9
SnowTex - N	3	1	-16.2	3	-38.1
SnowTex - AK	2	1	28.7	2	39.5
SnowTex-O	3	1	-1.3	3	-24.7
SnowTex-C	2	1	-0.5	2	-37.2
SnowTex-30-LH	3	1	-29.5	3	-35.6
Nexsil-20	2	1	-31.1	2	-42.7

Table 3.3 Zeta potential values for the nanoparticle dispersions with the reference nanoparticle dispersion without salt.   The shaded cells were used in the co-injection set-up to generate oil-in-water emulsion; cf. Table 3.2.   The green cells are dispersions that generated stable emulsion.   The yellow cells are dispersions that generated emulsions that coalesced within 24 hours of generation.   The red cells were dispersions that did not generate stable emulsions or generated emulsions that coalesced within one hour of their generation.   Cells with no color shading were zeta potential reference solutions that were not used in the co-injection set-up.

3.3.2 Critical Shear Rate Experiments

Critical shear rate experiments were performed using the 3 wt% NaCl, 2 wt% Nyacol DP 9711 dispersion that generated stable emulsion in the previous section. Stable emulsion was formed in the beadpack when the nanoparticle dispersion and mineral oil were injected above the critical shear rate. Below the critical shear rate, stable emulsion was not produced. The critical shear rate experiments were performed with five different bead sizes. Figure 3.2 shows the shear rate ranges tested for the five different bead sizes.
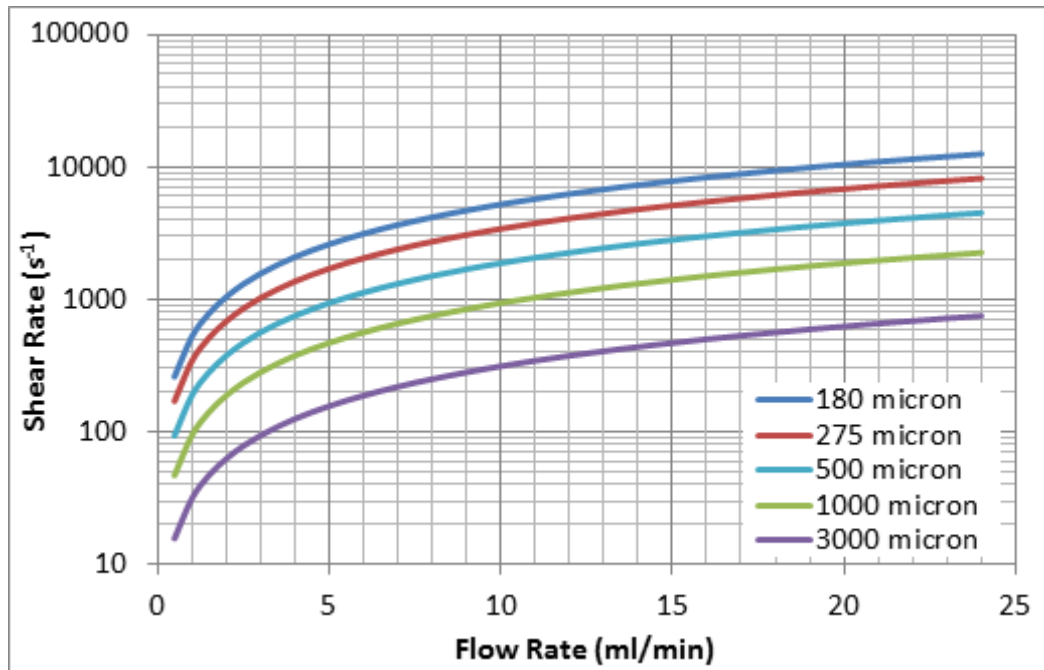
Figure 3.2 Plot of shear rate versus flow rate (from equation in Section 3.2.2) for different bead sizes in the HiP beadpack. The critical shear rate experiments were performed in these shear rate-ranges.

The following five figures show the effluent collected for the critical shear rate experiments. The table above the picture shows the bead size, flow rate, and the

26

corresponding shear rate for each sample. For each bead size a different critical shear rate window was apparent. Above the critical shear rate window stable emulsion was produced. Below the critical shear rate window stable emulsion was not produced. The critical shear rate window for each bead size is indicated by the red line in each image of the effluent.

180 Micron Beads						
Total Flow Rate (mL/min)	1	1.5	2	6	12	18	24
Shear Rate (s^{-1})	520	781	1,042	3,125	6,250	9,375	12,500
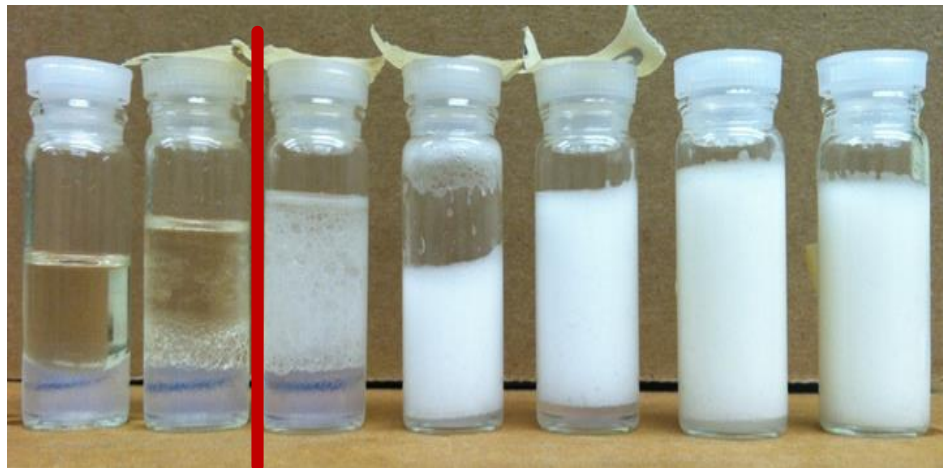
Figure 3.3 The effluent for the critical shear rate experiment performed in 180 micron beads. The critical shear rate was between 781 s^{-1} and 1,042 s^{-1}. The red line indicates the critical shear rate window. Nanoparticle dispersion (3 wt% NaCl, 2 wt% Nyacol DP 9711) and mineral oil co-injected at 1:1 phase ratio.

275 Micron Beads						
Total Flow Rate (mL/min)	1	1.5	2	6	12	18	24
Shear Rate (s^{-1})	341	511	681	2,045	4,091	6,136	8,182

Figure 3.4 The effluent for the critical shear rate experiment performed in 275 micron beads. The critical shear rate was between 341 s^{-1} and 511 s^{-1}. The red line indicates the critical shear rate window. Nanoparticle dispersion (3 wt% NaCl, 2 wt% Nyacol DP 9711) and mineral oil co-injected at 1:1 phase ratio.

500 Micron Beads						
Total Flow Rate (mL/min)	1	1.5	2	6	12	18	24
Shear Rate (s^{-1})	187	281	375	1,125	2,250	3,375	4,500

Figure 3.5 The effluent for the critical shear rate experiment performed in 500 micron beads. The critical shear rate was between 187 s^{-1} and 281 s^{-1}. The red line indicates the critical shear rate window. Nanoparticle dispersion (3 wt% NaCl, 2 wt% Nyacol DP 9711) and mineral oil co-injected at 1:1 phase ratio.

1,000 Micron Beads					
Total Flow Rate (mL/min)	2	4	6	12	18	24
Shear Rate (s⁻¹)	188	375	681	2,045	4,091	6,136

Figure 3.6 The effluent for the critical shear rate experiment performed in 1,000 micron beads. The critical shear rate was between 188 s^{-1} and 375 s^{-1}. The red line indicates the critical shear rate window. Nanoparticle dispersion (3 wt% NaCl, 2 wt% Nyacol DP 9711) and mineral oil co-injected at 1:1 phase ratio.

3,000 Micron Beads					
Total Flow Rate (mL/min)	2	4	6	12	18	24
Shear Rate (s^{-1})	62	125	188	375	562	750
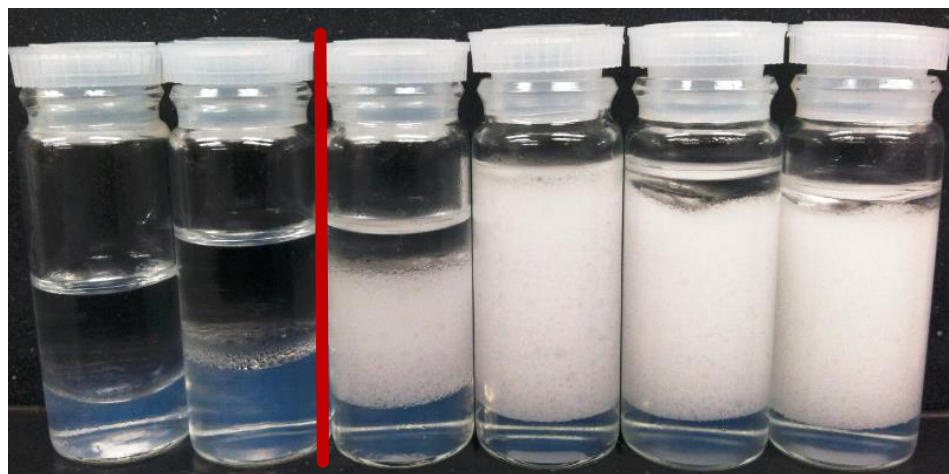
Figure 3.7 The effluent for the critical shear rate experiment performed in 3,000 micron beads.   The critical shear rate was between 125 s^{-1} and 188 s^{-1}. The red line indicates the critical shear rate window.   Nanoparticle dispersion (3 wt% NaCl, 2 wt% Nyacol DP 9711) and mineral oil co-injected at 1:1 phase ratio.

3.3.2.1 Effect of bead size on critical shear rate

From the critical shear rate experiments it is apparent that the critical shear rate to produce stable emulsion increases as the bead size was decreased. For example at 781 s^{-1} stable emulsion was not produced in the 180 micron beadpack but at 511 s^{-1} stable emulsion was produced in the 275 micron beadpack.   Similar results are apparent in the experiments performed in the 500, 1000, and 3000 micron beadpacks.   Figure 3.8 shows

31

how the critical shear rate for producing stable emulsion (for a 1:1 phase ratio) decreases as the bead size in the beadpack was increased. The dependence on bead size is very strong for the three smallest bead sizes. The dependence is weak for larger bead sizes, perhaps because of the transition from pore-throat-dominated flow to wall-bead-gap-dominated flow. Co-injection of the nanoparticle dispersion and mineral oil at or above the blue points on Figure 3.8 produced stable emulsions. Conversely, when the two fluids were co-injected at shear rates lower than the red points on Figure 3.8 a stable emulsion did not form for a particular bead size.

As the bead size was increased the ratio of the bead pack internal diameter to bead size decreased significantly, possibly transitioning from pore-throat-dominated flow wall-bead-gap dominated flow. For the smaller beads, 180, 275, 500 μm, there were pores and pore throats in the beadpack. When the beadpack was packed with 3,000 micron beads there were no pore throats in the beadpack, just irregular gaps between tube walls and beads.
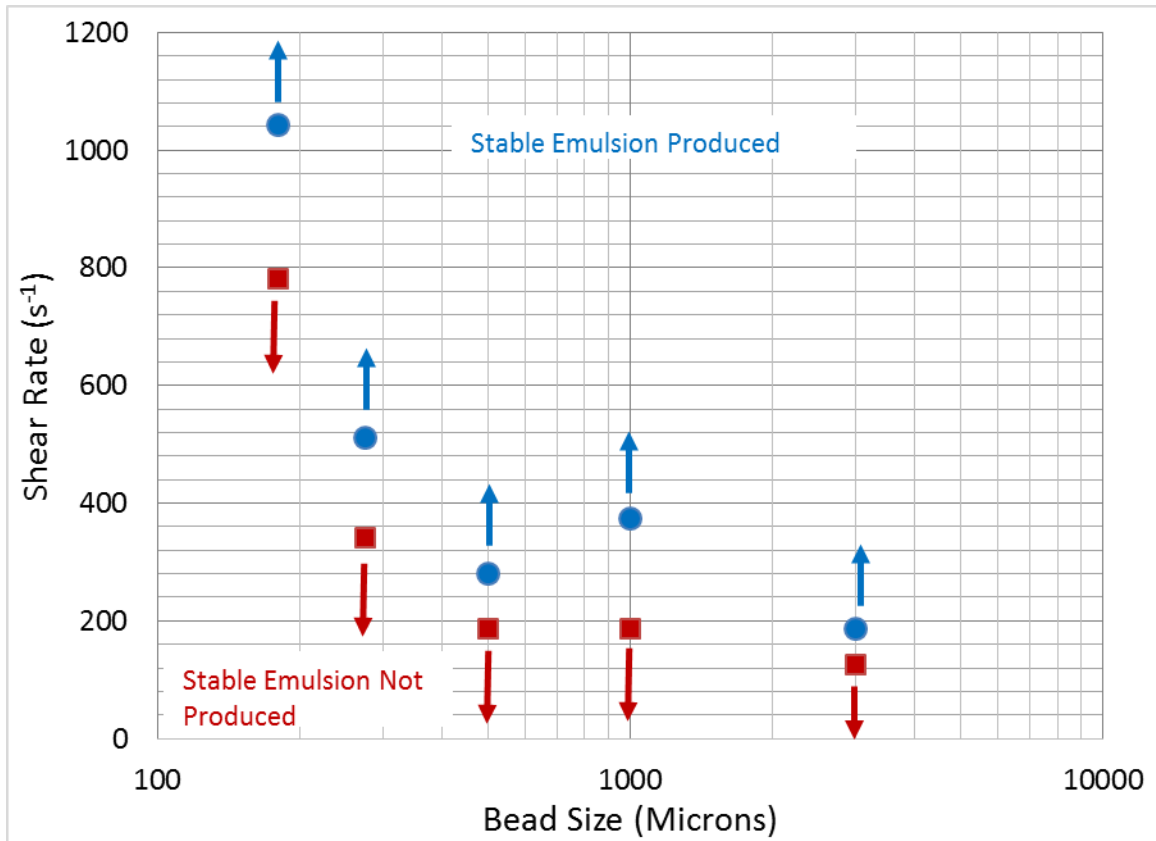
Figure 3.8 Critical shear rate for generating stable emulsion by co-injection decreases as bead size increases in the beadpack through which the fluids flow. Stable emulsion was produced at each of the blue points and any shear rate above. Stable emulsion was not produced for the red points or any shear rate below them. All experiments conducted at a 1:1 phase ratio of nanoparticle dispersion (3 wt% NaCl, 2 wt% Nyacol DP 9711) and mineral oil. All experiments conducted at ambient temperature and pressure. See text for discussion of pore throats and gaps between tube walls and beads.

3.3.2.2 Effect of shear rate on emulsion droplet size

Images of the emulsions produced in the critical shear rate experiments were taken with the Nikon microscope setup. The average droplet size was calculated using the ImageJ software; this requires the user to select individual droplets in the image, and

33

an effort was made to choose representative droplets.   Figure 3.9 shows the microscopic

images taken of the different emulsions generated in the critical shear rate experiments.
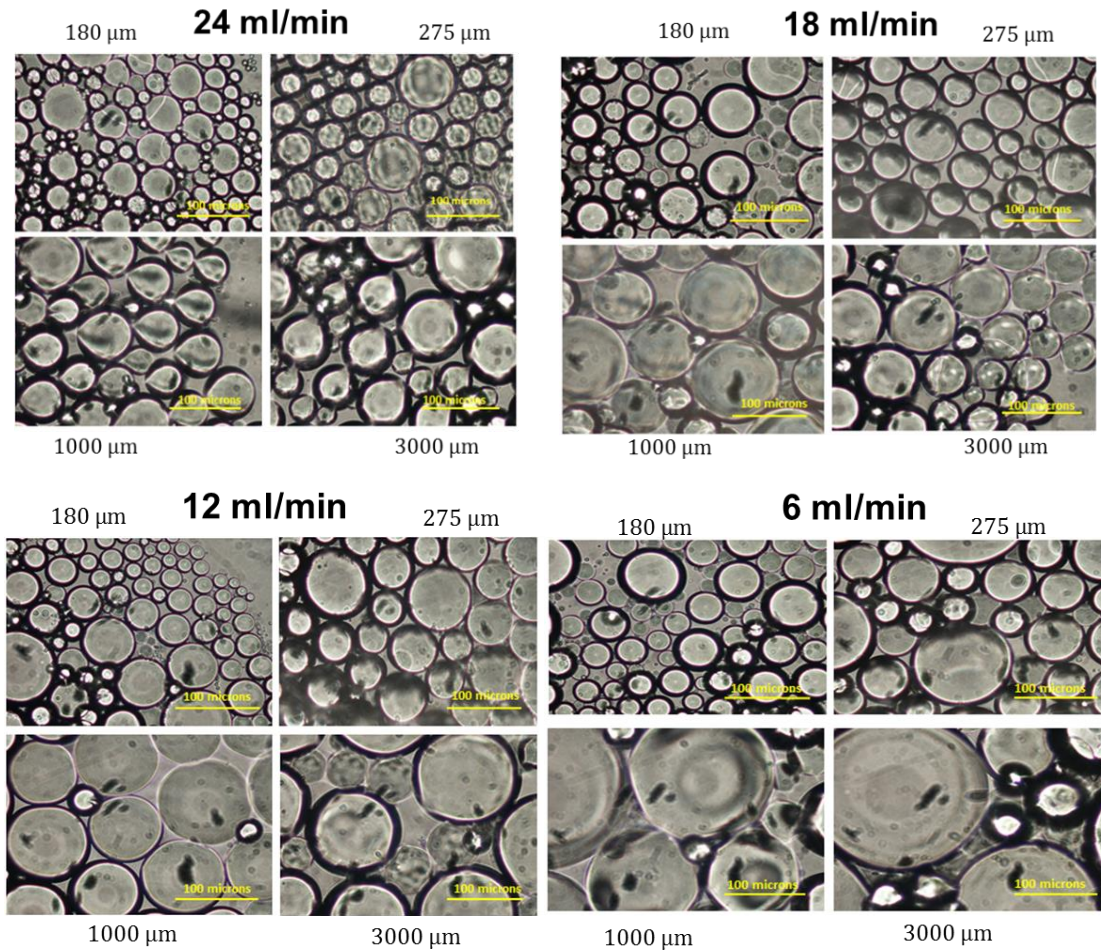
Figure 3.9 Microscopic images of the emulsions produced with the same total flow rate in
the beadpack for different size beads.   Yellow line is a scale bar of 100
microns.   Nanoparticle dispersion (3 wt% NaCl, 2 wt% Nyacol DP 9711)
and mineral oil co-injected at 1:1 phase ratio.

Several observations were made from visual inspection of Figure 3.9.   First, for a given bead size the droplet size of the emulsions produced appears to decrease with increasing flow rate.   This is much more apparent in the case of the emulsions produced with 1,000 and 3,000 micron beads than it is with the smaller beads.   For 1,000 and 3,000 micron beads, the emulsion droplets produced at 6 and 12 mL/min appear to have much larger diameters than the droplets produced at similar flow rates.   The second observation is that for a given flow rate the emulsion droplets produced with smaller beads appear to be smaller than those produced with larger beads.   This is very clear in the images of the emulsions generated at 6 and 12 mL/min.

The average droplet size for each emulsion was calculated using ImageJ.   Figure 3.10 plots the average droplet diameter versus the shear rate it was produced with.   The average droplet sizes are also categorized by the bead size they were generated with.

35
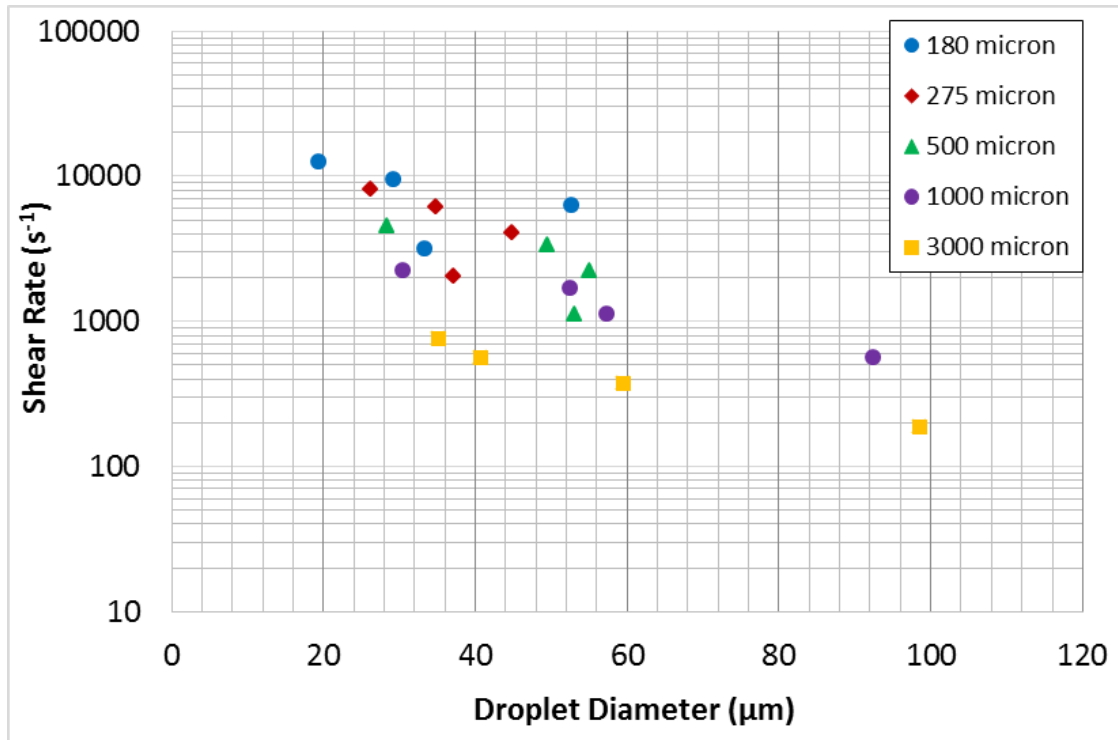
Figure 3.10 Average droplet diameter of emulsions generated in the critical shear rate experiments plotted against the shear rate they were produced with. Water-in-oil emulsions composed of nanoparticle dispersion (3 wt% NaCl, 2 wt% Nyacol DP 9711) and mineral oil.

From Figure 3.10 it is apparent that as shear rate increases the average droplet size of an emulsion decreases. With the larger beads (1,000 and 3,000 µm), increasing the shear rate generated emulsions with smaller average droplet sizes. When the shear rate was increased in the smaller beads (180 and 275 µm), the overall trend was a decrease in droplet size however the difference in droplet sizes was not as large as it was in the larger beads. This may have been caused by gap flow in the larger beads versus pore throat flow in the smaller beads.

3.3.2.3 Effect of total flow rate on droplet size

Figure 3.11 plots the average droplet size of the generated emulsion versus the total flow rate of the two phases. The droplet sizes are also grouped by the bead size they were generated with. There is a wide droplet size range at small flow rates for the different bead sizes. Conversely, at large flow rates the emulsions have similar droplet sizes. The hypothesis is that at larger flow rates the gaps in the larger beadpacks and the pore throats in the smaller beadpacks act the same producing similar emulsions. At lower flow rates the difference between flowing through gaps versus pores produces emulsions with different droplet sizes.
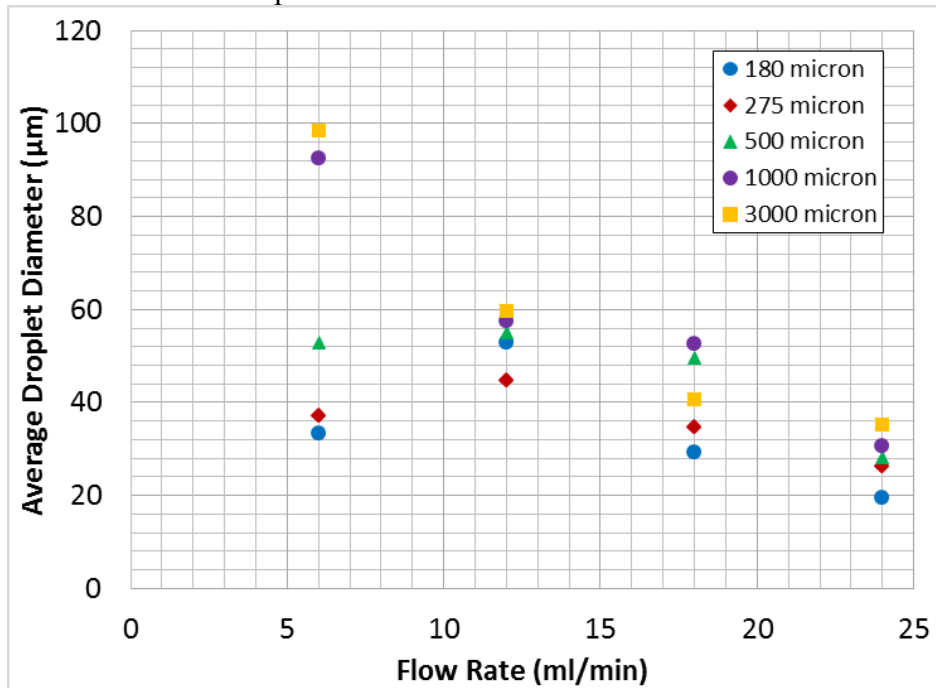
Figure 3.11 Average droplet diameter versus the total flow rate the emulsion was generated with. Emulsions are grouped by the bead size they were generated with. Water-in-oil emulsions composed of nanoparticle dispersion (3 wt% NaCl, 2 wt% Nyacol DP 9711) and mineral oil.

3.3.3 Emulsion Viscosity

The rheology of the stable emulsions generated by co-injection through the beadpack was measured. The nanoparticle stabilized oil in water emulsions are found to be highly shear thinning power-law fluids, i.e. as the shear rate increases the viscosity of the emulsion decreases. The shear stress, τ, of a power law fluid is given by:

$$\tau = K\dot{\gamma}^n$$

where K is the consistency index, $\dot{\gamma}$ is the shear rate, and n is the flow behavior index.

Figure 3.12 below, shows the rheology of the emulsion generated by co-injecting mineral oil and the Nyacol DP9711 nanoparticle dispersion through a 180 micron beadpack at a 1:1 ratio at a total flow rate of 24 mL/min. As the shear rate in the rheometer is increased the viscosity of the emulsion decreases. From a power law curve fit using Microsoft Excel, this emulsion has a flow consistency index (K) of approximately 15800 and a flow behavior index (n) of -0.84. At the shear rate in the beadpack used to generate the emulsion, the viscosity of the emulsion would be about 6 cP. The viscosity of the component fluids is given in Table 3.1.
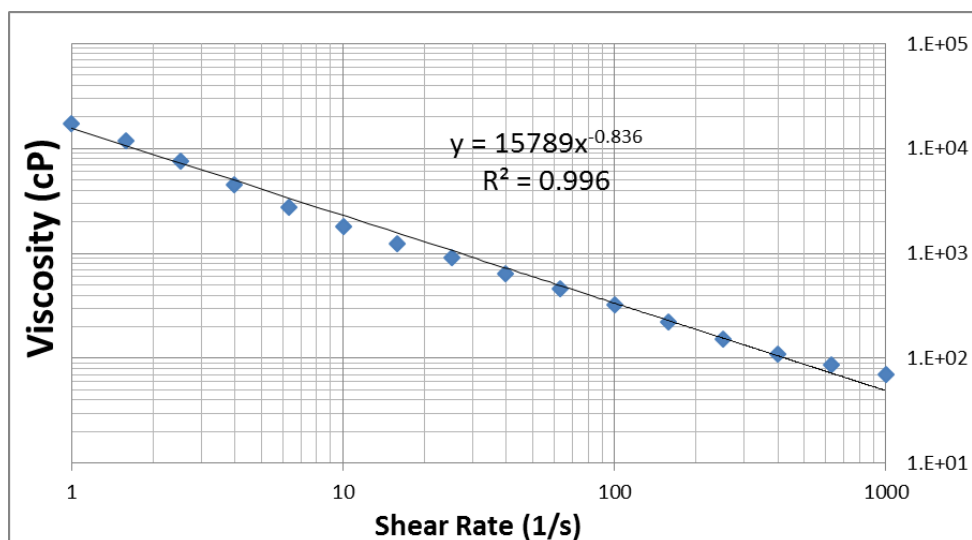
Figure 3.12 Rheology of nanoparticle stabilized emulsion.   The emulsion was generated by co-injecting mineral oil and the Nyacol DP9711 nanoparticle dispersion through a 180 micron beadpack at a 1:1 ratio at a total flow rate of 24 mL/min.

3.3.4 Emulsion Generation with Different Oils

Different oils were used to generate stable emulsions. The emulsions were all generated by co-injecting the oil phase and Nyacol DP 9711 dispersion through the HiP beadpack.   This dispersion was chosen over the other nanoparticle dispersions that stabilized emulsions in the beadpack because of the previous research conducted by Roberts (2011) where DP 9711 generated stable dodecane-in-water emulsions by co-injection through sandstone fractures. The dispersion was 2 wt% nanoparticles and 3 wt% NaCl.   Table 3.3 shows the viscosity of the oils used to generate emulsions.   The oil viscosity was measured with the rheometer.

Oil	Mineral Oil	Texaco White Oil	Dodecane	n-Octane
Viscosity (cP)	41.5	26.6	1.28	0.49

Table 3.3 Bulk viscosity of the oils used to generate emulsions.

The emulsions made with mineral oil, Texaco White Oil, and dodecane were all stabilized by injecting the nanoparticle dispersion and oil phase using the same flow conditions outlined in Section 3.3.1.   Stable emulsion was not formed with n-octane at these conditions.   The n-octane emulsion was generated using the same 1:1 phase ratio but at a total flow rate of 40 mL/min.   This shows that the critical shear rate depends on the oil phase; presumably the shear stresses were too small in the octane to generate sufficient droplets at 24 mL/min, but increasing the shear rate by increasing flow rate to 40 mL/min gave sufficient shear stress.

The critical shear rate for mineral oil in 180 micron beads was between 781 and 1,042 s^{-1}.   The generation of the octane emulsion suggests the critical shear rate for octane in 180 micron beads is between 12,500 and 20,800 s^{-1}.   Multiplying the critical shear rate by the viscosity of the oil phase gives a critical shear stress.   The critical shear stress for mineral oil is between 32 and 43 pascals.   The critical shear stress for octane is between 6 and 10 pascals.

The emulsion droplet size was then analyzed using the microscope and ImageJ. Table 3.4 shows the following for each emulsion: average droplet diameter, median droplet diameter, and number of droplets measured for each emulsion.

Emulsion	Mineral Oil	Texaco White Oil	Dodecane	n-Octane
Average Droplet Diameter (μm)	23.2	23.4	29.0	22.2
Median Diameter (μm)	22.0	23.0	29.0	22.0
# of droplets measured	130	167	158	245

Table 3.4 The average droplet diameter, median diameter, and number of droplets measured for the emulsions generated with different oils.

The rheology of each emulsion was measured. Figure 3.13 plots emulsion viscosity as a function of shear rate. The emulsions exhibit highly shear-thinning behavior. The emulsions have very similar viscosities even though the different oils used to make the emulsions have different viscosities. This is evidence that emulsion viscosity is dependent on droplet size and independent of the viscosity of the oil making up the droplets.
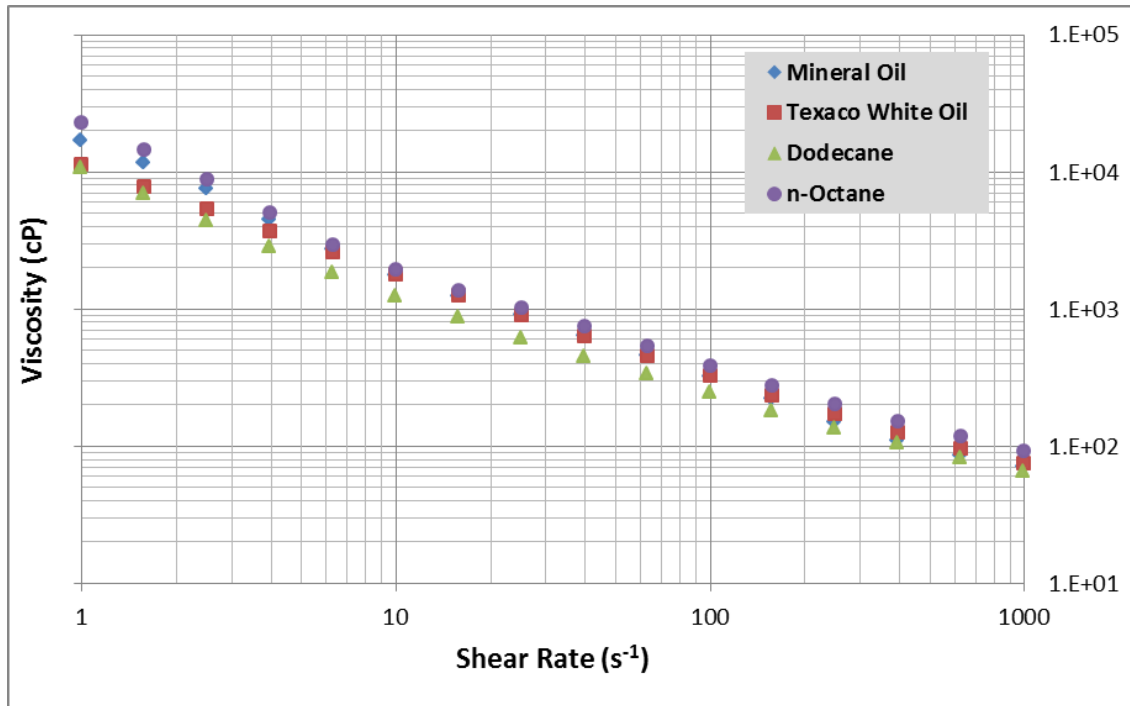
Figure 3.13 The rheology of the emulsions generated with different oils and 3 wt% NaCl, 2 wt% Nyacol DP 9711 nanoparticle dispersion with 180 micron beadpack at shear rates of 12,500 s^{-1} (20,800 s^{-1} for octane). The dispersion and oil were injected at 1:1 phase ratio. The average droplet sizes of the emulsions are in Table 3.4.

3.3.5 Effect of Droplet Size on Emulsion Viscosity

The previous section showed that emulsion rheology is independent of oil viscosity for emulsions with similar droplet sizes. Figure 3.14 shows how emulsion viscosity is controlled by the emulsions droplet size. Two different mineral emulsions were generated by co-injecting mineral oil and the Nyacol DP9711 nanoparticle dispersion used in the critical shear rate experiments through the HiP beadpack at a 1:1 phase ratio. The emulsion with an average droplet diameter of 24 microns was generated with 180 micron beads and a total flow rate of 24 mL/min. The emulsion

with an average droplet diameter of 62 microns was generated with 500 micron beads and a total flow rate of 12 mL/min. The emulsion with the smaller droplet size is more viscous over the entire range of shear rate. The smaller droplet emulsion is more than twice as viscous as the larger droplet emulsion between 1-100 s^{-1}. Between 100-1000 s^{-1}, the difference in viscosity is not as large but the 24 micron emulsion is still more viscous than the 62 micron emulsion.
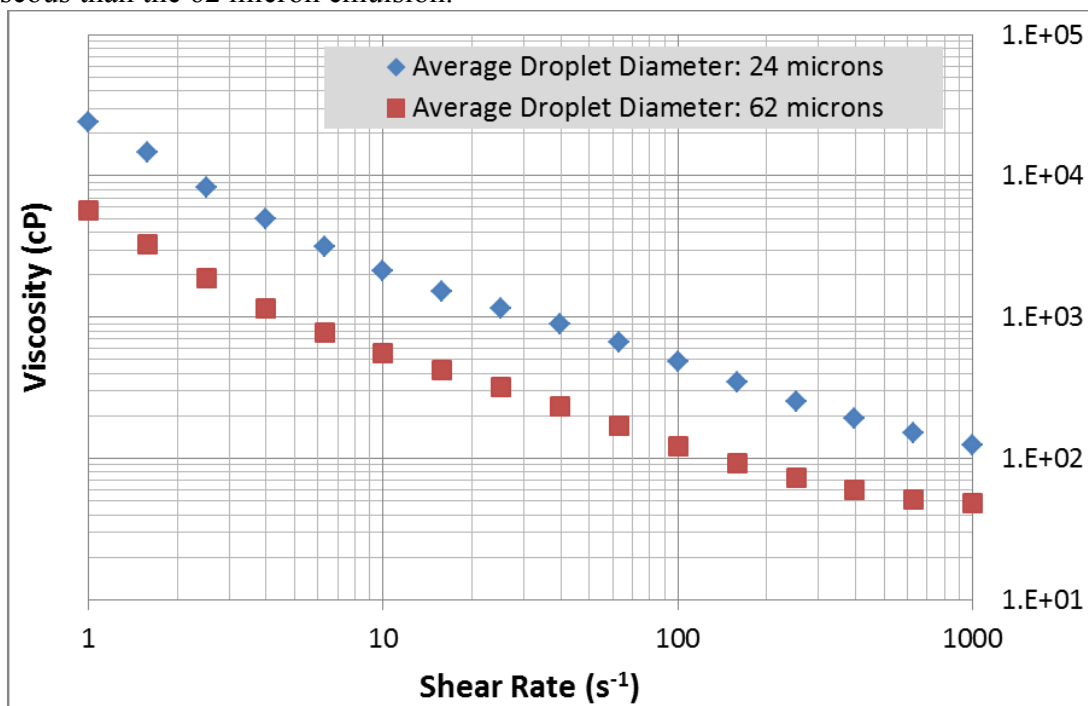
Figure 3.14 Rheology of two mineral oil-in-water emulsions (stabilized with 3 wt% NaCl, 2 wt% Nyacol DP 9711 nanoparticle dispersion) generated with flow rates and bead sizes chosen to yield different droplet sizes (see text).

3.3.6 Effect of Time on Emulsion Droplet Size and Viscosity

To test the stability of emulsions over time a newly generated emulsion was stored in a closed container at atmospheric pressure and room temperature for

approximately 1 month.   The droplet size and rheology were measured the same day the emulsion was initially generated in the beadpack.   The emulsion was generated by injecting nanoparticle dispersion (3 wt% NaCl, 2 wt% Nyacol DP 9711) and mineral oil through 500 micron beads with a total flow rate of 12 mL/min at a 1:1 phase ratio.   The rheology and droplet size were measured approximately 1 month later.   The average droplet size remained the same and the rheology of the emulsion was unchanged. Figure 3.15 shows the rheology and microscopic images of the emulsion the day it was generated and one month later.
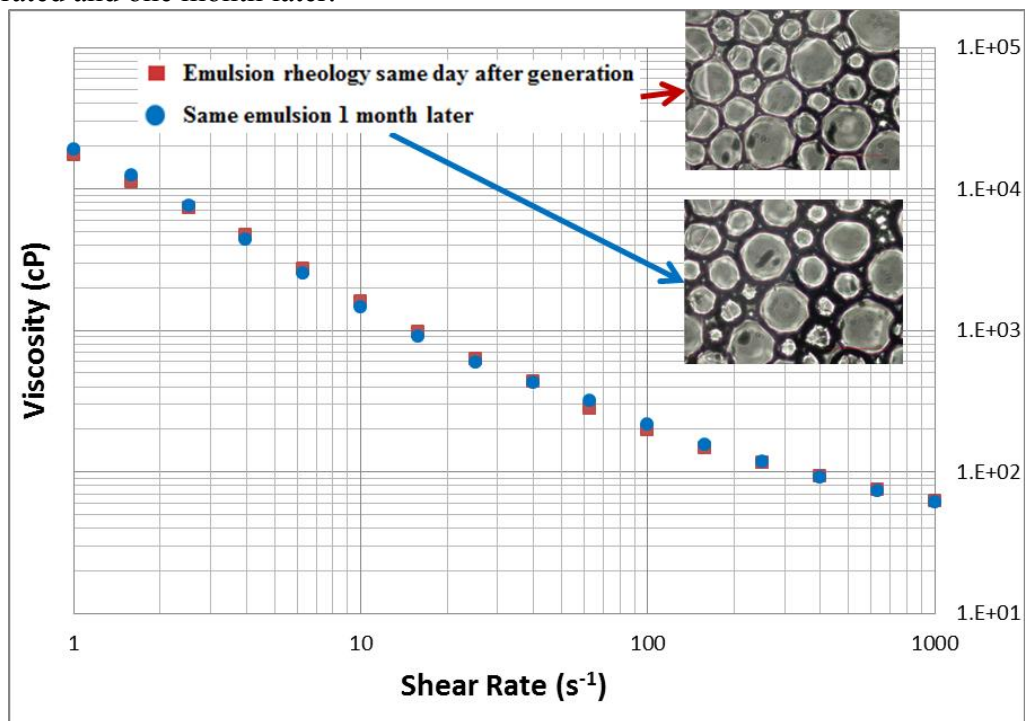
Figure 3.15 The rheology of a mineral oil-in-water emulsion the day it was generated with 500 micron beads and 1 month after it was stored at ambient conditions.   Microscopic images of the emulsion are also shown. Mineral oil-in-water emulsion (stabilized with 3 wt% NaCl, 2 wt% Nyacol DP 9711 nanoparticle dispersion) generated at a total flow rate of 12 mL/min, 1:1 phase ratio.

3.3.7 Reproducibility of Generating Emulsions by Co-injection

The next two chapters present the results of flowing large volumes of emulsion through beadpacks and sandstone cores. The emulsions used in those chapters were generated by co-injecting nanoparticle dispersion and oil through the beadpack. It was important that different batches of emulsions generated using the same conditions had similar droplet size and rheology. Different batches of emulsion made with the same conditions displayed consistent rheology and average droplet size. Figure 3.16 shows the droplet distribution for two different emulsions made using the same conditions except the beadpack had a different packing of 180 micron beads. The two emulsions displayed approximately normal distributions and had approximately the same droplet size. All of the emulsions generated through co-injection displayed a normal distribution of droplet size. Because the emulsion droplet size distribution was normal, the emulsions used throughout this thesis were classified by their average droplet size.
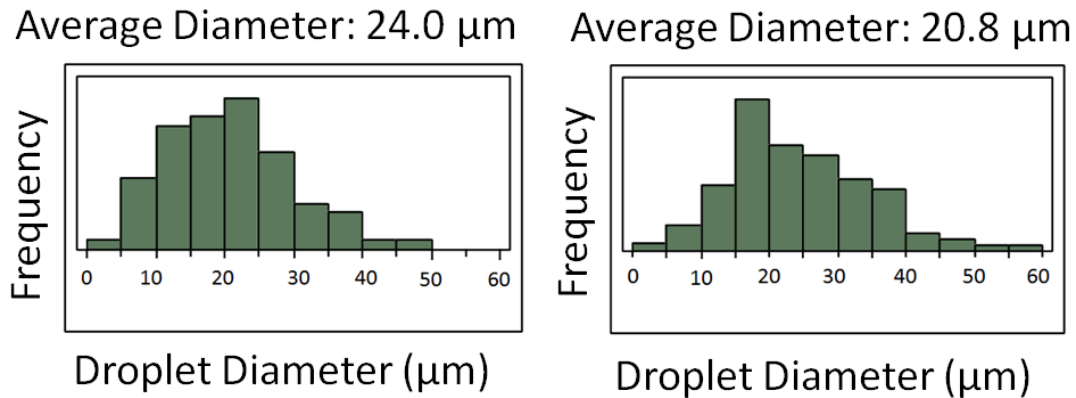
Figure 3.16 The droplet size distribution and average droplet diameter for two different emulsions generated under the same conditions with 180 micron beads. Mineral oil-in-water emulsions (stabilized with 3 wt% NaCl, 2 wt% Nyacol DP 9711 nanoparticle dispersion) generated at a total flow rate of 24 mL/min, 1:1 phase ratio.

45

The rheology of the two emulsions was measured with the rheometer. The results are shown in Figure 3.17. The two emulsions, as expected, have nearly identical viscosity behavior.
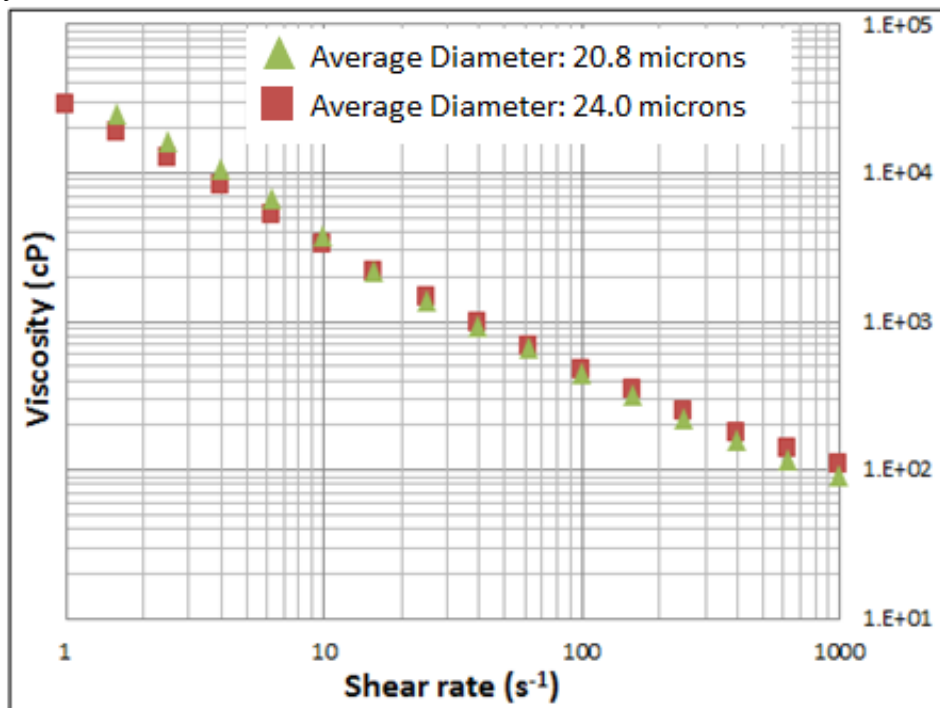
Figure 3.17 The rheology measurements of the two different emulsions made using the same conditions just different packings of 180 micron beads. Mineral oil-in-water emulsions (stabilized with 3 wt% NaCl, 2 wt% Nyacol DP 9711 nanoparticle dispersion) generated at a total flow rate of 24 mL/min, 1:1 phase ratio.

3.4 DISCUSSION

Three nanoparticle dispersions out of the twelve tested were able to generate stable oil-in-water emulsions in the beadpack at the conditions studied here. The three nanoparticle dispersions all had similar nanoparticle size, similar concentration, and some proprietary surface treatment. The Nyacol DP 9711 nanoparticles had a diameter of

approximately 20 nm. The EOR-25 nanoparticles were approximately 25 nm in diameter. The IPA-ST particles were approximately 10-15 nm in diameter. The surface treatments are proprietary to Nyacol Nano Technologies (DP 9711) and Nissan Chemical (EOR-25 and IPA-ST). The nanoparticle concentrations of these three dispersions were diluted to 2 wt% for DP 9711, 3 wt% for IPA-ST, and 5 wt% for EOR-25. A 1 wt% nanoparticle concentration dispersion made with EOR-25 did not generate a stable emulsion indicating the existence of a critical nanoparticle concentration to generate a stable emulsion for this particle type.

It was shown that there is a critical shear rate associated with generating an emulsion by co-injection. Previous work by Espinosa (2011), Roberts (2011), and Hariz (2012) all showed evidence of a critical shear rate to generate nanoparticle stabilized emulsions/foams. The ability to generate stable emulsions is related to the amount of energy supplied to the fluids giving rise to a critical shear rate in the co-injection setup. Above the critical shear rate there is adequate shear between the two fluids to snap off individual oil droplets from the bulk oil phase into the dispersion. The nanoparticles adhere to the droplet surface, preventing them from coalescing and thereby creating stable emulsions. The nanoparticles at the oil/water interface create an energy barrier to prevent coalescence of the individual oil droplets. At the critical shear rate just enough energy is provided in the form of shear to snap off individual oil droplets from the continuous oil phase. Below the critical shear rate, the amount of energy supplied is not high enough to snap off individual oil droplets from the continuous oil phase or, if droplets are created, there is not enough energy to promote rapid nanoparticle adhesion to

47

the droplet surfaces, so no emulsion is formed and the fluids flow through the beadpack as two separate continuous phases.

The critical shear rate increases as the pore throat size of the beadpack was decreased. Evidently it takes more energy to stabilize an emulsion in smaller pore throats. This most likely arises from the generated emulsion droplets having to pass through smaller pore throats. The emulsion droplets are more likely to coalesce as they travel through smaller pore throats, compared to larger pore throats, because the droplets have larger curvature. This causes an increase in the shear rate in smaller pore throats because the flow rate must be high enough to generate stable droplets and then propagate them through the small pore throats. In the larger bead sizes the droplets were much smaller than the pore throats so the critical shear rate arose from simply generating a stable emulsion from snap off.

In the critical shear rate experiments it was evident that emulsion droplet size was correlated with shear rate but not bead size. Because the emulsion droplets were much smaller than the average pore throat size, except for the 180 and 275 micron beads, the emulsion droplet size was not affected by the bead size but the amount of shear in the beadpack. When the pore throats began to approach the size of the droplets an increase in droplet strain caused the critical shear rate to increase for the 180 and 275 micron beads.

All of the experiments performed in this chapter were performed at a 1:1 phase ratio. Although the phase ratio was never altered in the critical shear rate experiments, it is expected that changing the phase ratio of the two fluids would not affect the critical shear rate except at large aqueous to oil volume ratios $(q_w/q_o \geq 4)$. Using a Nyacol

DP 9711 nanoparticle dispersion, Roberts (2010) found that stable emulsion could be generated at with several different phase ratios (q_w/q_o from 0.25 to 2) at equivalent shear rates.   It was not until the phase ratio, q_w/q_o, was raised to 4 that stable emulsion was not produced above the critical shear rate.   Espinosa (2011) found that the critical shear rate to generate nanoparticle stabilized CO_2 foams was independent of phase ratio.

In the co-injection experiments with different oils three oils with quite different viscosities were able to generate stable emulsion at a shear rate of 12,500 s^{-1}. Mineral oil (41.5 cP), Texaco White Oil (26.6 cP), and dodecane (1.28 cP) were all more viscous than the nanoparticle dispersion (1.06 cP) used to generate the emulsions.   A higher shear rate of 20,830 s^{-1} was required to stabilize an emulsion with octane.   The octane (0.49 cP) was less viscous than the nanoparticle dispersion.   This indicates that the oil viscosity may only be factor in emulsion stabilization if the oil is less viscous than the nanoparticle dispersion, in which case more shear is required to stabilize an emulsion than for oil that is more viscous than the dispersion. The critical shear stress range for mineral oil and octane were different suggesting that emulsion generation may be independent of shear stress. The increase in shear rate required to stabilize the octane emulsion was most likely due to snapping off oil droplets that are less viscous (octane) into than the continuous phase (nanoparticle dispersion).

It was shown in Section 3.3.5 that the viscosity of the nanoparticle stabilized oil-in-water emulsions is a function of droplet size.   This is typical of other emulsions stabilized with surfactants (Otsubo and Prud'homme 1994).   Otsubo and Prud'homme (1994) showed that increasing the droplet size caused a decrease in emulsion viscosity over the entire shear rate range for surfactant stabilized oil in water emulsions.   The

49

same behavior was observed for the nanoparticle stabilized oil-in-water emulsions generated in this chapter.

The shear thinning behavior is similar to other emulsions stabilized with surfactants. Emulsions typically become more viscous and shear thinning as the volume of the dispersed phase is increased (Tadros 2013). The nanoparticle stabilized emulsions display similar shear thinning behavior as other surfactant stabilized emulsions indicating that the nanoparticles do not affect the power law behavior (Otsubo and Prud'homme 1994).

3.5 CONCLUSIONS

Highly stable, shear thinning oil-in-water emulsions were generated by co-injecting nanoparticle dispersion and oil phase through a beadpack. Eleven different nanoparticle dispersions, with different particles, were used in the co-injection system. Only three types of nanoparticle dispersions were able to generate stable emulsions in the beadpack at the conditions studies here (1:1 phase ratio, shear rates ranging from 200 to 20,800 s^{-1}, ambient temperature and pressure, nanoparticle concentrations of 2 to 5 wt%, salinity of 1 to 3 wt%). The nanoparticle size of the dispersions ranged from 10-25 nm in diameter and the nanoparticles had a proprietary surface treatment/modification.

Critical shear rate experiments were performed using a Nyacol DP 9711 dispersion and mineral oil. Stable emulsions were produced over a range of shear rates for different bead sizes. The critical shear rate for producing a stable emulsion was found for five different bead sizes. As bead size increased, the critical shear rate to generate stable emulsion decreased. The stable emulsions were characterized by their average droplet size and their rheology. Emulsions produced at high shear rates had smaller

average droplet size and were more viscous than emulsions produced at lower shear rates. In the large beads (1000 and 3000 microns) the average droplet size of the emulsion was highly dependent on the shear rate. The average droplet size of the emulsions produced in smaller beads was less dependent on shear rate although in general the average droplet size decreased with increasing shear rate.

Stable emulsions were generated using three different oils at the same flow rates, phase ratios, nanoparticle dispersion (2 wt% Nycol DP 9711, 3 wt% NaCl) in the same beadpacks. Stable octane-in-water emulsion was generated using the same conditions except for a higher flow rate. The droplet size and rheology of each emulsion was measured. The average droplet size of each emulsion was approximately the same. The emulsions displayed the same rheology because of their similar droplet size, proving that emulsion viscosity is independent of the bulk oil viscosity. Nanoparticle stabilized emulsions viscosity is highly dependent on droplet size. Emulsions with small droplets are more viscous than emulsions with large droplets. The emulsions generated by co-injection retained their droplet size and rheology over time indicating their robust stability. The emulsions generated in the beadpack displayed normal droplet size distributions and the emulsions properties were reproducible for different batches of emulsion generated using the same conditions.

51

Chapter 4

Emulsion Flow through Beadpacks

For emulsions to be used in conformance control/mobility control applications, it is necessary to understand their rheology and stability in reservoirs. It should not be taken for granted that the batch emulsion rheology reported in Chapter 3 will be the same as the rheology of the emulsion when it flows through porous media. In Chapter 3 emulsions were generated by flowing two phases through the beadpack. This chapter will investigate the stability and rheology of injecting the stable, already formed emulsions through the beadpack.

CO_2 foams are often used to improve mobility control. The ideal foams used for mobility control will propagate through the reservoir by the breaking and remaking of the lamellae, thin liquid films separating gas bubbles (Morrow 1990). The transport of foams is different than emulsions in that emulsion transport is generally viewed as stable droplets flowing in a continuous phase, i.e. the droplets are not constantly breaking and reforming. The transport and stability of injecting statically stable emulsions through the beadpack will be investigated in this chapter, specifically the result of injecting emulsions through different size pores at different flow rates.

4.1 MATERIALS AND EXPERIMENTAL PROCEDURE

In this section the materials and equipment used for beadpack experiments will be discussed. In order to investigate emulsion flow and stability in porous media, experiments were performed in which stable emulsion was injected through a beadpack with varying conditions.

52

4.1.1 Materials

Emulsion Injected

Two different emulsions were used in the beadpack experiments. Both were made using a Nyacol DP9711 nanoparticle dispersion and light mineral oil. This dispersion was 2 wt% nanoparticles and 3 wt% NaCl. One emulsion was generated by co-injecting a 1:1 ratio of mineral oil and nanoparticle dispersion through a 180 μm beadpack at a total flow rate of 24 mL/min. The second emulsion was generated by co-injecting a 1:1 ratio of mineral oil and nanoparticle dispersion through a 500 μm beadpack at a total flow rate of 12 mL/min. Properties of each emulsion are described in Chapter 3 (see Figure 3.14). The two emulsions were generated continuously to produce a batch of approximately 1 liter. A batch of emulsion generated at a total flow rate of 24 mL/min was generated for approximately 35 minutes, while it took approximately 70 minutes a batch for the emulsion produced at a total flow rate of 12 mL/min. Excess nanoparticle dispersion was present in the effluent from the beadpack for both emulsions. Because oil and nanoparticle dispersion were injected at a 1:1 phase ratio, there was 500 mL of each phase present in a 1 liter batch. For 1 liter of effluent collected, approximately 760 mL of stable emulsion was produced with 240 mL of excess nanoparticle dispersion and no excess mineral oil; therefore, both emulsions were approximately 66% mineral oil by volume. The rheology and droplet size of each batch were measured. The average droplet diameter for the emulsion made in the 180 micron beadpack ranged from 20 to 24 microns. The average droplet diameter for the emulsion made in the 500 micron beadpack ranged from 50 to 62 microns. In this chapter the two different emulsions will be denoted by their average droplet size. The emulsions

generated in the 180 micron beadpack will be denoted by an average droplet diameter of 24 microns.   The emulsions generated in the 500 micron beadpack will be denoted with an average droplet diameter of 62 microns.   The rheology of each batch of emulsion was measured for consistency.   Figure 3.13 show the rheology of the two emulsions used in this chapter.

Initial Saturations

DI water, light mineral oil, and a polyethylene glycol (PEG) solution were used in different experiments to saturate the beadpack prior to injecting the emulsion.   The PEG solution was 5 wt% PEG, 2 wt% NaCl in DI water.   The polyethylene glycol has an average molecular weight of 1000 and was purchased from Fisher Scientific.

Beadpack and Beads

Two different beadpacks were used in these experiments.   Majority of the experiments was performed in the same beadpack used in the co-injection set up. The second beadpack used in these experiments was longer and wider than the HiP beadpack. The larger beadpack had an internal diameter of 2.13 cm and was 30.5 cm long.   Several different bead sizes were used in the beadpack experiments.   All beads were made of glass and were spherical in shape.   The sizes of the beads used in this chapter were: 52 μm, 105 μm, 180 μm, 500 μm, 1000 μm, and 3000 μm. The larger beadpack ID is sufficient to ensure most injected fluids move through pore throats within the pack even for the largest beads, in contrast to the situation in the narrow beadpack.

54

4.1.2 Beadpack Emulsion Injection Set-Up

The beadpack injection set-up involves many of the same components used in the co-injection apparatus; however there are some key differences. Figure 4.1 is a schematic of the beadpack setup with the key components labeled. A Teledyne ISCO syringe pump was used to inject drive water into the accumulator. Inside the accumulator is a movable piston. As the drive water is injected into the accumulator it moves the piston displacing the emulsion to the beadpack. A pressure transducer was used to measure the pressure drop across the bead pack. Eleven emulsion injection experiments were performed before the pressure transducer was implemented into the setup, so there is no pressure data for those experiments. The fraction collector was used to collect the effluent from the beadpack.
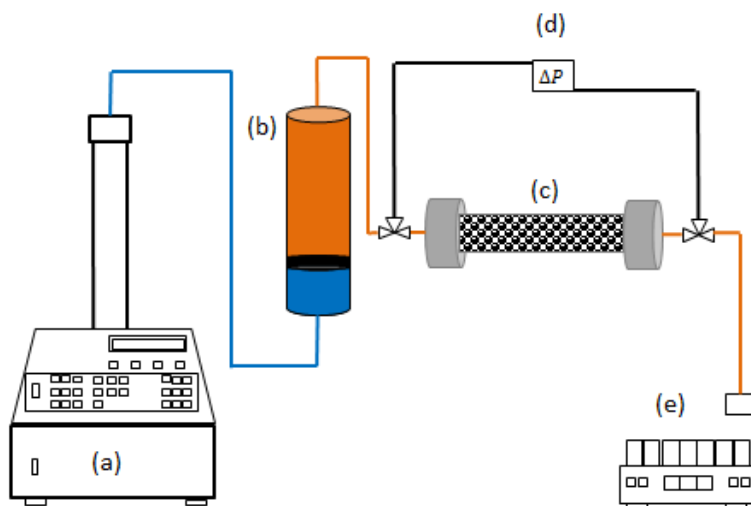
Figure 4.1 Beadpack injection schematic: (a) syringe pump (b) accumulator containing stable emulsion (c) bead pack (d) pressure transducer (e) fraction collector. Pressure transducers were not used in Beadpack Experiments 1-11.

Pump

One syringe pump was used for the emulsion injection.   The pump is a D-Series Model 1000 Teledyne ISCO (Lincoln, NE) syringe pump.   This pump is capable of pumping up to 408 mL/min and has a maximum operating pressure of 2000 psi.

Accumulator

A 400 mL accumulator was incorporated in the system to avoid loading the emulsion and the nanoparticles within it directly into the pumps.   Inside the accumulator is a movable piston.   The procedure for loading the accumulator will be outlined in Section 4.1.3.

Data Acquisition

A differential Rosemount pressure transducer was used to record the pressure drop across the beadpack.   This transducer is a differential pressure transducer model 3051CD5A22A1A.   The transducers and the data acquisition card are powered by a power supply unit.   The data acquisition card allows the pressure to be monitored and recorded from the computer.   From the computer, the pressure is displayed and recorded using the program LabView.   The pressure data has been corrected to remove any offset (i.e. so a zero flow rate corresponds to a zero pressure drop).   The pressure transducer has a maximum working pressure drop of 2,000 psi however the transducers have been calibrated to operate in the pressure ranges for the beadpack experiments.

4.1.3 Beadpack Experimental Procedure

This section will outline the experimental procedure used for injecting emulsion into the beadpack.   The procedure outlined below was used after the accumulator was loaded with emulsion and was allowed to sit for approximately two hours to ensure that

emulsion was the only fluid injected into the beadpack. Two hours provides sufficient time for any excess nanoparticle dispersion to drain to the bottom of the accumulator. The difference in density between the emulsion and excess nanoparticle dispersion cause the nanoparticle dispersion to collect at the bottom of the accumulator.   The procedure for loading the accumulator will be discussed in detail.

1. Load syringe pump with fluid that will be used to initially saturate the beadpack (either mineral oil, DI water, or PEG solution)

2. Change beadpack to put in fresh beads (beadpack filling procedure outlined earlier)

3. Connect beadpack to syringe pump and inject the saturating fluid (over 20 pore volumes were injected to ensure complete saturation)

4. Disconnect beadpack from syringe pump and empty the syringe pump

5. Load syringe pump with drive water

6. Connect the pump to the accumulator loaded with emulsion

7. Attach transducer lines and begin recording pressure drop with LabVIEW

8. Have a waste beaker to collect any excess fluid in lines or any excess oil in the accumulator.   Pump any excess fluid in the lines until emulsion is seen leaving the line attached to the top of the accumulator that will be connected to the beadpack

9. Once emulsion is flowing out of the line connect it to the beadpack

10. Collect effluent with fraction collector

Loading the Accumulator

In order to load the accumulator, the piston was first moved to the bottom of the accumulator. Then the emulsion is poured into the accumulator. During the emulsion loading process it was common some of the excess nanoparticle dispersion, from the emulsion generation process, to flow into the accumulator along with the emulsion. In order to ensure that only emulsion was injected into the beadpack and not a mixture of
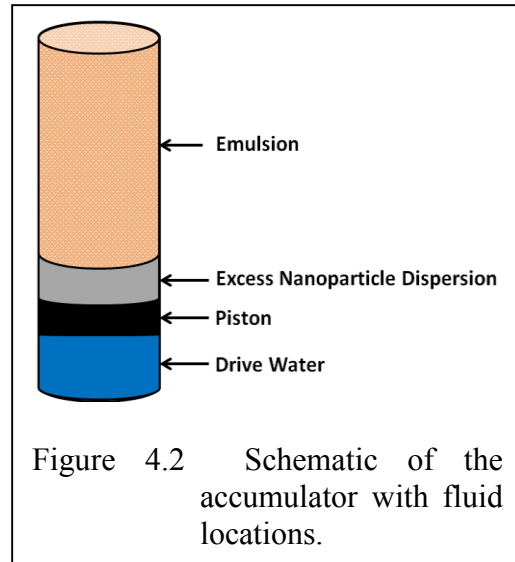
Figure 4.2 Schematic of the accumulator with fluid locations.

emulsion and nanoparticle dispersion, the accumulator was positioned vertically. This allowed for the denser nanoparticle dispersion to settle to the bottom of the accumulator with the less dense emulsion sitting above it. Although the settling process took approximately 30 minutes to complete, the emulsion and nanoparticle dispersion were positioned vertically for at least two hours before an experiment was performed to ensure that only emulsion was injected into the beadpack.

4.2 DATA ANALYSIS

4.2.1 Permeability of the Bead Pack

The permeability of the bead pack was calculated using the same equation in section 3.2.1.

4.2.2 Shear Rate in the Beadpack

The shear rate in the beadpack was calculated using the same equation in section 3.2.2.

4.2.3 Reynolds Number Calculation

The Reynolds number, Re, was calculated for experiments where the apparent viscosity was calculated using Darcy's law. Darcy's law only applies for slow, creeping flow ($Re < 1$). The following equation was used to calculate Reynolds number:

$$Re = \frac{\rho v_s D}{\mu}$$

where ρ is the density of the fluid (g/cm^3), v_s is the superficial velocity (cm/s), and D is the bead diameter (cm), and μ is the viscosity of the fluid (g/cm/s). For the experiments in this section where Darcy's law was used to calculate apparent viscosity the Reynolds number was less than one.

4.2.4 Apparent Viscosity Calculation

The apparent viscosity, μ_{app}, of the emulsion while flowing through the beadpack was calculated from Darcy's law:

$$\mu_{app} = \frac{kA}{Q} \frac{(P_i - P_o)}{L}$$

where k is the permeability of the beadpack (cm^2), A is the cross-sectional area of the beadpack (cm), P_o and P_i are the outlet and inlet pressure (Pa), Q is the volumetric flow rate (cm^3/s), and L is the length of the bead pack (cm). Gravity is not accounted for because the beadpack was positioned horizontally for all experiments.

4.3 RESULTS AND DISCUSSION

In this section the results from the emulsion injection experiments will be presented and discussed in detail. For many of the experiments photographs of the effluent are shown. The effluent was collected in 15 mL centrifugal tubes. The pore volume of the beadpack was approximately 1 mL. One test tube contains several pore volumes of effluent. Table 4.1 is a summary of all the beadpack experiments presented in this section.

Chapter 4 Beadpack Emulsion Injection Experiment Summary							
Beadpack Experiment	Flow Rate (mL/min)	Bead Diameter (μm)	Emulsion Droplet Diameter (μm)	Shear Rate (s⁻¹)	Initial Saturation	PV of emulsion injected	PV injected when stable emulsion arrived in effluent
1	0.5	105	62	446	DI Water	52	Never
2	0.5	52	24	901	DI Water	37	Never
3	0.5	52	24	901	DI Water	34	Never
4	0.1	105	24	89	DI Water	11	4
5	0.5	500	62	94	DI Water	45	Never
6	0.5	500	62	94	DI Water	93	45
7	0.5	500	24	94	DI Water	95	8
8	0.5	180	24	260	DI Water	92	13
9	4	500	24	750	DI Water	95	11
10	4	180	24	2083	DI Water	96	9
11	0.5	180	24	260	Mineral Oil	93	Never
12	0.5	500	24	94	Mineral Oil	225	40
13	0.5	500	24	94	DI Water	190	13
14	0.5	500	24	94	DI Water	215	10
15	0.5	52	24	901	DI Water	76	75
16	2	180	24	1042	DI Water	350	20
17	0.5	1000	24	47	DI Water	100	5
18	0.5	1000	24	47	DI Water	100	3
19	0.5	1000	24	47	DI Water	100	4
20	0.5	1000	24	47	DI Water	100	2
21	0.5	500	24	94	PEG Solution	150	Never
22	1	500	62	8	DI Water + some crude oil	8	Never
23	4	500	62	32	DI Water	9	Never
24	14	3000	24	535	DI Water	9	1.5
25	14	3000	24	535	Mineral Oil	6	2.2

Table 4.1 A summary of all of the beadpack experiments presented in this chapter. Experiments 1-11 in grey color were performed without the pressure transducer. Experiments 1-21 were all performed in the HiP beadpack. Experiments 22-25 were performed in the larger beadpack (see section 4.1 for dimensions).

4.3.1 Emulsion Injection Experiments without Pressure Data

In this section the emulsion injection experiments without pressure data will be presented. The two different emulsions outlined in the previous section will be denoted by their average droplet size (24 microns and 62 microns). These emulsions were injected through the beadpack with different bead sizes and initial saturations. The experiments in this section were all performed in the HiP beadpack that was used to generate emulsions in the previous chapter.

4.3.1.1 Emulsion coalescence caused by small pores

Beadpack Experiments 1-4 were performed to see whether emulsion droplets could remain intact while flowing through smaller pore throats or whether flow caused coalescence. A good approximation for the pore throat diameter in a uniform packing of spheres is one third of the bead diameter. Beadpack Experiment 1 in Figure 4.3 shows the effluent when an emulsion with an average droplet diameter of 62 microns was injected through 105 micron beads. The pore throats in the bead pack were approximately 35 microns. The ratio of average droplet size to pore throat size was approximately 1.8. The injected emulsion droplets did not survive passage through the beadpack; the effluent from the beadpack consisted of two separate phases, with all the droplets having coalesced. This was a surprising result because the emulsion was extremely stable under static environment; however when the emulsion was injected through the beadpack the emulsion became unstable. The shear rate for Beadpack Experiment 1 was 446 s^{-1}. Though the oil phase and dispersion phase used to generate the emulsion must have been flowing through the bead pack after coalescence, evidently the emulsion did not reform because the shear rate was below the critical shear rate

required to generate an emulsion in this beadpack. Although no critical shear rate was found for this particular bead size in the critical shear rate experiments because 105 μm beads were not used in the critical shear rate experiments (Section 3.2.2), the critical shear rate for 180 micron beads was approximately 1,000 s^{-1} and previous results showed that the critical shear rate increased for decreasing bead size. Thus it was likely that the critical shear rate for 105 micron beads would be higher than 446 s^{-1}, which was the shear rate for Beadpack Experiment 1.

Beadpack Experiment 1					
Average Emulsion Droplet Diameter (μm)	Flow Rate (mL/min)	Emulsion Pore Volumes Injected	Bead Size (μm)	Initial Saturation	Shear Rate (s^{-1})
62	0.5	52	105	DI Water	446
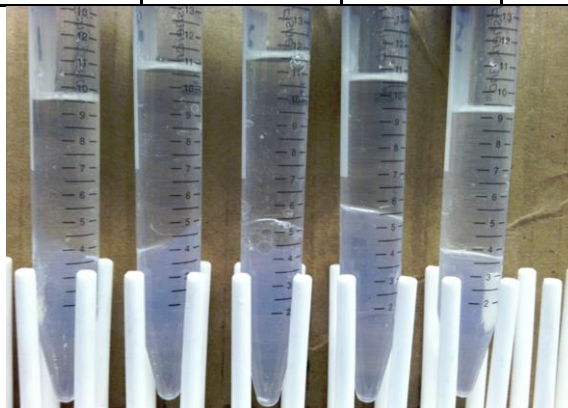
Figure 4.3 Experimental conditions and effluent from Beadpack Experiment 1. Only the constituent phases from the broken emulsion were produced for the duration of the experiment (note meniscus near the midpoint of each effluent sample). The volume ratio of the effluent is the same as the injected emulsion, which was approximately 2:1 mineral oil to aqueous nanoparticle dispersion.

Breaking a stable emulsion is generally difficult and it was particularly surprising that this emulsion was broken by flowing through a beadpack, since it was originally generated by flowing the two phases through a bead pack. To explore this phenomenon further, Beadpack Experiments 2 and 3 injected the emulsion with an average droplet diameter of 24 microns through 52 micron beads. The ratio of droplet diameter to pore throat size was approximately 1.4. Figure 4.4 shows that the emulsion completely coalesced for the entire 37 pore volumes injected. Experiment 3 was a repeat of Experiment 2, shown in Figure 4.5, and the emulsion coalesced for the 34 pore volumes injected. As in Beadpack Experiment 1, the statically stable emulsion was broken by flowing through a beadpack. Emulsion was not regenerated in the beadpack because it was injected below the critical shear rate to produce emulsion for this beadpack with 52 micron beads. The critical shear rate for 180 micron beads was approximately 1,000 s^{-1} and previous results showed that the critical shear rate increased for decreasing bead size, so the critical shear rate for 52 micron beads would be higher than 901 s^{-1} (shear rate for Beadpack Experiments 2 and 3).

Beadpack Experiment 2					
Average Emulsion Droplet Diameter (μm)	Flow Rate (mL/min)	Emulsion Pore Volumes Injected	Bead Size (μm)	Initial Saturation	Shear Rate (s^{-1})
24	0.5	37	52	DI Water	901

Figure 4.4 Experimental conditions and effluent from Beadpack Experiment 2.   Only the constituent phases from the broken emulsion were produced for the entire duration of the experiment.

Beadpack Experiment 3					
Average Emulsion Droplet Diameter (μm)	Flow Rate (mL/min)	Emulsion Pore Volumes Injected	Bead Size (μm)	Initial Saturation	Shear Rate (s^{-1})
24	0.5	34	52	DI Water	901
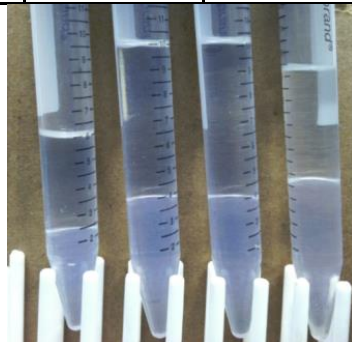
Figure 4.5 Experimental conditions and effluent from Beadpack Experiment 3.   Only the constituent phases from the broken emulsion were produced for the entire duration of the experiment.

In Beadpack Experiment 4, the droplet diameter to pore throat ratio was lowered below 1 by injecting an emulsion with an average diameter of 24 microns through 105 micron beads. These beads had an average throat diameter of approximately 35 microns making the ratio of droplet diameter to pore throat size 0.69. Figure 4.6 shows stable emulsion was produced in the effluent, along with a small volume of oil and 5 mL of aqueous phase. The latter must comprise the 1 mL of DI water initially present in the beadpack, any aqueous phase in the effluent lines at the beginning of emulsion injection, and several mL of nanoparticle dispersion. A probable explanation for the large amount of aqueous phase is that the effluent line from outlet of the beadpack to the fraction collector was not emptied before injection. This line contained 2 to 3 mL of dead volume and likely contained DI water. This would account for the excess aqueous phase in the effluent. A little less than 1 mL of aqueous nanoparticle dispersion would account for the free oil phase at the top of the effluent. This is consistent with the total amount of aqueous phase in the effluent: 3 mL from dead volume, 1mL from the DI displaced from the beadpack, and approximately 1mL from the nanoparticle dispersion from the coalesced emulsion. As with Experiments 1-3, the emulsion was injected below the critical shear rate, but unlike those experiments stable emulsion was produced. The critical shear rate for 180 micron beads was approximately 1,000 s^{-1} and previous results showed that the critical shear rate increased for decreasing bead size, so the critical shear rate for 105 micron beads would be higher than 89 s^{-1} (shear rate for Beadpack Experiment 4). Therefore, small droplets survived the passage through pores because the shear rate was not high enough to generate new droplets. The presence of oil and nanoparticle dispersion in the effluent indicates that emulsion coalescence occurred.

Thus another interpretation of this experiment is that most if not all of the injected emulsion broke, just as in Experiments 1-3, yet much of the coalesced oil was redispersed into an emulsion.

Beadpack Experiment 4					
Average Emulsion Droplet Diameter (μm)	Flow Rate (mL/min)	Emulsion Pore Volumes Injected	Bead Size (μm)	Initial Saturation	Shear Rate (s^{-1})
24	0.1	11	105	DI Water	89

Figure 4.6 Experimental conditions and effluent from Beadpack Experiment 4. Stable emulsion was produced in the effluent. Nevertheless a small amount of oil phase and aqueous phase were also produced (see top of sample tube) indicating a moderate degree of coalescence also occurred. Approximately 2 to 3 mL of aqueous phase contained in the effluent was from dead volume in the effluent line (see text).

4.3.1.2 Emulsion injection below the critical shear rate

In Beadpack Experiment 4 stable emulsion was produced in the effluent when emulsion was injected below the likely value of critical shear rate, although the critical shear rate was not explicitly determined for 52 or 105 micron beads. Beadpack

Experiments 5-8 were performed to see if an emulsion would remain stable while flowing below the critical shear rate to generate an emulsion for a particular bead size that was used in the critical shear rate experiments (Section 3.3.2). From the critical shear rate experiments, the critical shear rate window for 500 micron beads was between 187 s^{-1} and 281 s^{-1}. The emulsion in Beadpack Experiment 5 was injected into a 500 micron beadpack below the critical shear rate at 94 s^{-1}. Figure 4.7 shows that the emulsion completely coalesced. This is surprising for two reasons: first because the emulsion was generated with 500 micron beads, and second because the droplet size (62 microns) is smaller than the throat size (~160 micron). On the other hand, the small shear rate leads to the expectation that the emulsion would not be regenerated if droplets were to coalesce as a result of traveling through the pore throats. This expectation is consistent with the observation, but the reason for the coalescence remains unclear. As will be seen in subsequent experiments, this observation recurs and is a central discovery in this thesis.

Beadpack Experiment 5					
Average Emulsion Droplet Diameter (µm)	Flow Rate (mL/min)	Emulsion Pore Volumes Injected	Bead Size (µm)	Initial Saturation	Shear Rate (s⁻¹)
62	0.5	45	500	DI Water	94

Figure 4.7 Experimental conditions and effluent from Experiment 5. Only the constituent phases from the broken emulsion were produced for the entire duration of the experiment.

Beadpack Experiment 5 was replicated in Beadpack Experiment 6 but the emulsion was injected for a longer period of time. In Beadpack Experiment 5 the emulsion was injected for approximately 45 pore volumes. In Beadpack Experiment 6 the emulsion was injected for approximately 93 pore volumes. In Beadpack Experiment 6, Figure 4.8, the emulsion broke for approximately the first 45 pore volumes, with the component phases being produced in the effluent. But after this point stable emulsion was produced in the effluent. The dynamic behavior is remarkable; evidently the conditions within the beadpack are slowly evolving from one constant state (all emulsion

droplets coalesce and the effluent consists of the two separated phases) to another constant state (injected emulsion droplets apparently survive and are produced in the effluent, or alternatively the regeneration of emulsion from the coalesced phases can occur after a sufficient injection volume, despite the small shear rate).   The presence of oil (top of the last three samples in Figure 4.8) clearly indicates that droplets are continuing to coalesce even when mostly emulsion is being eluted from the beadpack.

Beadpack Experiment 6					
Average Emulsion Droplet Diameter (μm)	Flow Rate (mL/min)	Emulsion Pore Volumes Injected	Bead Size (μm)	Initial Saturation	Shear Rate (s^{-1})
62	0.5	93	500	DI Water	94

Figure 4.8 Experimental conditions and effluent from Beadpack Experiment 6. Only the constituent phases from the broken emulsion were produced for the first 45 pore volumes. Stable emulsion was produced after 45 pore volumes of injection though coalesced phases also continued to be produced along with the emulsion.

In Beadpack Experiment 6 the injected emulsion had an average droplet size of 62 microns and coalesced for the first 45 pore volumes of the injection. Beadpack Experiment 7 was a replicate of Beadpack Experiment 6 except the injected emulsion had an average droplet size of 24 microns. The hypothesis was that smaller droplets would remain stable in the beadpack therefore stable emulsion would be produced in the effluent sooner. Figure 4.9 shows the results of the experiment. Though the first 8 PV of injected emulsion completely coalesced (1st effluent sample), stable emulsion was

71

subsequently produced in the effluent (2nd effluent sample).   Coalescence continued after 8 PV, as large volumes of aqueous phase and small volumes of oil phase were produced along with the emulsion. The results from Beadpack Experiments 6 and 7 indicate that large droplets are less stable than small droplets while flowing through the beadpack; the pore throats in the beadpack are larger than both the droplet sizes.

Beadpack Experiment 7					
Average Emulsion Droplet Diameter (μm)	Flow Rate (mL/min)	Emulsion Pore Volumes Injected	Bead Size (μm)	Initial Saturation	Shear Rate (s^{-1})
24	0.5	95	500	DI Water	94

Figure 4.9 Experimental conditions and effluent from Beadpack Experiment 7.   Only the constituent phases from the broken emulsion were produced for the first 8 pore volumes (leftmost sample) but stable emulsion was produced along with the coalesced phases (small fraction of oil and large fraction of aqueous phase in each sample tube) for the remainder of the experiment.

Beadpack Experiment 8 was performed with a 180 micron beadpack.   The critical shear rate window for 180 micron beads was between 781 s^{-1} and 1042 s^{-1}.   The emulsion that was generated with the 180 micron beads was injected through 180 micron beads at a shear rate of 260 s^{-1}.   In Figure 4.10 only the constituent phases of the broken

72

emulsion were produced for approximately the first 13 pore volumes but then stable emulsion was produced in the effluent for the next 79 pore volumes. Unlike Beadpack Experiment 7, only emulsion is produced after the first 13 PV.   No oil phase and aqueous phase were evident in the effluent while stable emulsion was produced.   A possible explanation is the injected emulsion simply stopped coalescing after a sufficient volume has been injected.   Another possibility is that complete coalescence continued, but regeneration of the emulsion became possible after sufficient volume was injected, despite the shear rate being below the critical shear rate.

Beadpack Experiment 8					
Average Emulsion Droplet Diameter (μm)	Flow Rate (mL/min)	Emulsion Pore Volumes Injected	Bead Size (μm)	Initial Saturation	Shear Rate (s^{-1})
24	0.5	92	180	DI Water	260
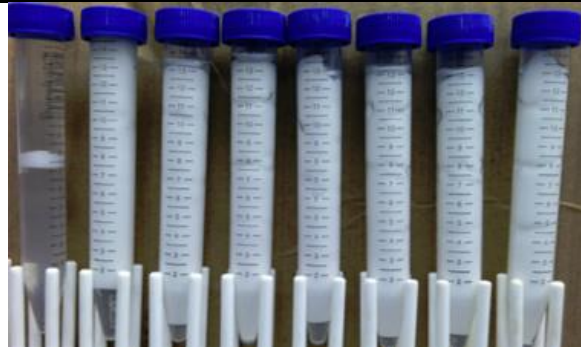
Figure 4.10 Experimental conditions and effluent from Beadpack Experiment 8.   Only the constituent phases from broken emulsion were produced for the first 13 pore volumes whereas only stable emulsion and no free phase (neither oil nor aqueous) was produced for the remainder of the experiment.

4.3.1.3 Emulsion injection above the critical shear rate

Beadpack Experiment 9 and 10 were performed where the emulsion was injected above the critical shear rate for the beadpack.   The critical shear rate was found for co-

injecting a 1:1 phase ratio, but the fractional flow from the coalesced emulsion creates a phase ratio of 2:1 mineral oil to nanoparticle dispersion. Previous work by Espinosa (2011) showed that generation of nanoparticle-stabilized foams in a beadpack was independent of phase ratio. Roberts (2010) found that nanoparticle-stabilized emulsion could be generated at several different phase ratios (q_w/q_o from 0.25 to 2) at equivalent shear rates. Thus, it is likely the critical shear rate to regenerate and emulsion from the coalesced phases is similar to the critical shear rate values reported in Chapter 3 for a 1:1 phase ratio.

The injected emulsion in Beadpack Experiment 9 and 10 had an average droplet diameter of 24 microns.   The flow rate was 4 mL/min for both the 500 and 180 micron beadpacks.   This flow rate corresponded to a shear rate of 2083 s^{-1} in the 180 micron beadpack and 750 s^{-1} in the 500 micron beadpack.   This was well above the critical shear rates for these two bead sizes.   The hypothesis was that when the emulsion was injected above the critical shear rate that stable emulsion would arrive in the effluent earlier than it arrived when emulsion was injected below the critical shear rate. But contrary to expectation, as shown in Figure 4.11 and 4.12, only the constituent phases from the broken emulsion were produced for approximately the first 11 pore volumes of emulsion injection.   After that point stable emulsion was produced in the effluent for the rest of the injection in both experiments.   In Beadpack Experiment 9 there was no excess oil phase but a small amount of nanoparticle dispersion was produced with the emulsion.   In Beadpack Experiment 10 there was a small amount of both excess oil and aqueous phase produced with the emulsion. This indicates emulsion coalescence still takes place even when the stable emulsion flows through the beadpack. The emulsion

broke for approximately the same amount of pore volumes injected when comparing Beadpack Experiments 7 and 8 (below the critical shear rate) to Beadpack Experiments 9 and 10 (above the critical shear rate).   These results refute the hypothesis, indicating the initial coalescence stage (typically first ~10 PV of effluent) during which only coalesced separate phases are produced is independent of shear rate.

Beadpack Experiment 9					
Average Emulsion Droplet Diameter (μm)	Flow Rate (mL/min)	Emulsion Pore Volumes Injected	Bead Size (μm)	Initial Saturation	Shear Rate (s^{-1})
24	4	95	500	DI Water	750

Figure 4.11 Experimental conditions and effluent from Beadpack Experiment 9.   Only the constituent phases from the broken emulsion were produced for the first 11 pore volumes (leftmost sample) but stable emulsion was produced for the remainder of the experiment.

Beadpack Experiment 10					
Average Emulsion Droplet Diameter (µm)	Flow Rate (mL/min)	Emulsion Pore Volumes Injected	Bead Size (µm)	Initial Saturation	Shear Rate (s⁻¹)
24	4	96	180	DI Water	2,083

Figure 4.12 Experimental conditions and effluent from Beadpack Experiment 10. Only the constituent phases from the broken emulsion were produced for the first 9 pore volumes but stable emulsion along with small volumes of oil and aqueous phases from coalesced emulsion was produced for the remainder of the experiment

4.3.1.4 Effect of initial saturation on emulsion stability

To this point all of the experiments performed in the beadpack had an initial saturation of DI water. The initial saturation of the beadpack was changed to mineral oil to see if it would affect the stability of the emulsion in the beadpack. The conditions for the Beadpack Experiment 11 were the same as Beadpack Experiment 8 except the initial saturation was changed to mineral oil. Recall that in Beadpack Experiment 8 the beadpack was saturated with DI water and stable emulsion was produced in the effluent after 13 pore volumes of emulsion were injected. When the initial saturation of the beadpack was changed from DI water to mineral oil it caused the emulsion to coalesce

76

for the entire 93 pore volumes injected.   Evidently the process of displacing the initially resident fluid in the beadpack influences rate of evolution from the droplets-coalescing constant state to the droplets-appear-in-effluent constant state that was observed in Beadpack Experiments 4, 6, 7, 8, 9, and 10.   The phase ratio of oil to aqueous phase in the tubes was the same as the phase ratio of the injected emulsion which was similar to the effluent in the other experiments where the emulsion completely coalesced (Beadpack Experiments 1, 2, 3, and 5).

Beadpack Experiment 11					
Average Emulsion Droplet Diameter (μm)	Flow Rate (mL/min)	Emulsion Pore Volumes Injected	Bead Size (μm)	Initial Saturation	Shear Rate (s^{-1})
24	0.5	93	180	Mineral Oil	260

Figure 4.13 Experimental conditions and effluent from Beadpack Experiment 11.   Only the constituent phases from the broken emulsion were produced for the entire duration of the experiment.

4.3.2 Emulsion Injection Experiments with Pressure Data

To provide more insight into the mechanisms governing the behavior of Beadpack Experiments 1-11 the pressure drop was recorded for Beadpack Experiments 12-25. To

enable comparison between experiments the apparent viscosity was calculated from the pressure data using the equation in Section 4.2.4. Relative permeability caused by multiphase flow is thus lumped into the calculation of apparent viscosity. The pressure drop and apparent viscosity are plotted on the same graph for each experiment in this section. In some of the experiments not all of the effluent is shown because the amount of emulsion in the test tubes was constant as injection continued.

4.3.2.1 Pressure response during emulsion injection

Beadpack Experiments 1-11 all exhibited an initial period of duration about 10 PV during which the injected emulsion would coalesce and only two separate phases would elute from the beadpack. Stable emulsion was only present in the effluent after some amount of emulsion coalesced in the beginning of each experiment. The duration of the coalescence varied experiment by experiment but it was always greater than one pore volume. In almost all of the experiments, some coalescence continued within the beadpack even after stable emulsion was produced, because measurable volumes of separate oil and aqueous phases were also present in the effluent. The experiments presented in this section, Beadpack Experiments 12-16, exhibit an injection pressure build up phase that corresponds to the duration of producing only coalesced phases from the beadpack. After this buildup phase the injection pressure in the beadpack reaches what is called the dynamic pressure equilibrium. In this dynamic pressure equilibrium period the injection pressure fluctuates as stable emulsion often accompanied by the constituent phases are produced from the beadpack.

In Beadpack Experiment 12, Figure 4.14, emulsion was injected into a mineral oil saturated beadpack. The droplet diameter of the emulsion was 24 microns and it was

78

injected through 500 micron beads at a flow rate of 0.5 mL/min.   This experiment is similar to Beadpack Experiment 7 only the initial saturation of the emulsion was changed to from DI water to mineral oil.   In Beadpack Experiment 7 stable emulsion was produced in the effluent after 8 pore volumes of emulsion were injected.

Beadpack Experiment 12				
Average Emulsion Droplet Diameter (μm)	**Flow Rate (mL/min)**	**Bead Size (μm)**	**Initial Saturation**	**Shear Rate (s⁻¹)**
24	0.5	500	Mineral Oil	94
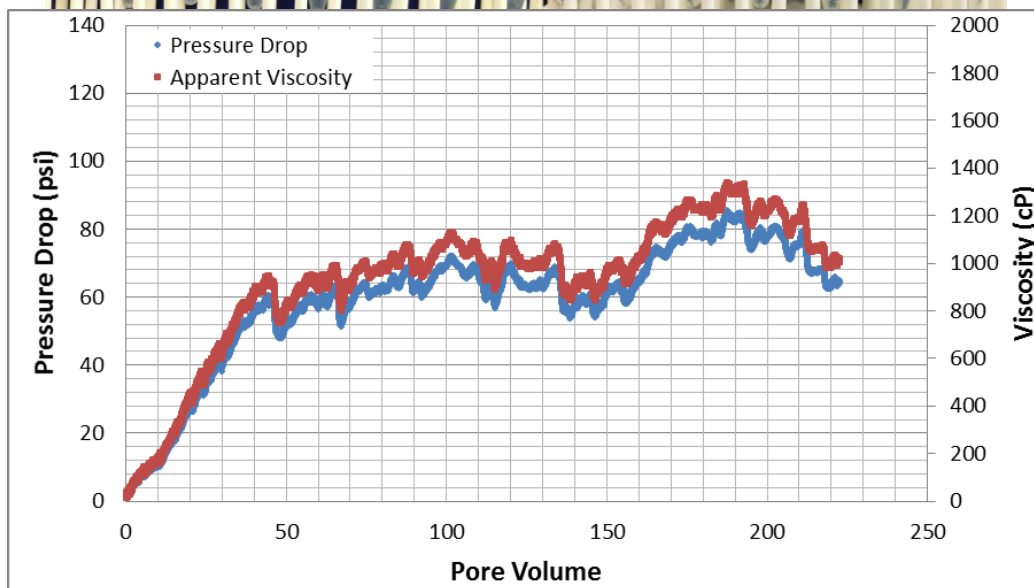
Figure 4.14 Experimental conditions, pressure data, and effluent from Beadpack Experiment 12. Each sample tube holds approximately 12 PV of effluent. Only the constituent phases from the broken emulsion were produced for the first 40 pore volumes, but stable emulsion was produced along with some free oil and aqueous phases for the remainder of the experiment.

In Beadpack Experiment 12 the pressure steadily builds across the beadpack for the first 40 pore volumes of injection. During this time the effluent consisted only of the two phases resulting from coalesced emulsion. At approximately 40 pore volumes

the pressure drop reached the dynamic equilibrium.   As the emulsion injection continued, the pressure began to fluctuate and the amount of emulsion in the effluent increased but eventually stabilized. The initial saturation of mineral oil appeared to have a significant effect on emulsion stability when comparing the effluent of Beadpack Experiment 7 and 12.   The viscosity of the injected emulsion from the rheometer at 94 s^{-1} (the shear rate in the beadpack) is approximately 353 cP.   The apparent viscosity in the beadpack is approximately 1100 cP.   The difference between the apparent viscosity in the beadpack and the rheometer viscosity will be discussed in further detail later in the Chapter.

The same type of pressure response is shown in Beadpack Experiment 13.   In Beadpack Experiment 13 emulsion with an average droplet diameter of 24 microns was injected through 500 micron beads that were initially saturated with DI water. This experiment was a replication of Beadpack Experiment 7, where stable emulsion was produced in the beadpack along with some free oil and aqueous phases after 8 pore volumes of emulsion were injected.   The initial pressure buildup period lasted for approximately 50 pore volumes. It is possible that the coalescence/regeneration front traveled more slowly in Beadpack Experiment 13 compared to Beadpack Experiment 7 due to local variations, causing the late time arrival of emulsion in Beadpack Experiment 13. Some stable emulsion was produced in the effluent during this period but majority of the emulsion coalesced.   After 50 pore volumes of injection the pressure reached the dynamic pressure equilibrium and began to fluctuate.   During this period of injection

there was an increase in the amount of stable emulsion present in the effluent compared to the pressure buildup stage and the amount of stable emulsion in the effluent stabilized. Approximately 100 pore volumes of effluent are shown in the image. The rest of the effluent, not shown, was indistinguishable from the last four tubes in the image. In tubes 5 and 8 in Figure 4.15, emulsion and aqueous phase are present but a very small amount (no oil in some effluent tubes) of oil phase was present. This indicates that some of the aqueous nanoparticle dispersion may have drained from the produced emulsion but the oil droplets remained intact. The apparent viscosity in the beadpack was approximately 1700 cP. The emulsion viscosity from the rheometer at 94 s^{-1} (the shear rate in the beadpack) was approximately 353 cP. The difference between the apparent viscosity in the beadpack and the rheometer viscosity will be discussed in further detail later in the Chapter.

Beadpack Experiment 13				
Average Emulsion Droplet Diameter (μm)	Flow Rate (mL/min)	Bead Size (μm)	Initial Saturation	Shear Rate (s⁻¹)
24	0.5	500	DI Water	94

Figure 4.15 Experimental conditions, pressure data, and effluent from Beadpack Experiment 13. Each sample tube holds approximately 12 PV of effluent. Only the constituent phases from the broken emulsion were produced for the first 13 PV, but stable emulsion was produced along with some free oil and aqueous phases for the remainder of the experiment. Very little to no free oil was observed in the last four effluent tubes. It took approximately 50 PV before a constant state of emulsion elution was reached in the beadpack.

Beadpack Experiment 13 was repeated in Beadpack Experiment 14. In Beadpack Experiment 13 it took approximately 50 PV before the beadpack reached a constant state. In Beadpack Experiment 14 the injection pressure buildup period was approximately 10 pore volumes before reaching a constant state. This was quite similar to Beadpack Experiment 7, indicating that the coalescence/regeneration front was moving at similar speeds. During the injection pressure buildup period the effluent consisted only of coalesced emulsion, i.e. the oil and aqueous phases. Stable emulsion was only present in the effluent after the dynamic equilibrium injection pressure was reached. The apparent viscosity in the beadpack was approximately 2000 cP. The emulsion viscosity measured by the rheometer at 94 s^{-1} (the shear rate in the beadpack) was approximately 353 cP. This indicates that the coalescence of droplets is a high resistance to flow process and contributes to the overall pressure drop along with the apparent viscosity of the regenerated emulsion as it flows through the beadpack. In Beadpack Experiments 12, 13 and 14 the pressure response supports the interpretation of the effluent phases as a moving front that separates constant states in the beadpack. One constant state is associated with emulsion coalescence, no emulsion droplets exiting the beadpack, while the second constant state is associated with an approximately constant and large pressure gradient, some emulsion droplets exit the beadpack but coalescence still occurs. The speed of the front appears to be correlated to the injected emulsion droplet size as the constituent phases of the emulsion were produced for a longer duration for larger droplets than smaller droplets, which regenerated more quickly. The speed of the advancing front, as shown in previous and subsequent experiments, appears to be dependent on bead

size.   The advancing front moves faster through larger beads and slower through smaller beads.

Beadpack Experiment 14				
Average Emulsion Droplet Diameter (μm)	Flow Rate (mL/min)	Bead Size (μm)	Initial Saturation	Shear Rate (s⁻¹)
24	0.5	500	DI Water	94
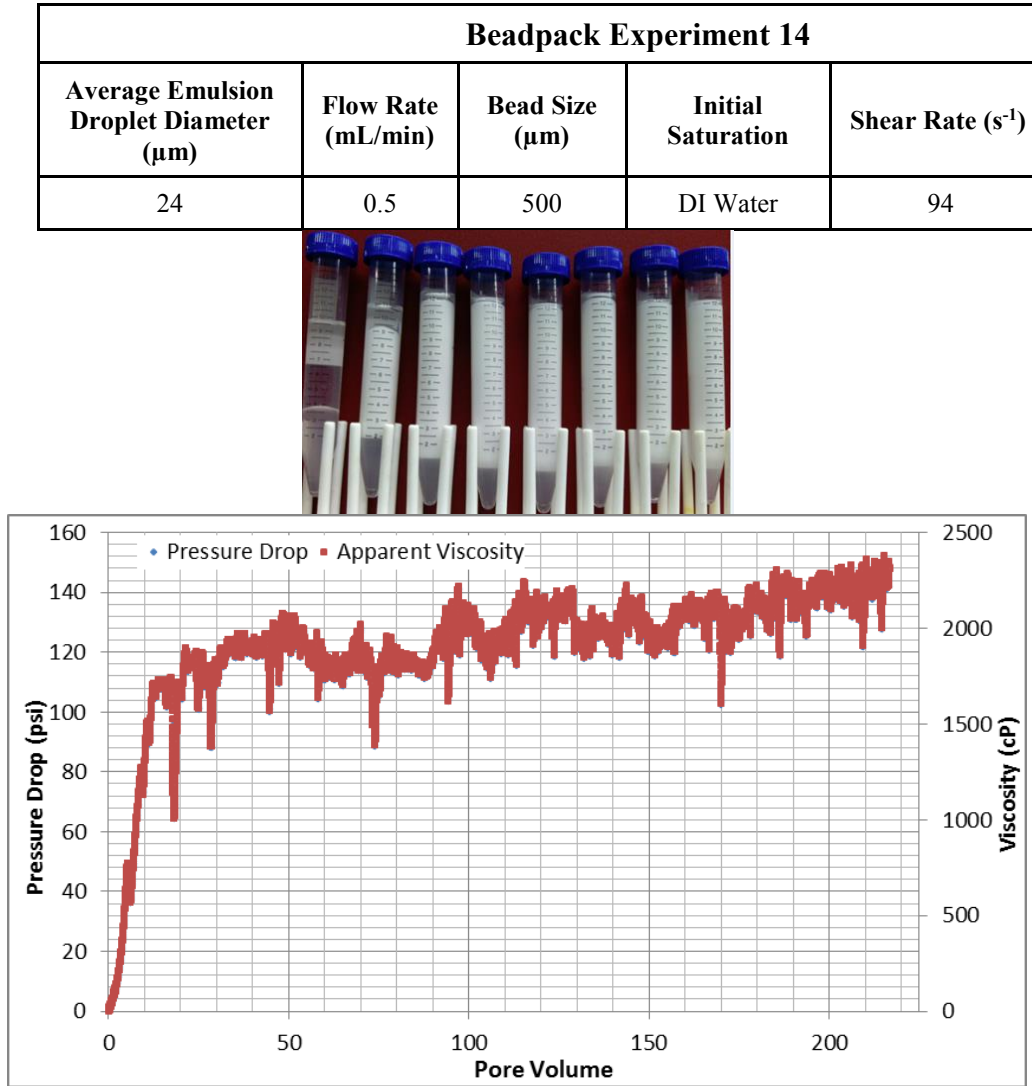
Figure 4.16 Experimental conditions, pressure data, and effluent from Beadpack Experiment 14.   Only the constituent phases from the broken emulsion were produced for the first 10 pore volumes, but stable emulsion along with small volumes of oil and aqueous phases from coalesced emulsion was produced for the remainder of the experiment. Each sample tube holds approximately 14 PV of effluent.

One interpretation of Beadpack Experiment 12, 13, and 14 is that stable emulsion exists and is flowing throughout the beadpack. The apparent viscosity of the emulsion was calculated from the pressure data using the equation in Section 4.2.4.   In this situation, the apparent viscosity can be compared with the viscosity of emulsions measured in the rheometer at the same shear rate.   The average apparent viscosity after the initial pressure buildup period was used for this comparison.   Figure 4.17 show the bulk viscosity of the injected emulsion versus the apparent emulsion viscosity for Beadpack Experiments 12, 13 and 14.   The apparent viscosity in the beadpack was significantly higher than the bulk emulsion viscosity.   The mesh end caps, used to hold the beads in the beadpack, most likely caused the increase in apparent viscosity of the emulsion.   The mesh had a sieve size of 50 microns and required additional pressure for the emulsion droplets to pass through increasing the total pressure drop.   This pressure drop was used to calculate the apparent viscosity although it was not the actual pressure drop from the emulsion flowing through the beadpack.
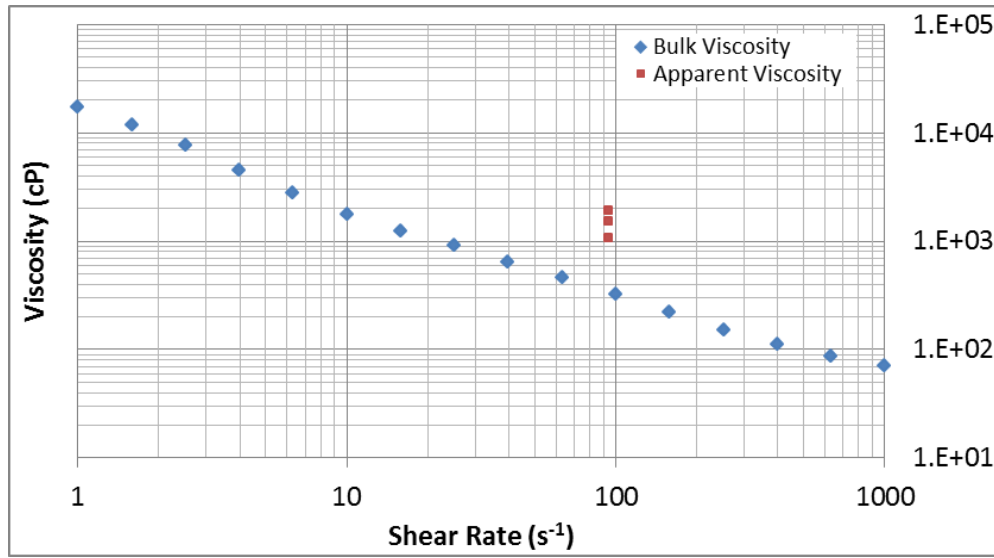
Figure 4.17 The bulk viscosity of the injected emulsion compared to the apparent viscosity of the emulsion flowing through the beadpack for Experiments 12, 13 and 14 after reaching the dynamic pressure equilibrium state.

Beadpack Experiment 15 was a replication of Beadpack Experiments 2 and 3. An emulsion with an average droplet diameter of 24 microns was injected through 52 micron beads.   The ratio of droplet diameter to pore throat size was approximately 1.4. As shown in Figure 4.18 the emulsion coalesced for the entire duration of the experiment except for the very last tube where there was a thin film of emulsion present.   In Beadpack Experiment 2 and 3 the emulsion coalesced for the duration of injection (37 and 32 PV). The pressure drop steadily increased for the entire duration of the experiment.   Emulsion injection was stopped early because the injection pressure was reaching the limit of the experimental set-up (2000 psi).   The small permeability (due to the small bead size) presumably caused the large pressure drop because the apparent

87

viscosity in the beadpack was not that large by the end of the experiment (300 cP). The advance of the transition between the emulsion coalescing constant state and emulsion elution constant state was much slower in the smaller permeability beadpack compared to Beadpack Experiments 12, 13, and 14. In those experiments larger beads (180 and 500 microns) were used and the transition between the two constant states arrived much sooner than in Beadpack Experiment 15 (52 microns). In Beadpack Experiment 2 and 3, only the constituent phases were produced which indicates a similar slow advance compared to Beadpack Experiment 15. This shows that bead size affects the speed of the transition between emulsion coalescence and emulsion elution from the beadpack. The transition arrives much slower, at least 70 PV, in smaller beads compared to larger beads where the transition arrived at approximately 10 PV.

Beadpack Experiment 15				
Average Emulsion Droplet Diameter (µm)	Flow Rate (mL/min)	Bead Size (µm)	Initial Saturation	Shear Rate (s⁻¹)
24	0.5	52	DI Water	901
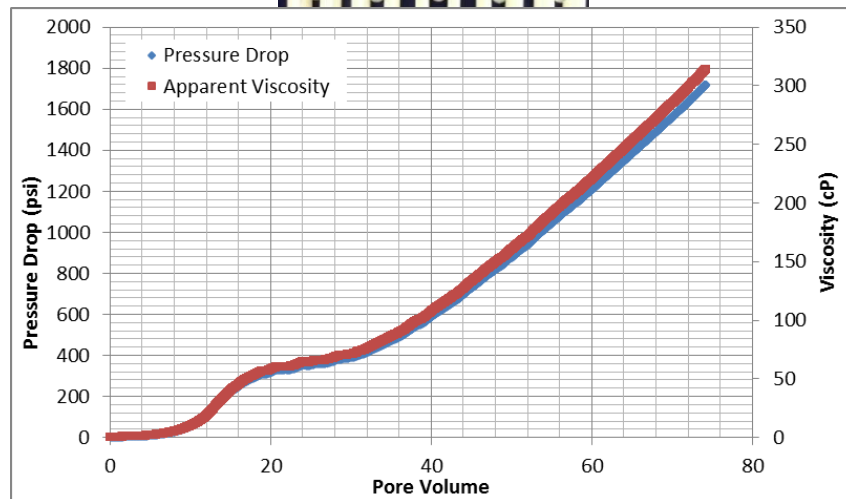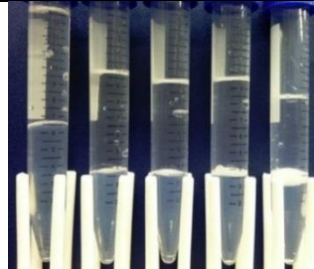
Figure 4.18 Experimental conditions, pressure data, and effluent from Beadpack Experiment 15. Only the constituent phases from the broken emulsion were produced for the duration of the experiment except for a very thin film of emulsion in the last test tube. Each sample tube holds approximately 12 PV of effluent.

In Beadpack Experiment 16 emulsion was injected at a higher flow rate (2 mL/min) through 180 micron beads. The initial saturation in the beadpack was DI water. The average emulsion droplet diameter was approximately 24 microns.

Approximately 20 pore volumes of emulsion were injected before the pressure reached the dynamic equilibrium pressure at which point stable emulsion was produced in the effluent. A picture of the effluent is not shown. As emulsion injection continued the pressure fluctuations in the beadpack became more ordered and regular. The first graph in Figure 4.17 shows the pressure drop for the entire experiment. The second graph is a closer view between 250 and 370 pore volumes, where the pressure drop became very periodic and regular. The apparent viscosity was on average approximately 200 cP. The viscosity of the emulsion from the rheometer at the same shear rate was approximately 47 cP. The difference between the apparent viscosity and the beadpack was not nearly as large as it was in Beadpack Experiments 12-14 where emulsion was injected through 500 micron beads. In those experiments the difference between the apparent viscosity in the beadpack and the emulsion viscosity from the rheometer at the same shear rate was on average 1250 cP. In Beadpack Experiment 16 the difference was only 153 cP. The reason the apparent viscosity is closer to the rheometer viscosity in the 180 micron beads is from the increase in pressure drop from the reduction in permeability. Because the 180 micron beadpack is less permeable than the 500 micron beadpack, a larger pressure drop is recorded as the result of the emulsion injection in the 180 micron beadpack. The increase in pressure drop minimizes the pressure drop contribution from the mesh end caps. This is why the apparent viscosity more closely matches the rheometer viscosity in the 180 micron beadpack.

This was the first time a very regular, periodic pressure profile was observed in the effluent. The hypothesis was that the mesh end caps were the cause of this behavior. The proposed mechanism was that the large droplets were continuously trapped in the

mesh screens that were placed at the exit and entrance of the beadpack.   As more and more droplets were trapped, the pressure continued to build while the smaller droplets drained through the mesh.   At some critical pressure the larger droplets were forced to deform and flow through the mesh.   This process was then repeated over and over causing the very regular periodic pressure profile.   The next section investigated whether or not the mesh was the cause of the regular periodic pressure profile.

Beadpack Experiment 16				
Average Emulsion Droplet Diameter (μm)	Flow Rate (mL/min)	Bead Size (μm)	Initial Saturation	Shear Rate (s⁻¹)
24	2	180	DI Water	1,042
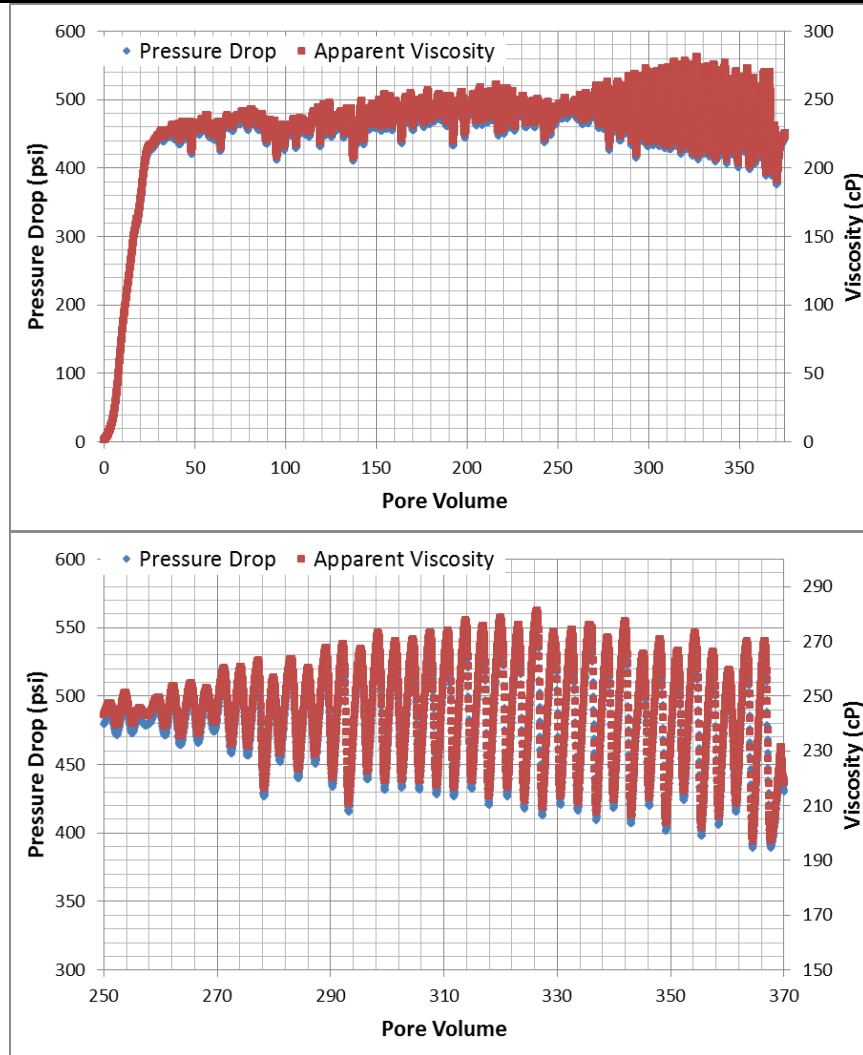
Figure 4.19 Experimental conditions and pressure data from Beadpack Experiment 16. Only the constituent phases from the broken emulsion were produced for the first 20 pore volumes then stable emulsion was produced in the effluent. The late time pressure response is periodic with an interval of about 3 PV from peak to peak.

4.3.2.2 Periodic pressure profile in larger beads

To test whether the mesh was the cause of the regular periodic profile, emulsion was injected through the beadpack with 1000 micron beads. 1000 micron beads were used because they were large enough to stay lodged in the beadpack without the mesh end caps. In Beadpack Experiment 17 and 18 an emulsion with an average droplet diameter of 24 microns was injected through 1000 micron beads with the mesh end pieces in the beadpack. In Beadpack Experiment 19 and 20 the same emulsion was injected into through 1000 micron beads except the mesh pieces were removed from the beadpack. All of the beadpacks were initially saturated with DI water and the emulsion was injected at the same flow rate for all the experiments. In all of the experiments the same regular, periodic pressure response was observed indicating that the mesh end pieces were not the cause of this pressure response.

Beadpack Experiment 17 (with mesh)				
Average Emulsion Droplet Diameter (μm)	Flow Rate (mL/min)	Bead Size (μm)	Initial Saturation	Shear Rate (s⁻¹)
24	0.5	1000	DI Water	47
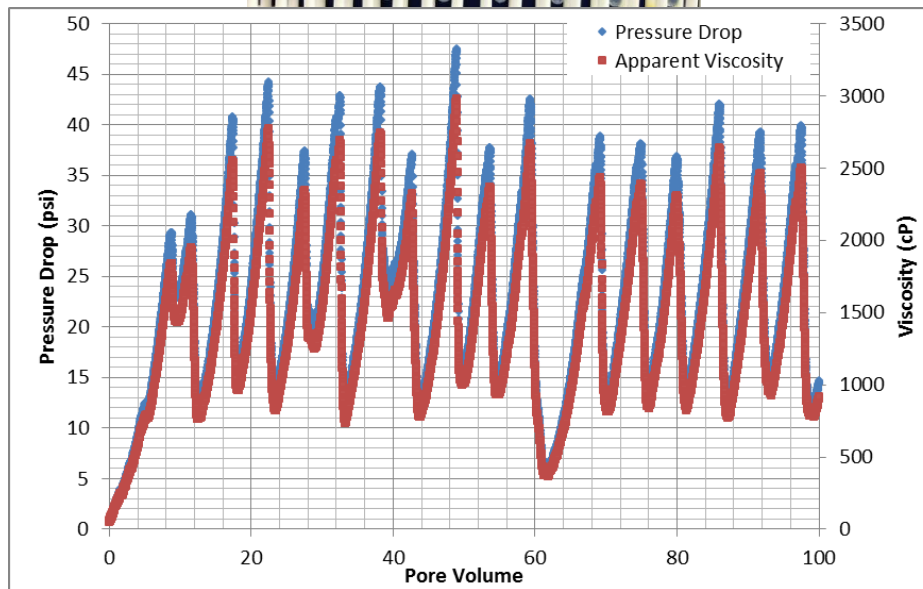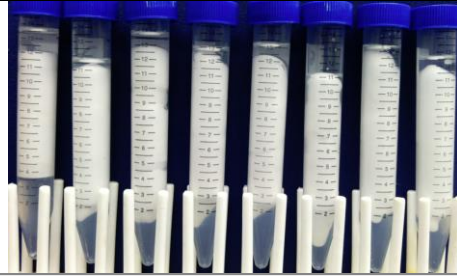
Figure 4.20 Experimental conditions, pressure data, and effluent from Beadpack Experiment 17. Each tube contains approximately 14 PV of effluent. Only the constituent phases from the broken emulsion were produced for the first 5 pore volumes but stable emulsion along with small volumes of coalesced emulsion was produced for the remainder of the experiment.

Beadpack Experiment 18 (with mesh)				
Average Emulsion Droplet Diameter (μm)	Flow Rate (mL/min)	Bead Size (μm)	Initial Saturation	Shear Rate (s⁻¹)
24	0.5	1000	DI water	47
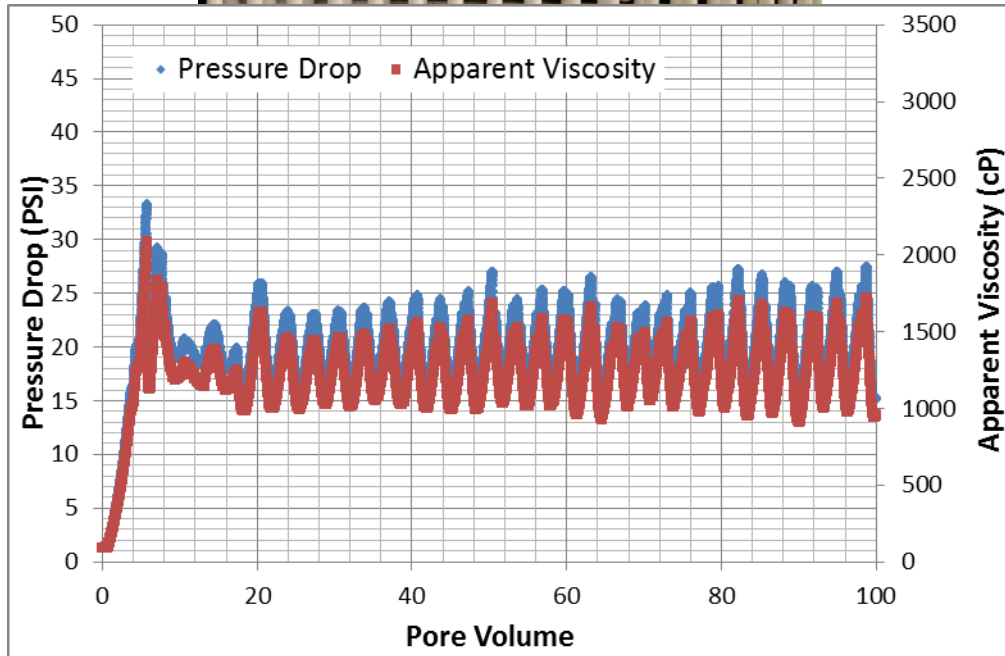
Figure 4.21 Experimental conditions, pressure data, and effluent from Beadpack Experiment 18. Each tube contains approximately 12 PV of effluent. Only the constituent phases from the broken emulsion were produced for the first 3 pore volumes but stable emulsion along with small volumes of coalesced emulsion was produced for the remainder of the experiment.

Beadpack Experiment 19 (without mesh)				
Average Emulsion Droplet Diameter (µm)	Flow Rate (mL/min)	Bead Size (µm)	Initial Saturation	Shear Rate (s^{-1})
24	0.5	1000	DI Water	47
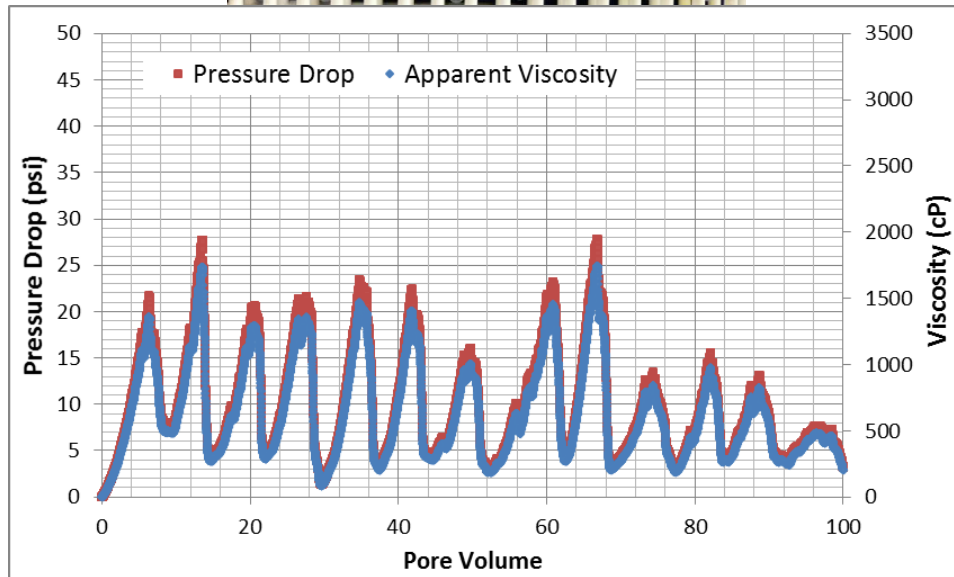
Figure 4.22 Experimental conditions, pressure data, and effluent from Beadpack Experiment 19. Each tube contains approximately 12 PV of effluent. Only the constituent phases from the broken emulsion were produced for the first 4 pore volumes but stable emulsion was produced along with significant volumes of coalesced emulsion for the remainder of the experiment.

Beadpack Experiment 20 (without mesh)				
Average Emulsion Droplet Diameter (μm)	Flow Rate (mL/min)	Bead Size (μm)	Initial Saturation	Shear Rate (s^{-1})
24	0.5	1000	DI Water	47
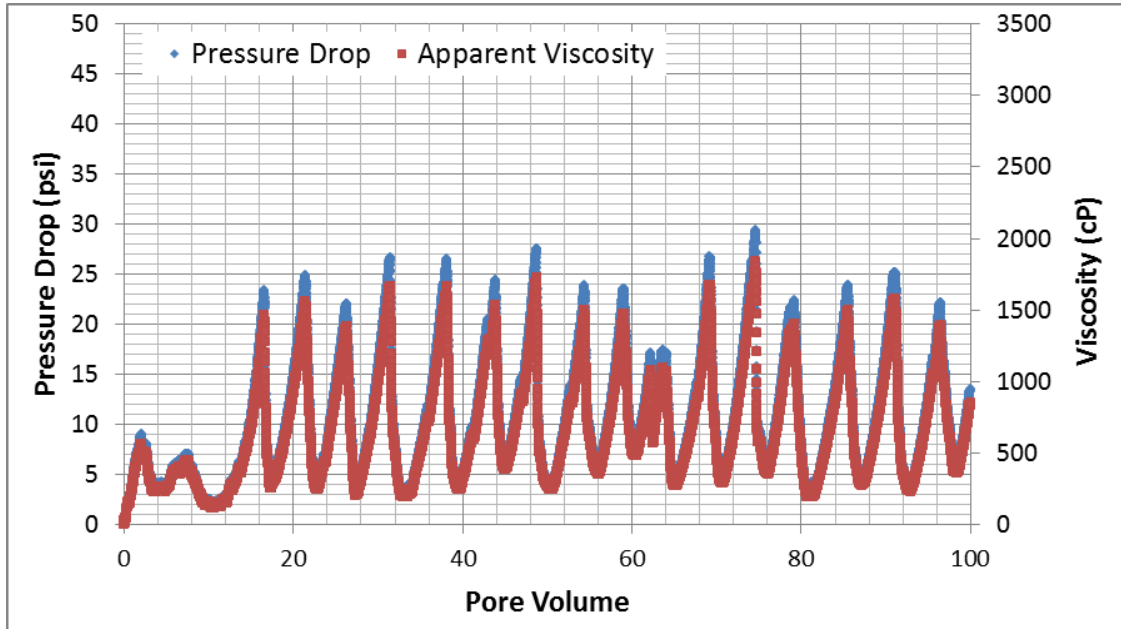
Figure 4.23 Experimental conditions, pressure data, and effluent from Beadpack Experiment 20. Only the constituent phases from the broken emulsion were produced for the first 2 pore volumes but stable emulsion was produced along with significant volumes of coalesced emulsion for the remainder of the experiment.

In Beadpack Experiments 17-20, with and without the mesh in the beadpack endcaps, the pressure response was oscillatory and extremely regular, indicating the periodicity arises from processes within the beadpack not the mesh. Emulsion was eluted from the beadpack within 5 pore volumes for each of these experiments. This indicates that if an emulsion coalescence/regeneration front is advancing through the

beadpack, it moves faster through larger beads. The emulsion viscosity from the rheometer at 47 s^{-1} (the shear rate in the beadpack) was approximately 632 cP. In the Beadpack Experiments 19 and 20 (without mesh) the rheometer viscosity falls within the range of apparent viscosities in the beadpack, however it is hard to compare the viscosities because of the oscillatory behavior. The apparent viscosity in Beadpack Experiments 17 and 18 was higher than in the experiments performed without mesh confirming the earlier hypothesis that the mesh end pieces were contributing to the increase in the emulsion apparent viscosity. This confirmed that the mesh contributed to the difference between the emulsion rheometer viscosity and apparent viscosity in the beadpack seen in Section 4.3.2.1. The amplitude of the periodic variation in pressure drop was much larger in the 1000 micron beads compared to the 180 micron beads (Beadpack Experiment 16). In Beadpack Experiments 17-20 the pressure drop stops increasing at certain pressure value that is roughly constant on average. The pressure drop then began to decrease after reaching the maximum pressure value. The pressure drop stops decreasing at a certain pressure value that is roughly constant on average.

The periodicity of the pressure profile suggests that there are possibly two competing processes occurring in the beadpack. The other beadpack experiments all showed an initial buildup period that was associated with emulsion coalescing. The hypothesis is that some of the emulsion droplets are coalescing as they travel through the beadpack. During this period of coalescence the pressure builds up steadily. At a certain point the pressure begins to drop as newly generated shear thinning emulsion is generated. This process is repeated over and over as more emulsion is injected into the beadpack which causes the oscillatory behavior. It is possible the gap-dominated flow

98

in the 1,000 micron beadpack contributed to the oscillatory behavior. This is why it was not observed in the other experiments, with smaller beads, except in the late time of Beadpack Experiment 16.

4.3.2.3 Slipping effect with PEG coated beads

It is possible that the interaction between the emulsion droplets and bead surfaces was contributing to the periodic pressure behavior in the beadpack. To gain further insight on the interactions between the emulsion droplets and the bead surfaces polyethylene glycol was used to initially saturate the beadpack. The hypothesis was that the PEG molecules would coat the individual bead surfaces and allow the emulsion droplets to slip past the beads lowering the pressure drop across the beadpack, possibly leading to less emulsion coalescence. The PEG solution discussed in section 4.1.1 was used to initially saturate the beadpack. Over 100 pore volumes of the PEG solution were injected into the beadpack to ensure the beads were sufficiently coated. One experiment was performed where emulsion was injected through 500 micron beads after PEG injection.

In Beadpack Experiment 21, Figure 4.24, majority of the emulsion coalesced however a very small amount remained stable. This behavior is qualitatively similar to many of the other experiments, and it is therefore of interest to consider whether a single theory could explain this entire class of experiments. Similar to other emulsion injection experiments, the pressure drop was large suggesting there was viscous emulsion flowing inside the beadpack. If the emulsion immediately broke upon entering the beadpack and emulsion was never regenerated inside the beadpack then the pressure data should be

99

similar to mineral oil and brine flowing through the beadpack at the same phase ratio in the absence of nanoparticles, i.e. steady two-phase flow, with pressure response dictated by relative permeability curves and phase viscosities. When brine and mineral oil were co-injected at the same phase ratio and flow rate as the emulsion was the steady state pressure drop was approximately 6 psi. In Beadpack Experiment 21, the pressure drop across the beadpack was much higher than 6 psi although very little stable emulsion was seen in the effluent. This suggests that when the emulsion was injected into the beadpack it coalesced and new emulsion was generated inside the beadpack but it was not stable enough to remain stable in the effluent.

\

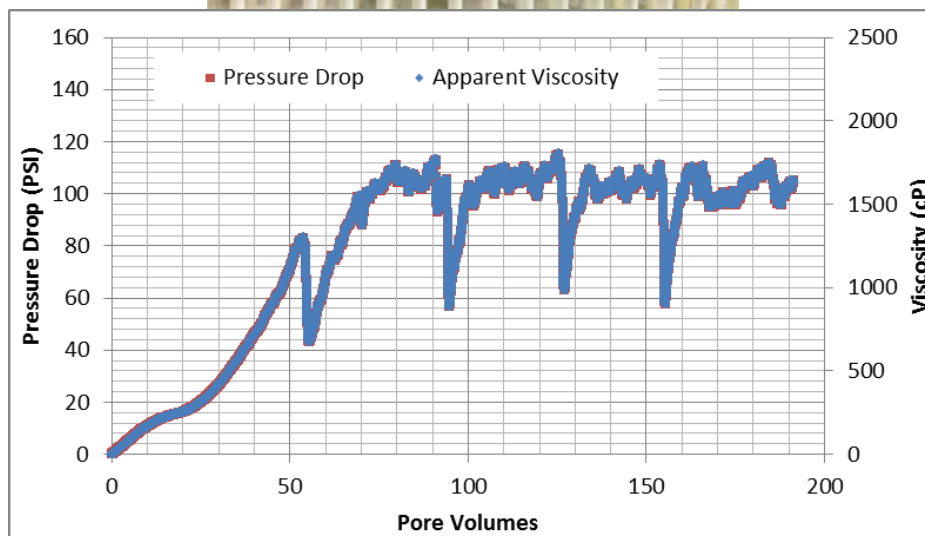| Beadpack Experiment 21				
Average Emulsion Droplet Diameter (µm)	Flow Rate (mL/min)	Bead Size (µm)	Initial Saturation	Shear Rate (s^{-1})
24	0.5	500	PEG solution	94
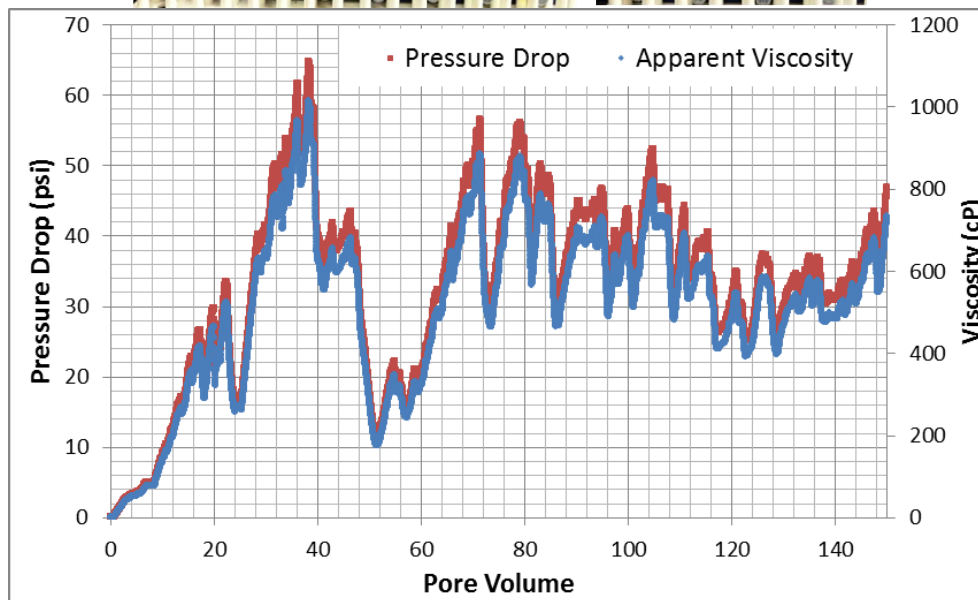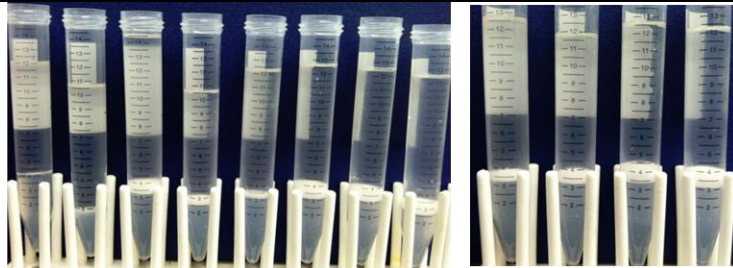
Figure 4.24 Experimental conditions, pressure data, and effluent from Beadpack Experiment 21. Each tube contains approximately 12 PV of effluent. Majority of the emulsion coalesced with constituent phases from the broken emulsion present in the effluent for the entire duration. A thin film of emulsion was present in some of the effluent tubes.

4.3.2.4 Emulsion injection into larger beadpack

All of experiments up to this point were performed in the HiP beadpack. Beadpack Experiments 22-25 were performed in a beadpack larger than the HiP beadpack (see section 4.1 for beadpack dimensions). The pore volume of the HiP beadpack was approximately 1 mL. The larger beadpack used in this section had a length of 30.5 cm, an internal diameter of 2.13 cm, and a pore volume of approximately 39 mL.

The large beadpack was initially filled with an unknown crude oil from a previous student's work. The beadpack was thoroughly rinsed and cleaned with soap and hot water. The beadpack was also rinsed with hexane to remove any remaining crude oil. The beadpack was filled with 500 micron beads and flushed with DI water. During the flush with DI water zero crude oil came out of the bead pack. In Beadpack Experiment 22 a 62 micron diameter emulsion was injected at 1 mL/min into the DI water saturated beadpack. The broken emulsion displaced some remaining crude oil from the beadpack that was left behind during the cleaning process as seen in Figure 4.24. Only the constituent phases from the broken emulsion were produced for the entire duration of the experiment. Because the phase initially saturating the beadpack influences the behavior of the emulsion (Beadpack Experiments 8, 11, 12, 13, and 14), the uncertain initial state of the beadpack in this experiment makes interpreting the results difficult.

In Beadpack Experiment 23 the beadpack was filled with 500 micron beads and was initially saturated with DI water. The 62 micron diameter emulsion was injected at 4 mL/min, four times larger than it was injected in Beadpack Experiment 22. The large pressure drop across the beadpack suggested that emulsion was flowing inside the

beadpack although very little stable emulsion was present in the effluent. The apparent viscosity inside the beadpack was approximately 8 times higher when injecting the emulsion at 4 mL/min compared to 1 mL/min even though the two effluents suggested that the emulsion coalesced. The proposed explanation for these observations is that in both cases the emulsion coalesced as it entered the beadpack. The two phases from the broken emulsion regenerated new emulsion at some distance downstream in the beadpack, and more emulsion was generated at the larger flow rate than in the smaller flow rate. But in both cases the emulsion that was regenerated in the beadpack was not stable enough to remain intact in the effluent.

Beadpack Experiment 22				
Average Emulsion Droplet Diameter (µm)	Flow Rate (mL/min)	Bead Size (µm)	Initial Saturation	Shear Rate (s⁻¹)
62	1	500	DI water and some crude oil	8
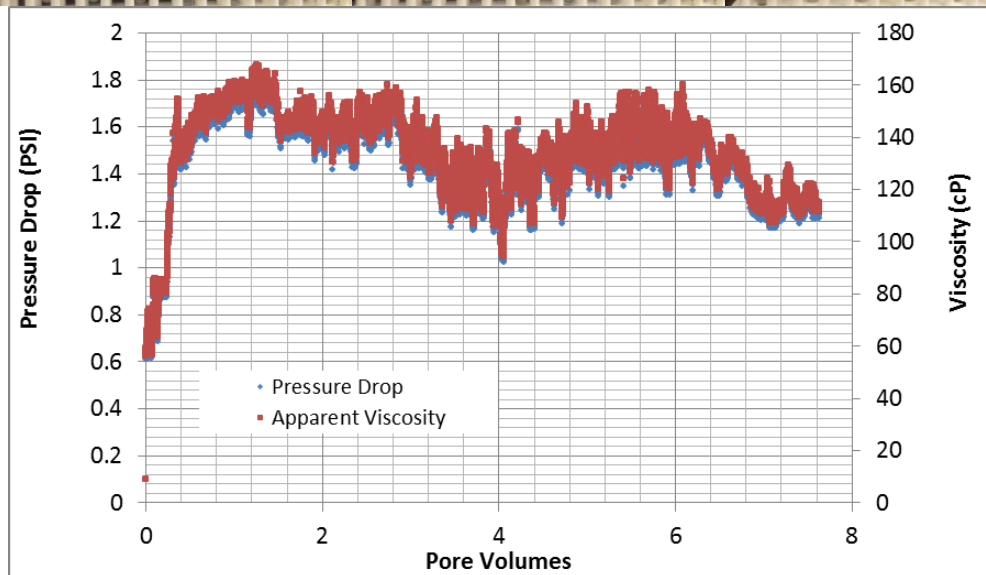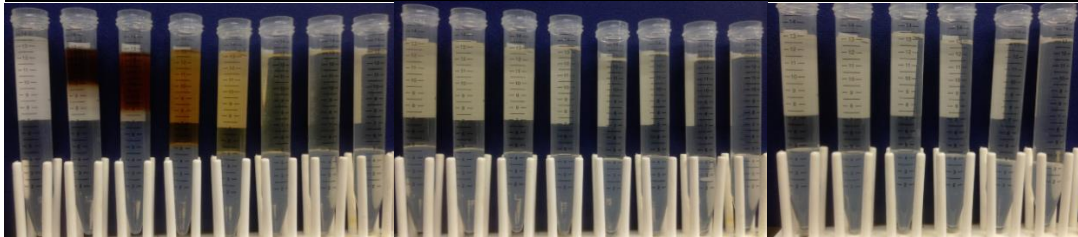
Figure 4.25 Effluent from Beadpack Experiment 22.   Each tube contains approximately 0.35 PV of effluent.   Only the constituent phases from the broken emulsion were produced for the duration of the experiment.

Beadpack Experiment 23				
Average Emulsion Droplet Diameter (µm)	**Flow Rate (mL/min)**	**Bead Size (µm)**	**Initial Saturation**	**Shear Rate (s⁻¹)**
62	4	500	DI Water	32
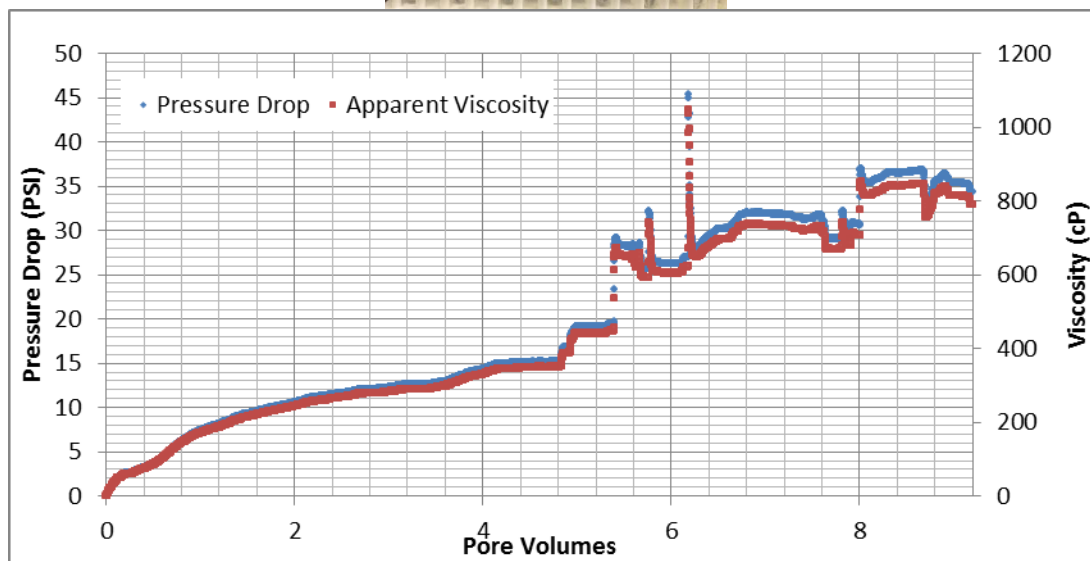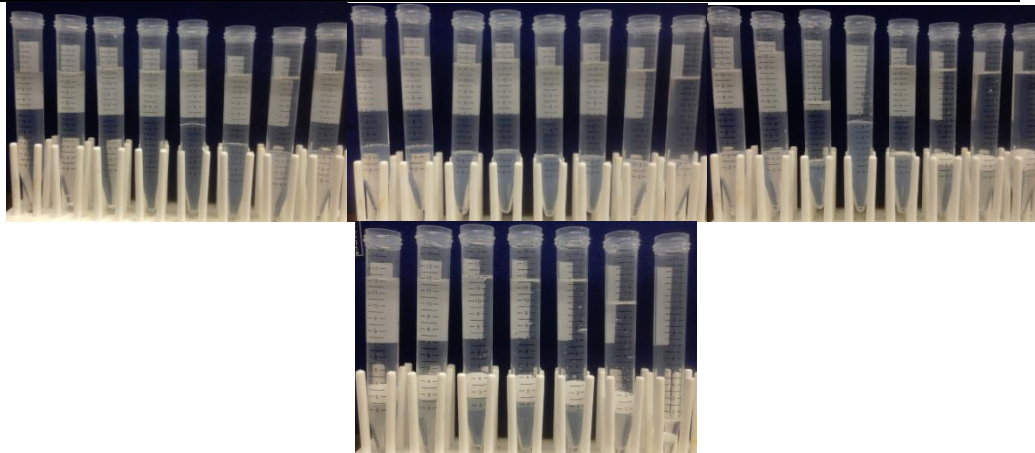
Figure 4.26 Effluent from Beadpack Experiment 23.   Each tube contains approximately 0.3 PV of effluent.   Only the constituent phases from the broken emulsion were produced for almost the entire duration of the experiment.   A small amount of stable emulsion was collected after approximately 7 pore volumes of emulsion were injected.

105

There was evidence from the earlier beadpack experiments, performed in the small HiP beadpack, that when emulsion was injected into an oil saturated beadpack the duration of the coalescence period was much longer compared to when emulsion was injected into a water saturated beadpack. The next two experiments were performed to see if this same effect would occur in a longer and wider beadpack. In Beadpack Experiment 24 emulsion was injected into the bead pack saturated with DI water. The beadpack was filled with 3,000 micron beads. This large bead size was used so that emulsion coalescence would conceivably be caused by contact with the resident fluid and not from droplets flowing through small pore throats. In Beadpack Experiments 17-20, with 1,000 micron beads, emulsion was eluted from the beadpack quickly, compared to experiments with smaller beads. This suggests that either less coalescence occurs or that the regenerated emulsion more easily flows through larger pores. In Beadpack Experiment 25 emulsion was injected into the mineral oil saturated beadpack. The mineral oil was dyed red to help distinguish it from the clear mineral oil in the emulsion. The same flow rate was used for both experiments.

Stable emulsion was produced in the effluent of the water saturated beadpack after approximately 1.5 pore volumes of emulsion were injected. In the mineral oil saturated case, stable emulsion was produced after 2.2 pore volumes of emulsion were injected. The mineral oil initially in the beadpack caused the emulsion to coalesce for a longer period of time than when the beadpack was saturated with DI water. This is consistent with the results in the HiP beadpack however the effect appeared to be much less drastic in the larger beadpack. The difference in apparent viscosity was most likely

106

due to the fact that the emulsions were generated in different batches and had a slightly different droplet size.

Beadpack Experiment 24				
Average Emulsion Droplet Diameter (µm)	Flow Rate (mL/min)	Bead Size (µm)	Initial Saturation	Shear Rate (s^{-1})
24	14	3000	DI water	535
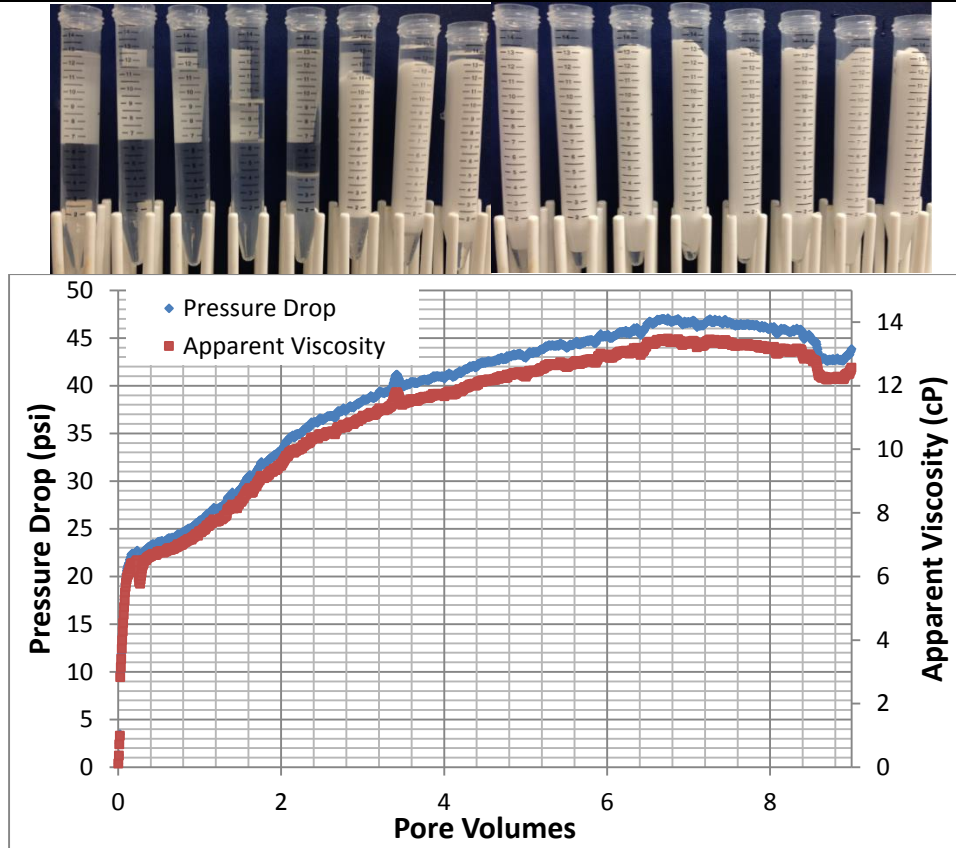
Figure 4.27 Effluent from Beadpack Experiment 24. The first five tubes (left) of effluent contain approximately a total of 1.5 PV of effluent. The other tubes (6-16) each contain approximatley 0.35 PV of effluent. Stable emulsion was present in the effluent after 1.5 pore volumes of emulsion were injected. No coalesced emulsion phases were produced after stable emulsion arrived in the effluent.

Beadpack Experiment 25				
Average Emulsion Droplet Diameter (μm)	Flow Rate (mL/min)	Bead Size (μm)	Initial Saturation	Shear Rate (s^{-1})
24	14	3000	Mineral Oil (Red Dye)	535
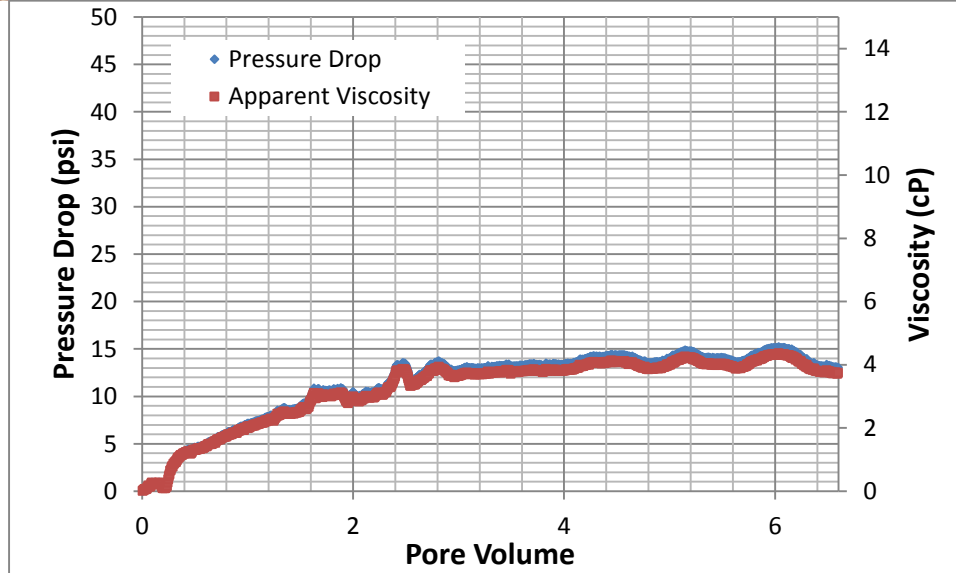
Figure 4.28 Effluent from Beadpack Experiment 25. Each sample contains approximately 0.35 PV of effluent. The red effluent is dyed mineral oil initially present in the effluent. Stable emulsion was present in the effluent after 2.2 pore volumes of emulsion were injected. No coalesced emulsion phases were produced after stable emulsion arrived in the effluent.

108

4.3.3 Mineral Oil-in-Water Emulsion Stability

The results from the beadpack experiments showed that the initial saturation of the beadpack caused significant changes in the transition time from producing only the constituent phases of the emulsion to emulsion elution. When the HiP beadpack was initially saturated with oil the duration of emulsion coalescence was on average approximately 66 PV compared to only approximately 10 PV for the DI water saturated beadpacks. The same effect was seen in the Beadpack Experiments 24 and 25 performed in the larger beadpack although it was much less drastic (only the constituent phases were produced for an additional 0.7 PV in the oil saturated beadpack compared to the water saturated beadpack). Batch experiments were performed to see if mineral oil had a similar effect on emulsion stability. Mineral oil-in-water emulsion was mixed in equal parts by volume with DI water and with mineral oil, each mixture in 20 mL disposable scintillation vials. The emulsion had an average droplet diameter of 24 microns. Three sets of each mixture were made. Two of the samples were sonified with a Branson Digital Sonifier for three minutes at a 25% amplitude. Two samples were vigorously shaken by hand for one minute. Two samples were left undisturbed. Figure 4.29 below shows the samples just after preparing the mixtures. The mineral oil was dyed red to help distinguish it from the emulsion.
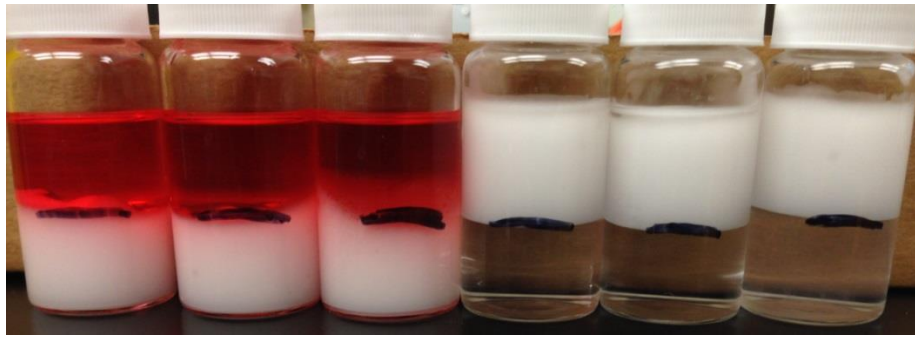
Figure 4.29 The batch experiment mixtures of emulsion, mineral oil, and DI water.   The first three on the left are the emulsion and mineral oil mixtures.   The first three from the right are the emulsion and DI water mixtures.   The black line shows the meniscus just after sample preparation.

The emulsion remained stable in the two samples that were left undisturbed. Putting mineral oil or DI water into contact with the emulsion did not cause any of the emulsion to coalesce.   Figure 4.30 shows the samples that were left undisturbed one day and one week after they were initially prepared.   The black indicates the position of the meniscus when the samples were initially prepared indicating that there was no change in the emulsion.
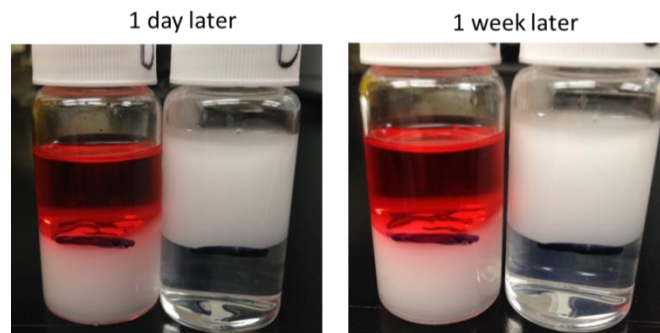
Figure 4.30 Photos of the emulsion/DI water mixture and the emulsion/mineral oil mixture day and 1 week later.   There was no change from when the samples were originally prepared.   The mineral oil was dyed red.

110

Two of the samples were shaken by hand for one minute each. Figure 4.31 shows the samples just after they were shaken, 1 day later, and 1 week later. Just after shaking the emulsion/DI water sample the mixture seemed to make a fairly uniform mixture while the emulsion/mineral oil sample appeared to be much less uniform. This behavior was expected because the emulsions are water external and not oil external. After one day the water/emulsion mixture completely separated back into separate phases. There was no additional emulsion produced because the meniscus returned to the same location as the original mixture. The mineral oil/emulsion mixture separated at a much slower rate because of the viscous nature of both the emulsion and mineral oil. The density difference that causes the emulsion and mineral oil to separate was not able to totally overcome the viscous forces of the emulsion, leaving some of the oil phase at the bottom of the vial. The emulsion is more attracted to the glass walls of the vial which gave the appearance that some of the red mineral oil was emulsified. After closer inspection of the vial, the walls had emulsion with the red mineral oil in a separate phase on the inner part of the vial. It was deemed that the mineral oil did not cause any of the emulsion to break because approximately the same amount of mineral oil was recovered from the vial when the contents were emptied and separated completely. This also proved that the excess mineral oil was not emulsified into the existing emulsion.
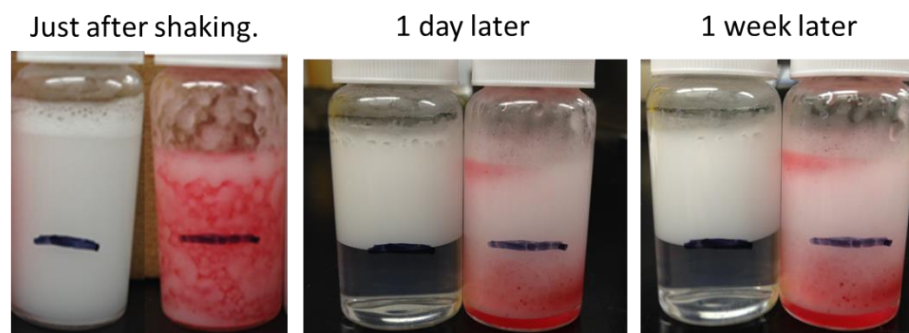
Figure 4.31 Photos of the emulsion/DI water and emulsion/mineral oil mixtures 1 day and 1 week after they were vigorously shaken by hand for one minute.

The other two mixtures were sonified with a Branson Digital Sonifier for approximately 3 minutes at 25% amplitude. The sonifier provides high frequency mechanical energy to a steel micro-tip which was centered at the meniscus of the samples. Figure 4.32 shows a photo of the sonified samples immediately after sonification, one day later, and one week later. During the sonification of the DI water/emulsion vial, a small amount of the DI water was emulsified. In Figure 4.32 there is emulsion below the original meniscus line indicating an increase in emulsion with sonification. Majority of the emulsion coalesced when the mineral oil/emulsion vial was sonified. In the Figure 4.32 there is a thin film of emulsion between the nanoparticle dispersion and mineral oil. Catastrophic phase inversion is believed to have caused the emulsion to break. Catastrophic phase inversion is when an oil-in-water emulsion changes to a water-in-oil emulsion and vice versa. Catastrophic phase inversion is induced by increasing the volume fraction of the dispersed phase and can cause drastic changes in the emulsion stability (Binks 1999). Binks et al. showed that catastrophic phase inversion occurs for both water-in-oil and oil-in-water emulsion

stabilized by silica particles for dispersed phase volume fractions around 0.7 (Binks 1999). Catastrophic phase inversion may have caused the generation of an unstable water-in-oil emulsion during sonification, majority of which coalesced.
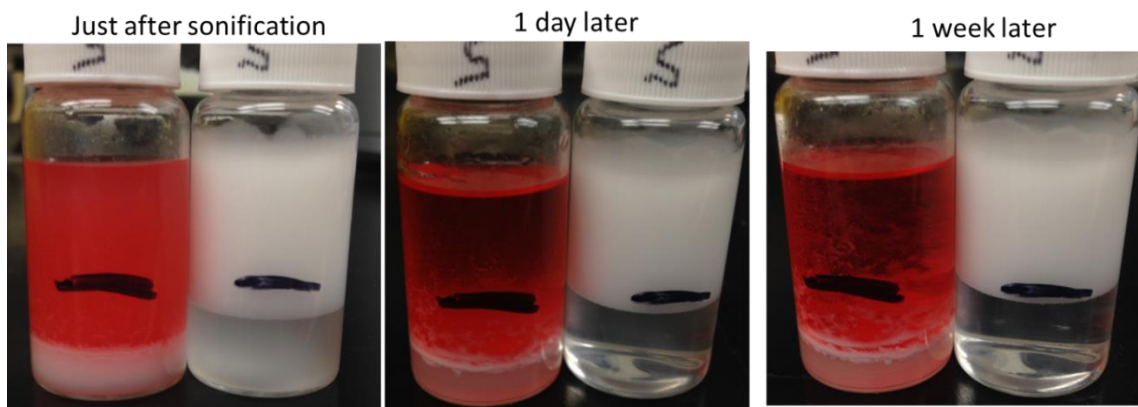
Figure 4.32 Photos of the emulsion/DI water and emulsion/mineral oil mixtures 1 day and 1 week after they were sonified for three minutes at 25% amplitude.

The observations from the batch experiments show that the presence of an excess oil phase can cause the emulsion to become unstable when enough mechanical energy is input into the sample. There was no mechanical energy input into the samples that were left undisturbed and as a result the emulsion remained stable in all three cases. A small amount of mechanical energy was input into the samples by shaking them by hand. The emulsion remained stable in these experiments too. When a large amount of energy was input into the samples via sonification, the emulsion became unstable for the oil/emulsion sample but remained stable for the water/emulsion sample. The hypothesis for the behavior in the beadpack is that as the emulsion is flowing through the beadpack it initially coalesces (pressure build up) and then transitions into a 2nd state where the emulsion begins to elute from the beadpack (pressure stabilization) . When the

113

beadpack is initially saturated with oil, the coalescence regime has a longer duration in terms of pore volumes because of a catastrophic phase inversion chain reaction. As the emulsion enters the beadpack it comes into contact with the oil. This causes the emulsion to coalesce at the front due to catastrophic phase inversion. The oil from the broken emulsion is no longer suspended in the aqueous phase which then acts like the oil initially present in the beadpack and causes the incoming emulsion to coalesce. This process is repeated over and over during the pressure build up, coalescence state. Then for some reason, still unknown, the emulsion transitions into the 2nd state where stable emulsion is eluted from the beadpack. This transition occurs later, in terms of pore volume of emulsion injected, in the oil saturated beadpack because of catastrophic phase inversion.

4.4 CONCLUSIONS

Two different emulsions were injected through beadpacks under various conditions. Both emulsions were generated by the co-injection procedure outlined in Chapter 3. One emulsion had an average droplet diameter of 24 microns while the other emulsion had an average droplet diameter of 62 microns. The bead size, flow rate, and initial saturation were varied in different experiments.

When greater than one, the average droplet diameter to pore throat ratio was sufficient enough to cause only the constituent phases of the emulsion to be produced in the effluent. Stable emulsion was not regenerated from the coalesced emulsion because they were injected below the critical shear rate. For experiments that meet these conditions, i.e. droplets larger than pore throats and injection rates smaller than the critical shear rate, emulsions were never produced. This implies either that the concept of

114

an advancing front does not apply in these experiments, or that the front exists but advances slowly, too slow to be observed in the duration of these experiments. The pressure drop steadily increased for the duration of these experiments which indicate that a front was in fact moving through the beadpack, however, the movement was so slow that the transition to the emulsion elution constant state was not observed. Conversely, stable emulsion was produced in the effluent when the average droplet diameter to pore throat ratio was decreased below one and emulsion was injected below the critical shear rate. Emulsion was produced in the effluent after a period during which only the constituent phases of the emulsion were produced in the effluent for some time. This was similar to the experiments previously discussed except there was an eventual transition to an emulsion elution constant state. For these experiments, the pressure would steadily increase when only the constituent phases of the emulsion were produced in the effluent. This behavior was consistent with the pressure drop and effluent in the experiments where emulsion was never produced. When emulsion was eluted from the beadpack, after the period of coalescence, the pressure gradient stopped increasing at a steady rate and began to fluctuate and relatively stabilize. Coalesced emulsion was also produced simultaneously with the stable emulsion. During this time of pressure fluctuation the amount of emulsion and constituent phases leaving the beadpack was constant. This is consistent with the movement of an emulsion coalescence/regeneration front through the beadpack. The front moved slower through smaller beads and faster through larger beads.

The initial period of coalescence was much longer, in terms of pore volumes, for the emulsion with an average droplet diameter of 62 microns than it was for the emulsion with an average droplet diameter of 24 microns. This indicated that emulsions with

115

larger droplets are more prone to coalescence when flowing through porous media than emulsions with smaller droplets. It also indicates speed of the front is a strong function of the injected droplet size.

The dynamic behavior in the beadpack was classified as a transition between two constant states with different pressure responses. In the first state all of the droplets are coalescing and the effluent consists of two separate phases; during this time the pressure in the beadpack is steadily building. Then the conditions in the beadpack transition into a 2nd state where emulsion droplets survive their passage in the beadpack or, alternatively, emulsion droplets are regenerated from the coalesced phases (this alternative suggests that critical shear rate for regeneration differs from critical shear rate for co-injection); during this time the pressure stabilizes but fluctuates as droplets pass through pores. The timing of this transition between emulsion coalescence and emulsion elution was highly dependent on the beadpack conditions. In some cases the emulsion coalesced for the entire emulsion injection. Figure 4.33 summarizes the transition time, from emulsion coalescence to emulsion elution, as a function of bead size and initial saturation in the experiments where the emulsion with an average droplet diameter of 24 microns was injected into the HiP beadpack. The amount of injected pore volumes is shown for experiments where stable emulsion never eluted from the beadpack (No Elution in Figure 4.33). The timing of transition from coalescence to emulsion elution, in terms of pore volumes injected, is plotted for experiments where stable emulsion was produced in the effluent (Elution in Figure 4.33).

Figure 4.34 summarizes the transition time, from emulsion coalescence to emulsion elution, as a function of bead size and shear rate in the experiments where the

116

emulsion with an average droplet diameter of 24 microns was injected into the HiP beadpack. The same convention of emulsion elution and no elution in Figure 4.31 was used in Figure 4.34. Figure 4.34 does not take into account the initial saturation of the beadpack which affected emulsion stability.

Figure 4.35 is a summary, in terms of emulsion elution and coalescence, for all of the emulsion injections where the 24 micron diameter emulsion was injected into the HiP beadpack. It plots the bead size and shear rate of from each experiment. The data is broken down into two categories, emulsion elution and emulsion coalescence. The experiments plotted in the emulsion elution category were plotted if any emulsion was eluted from the beadpack at any point in time during the emulsion injection. The constituent phases from the broken emulsion were produced for the entire injection duration, for the experiments plotted in the coalescence group. Some of the experiments from the two categories overlap because this plot does not take into account the initial saturation of the beadpack, which was a factor in emulsion stability.

117
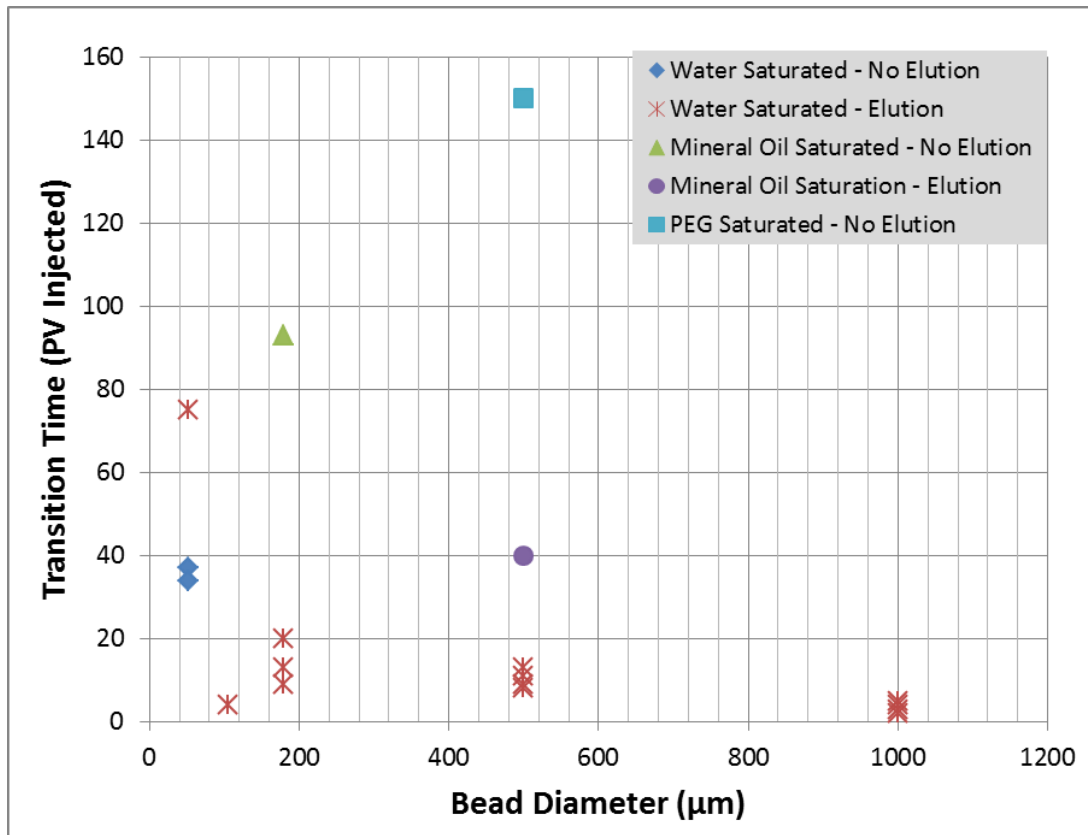
Figure 4.33 The transition time from emulsion coalescence to emulsion elution as a function of bead size and initial saturation. For the experiments where emulsion coalesced for the entire injection, the pore volumes of emulsion injected is plotted. The time of transition, in terms of PV, is shown for experiments when emulsion was present in the effluent. The data plotted are only for the experiments where the 24 micron emulsion was injected into the HiP beadpack, that is, the small rather than the large beadpack.

118
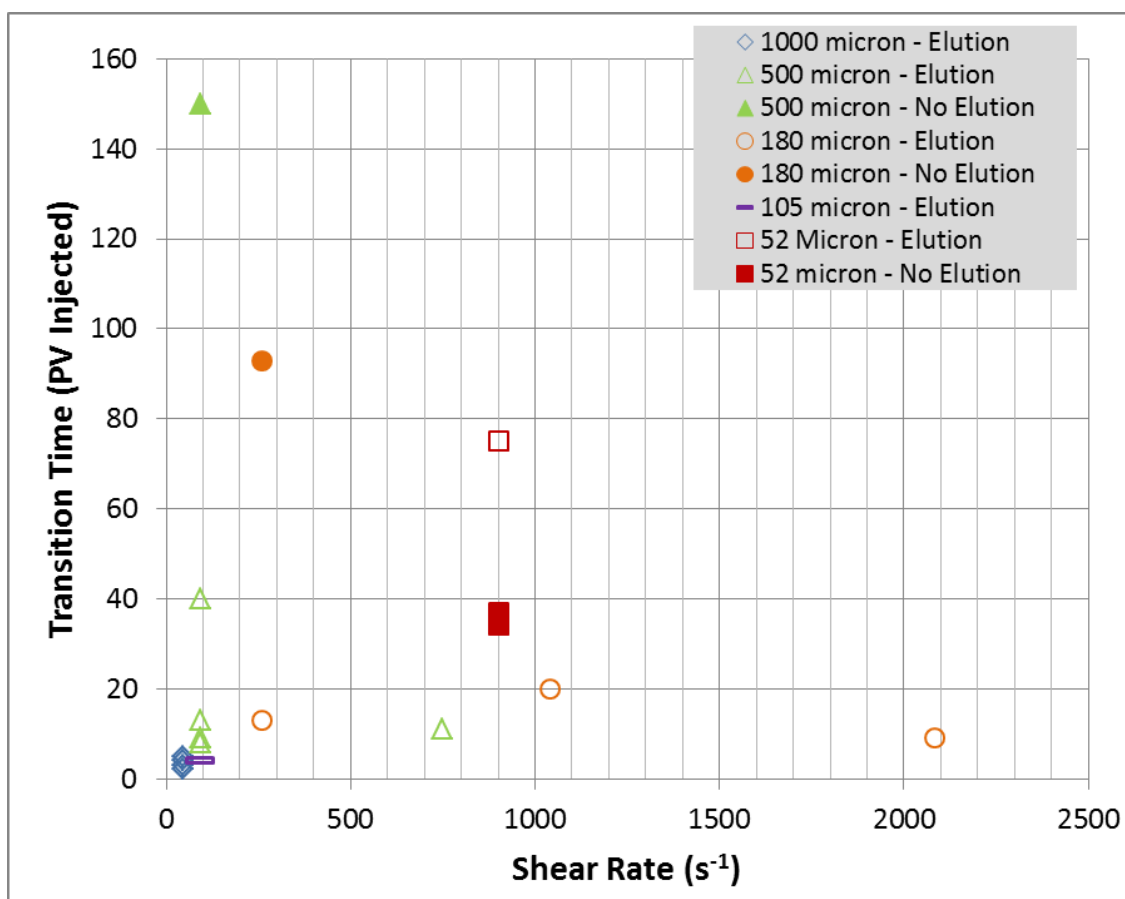
Figure 4.34 The transition time from emulsion coalescence to emulsion elution as a function of bead size and shear rate. For the experiments where emulsion coalesced for the entire injection, the pore volumes of emulsion injected is plotted. The time of transition, in terms of PV, is shown for experiments when emulsion was present in the effluent. This did not take into account initial saturation. The data plotted are only for the experiments where the 24 micron emulsion was injected into the HiP beadpack.

119
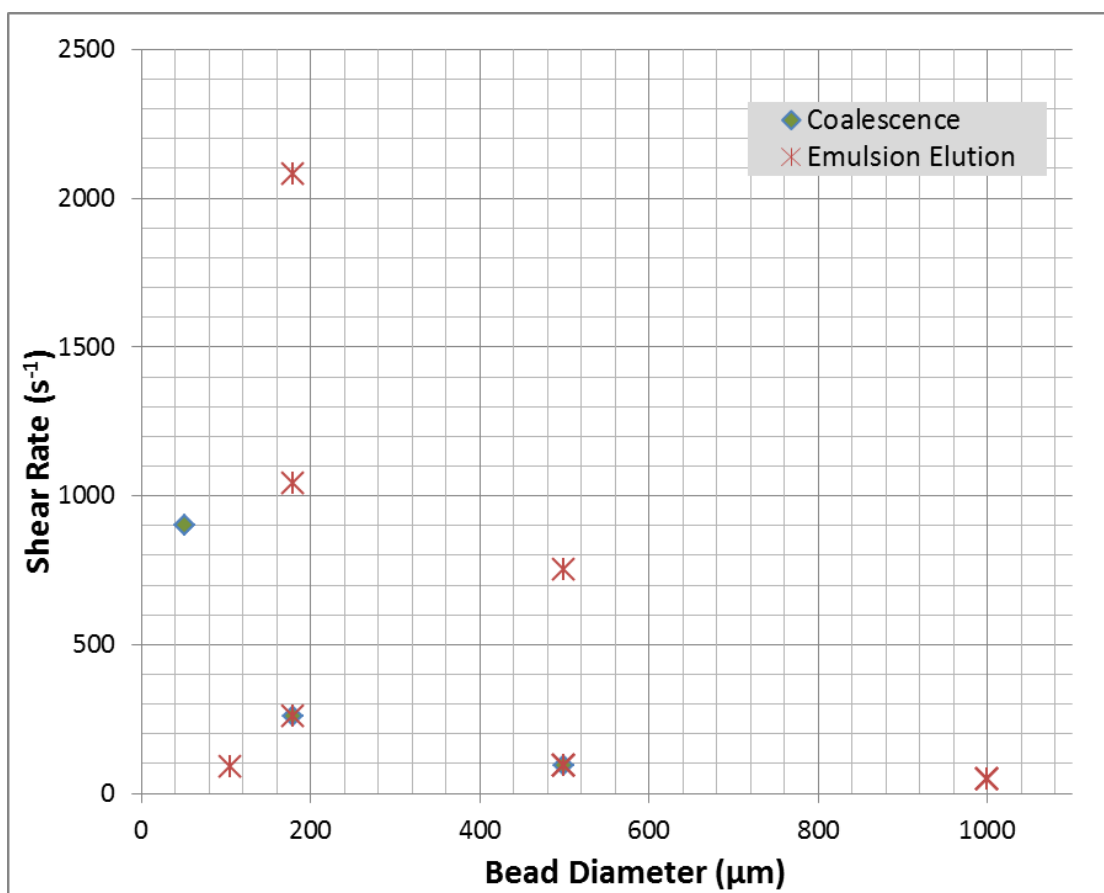
Figure 4.35 A summary of the emulsion injection experiments as a function of bead size and shear rate. Experiments are categorized into two groups, experiments where emulsion eluted from the beadpack and experiments for which the constituent phases from the broken emulsion were produced for the entire duration of injection. This did not take into account the initial saturation or when the emulsion elution occurred, in terms of PV's. The data plotted are only for the experiments where the 24 micron emulsion was injected into the HiP beadpack. Some experiments overlap so only one point is shown.

The initial saturation of the beadpack had a significant effect on emulsion stability. When emulsion was injected into a beadpack that was saturated with oil it would cause the only the constituent phases from the emulsion to be produced in the effluent for a significantly longer amount of time, in terms of pore volumes injected, than when it was injected at the same conditions into a beadpack that was saturated with water. The hypothesis for this behavior was a mechanism by which catastrophic phase inversion causes the emulsion to become unstable and the oil that is broken out of the emulsion causes the incoming emulsion to break, similar to a chain reaction. Evidence of this mechanism was shown in batch experiments where catastrophic phase inversion caused emulsion to break when a sample of emulsion and excess oil was sonified. When a mixture of emulsion and water was sonified the emulsion remained stable, indicating the excess oil was the cause of the emulsion coalescence and not just the sonification.

In almost all of the experiments some emulsion appeared to coalesce in the beadpack according to the effluent. Conversely, the pressure drop and apparent viscosity indicated that emulsion was flowing through the beadpack during these experiments. The hypothesis for this behavior is that the emulsion coalesced as it entered the beadpack and new emulsion was generated based on the shear rate in the beadpack. The newly regenerated emulsion was stable while flowing through the beadpack, causing an increase in the apparent viscosity, but was not stable enough to remain in the effluent after exiting the beadpack.

Chapter 5

Coreflood Experiments

In order to build upon the experiments completed with beadpacks, a variety of different coreflood experiments were performed. The HiP beadpack dimensions are 0.44 cm inner diameter, 15.24 cm in length and for large beads the ratio of bead size to packing ID causes potentially significant artifacts in the flow regime and hence the emulsion behavior. These artifacts do not arise in corefloods. Moreover, application of nanoparticle-stabilized emulsions in the field will involve flow through sedimentary rocks. The coreflood materials, experimental setups, procedure, and results will be discussed in this chapter. All experiments were performed at ambient temperature and an outlet pressure of 0 psig. The injection rates varied from 0.1 to 40 mL/min. The initial saturation of the core varied from brine saturated, residual water saturated, and residual oil saturated.

5.1 MATERIALS USED

Sandstone Cores

Two different sandstones were used in corefloods. Majority of the experiments were performed using Boise sandstone cores. Boise sandstone was used because of its availability, low clay content, and has relatively low heterogeneity. Berea sandstone, like Boise, has a low clay content and relatively low heterogeneity but is less permeable than Boise. The cores used in the coreflood experiments were 12" in length with a 1" diameter. Typical pore volumes are 33-37 mL for Berea sandstone and 40-45 mL for Boise sandstone.

Nanoparticle Stabilized Emulsions

Different emulsions were injected through the cores under different experimental conditions. These emulsions were generated by co-injection through the HiP beadpack filled with 180 μm beads. For the experiments in Sections 5.5.1 – 5.5.3, the emulsion effluent from the beadpack was allowed to settle in the accumulator before injecting the emulsion so that emulsion was the only phase injected into the core. In Section 5.5.5 diluted emulsion was injected into the core by routing the effluent directly to the core, this will be explained in more detail later in this chapter. In most cases these emulsions were stabilized using Nyacol DP9711 nanoparticle dispersion. However, other emulsions stabilized by different nanoparticle dispersions were used in some coreflood experiments. The type of emulsion used in each experiment will be indicated in the results section.

Organic Phases

Different organic phases were used in some of the coreflood experiments. Light mineral oil, n-octane, and dodecane were all used in some capacity. The physical properties of these oils are outlined in Table 3.3 in Section 3.3.4.

Aqueous Phases

Brine was used to initially saturate the core and was injected to measure core permeability. The brine was 2 wt% NaCl. It was typically prepared in large volumes (~ 3500 mL) by adding 70 grams of NaCl to 3,430 mL of DI water. Different nanoparticle dispersions were used in the coreflood experiments. All three nanoparticle

dispersions that stabilized emulsion in Chapter 3 were used (see Table 3.2 for specific concentrations). The primary dispersion used was the 3 wt% NaCl, 2 wt% Nyacol DP 9711 nanoparticle dispersion.

Effluent Sample Holders

Centrifugal tubes were used to collect the effluent from the corefloods. Each tube had a maximum capacity of 15 mL. In most experiments each sample tube contains approximately 12 mL of effluent which was approximately between for 0.25 to 0.30 PV depending on the core. Figure 5.1 below shows a sample of coreflood effluent with three different phases: mineral oil (top), emulsion (middle), and aqueous nanoparticle dispersion (bottom). The sample tubes contain a white label on the outer part of the tube and should not be confused with the white emulsion. Majority of the tubes were rotated so the label was not shown in the photos of the effluent but in some cases the labels are visible and should not be mistaken for emulsion.
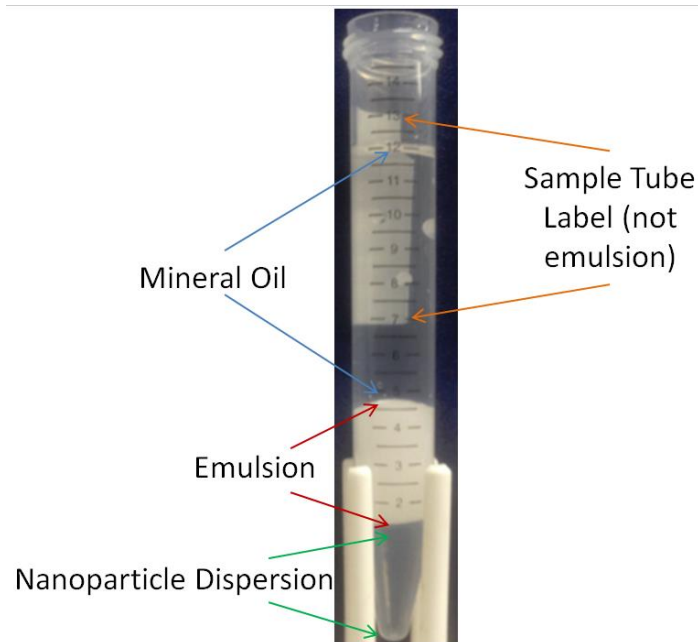
Figure 5.1 Three different fluids in effluent sample tube: organic oil phase (top), emulsion (middle), aqueous nanoparticle dispersion (bottom). The white sample label spans from the 7 mL marking to the 13 mL marking and should not be confused for emulsion in the photos of the effluent.

Pressure Transducers and Data Acquisition

Multiple Rosemount differential pressure transducers (model 3051CD5A22A1A) were used to record the pressure drop across the core. The differential transducers and the data acquisition card are powered by a power supply unit. The data acquisition card allows the pressure to be monitored and recorded from the computer. From the computer, the pressure is displayed and recorded using the program LabView. The pressure data has been corrected to remove any offset (i.e. so a zero flow rate corresponds to a zero pressure drop). The differential pressure transducer has a maximum working pressure drop of 2,000 psi however the transducers have been calibrated to operate in the pressure ranges for the beadpack experiments.

125

Summary of Coreflood Experiments in Chapter 5								
Experiment Type	Core	SS	ϕ	k (mD)	Initial Saturation	Injected Fluids	Flow Rate (mL/min)	Shear Rate (s^{-1})
Effect of Shear Rate on Emulsion Stability	E	Berea	0.29	251	Brine	Mineral Oil Emulsion	1	251
	B	Boise	0.29	499	Brine	Mineral Oil Emulsion	1	123
	C-1	Boise	0.28	690	Brine	Mineral Oil Emulsion	0.1	11
	C-2	Boise	0.28	690	End point from C-1	Mineral Oil Emulsion	1	106
	C-3	Boise	0.28	690	End point from C-2	Mineral Oil Emulsion	2	212
	D-1	Boise	0.27	828	Mineral Oil And Brine	Mineral Oil Emulsion	1, 2	99, 197
	D-2	Boise	0.27	828	Emulsion from endpoint of D-1	Mineral Oil Emulsion	4	395
	D-3	Boise	0.27	828	Emulsion from endpoint of D-2	Mineral Oil Emulsion	8	790
Comparing Co-injection to Emulsion Injection	M	Boise	0.29	655	Mineral Oil And Brine	Mineral Oil Emulsion then Co-injected	2	222
	N	Boise	0.29	720	Brine	Mineral Oil Emulsion then Co-injected	2	206
	O	Boise	0.29	710	Brine	Co-injected then mineral oil emulsion	2	207
Mobile Oil Recovery with Emulsion	P-1	Boise	0.28	776	Residual Water and Mineral Oil	Brine	3	300
	P-2	Boise	0.28	776	Residual Water and Mineral Oil	Octane Emulsion	0.1	10
	P-3	Boise	0.28	776	End Point from P-2	Brine	3	300
Residual Oil Recovery with Emulsion	Q-1	Boise	0.28	540	Residual Mineral Oil and Brine	Co-injected octane and brine	2	242
	Q-2	Boise	0.28	540	Residual Mineral Oil and Brine	Octane Emulsion	2	242
	T-1	Boise	0.29	900	Residual Oil Mineral Oil and Brine	Co-injected mineral oil and brine	2	183
	T-2	Boise	0.29	900	Residual Mineral Oil and Brine	Mineral Oil Emulsion	2	183
Emulsion Dilution Experiments	M-1	Boise	0.28	540	Brine	Diluted Mineral Oil Emulsion from Beadpack (1:1 NP dispersion to mineral oil)	40	4,842
	M-2	Boise	0.28	540	Emulsion Effluent from end point of M-1	Mineral Oil Emulsion	40	4,842
	R-1	Boise	0.28	720	Brine	Diluted Octane Emulsion From Beadpack	40	4,087
	R-2	Boise	0.28	720	Emulsion Effluent from end point of R-1	Highly Diluted Octane Emulsion From Beadpack	40	4,087
	R-3	Boise	0.28	720	Emulsion Effluent from end point of R-2	Non-diluted Octane Emulsion From Beadpack	40	4,087
Residual Oil Recovery with Nanoparticle Dispersion	G	Berea	0.24	408	Residual Water and Mineral Oil	IPA-ST nanoparticle dispersion (3 wt% NP and 2 wt% NaCl)	3, 6, 12, 24	446, 892, 1784, 3568
	I	Boise	0.28	908	Residual Water and Dodecane	DP 9711 nanoparticle dispersion (2 wt% NP and 3 wt% NaCl)	3, 6, 12, 25	278, 556, 1113, 2226

Table 5.1 Emulsion coreflood experiments reported in this thesis. Blue text indicates emulsion stabilized with the EOR-25 nanoparticle dispersion. Red text indicates emulsion stabilized by IPA-ST dispersion. All other emulsions stabilized with DP 9711 dispersion. See Table 3.2 for concentrations.

5.2 COREFLOOD EXPERIMENTAL SETUPS

This section will outline the different experimental setups and the different equipment used in the coreflood experiments. Three different setups were used to inject fluids through cores.

5.2.1 Emulsion/Nanoparticle Dispersion Experimental Setup

The following set-up was used when a single fluid was injected through the core. Figure 5.2 is a schematic for the emulsion injection experiments. The set-up is very similar to the emulsion injection experiments performed in the beadpack. In this configuration emulsion or nanoparticle dispersion is loaded into the accumulator (b) and pumped through the core by the syringe pump (a). The accumulator and syringe pump were the same ones used in Chapter 3 and 4. The sandstone core is housed in core holder (c). The effluent is collected with the fraction collector (f). Rosemount differential pressure transducers are used to measure the pressure drop across the core. Differential transducer (e) was used to measure the pressure drop across the entire core. Differential transducer (d) was used to measure the pressure drop along different sections of the core. The same setup was used when brine was injected to the core to measure permeability or waterflood except the accumulator was not used because the brine could be loaded directly into the syringe pump.
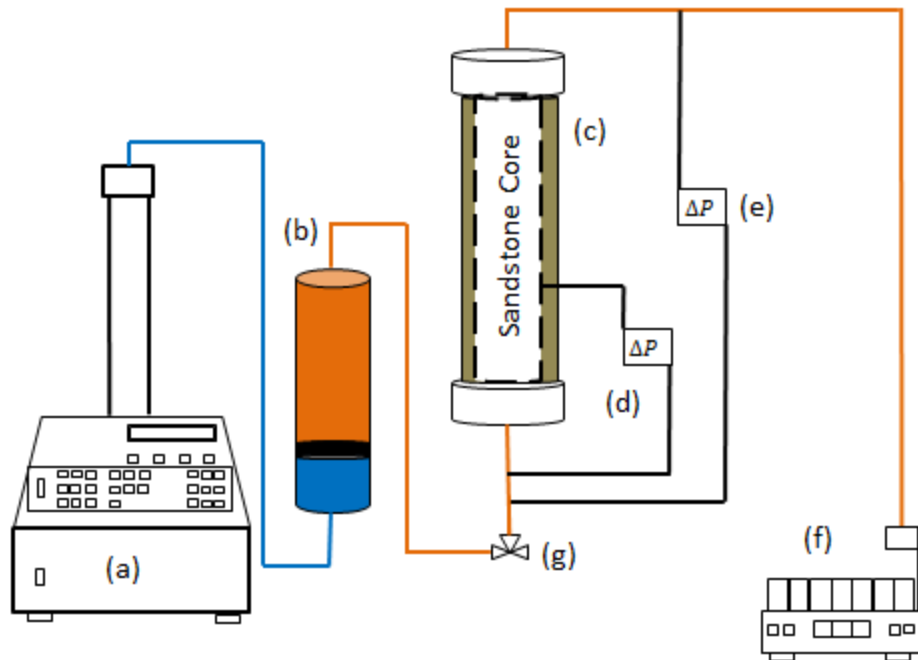
Figure 5.2 Schematic of core holder set-up: (a) syringe pump, (b) accumulator, (c) core holder with sandstone core, (d) differential pressure transducer, (e) differential pressure transducer, (f) fraction collector, and (g) three way valve.   This configuration was used anytime emulsion or nanoparticle dispersion was injected into the core.   The accumulator was bypassed when brine or oil was injected into the core because those fluids could be loaded directly into the syringe pump.

Core Holder

All of the corefloods in this thesis were performed using a Hassler type core holder.   It was manufactured by Phoenix Instruments Inc., and is designed to house cores up to 1" in diameter and 12" in length.   It has a working pressure of 2000 psi and a working temperature of 312 °F.   The core holder was mounted vertically using Unistrut metal framing.

Inside the core holder is a rubber sleeve made of Viton. Cores were placed directly into the Viton sleeve. The sleeve works as a seal for the core. This seal forces the injected fluids to flow into the core by preventing flow around the core. A hydraulic hand pump is used to apply confining pressure to the sleeve, by pumping mechanical pump oil, creating a seal between the core and sleeve. The core holder and sleeve both have 5 different pressure taps equally spaced. For some of the experiments the pressure taps were used to measure the pressure drop across certain sections of the core. In other experiments, the taps were not used in which case they were all sealed.

5.2.2 Co-injection Setup

Figure 5.3 shows the experimental configuration used to co-inject aqueous and organic fluids through the core. If nanoparticle dispersion was co-injected with an organic phase into the core then it was loaded into the accumulator (c). If brine was injected, instead of nanoparticle dispersion, it was loaded directly into syringe pump (b) and the accumulator was not used. The organic phase was loaded into the second syringe pump (b). The two fluids met a tee where they would then flow into the core in alternating slugs. The tee is designated in Figure 5.3 where the red line and green line meet. The differential transducers (e) were used to measure the overall pressure drop and the pressure drop along different sections of the core.

129
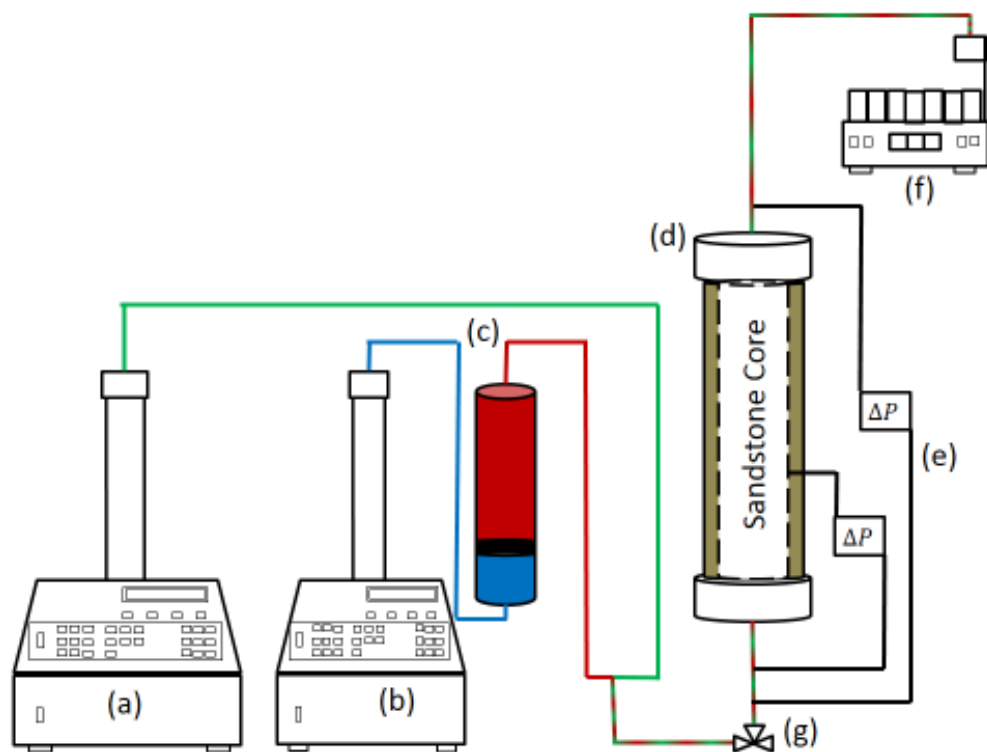
Figure 5.3 Schematic of core holder set-up: (a) oil syringe pump, (b) drive water syringe pump, (c) accumulator, (d) core holder with sandstone core, (e) differential pressure transducers, (f) fraction collector, and (g) three-way valve.   This configuration was used anytime an organic phase and an aqueous phase were co-injected into the core.

5.2.3 Emulsion Dilution Experimental Setup

Whenever emulsion was generated by co-injection through the beadpack, the effluent that was collected appeared to be 100% emulsion (white viscous fluid) for a short period of time. For experiments in which the injected phase ratio (volumetric flow rate of organic phase divided by volumetric flow rate of aqueous phase) was smaller than a threshold value (about 2.2, i.e. 69% organic phase and 31% aqueous phase),   excess aqueous phase would then drain from the collected emulsion leaving two phases in the

accumulator, emulsion and nanoparticle dispersion. It took approximately one hour for the excess nanoparticle dispersion to drain from the emulsion. The following experimental setup was used to inject dilute emulsions directly into the core before the excess phase had time to drain from the emulsion. This was used to test how the apparent viscosity of the emulsion would change when the volume fraction of droplets was smaller than the equilibrium value (the drained emulsion described above). Conceptually these experiments corresponded to injecting "dilute emulsion", where the dilution is done with excess nanoparticle dispersion.

Figure 5.4 shows the experimental set up for the dilute emulsion experiments. In these experiments nanoparticle dispersion and brine were co-injected through the beadpack (d) upstream of the core holder (e). Syringe pump (a) pumped the organic phase while syringe pump (b) used drive water to displace the nanoparticle dispersion from the accumulator (c). Before routing the effluent from the beadpack to the core, some of the beadpack effluent was collected in container (i) from a three way-valve (g). The beadpack effluent was only collected after the pressures on both pumps stabilized indicating steady state. The three way valve was turned to have the beadpack effluent enter the core once enough beadpack effluent was collected. The pressure drop was recorded across the core using a differential pressure transducer (f) and the effluent from the core was collected with the fraction collector (h).
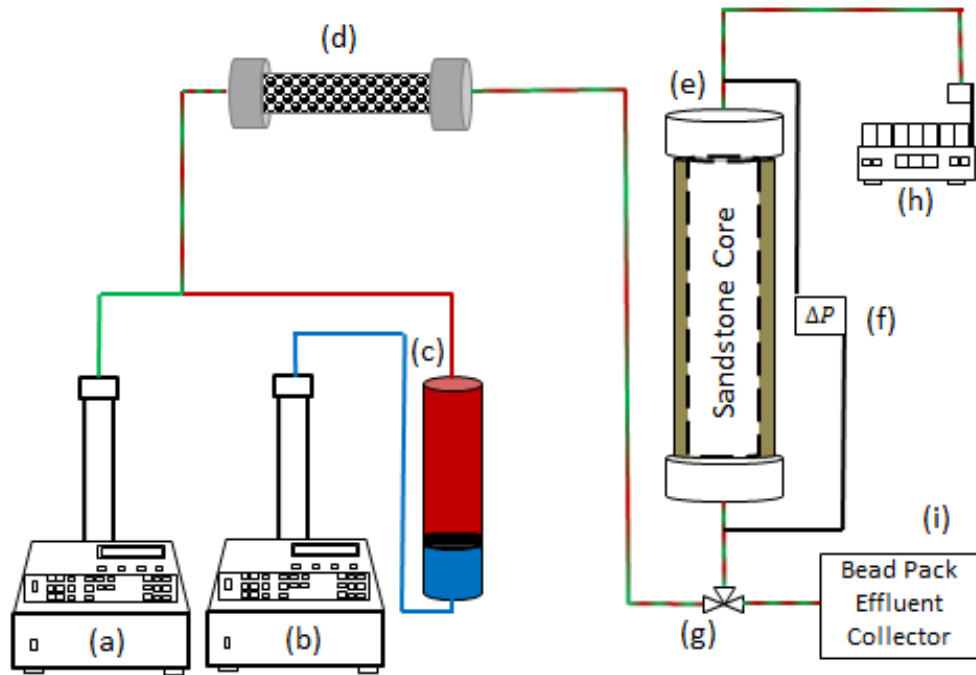
Figure 5.4 Schematic of core holder set-up: (a) oil syringe pump, (b) drive water syringe bump, (c) accumulator, (d) beadpack, (e) core holder with sandstone core, (f) differential pressure transducer, (g) three-way valve, (f) fraction collector for core effluent, and (i) container for beadpack effluent. This configuration was used to inject a dilute emulsion through the core.

5.3 COREFLOOD PROCEDURE

This section will outline the procedure for the coreflood experiments. The sandstone core preparation and loading procedure will first be outlined, including pressurizing the core holder. The procedure to prepare the sandstone core, measure permeability, and change the initial saturation of the core will be outlined.

5.3.1 Sandstone Core Preparation

The sandstone cores used in this experiment were cut from larger sections of Boise and Berea blocks.   During the cutting process the cores would become wet with water.   In order to measure the pore volume of the cores, the cores were dried so their dry weight could be recorded.   To dry the cores they were placed in a fume hood to dry for approximately two days to ensure that all of the water had evaporated from the core. To speed up the drying process, some of the cores were placed in an oven at approximately 40-50°C for several hours.

Once a core was dried and weighed the core was vacuumed using a model 1402 Welch Duoseal Vacuum Pump.   Cores were vacuumed for approximately 24 hours to remove any trapped air.   For 18-20 hours, the dry core was vacuumed then the core was saturated with brine.   The brine saturated core was vacuumed for approximately 4-6 more hours.   After the vacuuming procedure, the core was weighed a second time to measure its wet weight.

5.3.2 Loading Cores into the Core Holder

After the vacuum saturation the core was loaded into the core holder.   The core holder has two cylindrical end cap fittings. The top end cap has a hand-screw piece above it. This hand screw provides axial confining pressure to the core.   The bottom fitting has three prongs that fit into the core holder. Once the bottom fitting is pushed into the bottom of the core holder it must be turned by hand to lock into place creating a seal.

Before the both end cap pieces and hand-screw piece are removed to load a core the core holder needs to be de-pressurized. This can be done by turning a knob on the hand pump releasing any confining pressure.   Once the core holder is depressurized the

133

hand-screw piece and end caps are removed.   A steel rod can be used to gently push the previously used core out of the core holder.   The core should not be forced out of the core holder because this can damage the inner sleeve.   Before the new core can be loaded into the core holder the bottom end cap piece is flushed with brine to remove any fluid or dead volume from the line.   After the bottom piece is flushed with brine it is inserted into the core holder. The core is gently inserted into the top of the core holder by hand.   Once the core is in place the top end piece can be inserted into the core holder. The last step is to attach the hand-screw to the top end cap.   It is very important to tighten the hand-screw because this secures the top end cap and applies axial confining pressure.   If the core holder is pressurized while the hand-screw is not tightened pump oil will leak into the top of the sleeve and contaminate the core.

Applying Confining Pressure to Core Holder

Figure 5.5 is a schematic of how confining pressure was applied to the core by pumping mechanical pump oil with a hand pump.   The procedure for applying confining pressure is outlined below.
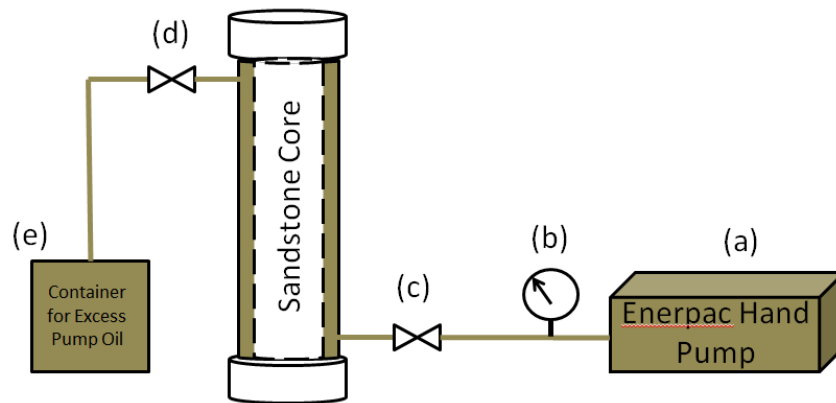
Figure 5.5 Schematic of confining pressure system: (a) hand pump, (b) pressure gauge, (c) two way valve, (d) two way valve, (e) pump oil container.

1. Make sure hand pump (a) is filled with mechanical pump oil

2. Open valve (c) and (d)

3. Begin manually pumping mechanical pump oil with hand pump (a)

4. Continue pumping until all of the air is displaced from the annulus leaving only pump oil is in the annulus

5. Close valve (d) and continue pumping while watching the pressure from gauge (b)

6. Stop pumping when desired pressure is reached

An Enerpac P-392 hydraulic hand pump was used to pump mechanical pump oil into the core holder annulus to pressurize the sleeve. It is capable of pumping up to 10,000 psi.

Typically the confining pressure applied was 2,000 to 2,500 psi. This was to ensure there was always a net total confining pressure of no less than 500 psi. Although the outlet pressure for the corefloods was always 0 psig, the apparent viscosity of the emulsion can be very large and consequently injection pressures as high as 1500 psig were encountered in experiments, hence the need for large confining pressure. The net confining pressure is the difference of the confining pressure as read from gauge (b) minus the pore pressure which is measured from the pressure transducers.

5.3.3 Core Permeability Measurement

After the core is loaded into the core holder and a proper confining pressure was applied the permeability of the core was measured. The core permeability was measured by injecting brine through the bottom of the core until a steady state pressure drop is reached. The permeability was calculated with the steady state pressure drop for each flow rate. The core permeability was taken as the average of the three different

permeabilities. The pressure drop was measured by the pressure transducer and recorded using LABView. It was sometimes necessary to correct the readings for a small offset of the baseline (should read zero pressure at zero flow rate) depending on the initial reading from the pressure transducer.

5.3.4 Saturating Core with Oil

Once a core's permeability was measured its initial saturations were changed for some experiments by injecting oil into the core. Dodecane, n-octane, and mineral oil were each used in different experiments. Typically over ten pore volumes of oil were injected through a core to ensure the core reached residual water saturation, S_{wr}. Oil was always injected through the top of the core so the less dense oil could displace the denser brine in gravity-stable and therefore more uniform manner. Injecting oil from the top of the core helps ensure that the core truly does reach residual water saturations by effectively using the density difference between oil and brine. The lines to the transducers were reversed whenever oil was injected through the top of the core so a positive pressure drop was recorded.

5.3.5 Waterflooding to reach residual oil saturation

Several experiments were performed in which emulsion was injected to recover residual oil. In order to reach residual oil saturation, S_{or}, the core was first saturated with oil using the procedure outlined in the previous section. Brine was injected through the bottom of the core to displace oil in a gravity-stable manner. Initially the brine injection was started at a low flow rate (2 mL/min) and then incrementally increased. The mobile oil bank was displaced during the first pore volume of brine was

136

injected.   After the oil bank was displaced only brine was seen in the effluent.   The flow rate was then increased to displace additional oil (incremental recovery is possible when the capillary number is increased).   After the flow rate was increased small amounts of additional oil were recovered.   The core was considered at residual oil saturation when an increase in flow rate would recover less than 1 mL of oil. Although it is possible to displace more oil at higher flow rates it would likely change the saturation very little (less than a 2% change in saturation). Typical flow rates for the waterfloods began at 2 mL/min and were increased incrementally to 6 mL/min and then finally 12 mL/min.

5.4 DATA ANALYSIS

5.4.1 Core Pore Volume

Before the core was saturated with brine it was dried and then weighed.   After the core was vacuumed and saturated with brine its wet weight was measured.   The cores pore volume, PV, was calculated from the following equation:

$$PV = \frac{M_{wet} - M_{dry}}{\rho_{brine}}$$

where M_{wet} is the mass of the core after it is saturated with brine (g), M_{dry} is the mass of the core dry (g), and ρ_{brine} is the density of the brine (g/mL).   The pore volumes of the cores typically ranged from 40-46 mL for Boise sandstone, corresponding to porosities between 0.26 and 0.29.

5.4.2 Core Permeability

Core permeability was calculated with Darcy's Law using at least two different flow rates to reach different steady state pressure drops. The permeability, k, is determined with the following arrangement of Darcy's Law:

$$k = \frac{\mu L Q}{A \Delta P}$$

where A is the cross-sectional area of the core (cm), ΔP is the pressure difference across the core (Pa), Q is the volumetric flow rate (cm^3/s), L is the length of the bead pack (cm), and μ is the viscosity of the brine (Pa*s).

Brine was typically injected at three different flow rates. The permeability was calculated with the steady state pressure drop for each flow rate. The core permeability was taken as the average of the three different permeabilities. Figure 5.6 shows a core permeability measurement.
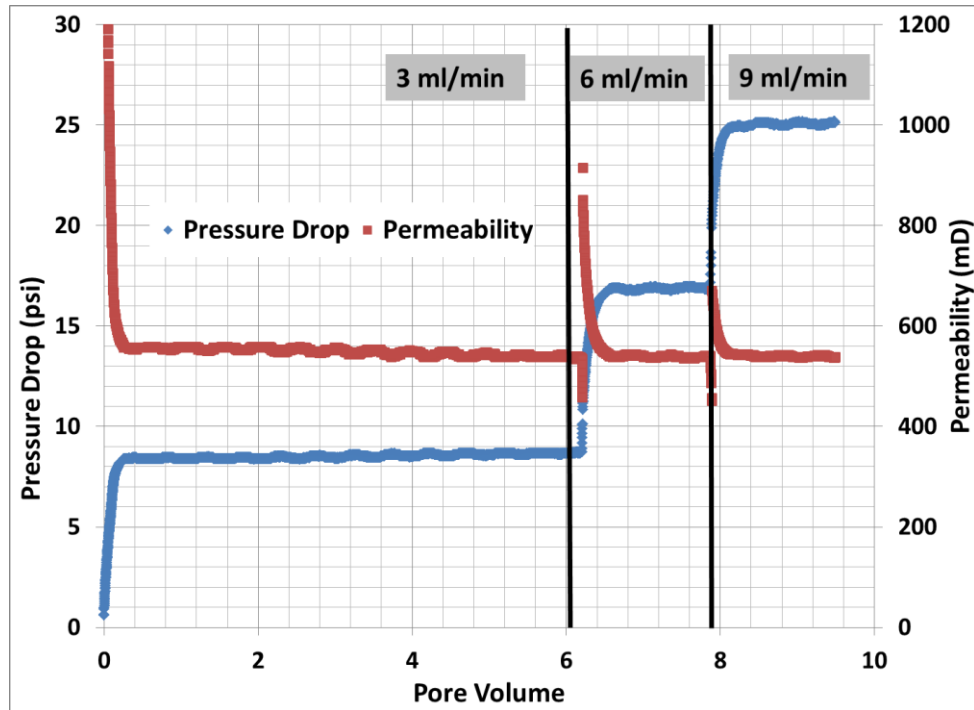
Figure 5.6 Example of pressure drop and calculated permeability of a sandstone core during a permeability measurement using brine.

5.4.3 Reynolds Number

The Reynolds number, Re, was calculated for experiments where the apparent viscosity or permeability was calculated using Darcy's law. Darcy's law only applies for slow, creeping flow ($Re < 1$). The following equation was used to calculate Reynolds number:

$$Re = \frac{\rho v_s D}{\mu}$$

where ρ is the density of the fluid (g/cm^3), v_s is the superficial velocity (cm/s), and D is the grain diameter (cm), and μ is the viscosity of the fluid (g/cm/s). The grain diameter for Boise Sandstone was estimated as 125 microns. For the experiments in this

139

section where Darcy's law was used to calculate apparent viscosity or apparent viscosity the Reynolds number was less than one.

5.4.4 Apparent Viscosity

The apparent viscosity, μ_{app}, of the emulsion/nanoparticle dispersion while flowing through the core was calculated from Darcy's law:

$$\mu_{app} = \frac{-kA}{Q} \frac{(P_o - P_i)}{L}$$

where k is the permeability of the core (cm^2), A is the cross-sectional area of the beadpack (cm), P_o and P_i are the outlet and inlet pressure (Pa), Q is the volumetric flow rate (cm^3/s), and L is the length of the bead pack (cm). Gravity is not accounted for because the beadpack was positioned horizontally for all experiments.

5.4.5 Residual Water Saturation

The residual water saturation, S_{wr}, was determined by comparing the brine displaced from the core during the oil injection to the pore volume of the core or:

$$S_{wr} = \frac{PV - displaced\ water\ during\ oil\ injection}{PV}$$

where PV is pore volume.

Figure 5.7 shows the pressure drop and relative permeability for a mineral oil flood to reach residual saturation. Mineral oil was injected at 11 mL/min for over 12 pore volumes to reach residual water saturation for this specific case.
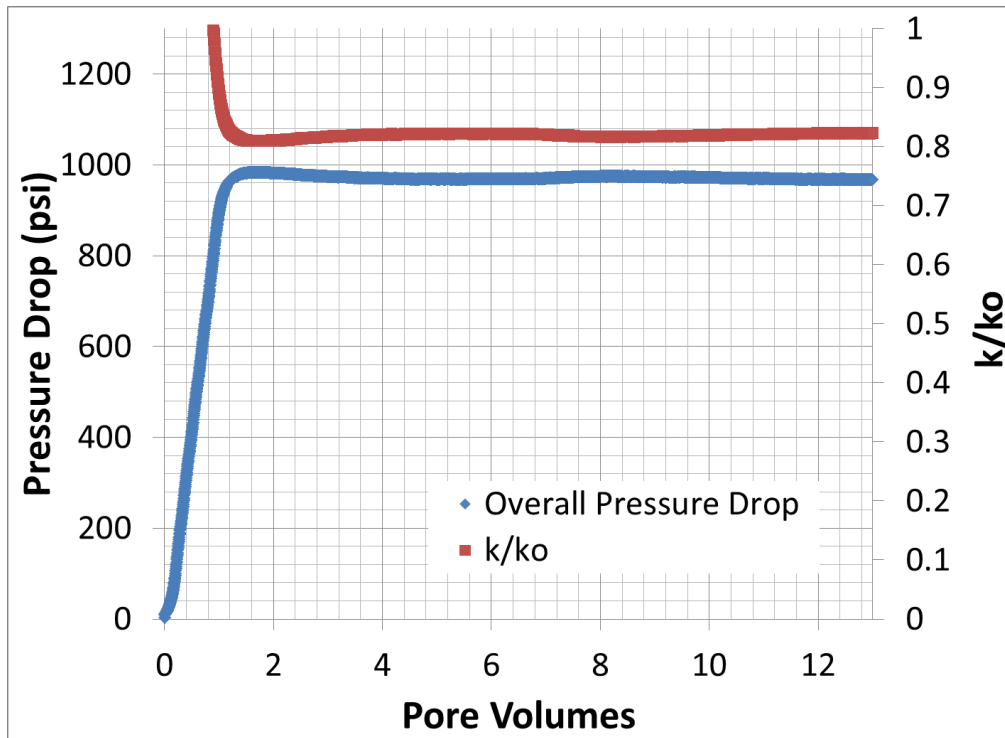
Figure 5.7 Example of the pressure drop and relative permeability from a mineral oil flood to reach residual brine saturation. Mineral oil was injected at 11 mL/min.

The effluent was collected in order to accurately measure the amount of water displaced from the core. This quantity was used to calculate the residual water saturation using the equation provided earlier in this section. Figure 5.8 shows the effluent collection for a mineral oil flood to reach residual water saturation. In this particular case the mineral oil, normally clear, was dyed red to help distinguish it from the brine.
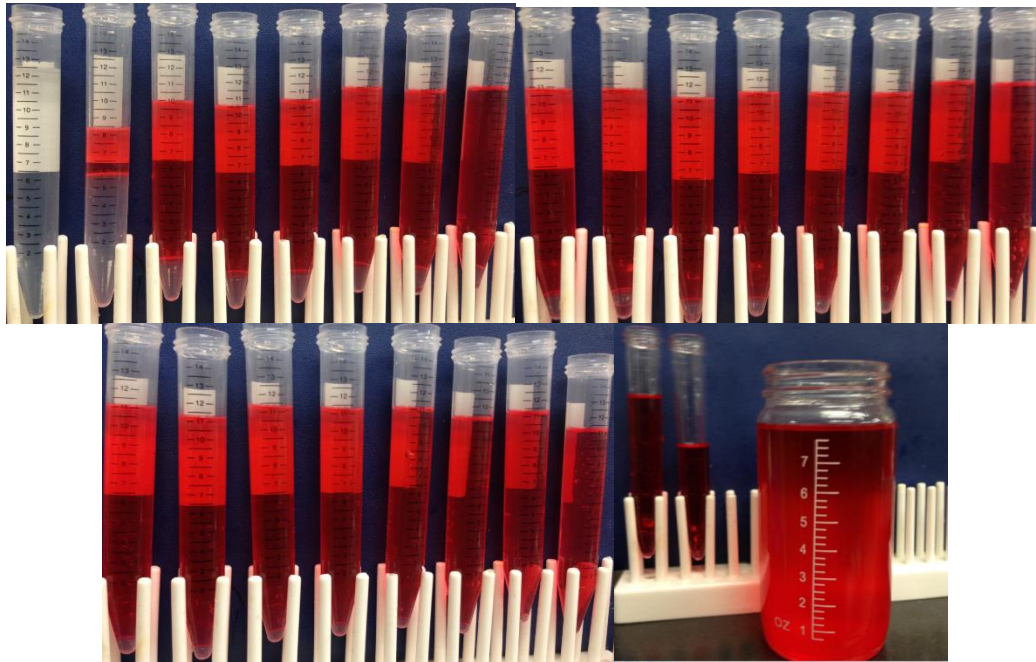
Figure 5.8 Example of effluent from mineral oil flood to reach residual brine saturation.

Normally the first 6 pore volumes were collected in the 15 mL centrifugal tubes to accurately estimate the amount of water displaced. After 6 pore volumes the effluent was collected in a larger container because little to no additional water was displaced after 6 pore volumes of oil were injected. For the cores used in this thesis the typical residual water saturation was between 30 to 40%. This procedure was used anytime a core was saturated with oil.

5.4.6 Residual Oil Saturation

The residual oil saturation, S_{or}, was determined by comparing the oil displaced from the core after waterflooding to the cores pore volume or:

$$S_{or} = \frac{PV(1 - S_{wr}) - oil\ displaced\ during\ waterflood}{PV}$$

where PV is pore volume.

Brine was injected into the core and the flow rate was incrementally increased to displace additional oil. The core was considered at residual oil saturation when an increase in flow rate did not recover an appreciable amount of oil (less than 1 mL of oil). Figure 5.9 shows the pressure drop and relative permeability for a brine injection that was used to get the core to residual oil saturation.
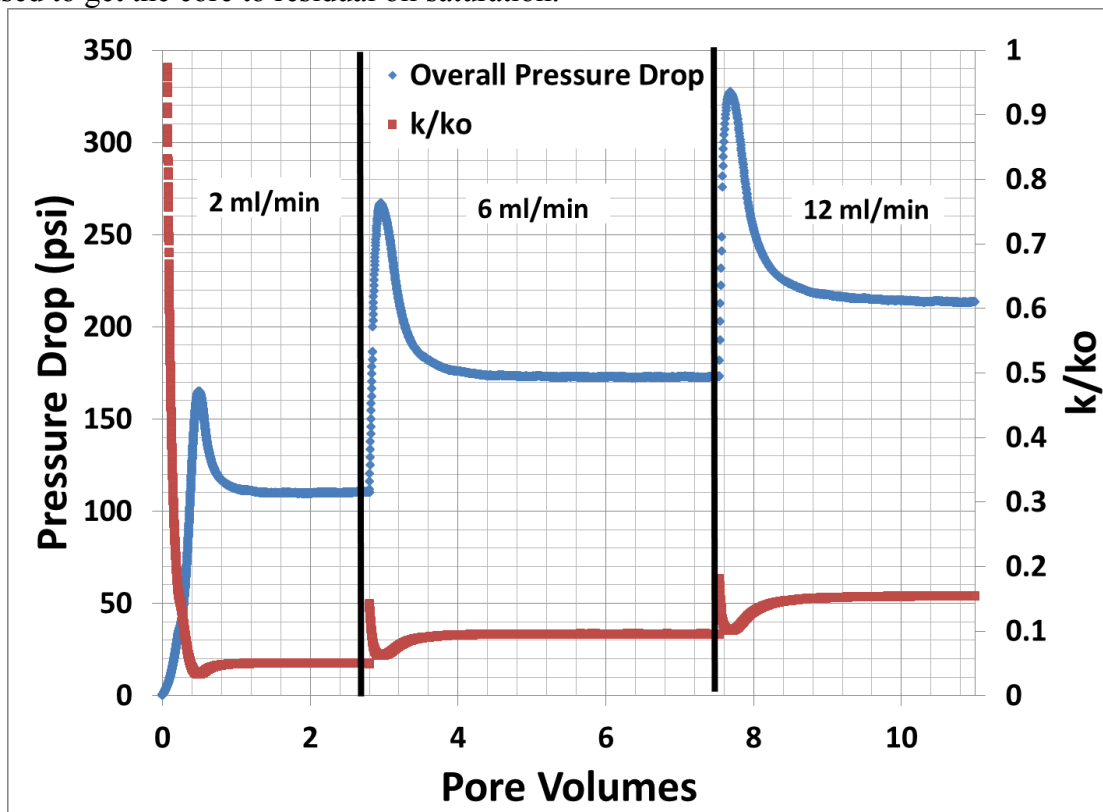
Figure 5.9 Example of the pressure drop and relative permeability for a waterflood that was used to reach residual mineral oil saturation.

The effluent for the entire waterflood was captured in 15 mL centrifugal tubes in order to accurately estimate how much oil was displaced. The amount of oil displaced from the waterflood was used to estimate the residual oil saturation using the equation provided earlier in this section. Figure 5.10 shows the effluent from a waterflood that was used to reach residual oil saturation.
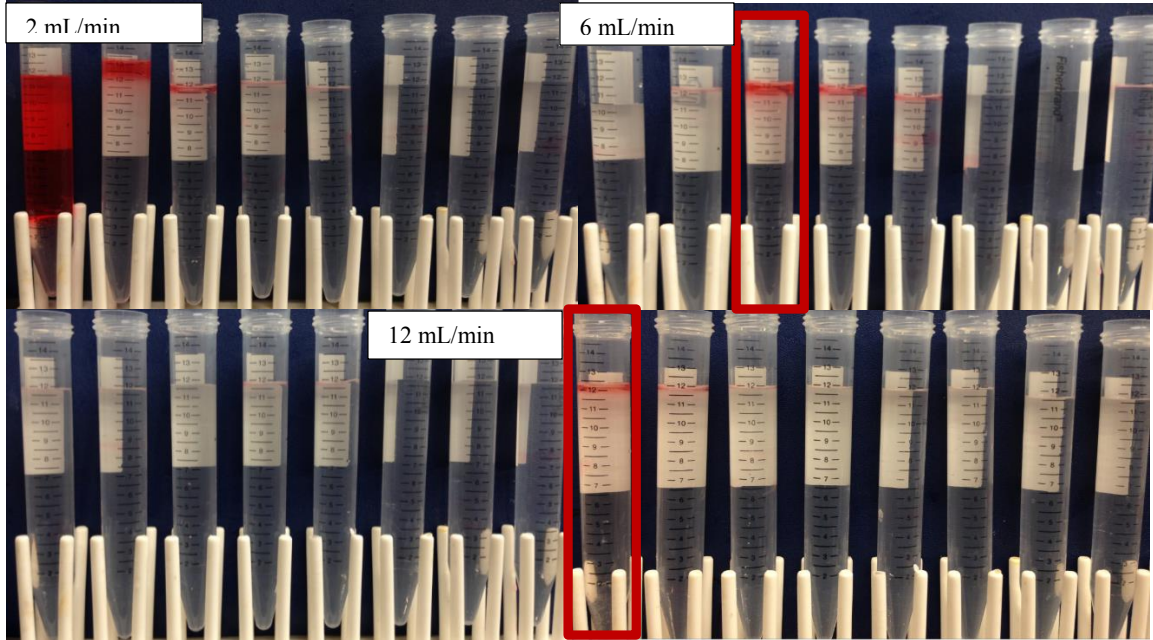
Figure 5.10 Example of the effluent from a waterflood to reach residual mineral oil saturation. The mineral oil was dyed red. The red rectangles around the centrifugal tubes indicate a change in flow rate; see Figure 5.9.

5.5 RESULTS

5.5.1 Emulsion Injection

Emulsion was injected through sandstone cores to further investigate emulsion flow and stability in porous media. In the Core E experiment, Figure 5.11, a mineral oil emulsion was injected into a brine saturated Berea sandstone core. The emulsion was

stabilized with the EOR-25 nanoparticle dispersion (Table 3.2 for specific concentrations). It was generated by co-injecting the nanoparticle dispersion and mineral oil through the 180 micron HiP beadpack at a 1:1 phase ratio with a total flow rate of 24 mL/min. The emulsion had an average droplet diameter of 25 microns and was approximately 75% mineral oil by volume. The pressure drop across the entire core was measured with one transducer. A second pressure transducer was attached to the pressure taps of the core holder. This transducer measured the pressure drop across a 4" section of the core. The 4" section that was measured was from the 2" of the core to the 6" of the core.

Figure 5.11 shows the experimental conditions, pressure drop, apparent viscosity, and effluent of the emulsion injection into Core E. The pressure drop across the core increased for the entire duration of the experiment although the pressure drop across the taps stabilized. A very small amount of stable emulsion (approximately 15% of the fractional flow during that period) was produced after approximately 5 pore volumes of emulsion were injected. Throughout the injection, mineral oil that had been dispersed as droplets in the injected emulsion was produced as a separate phase in the effluent, along with the aqueous phase that had been the external phase in the emulsion. The results of the experiment are consistent with the moving front hypothesis developed for the beadpack experiments in Chapter 4. The steadily building pressure gradient in Core E indicates the slow movement of a front which is associated with emulsion coalescence and regeneration in situ.

145

Core E – Berea Core					
k (mD)	ϕ	Pore Volume (mL)	Initial Saturation	Flow Rate (mL/min)	Shear Rate (s^{-1})
251	0.21	33	S_w=1	1	202
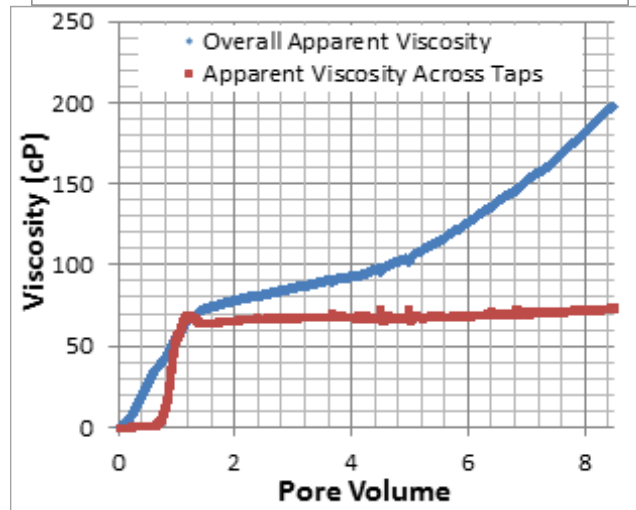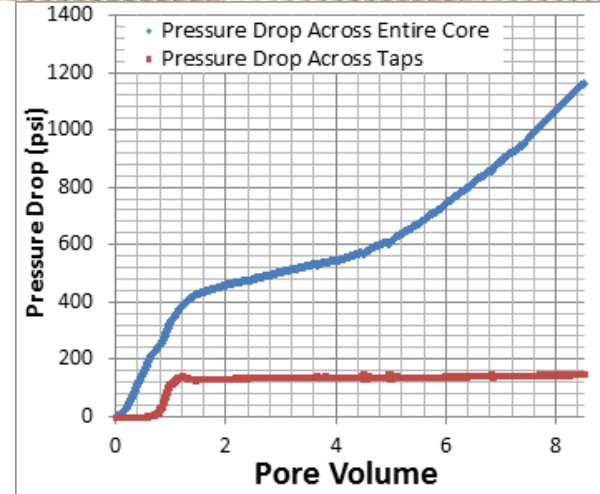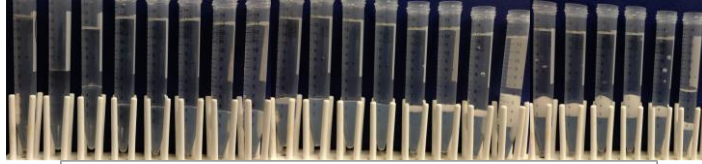
Figure 5.11 The experimental conditions, effluent, pressure drop and apparent viscosity of the emulsion injection into Core E. Taps located 2" and 6" from core inlet. Volume in each sample is 13 mL or 0.4 PV.

In the experiment in Core B (Figure 5.12) emulsion was injected into a brine saturated core. The emulsion was generated by co-injecting mineral oil and nanoparticle dispersion through the HiP beadpack. The dispersion was the Nycol DP 9711 dispersion used in the critical shear rate experiments (Section 3.3.2). The emulsion had an average droplet diameter of 24 microns and was approximately 66% oil by volume. This emulsion was used in the Core B and Core C experiments.

The injection pressure during the emulsion injection in Core B increased for the entire time that emulsion was injected. From the presence of oil phase and aqueous phase in the effluent it is apparent that the emulsion partially coalesced. The coalescence process within the core appears to be at steady state because the amount of emulsion in the effluent was consistent in each tube. At approximately 6 pore volumes the injection decreases significantly because all of the emulsion inside the accumulator was injected and the excess nanoparticle dispersion, at the bottom of the accumulator, was injected through the core (see Figure 4.2). This coincides with the pictures of the effluent in Figure 5.12 where only nanoparticle dispersion was collected (last 7 sample tubes).

Core B – Boise Core					
k (mD)	ϕ	Pore Volume (mL)	Initial Saturation	Flow Rate (mL/min)	Shear Rate (s^{-1})
499	0.29	45	$S_w=1$	1	123
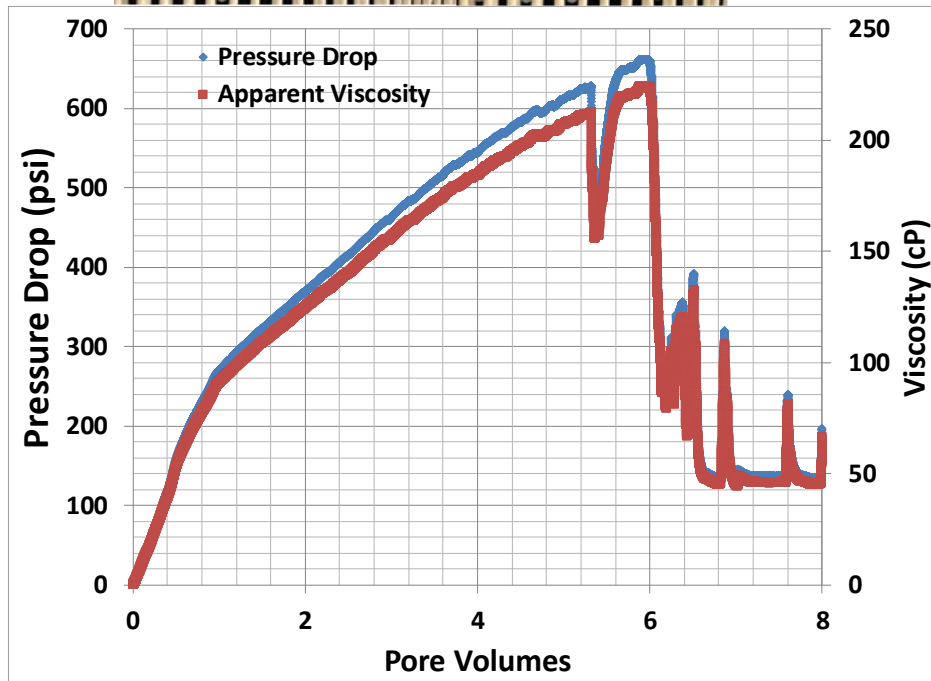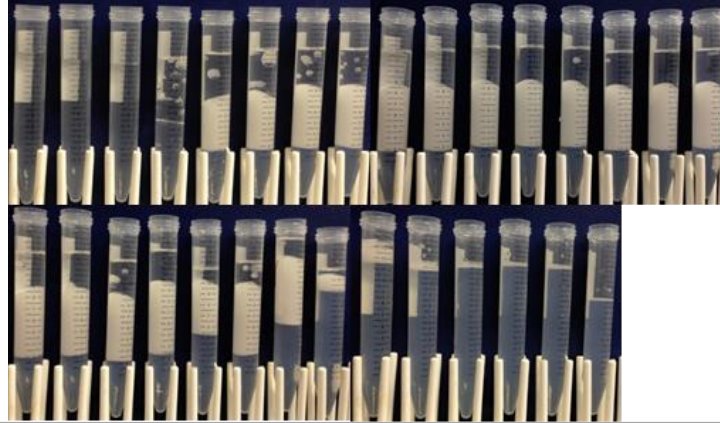
Figure 5.12 The experimental conditions, effluent, pressure drop and apparent viscosity of the emulsion injection into Core B.   The rapid decrease in pressure at 6 PV is from injecting the excess nanoparticle dispersion, which had settled at the bottom of the accumulator, through the core.   Volume in each sample is 12 mL or 0.27 PV.

The injected emulsion was compared to some of the effluent emulsion from the core. The effluent emulsions droplet diameter and rheology were measured. Figure 5.13 shows the viscosity and droplet size of the injected emulsion and the effluent emulsion.
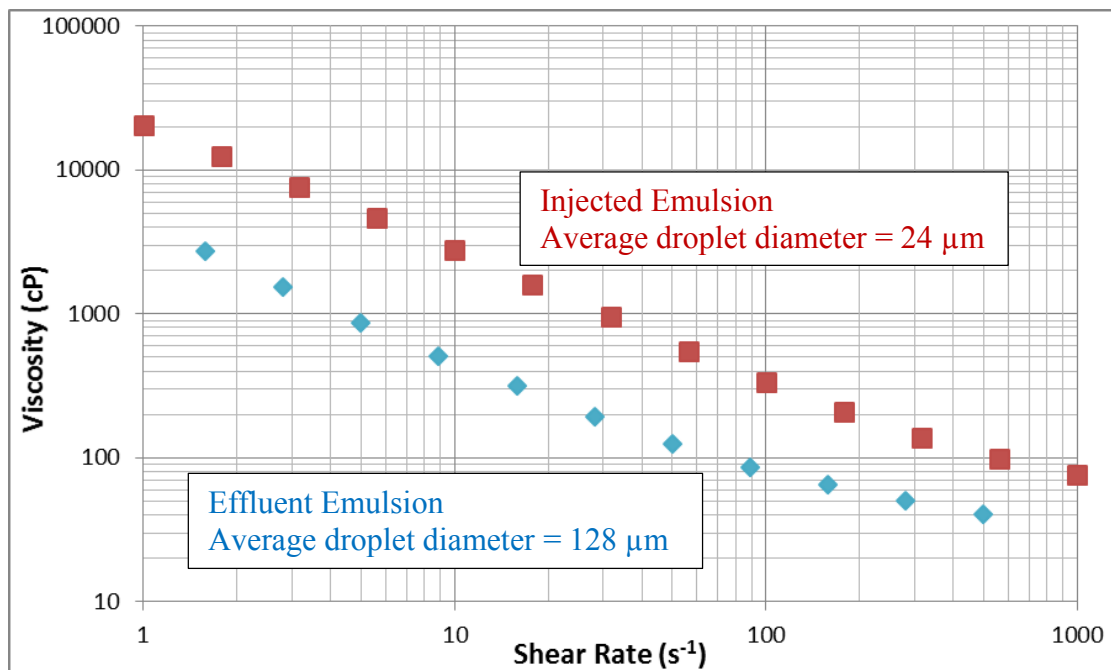
Figure 5.13 The rheology and droplet diameter of the emulsion injected into the core and the effluent emulsion from the Core B experiment.

The effluent emulsion had an average droplet diameter of 128 microns. The emulsion that was injected had an average droplet diameter of only 24 microns. Evidently the droplets of the injected emulsion coalesced into larger droplets as they passed through pore space, or they coalesced into a continuous oil phase which then generated a new

emulsion with 64 micron droplets as it flowed along with the nanoparticle dispersion in the core. The smaller viscosity of the effluent emulsion is consistent with the larger droplet size. The viscosity of the injected emulsion at 123 s^{-1} (the shear rate in Core B) was approximately 320 cP. The viscosity of the effluent emulsion at 123 s^{-1} was approximately 70 cP. During the emulsion injection the apparent viscosity was between 100 to 250 cP although the pressure drop never reached steady state when emulsion was being injected into the core. The apparent viscosity in the core was in between the injected emulsion viscosity and the effluent emulsion viscosity. Interestingly the apparent viscosity during the injection of nanoparticle dispersion (after 6 PV) was steady at 50 cP. This is much larger than the viscosity of the dispersion. This is consistent with the injected dispersion channeling through the more viscous fluids in the core (mineral oil, emulsion) to establish aqueous phase flow at a large residual saturation of non-aqueous phases. This is consistent with the appearance of only the aqueous phase in the effluent during this period, with occasional small volumes of emulsion whose production may correspond to the spikes in apparent viscosity.

Experiments E and B show that the injected emulsion can be broken and regenerated into new emulsion with larger droplets while flowing through a core. Given the observation in the beadpack emulsion generation experiments of Chapter 3 that fluids must reach a critical shear rate to generate stable emulsion, it is natural to speculate that Experiments E and B were conducted below an analogous critical shear rate for maintaining an emulsion. In Chapter 4 when emulsion was injected below the critical shear rate and coalesced in the beadpack, stable emulsion was not regenerated because the shear rate was not high enough. The Core C experiments (Figures 5.14, 5.15, and

5.16) were intended to determine whether a critical shear rate existed to maintain emulsion stability in the core. Emulsion was injected into the core at several different flow rates. As discussed next, at low shear rates the emulsion completely coalesced. As the shear rate was increased the amount of stable emulsion in the effluent also increased.

Emulsion was initially injected into Core C at 0.1 mL/min. Figure 5.14 shows the results of the experiment. The pressure drop continued to build throughout the duration of the experiment even though stable emulsion was not present in the effluent. This same behavior was seen in almost every beadpack experiment in Chapter 4. One possibility is that the same transition between two constant states hypothesized in Chapter 4 is occurring. In the first state all of the droplets are coalescing and the effluent consists of two separate phases; during this time the pressure in the beadpack is steadily building. This is similar to the pressure response and effluent in Core C. Another possible explanation of the pressure increase is that emulsion droplets that remained stable in the core were unable to pass through some pore throats, plugging them and reducing the permeability of the core. Other droplets coalesced, and only the separate mineral oil and dispersion phases were produced in the effluent. The phase ratio of the effluent was approximately the same as the phase ratio of the injected emulsion (66% mineral oil by volume). This shows that if emulsion droplets are being trapped in the pores the emulsion in the core is at approximately the same volume fraction as the injected emulsion.

151

Core C-1 – Boise Core					
k (mD)	ϕ	Pore Volume (mL)	Initial Saturation	Flow Rate (mL/min)	Shear Rate (s^{-1})
690	0.28	44	$S_w=1$	0.1	11
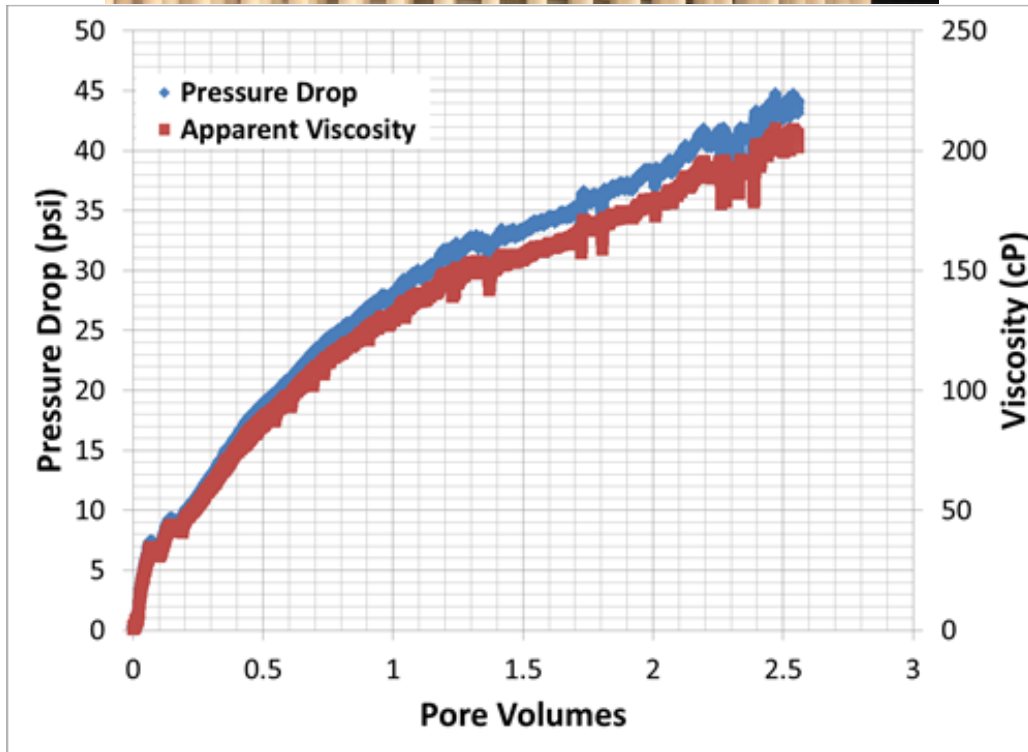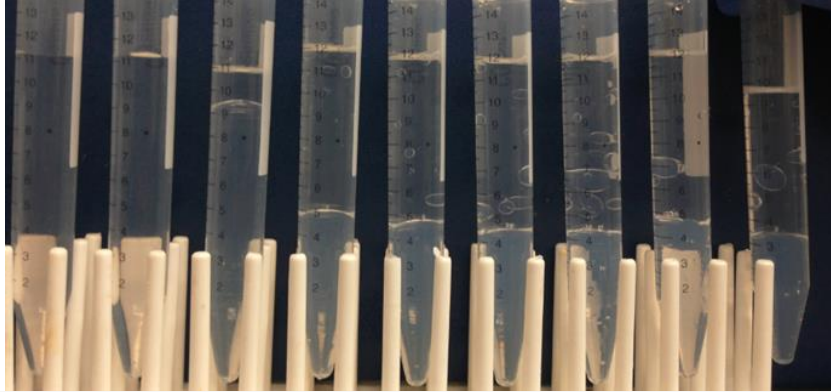
Figure 5.14 The experimental conditions, effluent, pressure drop and apparent viscosity of the emulsion injection into Core C at 0.1 mL/min.   Each tube contains 12 mL or 0.27 PV.

152

The flow rate of the emulsion was increased from 0.1 mL/min to 1 mL/min in the next stage of the Core C experiment (Figure 5.15). When the injection rate was increased there were two different fluids in the core for certain and possibly three: aqueous nanoparticle dispersion, mineral oil, and possibly some emulsion. The initial saturation was estimated by the effluent from Figure 5.14. A majority of the water (70%) originally in the core was displaced by the emulsion. The phase saturation in the core after the 0.1 mL/min injection was estimated by assuming that the water that was displaced from the core was replaced with the mineral oil and nanoparticle dispersion in the same proportion as they appear in the the effluent in Figure 5.14, i.e. the pore space that was occupied by the displaced water is now occupied by 66% mineral oil and 34% nanoparticle dispersion. Figure 5.15 shows the results of the experiment. When the emulsion was injected at 1 mL/min a very small amount of stable emulsion was produced in the effluent. Majority of the emulsion that was injected into the core coalesced even at the larger shear rate, 106 s^{-1}. The pressure drop continued to increase until approximately two pore volumes when the pressure drop stabilized.

Core C-2 – Boise Core						
k (mD)	ϕ	Pore Volume (mL)	Initial Saturation		Flow Rate (mL/min)	Shear Rate (s^{-1})
690	0.28	44	S_w=0.54	S_o=0.46	1	106

Figure 5.15 The experimental conditions, effluent, pressure drop and apparent viscosity of the emulsion injection into Core C at 1 mL/min, following the injection of 2.5 PV of emulsion at 0.1 mL/min (Figure 5.13). Each tube contains 12 mL or 0.27 PV.   See text for estimation of initial saturations.

154

In the next stage of the Core C experiment (Figure 5.16) the emulsion was injected at 2 mL/min to see if more stable emulsion would be produced in the effluent. Based on the effluent observed during injection at 1 mL/min, the core contained three different phases when the flow rate was increased: nanoparticle dispersion, mineral oil, and stable emulsion. Using the same analysis as above for the 1 mL/min stage of injection, the estimated phase saturations after the 1 mL/min stage are about the same as after the 0.1 mL/min stage. The difference is that that some stable emulsion occupied the pore space previously occupied by both mineral oil and nanoparticle dispersion. The initial saturation when injection at 2 mL/min began was estimated from the effluent of the previous experiment by assuming that the core now had 8% stable emulsion in addition to mineral oil and nanoparticle dispersion. It was assumed that this 8% emulsion was 66 % oil by volume.

When the emulsion was injected at 2 mL/min a greater volume fraction of stable emulsion was produced in the effluent compared to lower flow rates. When emulsion was injected at 1 mL/min the amount of emulsion in the effluent, based on steady fractional flow, was approximately 8%. At 2 mL/min, the amount of emulsion in the effluent, based on steady fractional flow, was approximately 25% during the first 1.9 pore volumes. Around 1.9 pore volumes the pressure decreases substantially and then continues to increase. A possible explanation is that some excess nanoparticle dispersion was trapped between two layers of emulsion in the accumulator. When the pressure drop decreases the effluent collected is primarily nanoparticle dispersion, tube 8 from the left in Figure 5.16. As the injection continues the pressure begins to rise again as if emulsion was the fluid injected into the core and the effluent becomes three different

155

phases again: mineral oil, emulsion, and aqueous phase. It is possible that the emulsion and excess nanoparticle dispersion were not given enough time to settle in the accumulator. In Figure 5.12, when all of the emulsion from the accumulator was injected into the core and the nanoparticle dispersion at the bottom of the accumulator was injected the pressure drop stabilized and only nanoparticle dispersion was observed in the effluent. Similar behavior would be expected in Figure 5.16 if only nanoparticle dispersion was injected but it is evident from the effluent and pressure data that most likely emulsion injection resumed after a small amount of nanoparticle dispersion was injected. The amount of emulsion present in the effluent increased when emulsion injection resumed, after the slug of nanoparticle dispersion was injected, to approximately 66 % by volume based on the fractional flow which was an increase from the 25 % during the first 1.9 pore volumes. One possible explanation is that as some emulsion droplets continue to plug pore throats the effective permeability is reduced which would increase the shear rate in the core and produce more stable emulsion from the two bulk phases.

There are several important implications from the experiments performed in Core C (Figures 5.14, 5.15, and 5.16). The dependence of emulsion stability in the core as a function of flow rate was observed. As the flow rate increased the volume fraction of stable emulsion in the effluent and presumably in the core also increased. This has serious implications if emulsions are to be injected to reservoirs. Near the wellbore where shear rates are high the emulsion may remain stable. As the emulsion moves farther away from the well bore the shear rate will decrease and the emulsion may coalesce as a result.

156

The results from Core B, C and E indicate that the coalescence of the injected emulsion must be responsible for a significant portion of the overall pressure drop. This indicates there may potentially be several different contributions to the overall pressure drop: the apparent viscosity of the injected emulsion, flow resistance due to the coalescence process, the apparent viscosity of regenerated emulsion, and multiphase flow of the coalesced oil and aqueous phases.

| Core C-3 – Boise Core						
k (mD)	ϕ	Pore Volume (mL)	Initial Saturation		Flow Rate (mL/min)	Shear Rate (s^{-1})
690	0.28	44	S_w=0.51 $\quad$ S_o=0.41 $\quad$ S_{em}=0.08		2	212
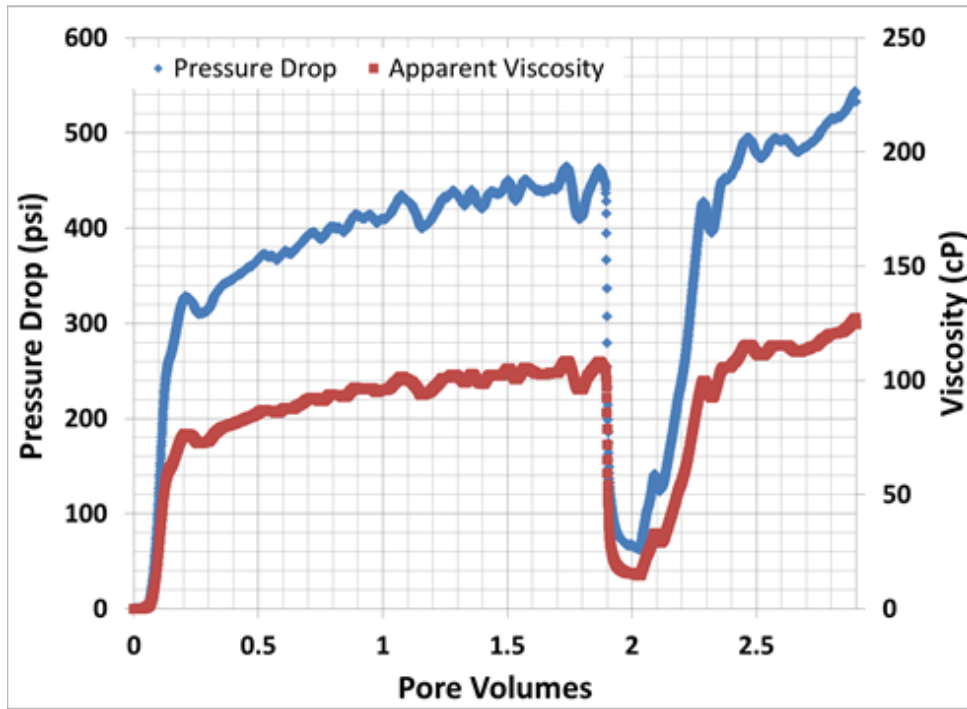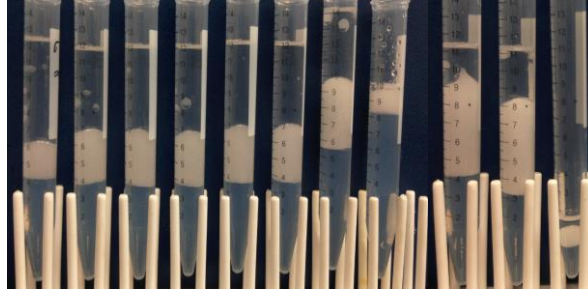
Figure 5.16 The experimental conditions, effluent, pressure drop and apparent viscosity of the emulsion injection into Core C at 2 mL/min, following injection of 3.25 PV at 1 mL/min (cf Figure 5.14). The pressure decrease at 2 PV is attributed to injection of excess nanoparticle dispersion. The subsequent build is from continuing emulsion injection (see text).

In the stages of the Core D experiment (Figures 5.17, 5.18, and 5.19) emulsion was injected into the core at various flow rates to see whether the flow rate affected the average droplet size of the effluent emulsion and to investigate further the effect of shear rate on emulsion stability. The experiments in Cores B and C showed a significant amount of emulsion coalescence in the core and that the effluent emulsion was drastically different than the injected emulsion (larger droplets, smaller viscosity). The hypothesis was that when emulsion was injected into the core at higher flow rates it would produce droplets that were smaller than effluent emulsion produced at lower flow rates. The Core D experiment (Figures 5.17, 5.18, and 5.19) showed that the emulsions display shear thinning behavior in porous media similar to their bulk rheology

The emulsion injected in the Core D experiments was stabilized with an IPA-ST dispersion that was 3 wt% nanoparticles and 2 wt% NaCl. The emulsion was generated in the 180 micron HiP beadpack with mineral oil and the nanoparticle dispersion each flowing at 12 mL/min. The effluent from the beadpack was collected in a container where excess nanoparticle dispersion drained from the emulsion. The average droplet diameter of the emulsion injected into Core D was 22 microns. The container containing the emulsion and excess nanoparticle dispersion was poured into the accumulator, trying to avoid adding the excess nanoparticle dispersion. Because some excess nanoparticle dispersion was poured into the accumulator, it was allowed to settle so that only 100% emulsion was injected into Core D.

The pressure drop across the entire core was measured with one transducer. A second pressure transducer was attached to the pressure taps of the core holder. This

159

transducer measured the pressure drop across a 4" section of the core.   The 4" section that was measured was from the 2" of the core to the 6" of the core.

Mineral oil and brine were injected into the core, prior to the emulsion injection experiments in Core D, at the same phase ratio as the injected emulsion (approximately 66% oil).   This gave a pressure baseline for how the emulsion would flow in the core if it entered the core completely coalesced and did not have any nanoparticles to stabilize emulsion in the core.   The steady state pressure drop for a total flow rate of 1 mL/min co-injection of brine and mineral oil in Core D was 53 psi.

In Figure 5.17 emulsion was injected at two different flow rates.   Initially the emulsion was injected into the core at 1 mL/min.   Less than 5% of the effluent was stable emulsion while flowing at 1 mL/min, based on the fractional flow. During this period the majority of the injected emulsion coalesced, but the pressure drop was much higher than 53 psi.   This indicates that the two separate phases (mineral oil, nanoparticle dispersion) were unlikely to be flowing in the core.   Instead it suggests that emulsion was possibly generated in situ as the phases flowed but was not stable enough to remain in the effluent.   When the flow rate was increased to 2 mL/min the amount of emulsion in the effluent, based on fractional flow, increased to approximately 84% of the effluent. This experiment indicates that a critical shear rate is required to maintain stable emulsion in the effluent.   The increase in shear rate from 99 to 197 s^{-1} resulted in a huge increase in the amount of stable emulsion produced in the effluent, suggesting that for this emulsion and this core, the critical shear rate is between 100 and 200 s^{-1}.   The pressure drop in the 4" section of the core was proportional to the pressure drop across the entire core based on the similar apparent viscosities.   It is evident there is a correlation

160

between the pressure drop behavior and the effluent. When there is no emulsion present in the effluent the pressure drop continues to rise. Conversely, when stable emulsion is steadily produced in the effluent the pressure drop is steady and large. This same behavior was observed in the beadpack experiments in Chapter 4.

In Figure 5.18 the emulsion was injected into the core at 4 mL/min. The initial state of the core was simply the state at the end of the 2 mL/min injection stage. The shear rate in the core was 395 s^{-1}. All of the effluent was stable emulsion. The pressure drop across the core reached a steady-state value within 1 pore volume. The pressure in the core was allowed to dissipate at the end of Figure 5.17 before the experiment in Figure 5.18 was performed. This is why the pressure drop across the core begins at 0 psi prior to emulsion injection.

In Figure 5.19 the emulsion was injected into the core at 8 mL/min. The shear rate in the core was 790 s^{-1}. Similar to the emulsion injection at 4 mL/min, all of the effluent was stable emulsion. The pressure drop across the core stabilized within one pore volume. Similarly, the pressure in the core was allowed to dissipate at the end of Figure 5.18 before the experiment in Figure 5.19 was performed. This is why the pressure drop across the core begins at 0 psi prior to emulsion injection.

161

| Core D-1 – Boise Core					
k (mD)	φ	Pore Volume (mL)	Initial Saturation	Flow Rate (mL/min)	Shear Rate (s⁻¹)
828	0.27	42	Mineral Oil and Brine	1, 2	99, 197
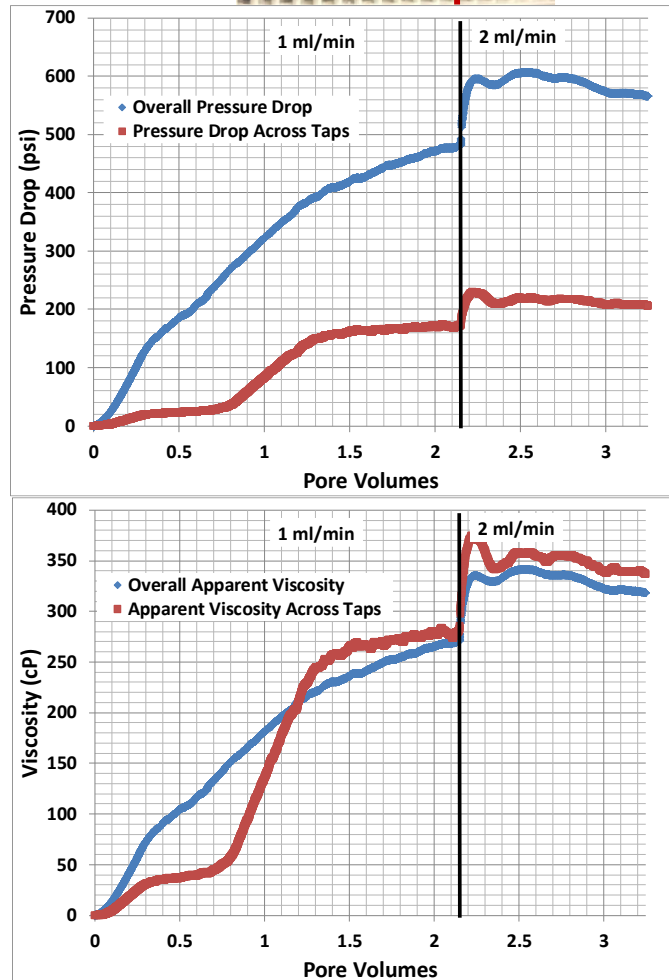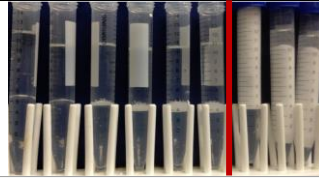
Figure 5.17 The experimental conditions, effluent, pressure drop and apparent viscosity of the emulsion injection into Core D at 1 and 2 mL/min. Red line in photo of effluent indicates change in flow rate.   Each tube contains 13 mL or 0.31 PV.

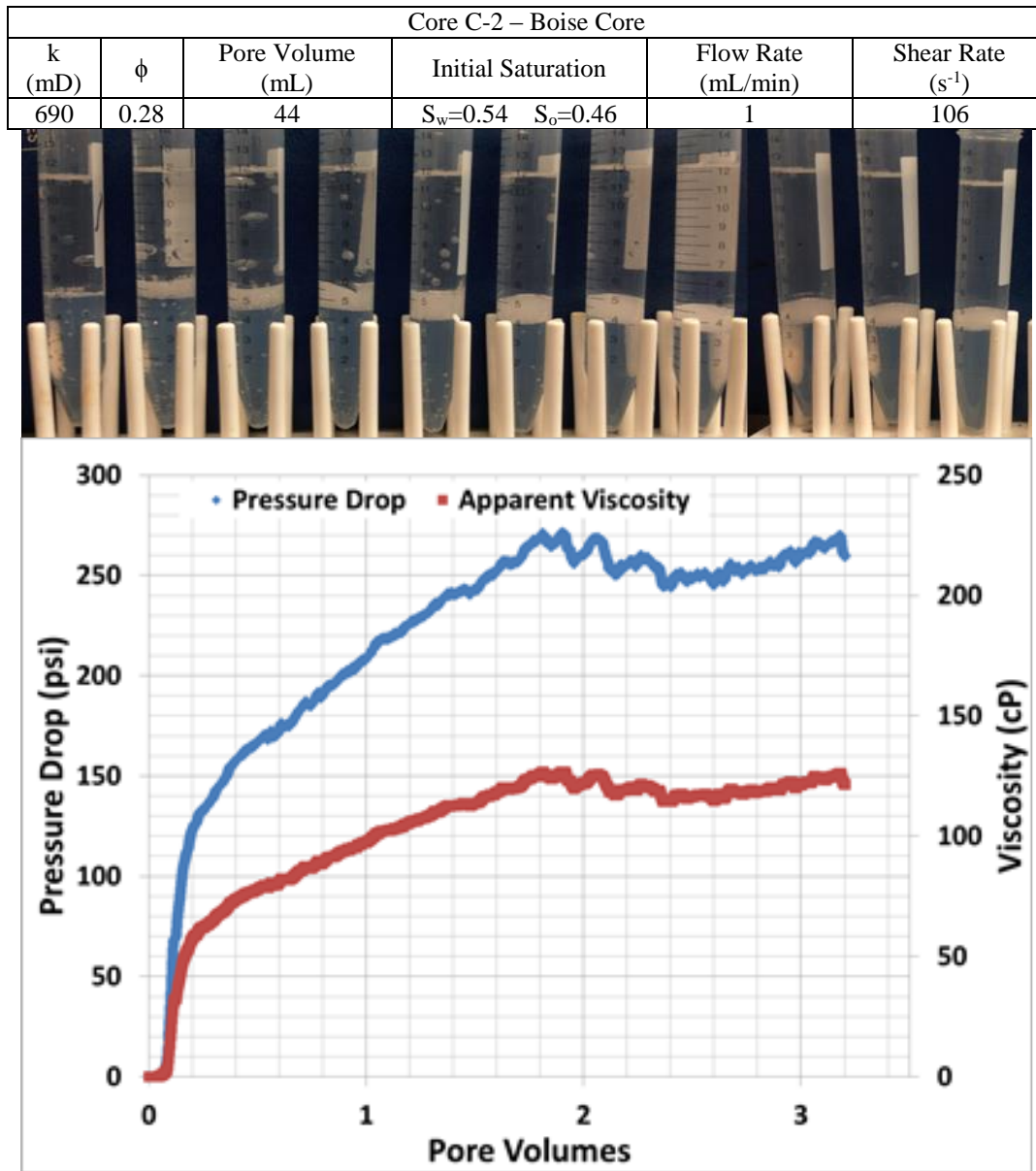| Core D-2 – Boise Core					
k (mD)	ϕ	Pore Volume (mL)	Initial Saturation	Flow Rate (mL/min)	Shear Rate (s^{-1})
828	0.27	42	Emulsion	4	395
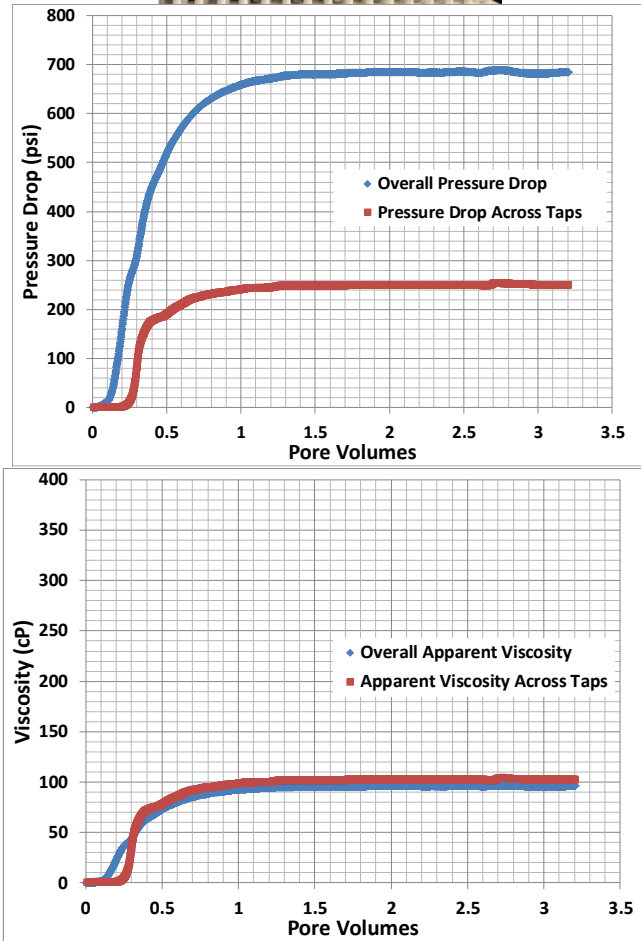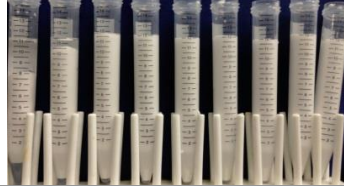
Figure 5.18 The experimental conditions, effluent, pressure drop and apparent viscosity of the emulsion injection into Core D at 4 mL/min, following steady injection of emulsion at 2 mL/min (cf 5.16). Initial saturation estimated that mainly emulsion is present in the core based on effluent history at 2mL/min. Each tube contains 13 mL or 0.31 PV.

Core D-3 – Boise Core					
k (mD)	ϕ	Pore Volume (mL)	Initial Saturation	Flow Rate (mL/min)	Shear Rate (s^{-1})
828	0.27	42	Emulsion	8	790
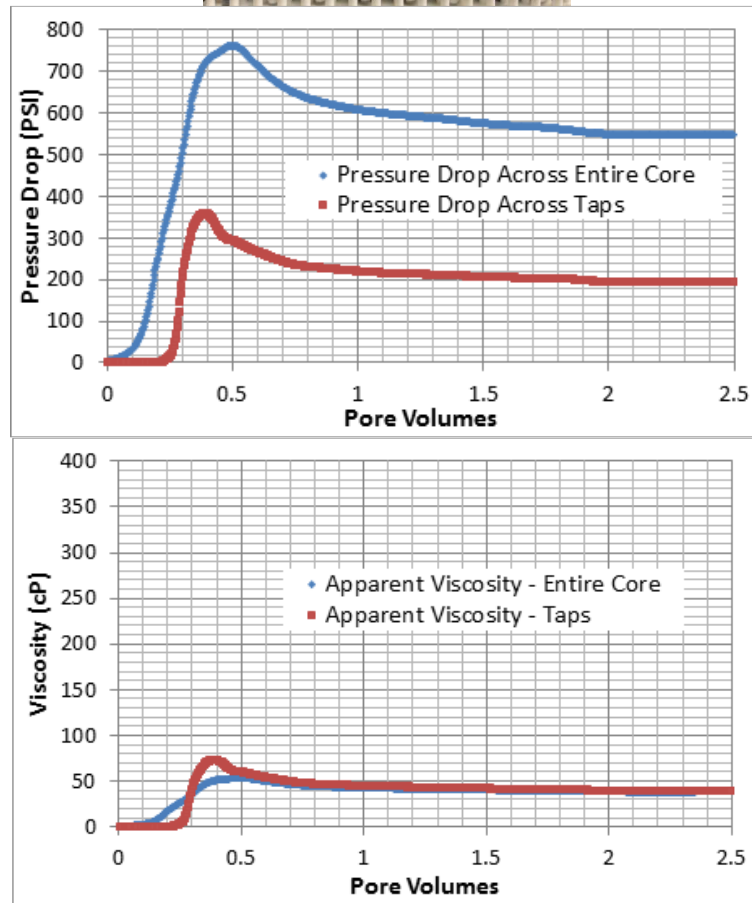
Figure 5.19 The experimental conditions, effluent, pressure drop and apparent viscosity of the emulsion injection into Core D at 8 mL/min. following steady injection of emulsion at 4 mL/min (cf 5.16). Initial saturation estimated that mainly emulsion is present in the core based on effluent history at 4 mL/min. Each tube contains 13 mL or 0.31 PV.

When emulsion was injected at 2, 4, and 8 mL/min the pressure history reached steady-state. As the flow rate was increased, and in turn the shear rate, the apparent viscosity of the emulsion flowing in the core decreased. Assuming the emulsion was the same within the core at all three flow rates, this emulsion showed the same shear thinning behavior in porous media that it did in the rheometer. At shear rates of 197, 395, and 790 s^{-1}, the corresponding emulsion apparent viscosity was 320, 102, and 40 cP. The effluent emulsion rheology (Figure 5.20) and droplet size (Table 5.2) were measured. The average droplet size of the effluent emulsions did not change with flow rate. For all three emulsions the average droplet diameter was approximately 12 microns. The average droplet diameter of the injected emulsion was approximately 22 microns. This supports the hypothesis that the emulsion is coalescing and regenerating new emulsion as it flows through the core. Because the emulsions had approximately the same droplet size, the viscosities of the different emulsions were nearly identical.

At 2 mL/min the apparent viscosity in the core (320 cP) was higher than the injected emulsion bulk viscosity (168 cP) and the effluent emulsion viscosity (85 cP) at the same shear rate. Conversely, at 8 mL/min the apparent viscosity in the core (40 cP) was slightly lower than the effluent emulsion viscosity (48 cP) and lower than the injected emulsion viscosity (76 cP) at the same shear rate. At 4 mL/min the apparent viscosity in the core (102 cP) was between the viscosity of the injected emulsion (113 cP) and the viscosity of the effluent emulsion (78 cP) at the same shear rate. The trend for the in-core rheology was much steeper compared to the rheometer rheology of the bulk emulsions. Evidently the coalescing/regenerating process has different shear rate dependence than just shearing a bulk emulsion. It appears at 2 mL/min that the resistance

165

to flow associated to droplet coalescence contributes to the apparent viscosity in addition to the apparent viscosity of the effluent emulsion and injected emulsion. At 4 mL/min the flow resistance associated with droplet coalescence is much less and contribution to the apparent viscosity in the core is from a combination of effluent droplets and injected droplets flowing through the core. At 8 mL/min the coalescence/regeneration must be much closer to the core inlet because the apparent viscosity is very similar to the effluent emulsion viscosity indicating that the contribution to the apparent viscosity is from the regenerated droplets traveling through the core.
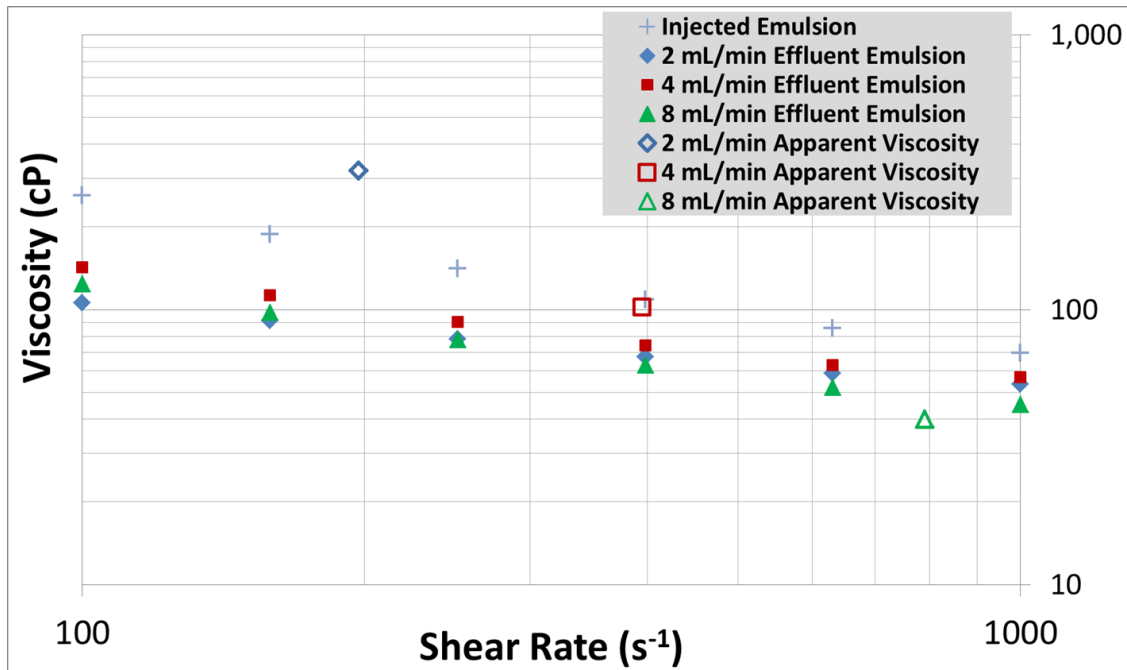
Figure 5.20 The rheology of the effluent emulsions produced from the emulsion injection at different flow rates in Core D.   Apparent viscosities are for the emulsion as it flows through Core D (cf Figs. 5.17, 5.18 and 5.19).

Effluent Emulsion	Average Droplet Diameter (µm)	Shear Rate (s⁻¹)	Apparent Viscosity in Core D (cP)	Effluent emulsion viscosity at equivalent shear rate from rheometer (cP)	Viscosity of injected emulsion at core shear rate (cP)
2 mL/min	13.0	197	320	85	168
4 mL/min	12.4	395	102	78	113
8 mL/min	12.8	790	40	48	76

Table 5.2 The apparent viscosity of the emulsion in Core D and the viscosity of the effluent emulsion from the core measured in the rheometer at equivalent shear rates.

5.5.2 Co-injection versus Emulsion Injection

The experiments in this section were performed to investigate the hypothesis that when emulsion was injected into the core it coalesced and was regenerated. If the injected emulsion completely coalesces within a short distance of the core inlet, then regenerates as the separated phases flow together down the core, the effluent history should be similar to co-injecting the nanoparticle dispersion and oil directly into the core. The injection pressure history should also be similar, with a possible increment due to the flow resistance associated with the coalescence process. A series of corefloods (Cores M, N, O) were performed to test this hypothesis. In Cores M and N a mineral oil-in-water emulsion was injected into the core. After the emulsion was injected, mineral oil and nanoparticle dispersion were co-injected into the core. The co-injection was performed at the same flow rate as the emulsion injection. The two phases were co-injected at the same phase ratio as the emulsion. The rheology and droplet size of the effluent emulsion from both the co-injection and emulsion injection were measured.

For the experiment in Core M, Figure 5.21, the pressure tap was arranged to measure the pressure drop across the first 6 inches of the core (the inlet half of the core). Because the overall pressure drop across the core was also measured, the second half pressure drop was calculated by subtracting the first half pressure drop from the overall pressure drop.

In the Core M experiment, a 69% mineral oil by volume emulsion was injected into the core for approximately 6.2 pore volumes at 2 mL/min (Figure 5.21). The emulsion was generated by co-injecting the same Nyacol DP9711 nanoparticle dispersion, used in the critical shear rate experiments, and mineral oil through the

beadpack at a total flow rate of 24 mL/min with a phase ratio of 69% mineral oil and 31% dispersion. The pumps were then stopped and the injection pressure was allowed to dissipate. Then mineral oil and nanoparticle dispersion were co-injected into the core. Mineral oil was injected at 1.38 mL/min and the nanoparticle dispersion was injected at 0.62 mL/min. Before injecting the emulsion and co-injecting the nanoparticle dispersion a baseline pressure drop was measured by co-injecting mineral oil at 1.38 mL/min and brine at 0.62 mL/min. The steady state apparent viscosity of the brine and mineral oil co-injection was 53 cP.

The overall pressure drop across Core M continued to rise throughout the emulsion injection and the co-injection. The same amount of effluent emulsion (Figure 5.22) was produced from the emulsion injection and the co-injection, approximately 72% of the effluent based on fractional flow (instantaneous, average). During the emulsion injection the apparent viscosity in the first half of the core is increasing at a higher rate than the apparent viscosity in the second half of the core. During co-injection the apparent viscosity in the second half of the core increases at a higher rate in the first half of the core until the two apparent viscosities reach the same value and begin to increase at the same rate. There are clear oscillations during the co-injection (though not periodic) in the co-injection stage while the emulsion injection is remarkably steady in comparison. It is possible that the smaller droplets from the injected emulsion are contributing to the creation of the larger droplets during the emulsion injection, while during the co-injection the droplets are formed as droplets from the oil phase are snapped off into the aqueous phase. The difference in behavior could simply be from a change in flow regime, i.e. the qualitative difference between emulsion injection and co-injection. Moreover similar

fractional flows of free oil phase and free dispersion phase (either from coalescence of injected emulsion or from un-emulsified co-injected phases) are apparent in the effluent for both stages of the experiment.

Despite clear differences in the pressure gradients within the core when emulsion is injected versus when oil and dispersion are co-injected, the emulsion injection and co-injection produced the same emulsion, as shown by measurements of rheology and droplet size of the emulsions produced by each stage of injection. The properties of effluent emulsion for the emulsion injection and co-injection were nearly identical. The effluent emulsion from the emulsion injection and from the co-injection both had an average diameter of 118 microns (Figure 5.24). In contrast, the injected emulsion had an average droplet diameter of 22 microns. The two effluent emulsions also have nearly identical rheology. In the plot of viscosity versus shear rate the effluent emulsions overlap for the entire range of shear rates, while the injected emulsion exhibits significantly larger viscosity at any given shear rate Figure 5.23. The results of Experiment M strongly indicate that emulsions coalesce completely when injected into this sandstone, but a new emulsion can be generated from the coalesced phases as they flow within the core. This is very similar to behavior in the bead pack experiments reported in Chapter 4. However the apparent viscosity of the fluids within the core exhibits qualitatively different behavior when an emulsion is injected versus when the constituent phases are co-injected.

For the emulsion injection, the apparent viscosity in the second half of the core is approximately the same as two phase flow of mineral oil and brine. It is also similar to the viscosity of the produced emulsion at the same shear rate. This suggests that

regenerated emulsion established in the second half of the core early on, presumably from a process still working its way through the first half of the core.

During co-injection, emulsion generation is occurring throughout the core because of the large pressure gradient that exists from the first stage of emulsion injection.   The rate of increase in the pressure gradient in the first half of the core is smaller compared to the emulsion injection because there is no flow resistance from the emulsion coalescence process during co-injection.

Core M – Boise Core					
k (mD)	ϕ	Pore Volume (mL)	Initial Saturation	Flow Rate (mL/min)	Shear Rate (s^{-1})
655	0.29	42	Mineral Oil and Brine	2	222
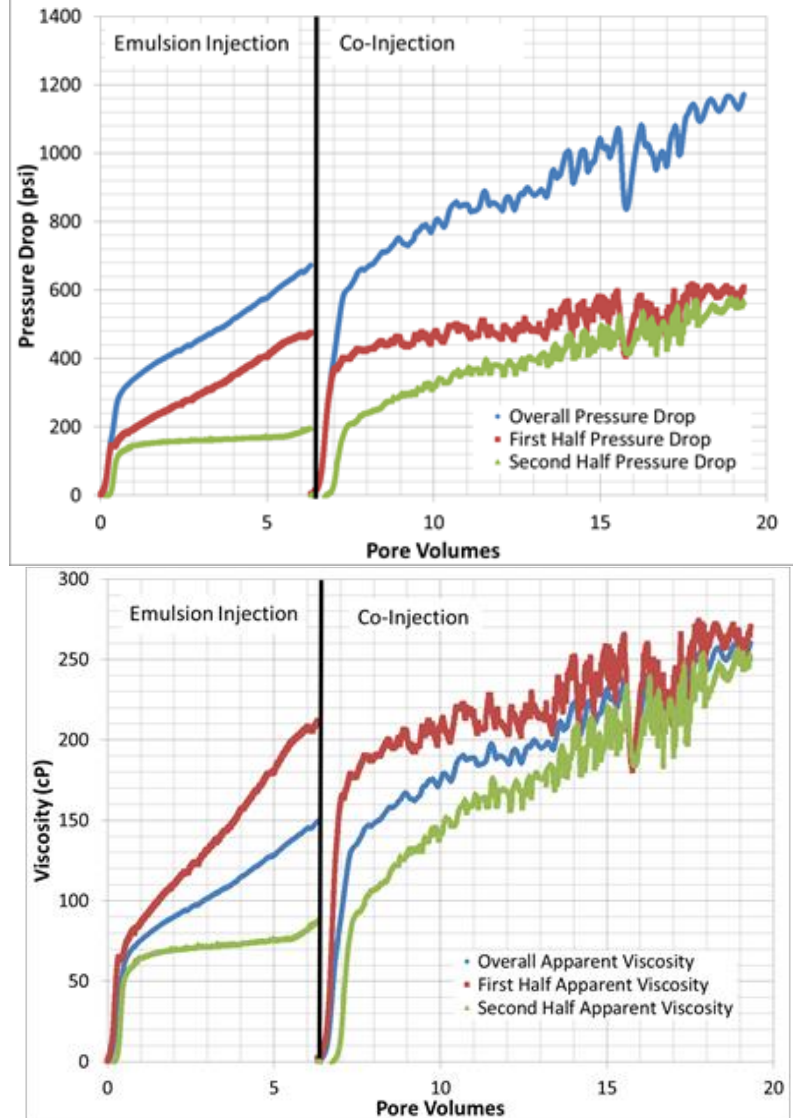
Figure 5.21 Experimental conditions, pressure data, and apparent viscosity for the emulsion injection/co-injection experiments in Core M. The core initially contained mineral oil and brine from the baseline co-injection of those phases (see text).
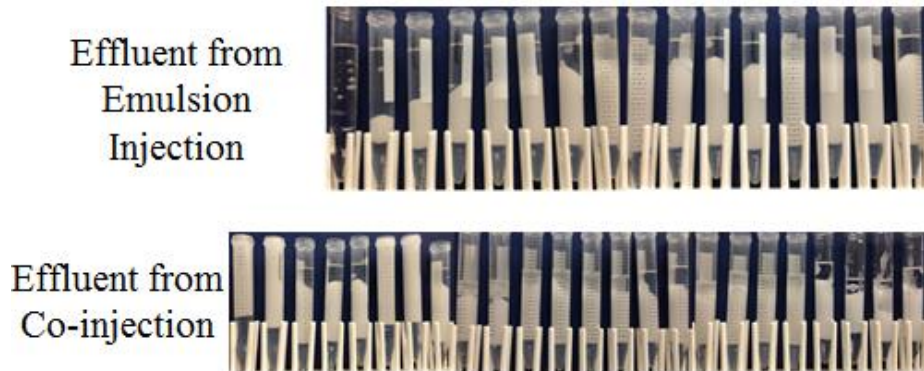
Figure 5.22 Images of the effluent from the emulsion injection and the co-injection in Core M. The same amount of emulsion was produced in both experiments. Each tube contains approximately 12 mL or 0.29 PV.
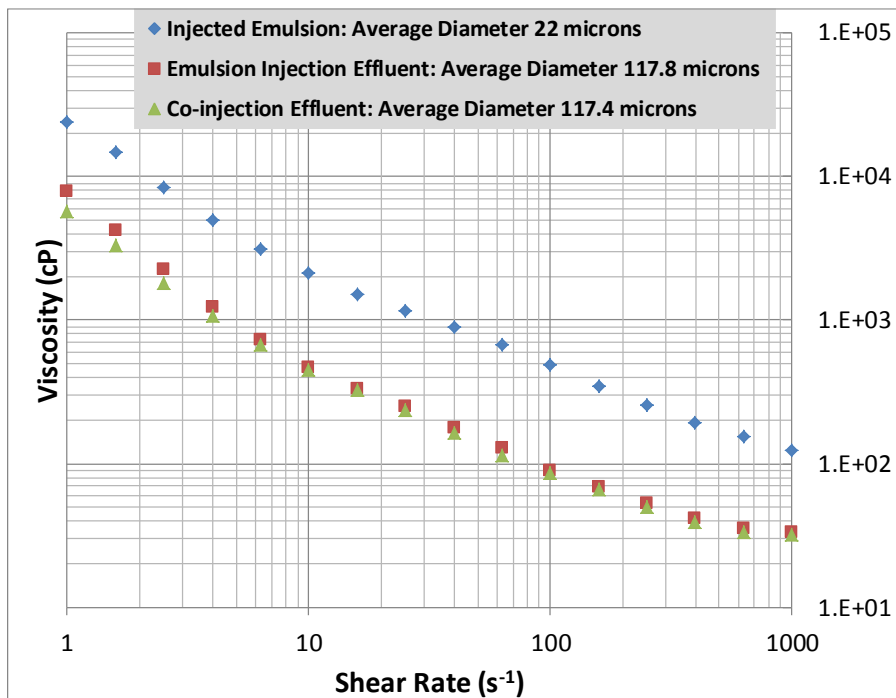
Figure 5.23 The rheology and droplet size of the two effluent emulsions from Core M. The rheology of the emulsion prior to injection is also shown.

Emulsion	Injected Emulsion	Emulsion Injection Effluent	Co-injection Effluent
Average Droplet Diameter (μm)	22.0	117.8	117.4
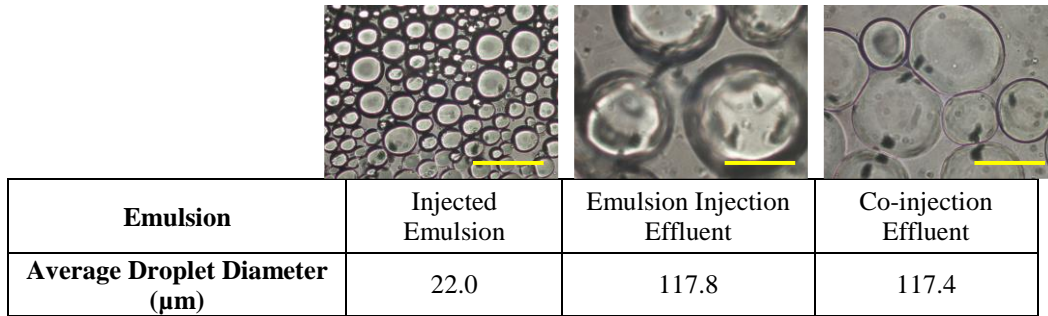
Figure 5.24 Microscopic images of the effluent emulsions and the injected emulsion from Core M experiments. The yellow line in the droplet images is a scale bar of 100 microns.

The experiments performed in Core M were replicated in Core N (Figure 5.25). The same 69% mineral oil by volume was first injected into Core N. Following the emulsion injection, the nanoparticle dispersion and mineral oil were co-injected through the core at using the same phase ratio and flow rate as the emulsion injection. The pressure tap was moved to measure the pressure drop across the first 2" of the core. The pressure drop across the last 10" of the core was calculated by subtracting the pressure drop across the first 2" of the core from the overall pressure drop.

The emulsion was injected at 2 mL/min for approximately 7.5 pore volumes (Figure 5.25). The apparent viscosity across the entire core continued to increase for the first 5 pore volumes before stabilizing. The amount of stable emulsion produced in the effluent was constant throughout the emulsion injection. Approximately 40% by volume of the effluent was stable emulsion. There were differences in the pressure histories and effluent emulsions from the experiments in Core N and M. In Core N the apparent viscosity across the first 2" of the core was steady, while the apparent viscosity across the

first 6" of the core was increasing for the emulsion injection. The apparent viscosity was building in the second 10" of Core N but was steady in the second 6" in Core M. The apparent viscosity in Core N stabilized but never did in Core M.

After injecting the prepared emulsion, mineral oil and the nanoparticle dispersion were co-injected through the core. The apparent viscosity for the co-injection returned to approximately the same stabilized apparent viscosity for the emulsion injection. As the co-injection continued the apparent viscosity became very regular and periodic. This was the first time this type of pressure history was seen in the core. The regular, periodic behavior was seen in several of the emulsion injection beadpack experiments showing this was not an inherent effect of the beadpack system.

The effluent from the co-injection differed from the effluent of the emulsion injection in several ways. The effluent from the co-injection was approximately 78% stable emulsion by volume compared to only 40% stable emulsion by volume for the emulsion injection effluent based on the instantaneous, average fractional flow (Figure 5.26). This was a different result than the effluent from the experiments in Core M, where the emulsion injection and co-injection yielded approximately the same amount of stable emulsion by volume (Figure 5.22). The effluent emulsion during the emulsion injection had an average diameter of 134 microns. The effluent emulsion during the co-injection had an average droplet diameter of 27 microns. This contrasts sharply with Experiment M, in which droplet sizes were the same for both emulsion injection and for co-injection. The rheology of effluent emulsions was slightly different, even though the droplet sizes were very different. From the plot of viscosity versus shear rate in Figure 5.27, the effluent emulsion from the co-injection was slightly more viscous than the

175

effluent emulsion from emulsion injection at shear rates from 1 to 10 s^{-1}. The two effluent emulsion viscosities overlap at 10 s^{-1}, with the effluent emulsion during emulsion injection becoming more viscous at shear rates between 10 to 1000 s^{-1}. Although the effluent emulsion during co-injection had a much smaller droplet size, the viscosity behavior in Figure 5.27 was similar to an emulsion with a much larger droplet size. The variance in the droplet size distribution is the most probable explanation for this rheology behavior. While the emulsion had an average droplet diameter of 26.8 microns, the emulsion had a wide distribution of different droplet sizes including a significant number of droplets with diameters larger than 100 microns. These large droplets must have been the controlling factor in the emulsion rheology and the reason the emulsion had a lower viscosity than an emulsion with an average droplet diameter of 26.8 microns with a normal distribution of droplets. The large size range of droplets can be seen in the microscopic image of the co-injection effluent (Figure 5.28).

The results in Core M and N were different even though the same procedure was used. The differences may have been caused by the propagation of an emulsion coalescence/regeneration front that slowly propagates throughout the core. The slow advance of the front causes the pressure to increase in certain sections. The increase in pressure at the front is due to the resistance to flow arising from the process of coalescence and emulsion regeneration. When the front exits the core the pressure stabilizes. The difference in the speed of the front in Cores M and N contributed to the difference in pressure response which may have been caused by the heterogeneities of the two cores.

176

Core N – Boise Core					
k (mD)	ϕ	Pore Volume (mL)	Initial Saturation	Flow Rate (mL/min)	Shear Rate (s^{-1})
720	0.29	44	$S_w=1$	2	206
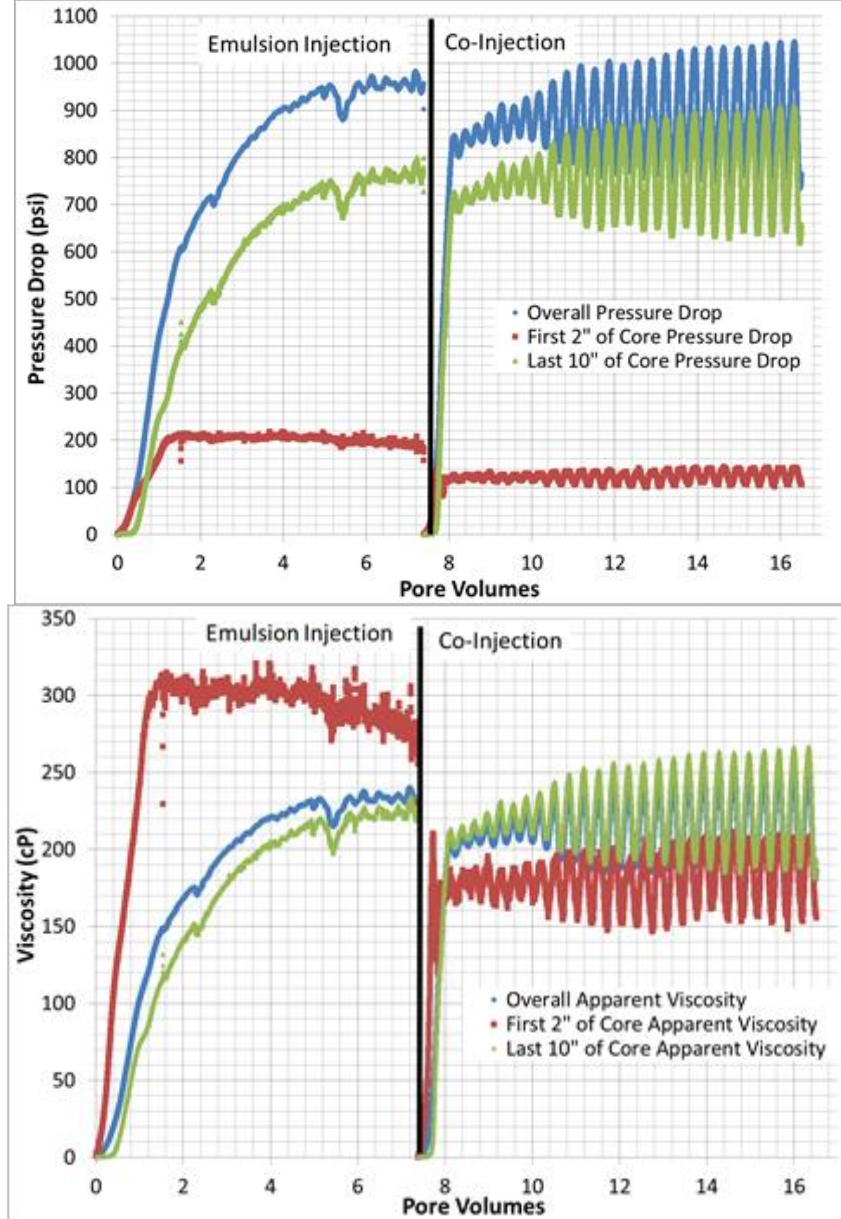
Figure 5.25 Experimental conditions, pressure data, and apparent viscosity for the emulsion injection/co-injection experiments in Core N.

177

Figure 5.26 The effluent from the co-injection and emulsion injection experiment in Core N.
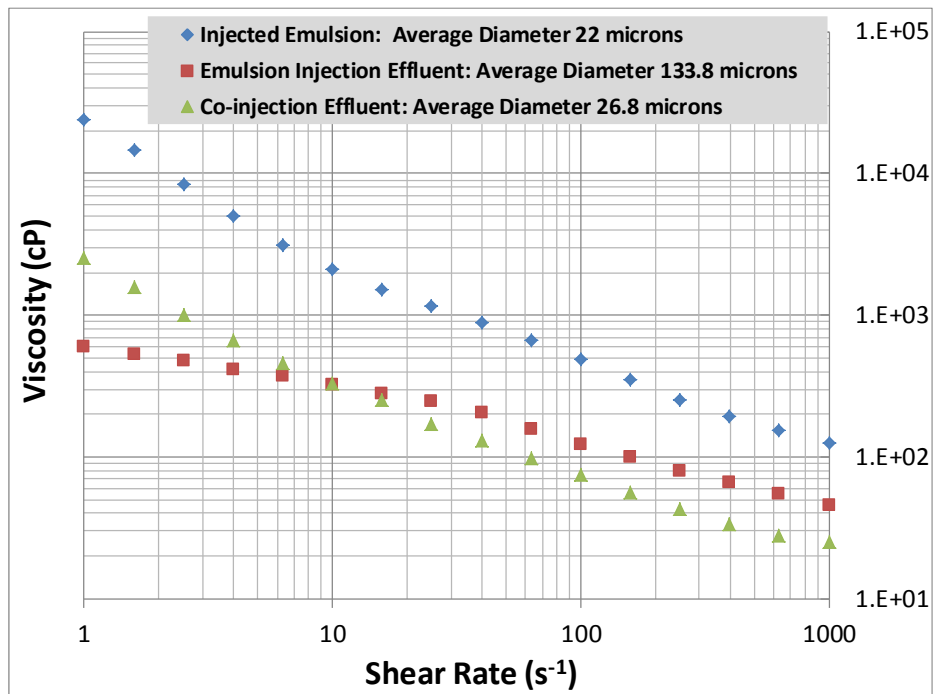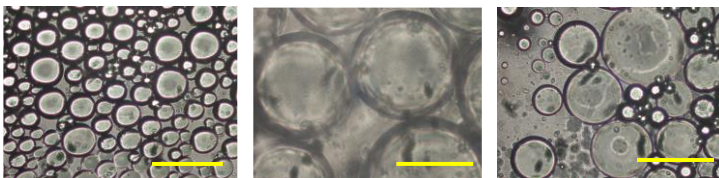
Figure 5.27 The rheology and droplet size of the two effluent emulsions from Core N. The rheology of the emulsion prior to injection is also shown.

Emulsion	Injected Emulsion	Emulsion Injection Effluent	Co-injection Effluent
Average Droplet Diameter (µm)	22.0	133.8	26.8

Figure 5.28 Microscopic images of the effluent emulsions and the injected emulsion from Core N experiments. The yellow line in the droplet images is a scale bar of 100 microns.

In the Core O experiment (Figure 5.29) the nanoparticle dispersion and mineral oil were co-injected into the core first. Following the co-injection, emulsion was injected into the core. Thus the sequence of fluids injected in the Core O experiment is reversed for the experiments in Cores M and N. The nanoparticle dispersion and mineral oil were co-injected at the same flow rate and phase ratio as the emulsion.   The injected emulsion was 69% oil by volume and was injected at 2 mL/min. This was the same emulsion used in the Core M and Core N experiments. For the co-injection, mineral oil was injected at 1.38 mL/min and the nanoparticle dispersion was injected at 0.62 mL/min.   The mineral oil and nanoparticle dispersion were co-injected for approximately 7 pore volumes.   The emulsion was injected for approximately 5 pore volumes following the co-injection.

In Figure 5.29 the apparent viscosity gradually increased for the entire duration of the co-injection.   The fractional flow of stable emulsion in the effluent was about 75% during co-injection. (Figure 5.30).   The apparent viscosity for the emulsion injection increased for the entire duration of the experiment, except in the first 2" of the core where

179

the apparent viscosity appeared to stabilize indicating the advancing of a front which then propagated through the 2nd 10" of the core. The apparent viscosity for the emulsion injection increased rapidly in first 2" of core but stabilized after about 2 PV for emulsion injection, indicating the slow passage of a front through that section. Consistent with the slow movement of a front, around 10 PV a similar rapid increase in apparent viscosity began in the 2nd 10" of the core. This increase coincides with the stabilization of viscosity in the first 2" of the core. This indicates the coalescence of injected emulsion is a high-resistance-to-flow process compared to generating an emulsion from the two continuous bulk phases. The fractional flow of stable emulsion in the effluent for the emulsion injection was approximately 75 % by volume, similar to the co-injection effluent (Figure 5.30). The average droplet diameter of the effluent emulsions was approximately the same. The average droplet diameter of the effluent emulsion from the co-injection was 119.6 microns. The average droplet diameter of the effluent emulsion from the emulsion injection was 135.4 microns. The microscopic images and droplet diameters are summarized in Figure 5.32. Because of the slightly smaller droplet diameter, the effluent emulsion from the emulsion injection was slightly more viscous than the effluent emulsion from the co-injection (Figure 5.31).

For the emulsion injection in Core M the apparent viscosity in the first 6" of the core increased steadily. This was similar to Core N where the apparent viscosity in the first 2" of the core increased rapidly and stabilized within 2 PV. This coincides with the slow movement of a coalescence/regeneration front that propagates through the core. The apparent viscosity was higher near the inlet because of the resistance to flow from injected droplet coalescence. Conversely, the apparent viscosity in the in the first 2" of

180

Core O was similar to the apparent viscosity in the last 10" after 1 PV had been co-injected. Because there were no injected droplets that contributed to the apparent viscosity near the core inlet, the apparent viscosity was similar throughout the entire core for the co-injection in Core O. When there was already emulsion present in the core and emulsion injection or co-injection resumed, the apparent viscosity would increase at a much higher rate compared to when the first injection began into a brine saturated core for the experiments in Core M, N, and O.

Core O – Boise Core					
k (mD)	ϕ	Pore Volume (mL)	Initial Saturation	Flow Rate (mL/min)	Shear Rate (s^{-1})
710	0.29	42	$S_w=1$	2	207
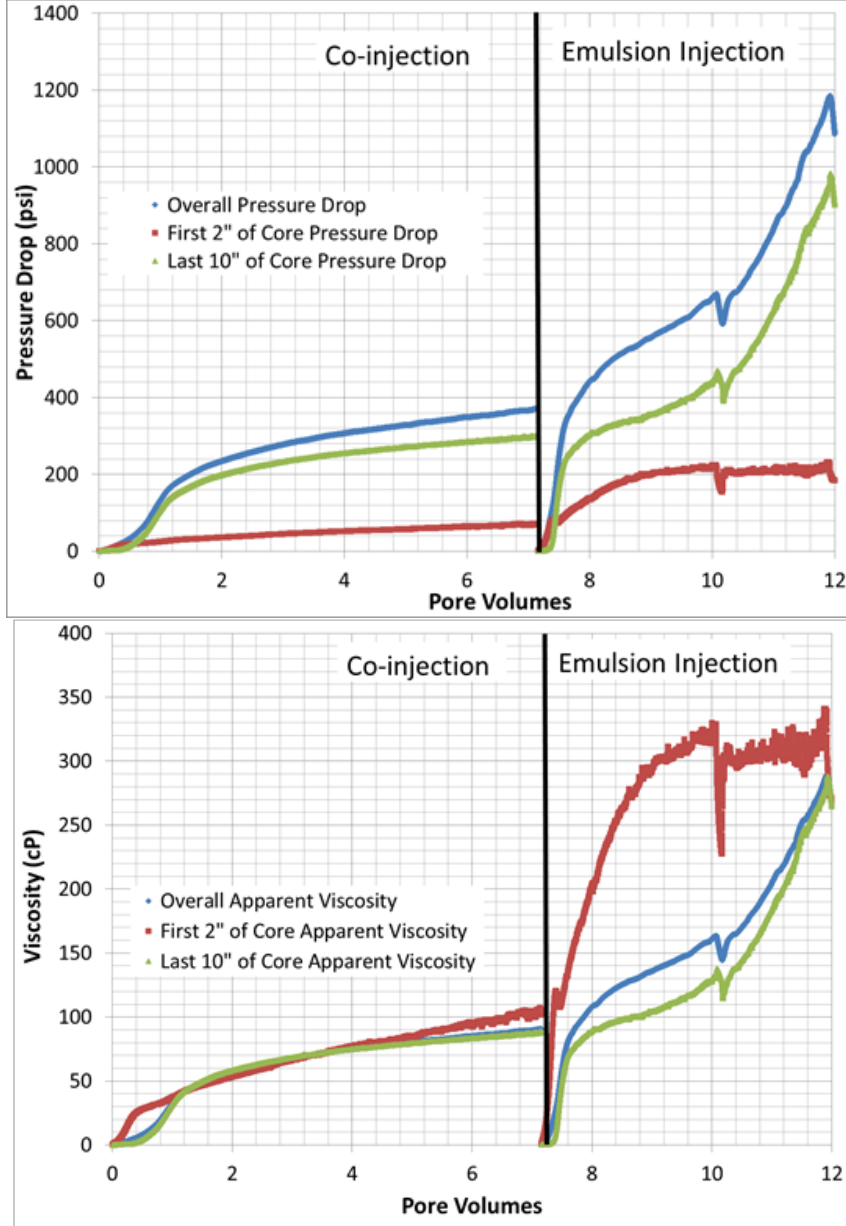
Figure 5.29 Microscopic images of the effluent emulsions and the injected emulsion from Core O experiments.

182

Figure 5.30 The effluent from the co-injection and the emulsion injection in Core O. Each tube contains 12 mL or 0.29 PV.
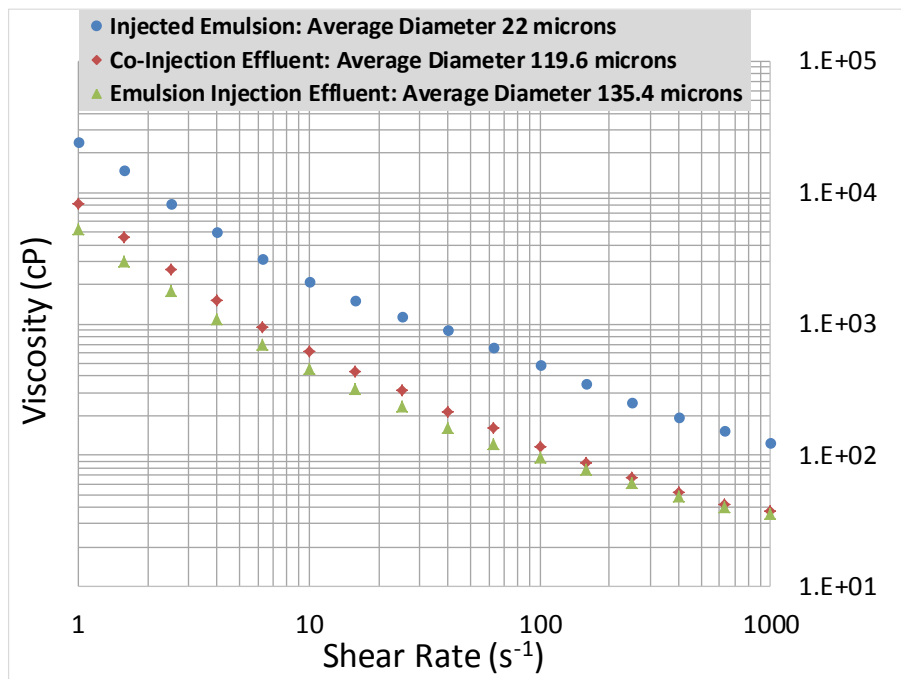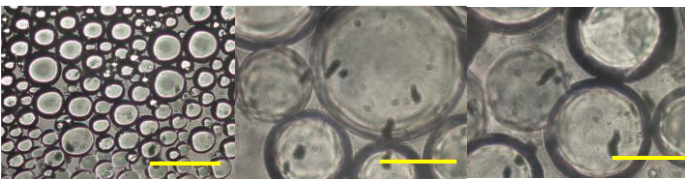
Figure 5.31 The rheology and droplet size of the two effluent emulsions from Core O. The rheology of the emulsion prior to injection is also shown.

Emulsion	Injected Emulsion	Emulsion Injection Effluent	Co-injection Effluent
Average Droplet Diameter (µm)	22.0	135.4	119.6

Figure 5.32 Microscopic images of the effluent emulsions and the injected emulsion from Core O experiments. The yellow line in the droplet images is a scale bar of 100 microns.

5.5.3 Oil Recovery Experiments

The experiments in Cores B, C, D, E, M, N and O indicate that nanoparticle stabilized emulsions are coalescing, most likely breaking entirely, as they flow through a core, and often (but not always) regenerating an emulsion. An important implication of this phenomenon is that such emulsions could be used to deliver recovery-enhancing fluids (in this case, an organic phase miscible with crude oil) to parts of a reservoir containing residual oil. The experiments in Cores P, Q and T were performed to test this implication: emulsions were injected into Boise sandstone core containing residual oil and the amount of oil produced was measured.

5.5.3.1 Mobile oil recovery with emulsion

The experiment in Core P was performed to see if an octane-in-water emulsion could be used to recover mineral oil, the premise being that coalesced droplets of octane

184

could mix with mineral oil droplets forming a bank of less viscous mobile oil phase that would flow ahead of the emulsion (or ahead of the phases coalesced from the emulsion). A water flood, following emulsion injection, would be able to displace majority of the octane from the coalesced emulsion because brine is more viscous than octane. Based on observations of the experiments in Cores E, D, and C of a critical shear rate for maintaining (or continually regenerating) an injected emulsion, the octane-in-water emulsion was injected through the core at a low flow rate in order to break the emulsion and avoid regeneration. This would offer the best chance creating an oil bank inside the core as the octane from the broken emulsion miscibly displaced the more viscous mineral oil.

An initial control experiment was performed. First, mineral oil was injected into the core to reach residual water saturation. The core was then waterflooded with 2 wt% brine to displace the mineral oil. This experiment determined how much mineral oil could be recovered by waterflooding alone. The control waterflood experiment is summarized in Figure 5.33. Because the viscosity of the brine is known, it is possible to infer the relative permeability of the aqueous phase at residual oil saturation, and this is the asymptotic value of k/k_o in the figure. This would correspond to an apparent viscosity of 16.5 cP.

After the waterflood, mineral oil was injected into the core again to reach residual water saturation. The octane-in-water emulsion was then injected at 0.1 mL/min, a flow rate that was shown earlier in this thesis to break a mineral oil-in-water emulsion. The results of the octane emulsion injection are shown in Figures 5.34 and 5.35. The octane emulsion properties are described in Section 3.3.3. A waterflood followed the emulsion

185

injection, to recover remaining octane left in the core. The results of the waterflood are shown in Figure 5.36.

There was approximately 28 mL of mineral oil in the core prior to the waterflood. Approximately 10 mL of mineral oil was recovered in the control waterflood experiment. The orange arrows in Figure 5.35 indicate recovered oil; the rest of the effluent was brine.

Core P-1 – Boise Core - Waterflood to Recover Mineral Oil (Control)						
k (mD)	ϕ	Pore Volume (mL)	Initial Saturation		Flow Rate (mL/min)	Shear Rate (s^{-1})
776	0.28	44	S_{oi}=0.64	$S_{w,irr}$=0.36	3	300

Figure 5.33 The experimental conditions, pressure drop, relative permeability, and effluent of the control waterflood in Core P. Each tube contains 12 mL or 0.27 PV. Orange arrows in the picture of the effluent indicate oil.

187

Core P-2 - Boise Core - Emulsion Injection						
k (mD)	ϕ	Pore Volume (mL)	Initial Saturation		Flow Rate (mL/min)	Shear Rate (s^{-1})
776	0.28	44	S_{oi}=0.64	$S_{w,irr}$=0.36	0.1	10
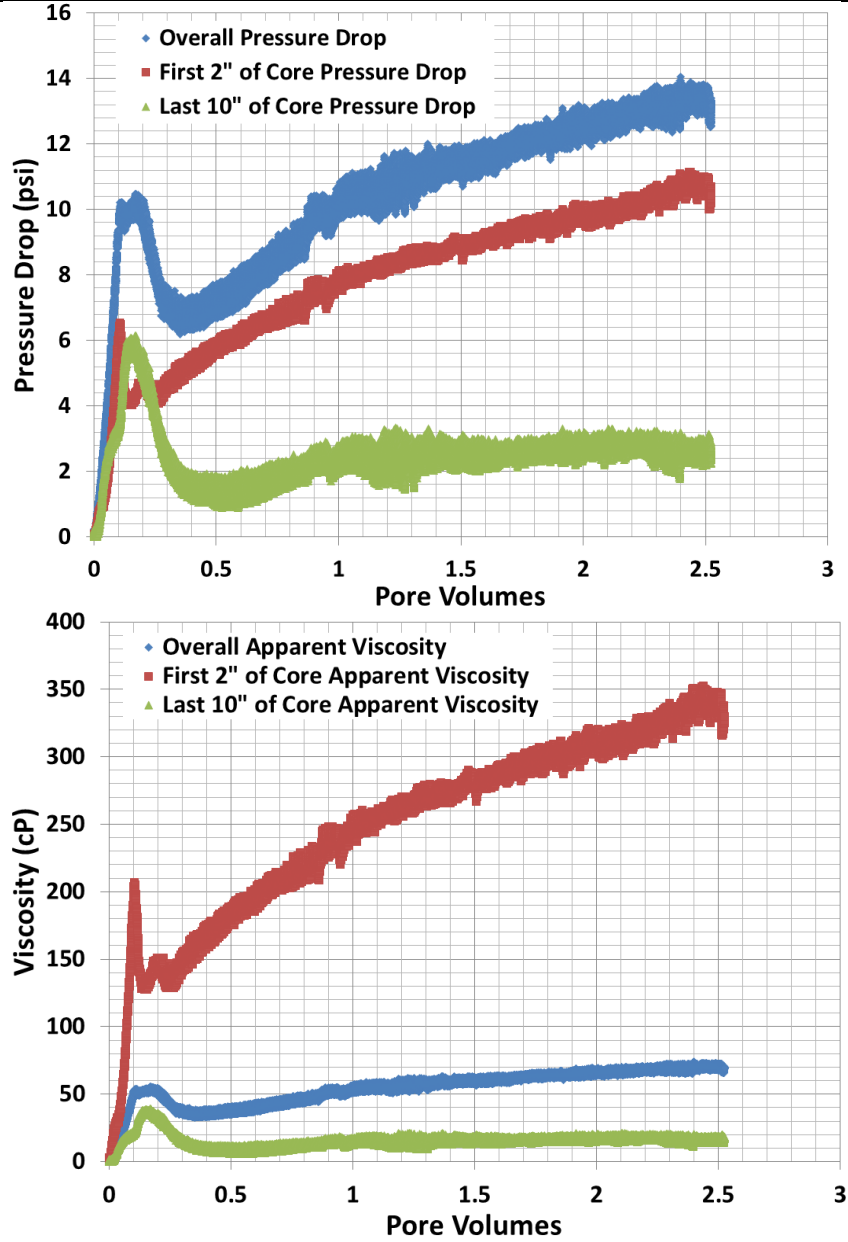
Figure 5.34 Experimental conditions, pressure data, and apparent viscosity of the octane emulsion injection into Core P.

188
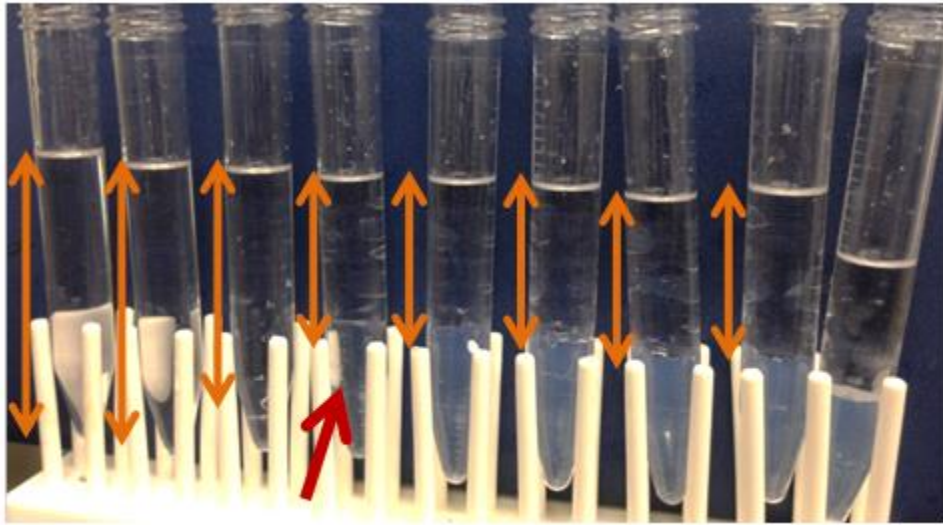
Figure 5.35 The effluent from the octane emulsion injection into core P which contains oil at S_o=0.64. The orange arrows indicate oil displaced from core. Arrival of nanoparticle dispersion is in tube number four indicated by red arrow. No emulsion was produced. Each tube contains 10 mL of effluent or 0.23 PV

There was approximately 28 mL of mineral oil in the core prior to the emulsion injection. Approximately 25 mL, total fluid in first three tubes in Figure 5.35, of oil was recovered before nanoparticle dispersion arrived in the effluent in tube four in Figure 5.35. The recovery of the mineral oil in this case was far more efficient than in the control waterflood, leaving a residual saturation to emulsion $S_{or,e}$ of only 7%. This calculation assumes that none of the 25 mL of recovered oil is octane from the emulsion that coalesced within the core. Qualitatively, it appeared that the emulsion injection yields smaller residual oil saturation than the waterflood but it is difficult to say how much of the oil recovered was injected octane without a more rigorous analysis of effluent oil phase composition.

During the emulsion injection the apparent viscosity in the first 2 inches of the core was at least three times higher than the apparent viscosity in the rest of the core. It is believed that the resistance to emulsion coalescence is the cause of the increase in pressure drop in the first 2" of the core. Another possibility is that some emulsion droplets were trapped in the first 2" of the core causing a reduction in the permeability of the core increasing the apparent viscosity of fluid flowing in that section of the core.

Analysis of the effluent led to the conclusion that some of the octane was trapped inside the core as emulsion droplets or as a residual phase trapped by capillary forces. The injected emulsion was approximately 80% octane by volume. Thus every mL of effluent nanoparticle dispersion corresponds to four mL of octane that must be produced in the effluent or remain within the core. The volume percentage of octane to the overall effluent of broken emulsion was somewhere between 55% and 60% during the steady state fractional flow in tubes 4 thru 8 in Figure 5.35. This indicates that some of the octane was trapped in the core. The follow up waterflood also provided evidence that the octane in the core was trapped as droplets.

The waterflood, after emulsion injection, did not displace any octane from the core and there appeared to be an early breakthrough of brine from the image of the effluent. The first test tube of the effluent in Figure 5.36 is nanoparticle dispersion with a thin film of emulsion above it (less 0.5 mL). The second test tube appears to have a small amount of nanoparticle dispersion because it is not completely clear. The third test tube appears to be all brine by its transparency. The pressure drop and relative permeabilities of the two waterfloods are nearly identical.

Core P-3 – Boise Core - Waterflood to Recover Octane						
k (mD)	ϕ	Pore Volume (mL)	Initial Saturation		Flow Rate (mL/min)	Shear Rate (s^{-1})
776	0.28	44	S_o=0.52	S_w=0.48	3	300
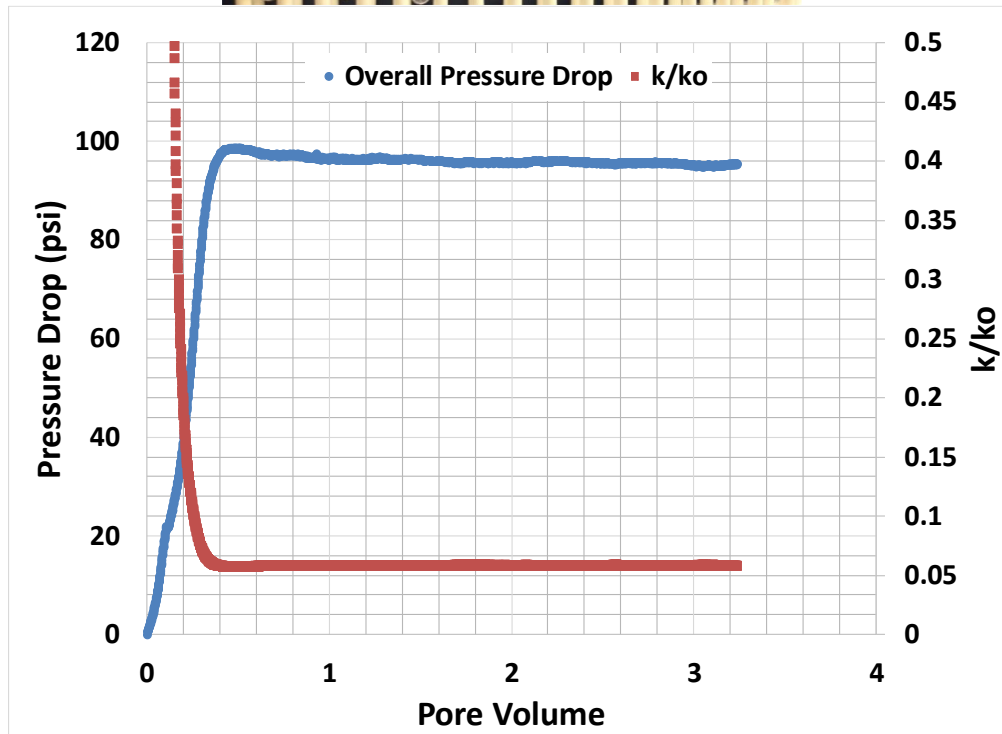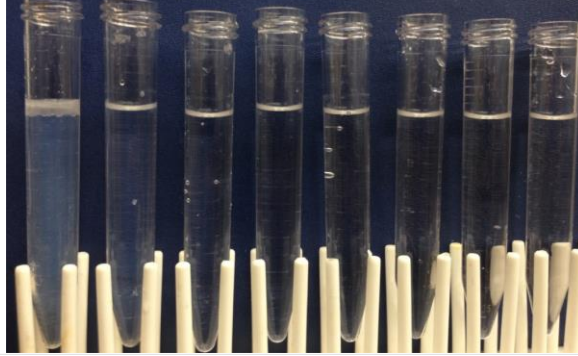
Figure 5.36 The experimental conditions, pressure data, and relative permeability of the waterflood, post emulsion injection, in Core P. Each tube contains 12 mL or 0.27 mL.

191

Several important observations were made during the Core P experiment. First an emulsion was used to displace nearly all of the oil from the core. It appeared, qualitatively that the emulsion injection recovered approximately 2.5 times more oil than the control water flood. The octane that was left in the core was not able to be recovered with a follow up waterflood. The most probable cause for this is that the emulsion did not completely break in the core. In the image of the effluent in Figure 5.35, it appeared that the emulsion broke but the pressure did not reach steady state indicating possible in situ generation of emulsion. The results of this experiment were the motivation for the experiments performed in the next section.

5.5.3.2 Residual oil recovery with emulsion

The key finding from the Core P experiment was that injecting an octane-in-water emulsion displaced what was believed to be all the mineral oil in the core, when the initial oil saturation was all mobile (S_{oi} = 1 - $S_{w,irr}$). This suggests that the emulsion flood prevents disconnection of the mineral oil as its saturation decreases, or in-situ coalescence of the injected emulsion miscibly displaces and recovers any mineral oil that does become disconnected. The experiments in Core Q and T were performed to further investigate this phenomenon.

The Core Q and T experiments presented in this section are similar to the Core P experiment. The first experiment performed in Core Q was a control experiment. First a Core Q was saturated with mineral oil to reach residual water saturation. Core Q was then waterflooded to reach residual oil saturation. Next, octane and brine were co-injected into Core Q to recover the residual mineral oil. The intention of this experiment was to get a baseline apparent viscosity and pressure drop as well as recovery

of residual oil by the octane.   Moreover if the emulsion completely breaks as it enters the core the displacement should behave as if brine (containing nanoparticles) and octane are flowing through the core.   The brine and octane were injected into the core at the same flow rate that the emulsion was injected in Figure 5.37.   The phase ratio of brine and octane during co-injection is the same as the volume ratio of aqueous phase and oil in the emulsion.   After the co-injection of brine and octane the core was flooded with isopropyl alcohol (IPA) to remove all of the oil and water in the core.   The brine was injected into the core to remove all of the IPA.   Mineral oil was injected into the core to reach residual brine saturation.   Then the core was waterflooded with brine to reach residual oil saturation.   Finally, the octane-in-water emulsion was injected into the core to recover the residual oil. An outline of the experimental procedure is provided below.

1. Inject mineral oil to reach residual water saturation

2. Waterflood to reach residual oil saturation

3. Co-inject octane and brine through the core at 0.4 mL/min of brine and 1.6 mL/min of octane

4. Flush core with IPA (20 pore volumes)

5. Flush core with brine (20 pore volumes)

6. Inject mineral oil to reach residual saturation

7. Waterflood to reach residual oil saturation

8. Inject octane-in-water emulsion that is 80% octane by volume at 2mL/min

In all of the experiments the mineral oil was dyed red to help distinguish it from the octane.   All of the red mineral oil that was recovered during the brine and octane co-injection was recovered within the first pore volume.   The steady-state apparent viscosity of the co-injection was approximately 9 cP in Figure 5.37.   After the co-injection, the octane-in-water emulsion was injected to recover residual oil after completing steps 4-7 in the experimental outline.

Core Q-1 – Boise Core - Brine and Octane Co-injection						
k (mD)	ϕ	Pore Volume (mL)	Initial Saturation		Flow Rate (mL/min)	Shear Rate (s⁻¹)
540	0.28	42	S_{or}=0.31	S_w=0.69	2	242
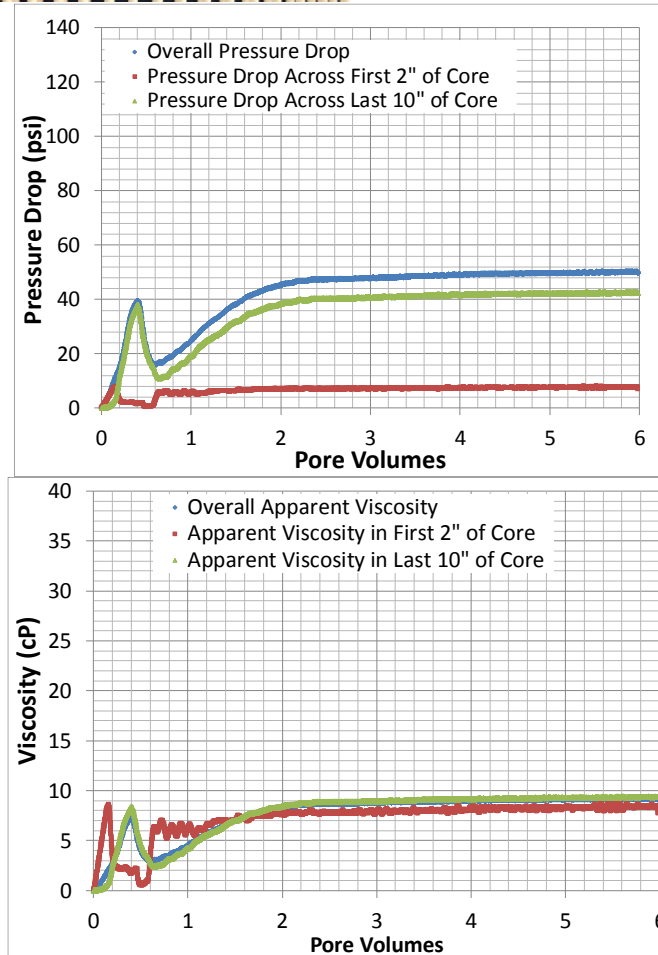
Figure 5.37 The effluent, pressure drop, and apparent viscosity of the brine and octane co-injection in Core Q.   Each tube contains 12 mL or 0.29 PV.   Residual oil (dyed red) was initially present at S_{or}=0.31.

195

Core Q-2 – Boise Core - Water-in-Octane Emulsion Injection						
k (mD)	ϕ	Pore Volume (mL)	Initial Saturation		Flow Rate (mL/min)	Shear Rate (s^{-1})
540	0.28	42	S_{or}=0.33	S_w=0.67	2	242
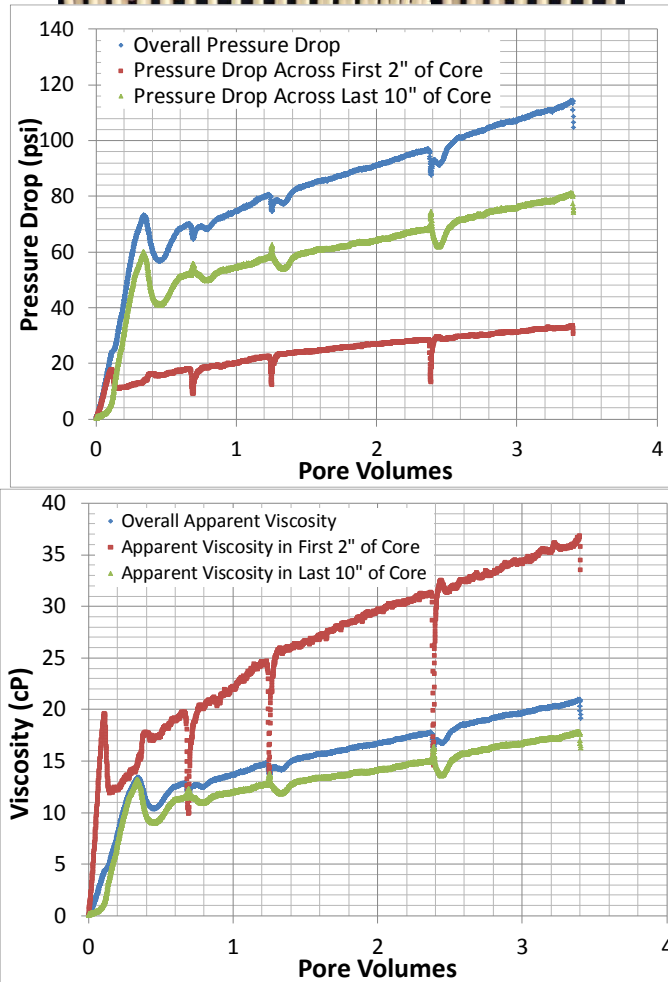
Figure 5.38 The effluent, pressure drop, and apparent viscosity of the octane-in-water emulsion injection in Core Q. Each tube contains 12 mL or 0.29 PV. Residual oil (dyed red) was initially present at S_{or}=0.33.

One pore volume is approximately four test tubes of effluent in Figures 5.37 and 5.38. The mineral oil was dyed red while the brine, nanoparticle dispersion, and mineral oil were all clear. There were 13 mL of residual oil in the core. Co-injection (Figure 5.37) displaced 28 mL of red, pink, and faintly red oil phase, consistent with miscible displacement of some but not all of the residual oil from the core. The 28 mL was the total amount of red, pink, and faintly red fluid in the first three test tubes in Figure 5.37. There was no red dye present after the fourth test tube (~1PV) in the co-injection in Figure 5.37. In contrast, in Figure 5.38 red dye was present in the first eight effluent test tubes (~2 PV). Approximately 50 mL of red, pink, and faintly red fluid was collected. In the first pore volume (first four tubes from the left in Figure 5.38) majority of the residual oil is recovered because these tubes are dark red to pink. As the emulsion injection continued the red color becomes fainter but is still present in the remaining test tubes. This indicates additional recovery of residual mineral oil compared to the control experiment. The similarity in the effluent oil volumes and color in Figures 5.37 and 5.38 confirms the hypothesis that coalescence or breaking of an injected emulsion occurs when it flows through a core at sufficiently small rate; moreover the coalesced oil phase persists (is not regenerated into stable droplets) long enough to contact residual oil and mobilize it. This constitutes a proof of the concept of delivery a recovery-enhancing fluid, in this case octane, to residual oil. This extends the finding from the experiment in Core P that delivery could be accomplished to mobile oil.

The pressure drop during co-injection increased to a peak as the oil bank formed during the first 0.5 PV, decreased as the oil bank was produced then steadily increased until a steady state saturation distribution was established in the core. This behavior is

consistent with expectations from fractional flow theory.   In contrast, the pressure drop increased for the entire duration of the emulsion injection, driven primarily by the large and growing apparent viscosity in the first 2" of the core. The increase in pressure in the first 2" of the core is associated with the emulsion resistance to droplet coalescence which increases the pressure drop. Majority of the injected emulsion coalesced according to the effluent. The increase then decrease in pressure gradient as the oil bank forms is visible in the first pore volume (red curve within 0.2 PV, blue and green curve within 0.4 PV) of pressure history in Figure 5.38, but the magnitude of the change is somewhat smaller than during co-injection.   The last 8 test tubes from the left in Figure 5.38 each contained approximately 1 mL of stable emulsion.   The pressure data indicates that there was emulsion flowing through the core because after the oil bank was produced, the pressure drop across the core was higher in the emulsion injection compared to the co-injection.   The apparent viscosity in the first 2 inches of the core was approximately twice as large as it was in the rest of the core.   This is an indication that more emulsion was present in the first 2 inches of the core compared to the rest of the core.

The experiments in Core T (Figures 5.39 and 5.40) presented in this section are identical to the emulsion injection/co-injection experiments in Core Q, except mineral oil was used   to create the emulsion instead of octane.   The experiments in Core T were performed to see what effect the less viscous octane had on the recovery of residual oil in the experiment. The following outline was used in the next set of experiments presented.

1. Inject mineral oil to reach residual water saturation

2. Waterflood to reach residual oil saturation

198

3. Co-inject emulsion and brine through the core to recover oil at (0.68 mL/min of brine and 1.32 mL/min of mineral oil)

4. Flush core with IPA (20 pore volumes)

5. Flush core with brine (20 pore volumes)

6. Inject mineral oil to reach residual saturation of brine

7. Waterflood to reach residual oil saturation

8. Inject mineral oil-in-water emulsion that is 66% mineral oil by volume at 2mL/min

The apparent viscosity for the co-injection of mineral oil and brine was approximately 62 cP (Figure 5.39). All of the recovered mineral oil (red dye) was recovered within the first four test tubes (~1 PV) in Figure 5.39. The fraction of residual oil recovered was 78%, meaning the residual oil saturation to the co-injected fluids was $S_{or,co}$=0.07. This was estimated by assuming all the residual mineral oil recovered was in the first two tubes in Figure 5.39. The red dye in the first two tubes was the same color as the residual mineral oil so it is safe to assume that this fluid was primarily residual mineral oil. It is difficult to quantify how much residual oil was recovered in the third and fourth tubes with lighter red color in Figure 5.39. There was no red dye in the fifth test tube indicating that all of the residual mineral oil to brine was recovered in the first pore volume of injection. After the co-injection experiment, the

mineral oil-in-water emulsion was injected after completing steps 4-7 in the experimental outline.

Figure 5.40 shows that the pressure drop continued to build for the entire duration of mineral oil emulsion injection to recover residual oil. The apparent viscosity in the core was higher in the emulsion injection versus the co-injection. Displaced mineral oil (red dye) was present in the first four test tubes in Figure 5.40. In the fifth test tube there was very little, if any red dye. The emulsion injection appeared to recover less of the residual mineral oil compared to the co-injection experiment. Stable emulsion was present in the third test tube and beyond. This suggests that the emulsion re-generated in the core more readily than in the Core Q experiment, so that less mineral oil from the emulsion was available to miscibly displace the residual. This in turn suggests that the conditions for emulsion coalescence and regeneration during flow in a core may depend on the composition and viscosity of the oil phase. This is consistent with the results in Section 3.3.4 where it took a higher shear rate to stabilize an octane-in-water emulsion ($20,830$ s^{-1}) than a mineral oil-in-water emulsion ($12,500$ s^{-1}).

Core T-1 – Boise Core – Mineral oil and Brine Co-injection (Control)						
k (mD)	ϕ	Pore Volume (mL)	Initial Saturation		Flow Rate (mL/min)	Shear Rate (s⁻¹)
900	0.29	45	S_{or}=0.34	S_w=0.66	2	183
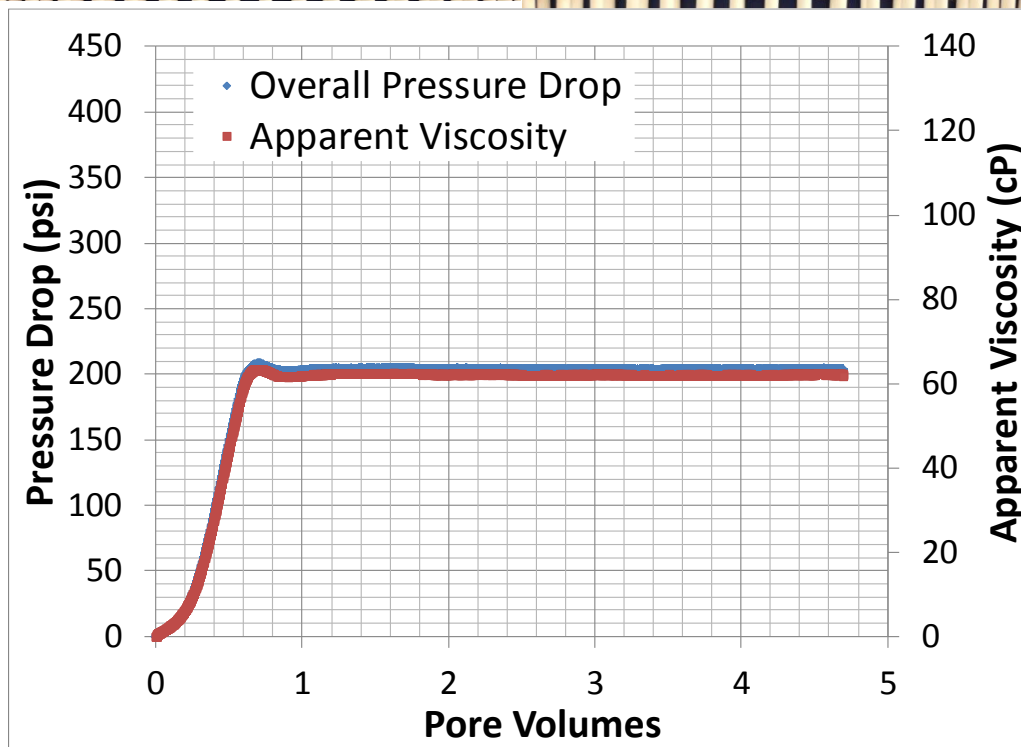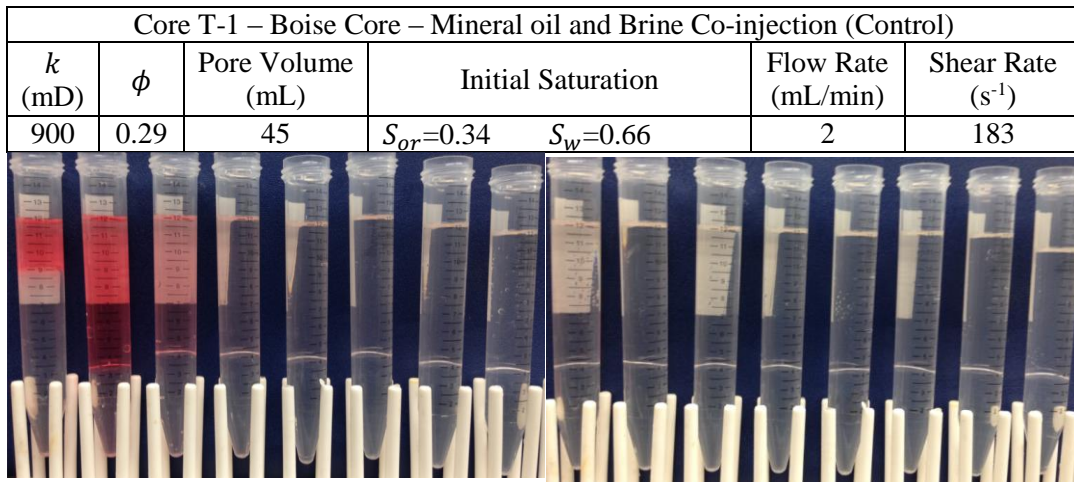
Figure 5.39 The experimental conditions, effluent, pressure drop, and apparent viscosity of the co-injection of brine and mineral oil in Core T.   Each tube contains 12 mL or 0.27 PV. Residual oil (dyed red) was initially present at S_{or}=0.34.

| Core T-2 – Boise Core – Mineral Oil Emulsion Injection						
k (mD)	ϕ	Pore Volume (mL)	Initial Saturation		Flow Rate (mL/min)	Shear Rate (s^{-1})
900	0.29	45	S_{or}=0.37	S_w=0.63	2	183
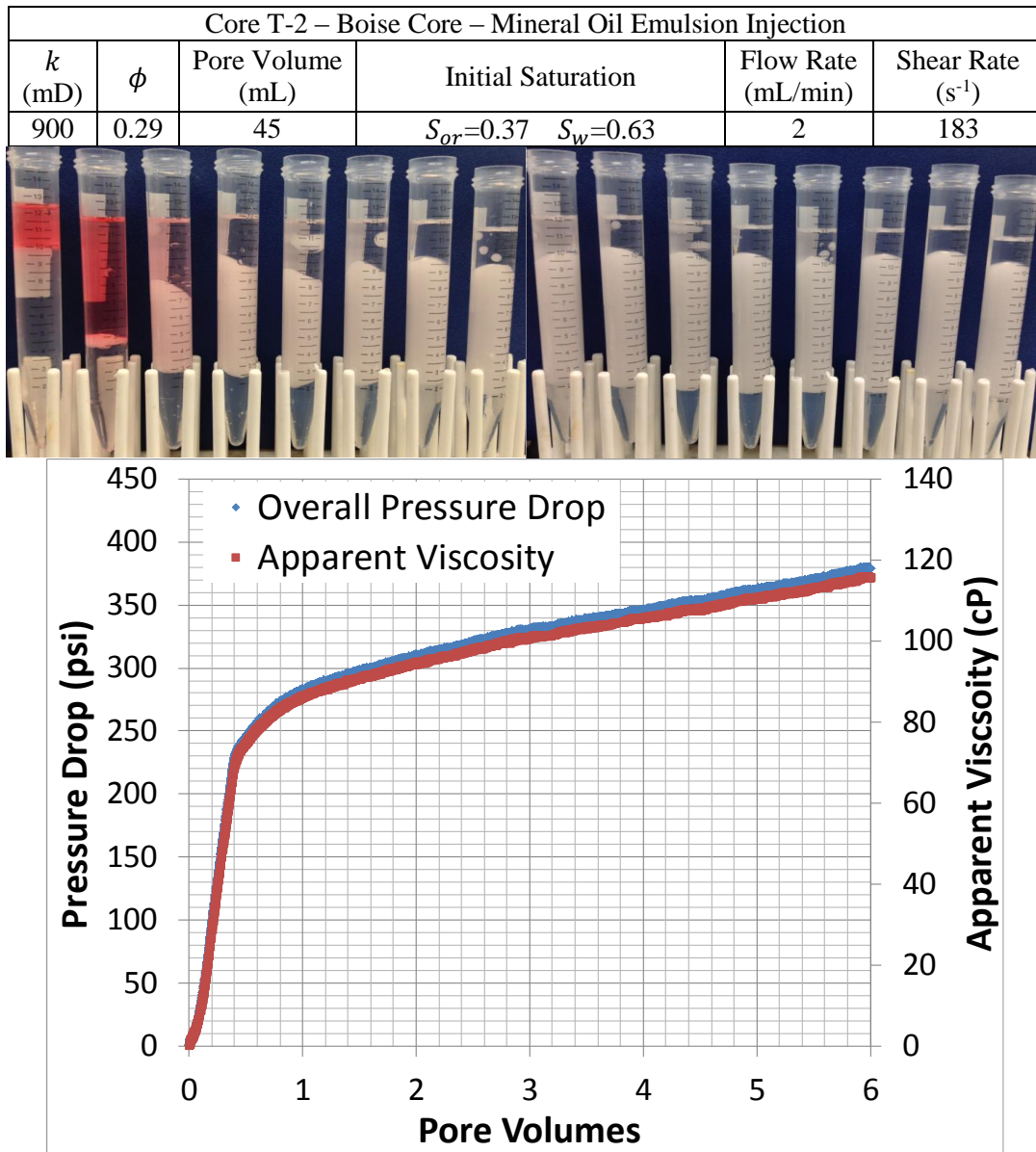
Figure 5.40 The experimental conditions, effluent, pressure drop, and apparent viscosity of the mineral oil-in-water emulsion injection in Core T. Each tube contains 12 mL or 0.27 PV. Residual oil (dyed red) was initially present at S_{or}=0.37.

To summarize, the octane-in-water emulsion recovered the most residual mineral oil compared to the other two co-injections and mineral oil emulsion injection. Residual mineral oil was still being recovered in the tenth test tube for the octane-in-water emulsion injection. For the other three experiments there was no presence of residual mineral oil after the fifth test tube. The hypothesis is that coalesced octane emulsion droplets caused the increase in oil recovery. It appeared that the octane emulsion coalesced according to the presence of free oil and aqueous phases in the effluent however the pressure data suggested that droplets were traveling through the core. It is believed the octane droplets were unstable as they traveled through the core, constantly coalescing and regenerating as they passed through the pore space. As the droplets coalesced some of the octane was able to mix with the residual mineral oil. Trapping of droplets also contributed to the recovery of mineral oil causing emulsion to travel through pore space that was bypassed in the other co-injection experiments. In contrast, the injected mineral oil emulsion remained stable as it traveled through the pore which didn't allow the mineral oil in the emulsion to mix with the residual mineral oil.

5.5.4 Octane-in-Water Emulsion Stability

This section was intended to investigate the stability of the octane-in-water emulsion. Specifically, it is important to determine whether the emulsion coalescence shown in Section 5.5.3 was primarily the consequence of flowing the through porous media or the result of the emulsion coming into contact with the resident fluids in the core. Batch experiments similar to those performed with the mineral oil-in-water emulsion were here performed with the octane-in-water emulsion, Chapter 4 Section 4.3.3. Brine (B), nanoparticle dispersion (D), and mineral oil (O) dyed red were

individually mixed with an octane-in-water emulsion (E). Each mixture was equal parts by volume emulsion and the other fluid (brine, dispersion, or mineral oil) in 20 mL disposable scintillation tubes. Three samples were made of each mixture (B/E, D/E, O/E). For each mixture, one of the samples was left undisturbed for a week; another was shaken vigorously by hand for 1 minute; the third was sonified for three minutes at 25% amplitude. Figure 5.41 shows the nine samples just after preparation.
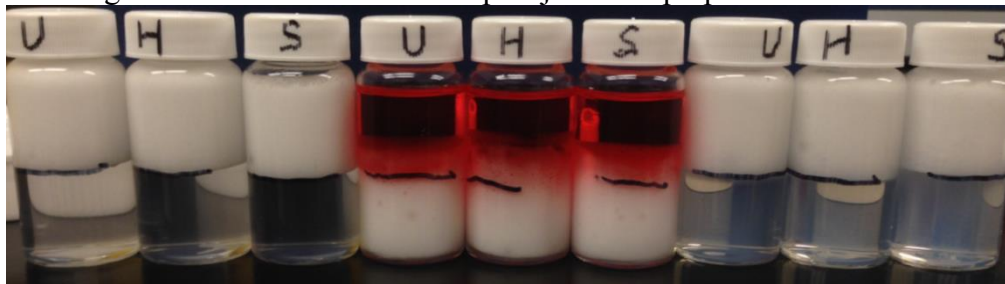
Figure 5.41 Photo of three samples of the B/E (octane emulsion/brine, left) mixture, the O/E (octane emulsion/red mineral oil, middle) mixture, and the D/E (octane emulsion/nanoparticle dispersion, right) mixture just after sample preparation. Cap labels U, H, S refer to modes of agitation (see text.)

There was no change in the samples that were left undisturbed. The octane emulsion did not coalesce when it was put into contact with brine, nanoparticle, dispersion, or mineral oil. Figure 5.42 shows the undisturbed samples after one week. The original meniscus, marked by the sharpie line (black) in Figure 5.41, is in approximately the same location as the meniscus one week later.
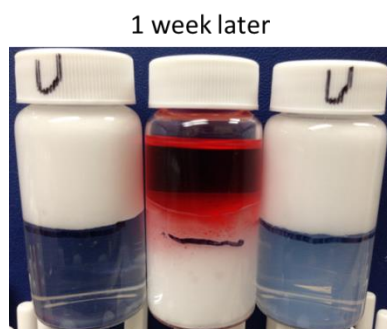
Figure 5.42 Photo of B/E, O/E, and D/E (left to right) samples after sitting undisturbed for one week.

There was no change in the samples that were shaken by hand. Figure 5.43 shows the vials just after shaking, 1 day later, and 1 week later. Within one day each samples meniscus returned to the original meniscus indicated by the black line.
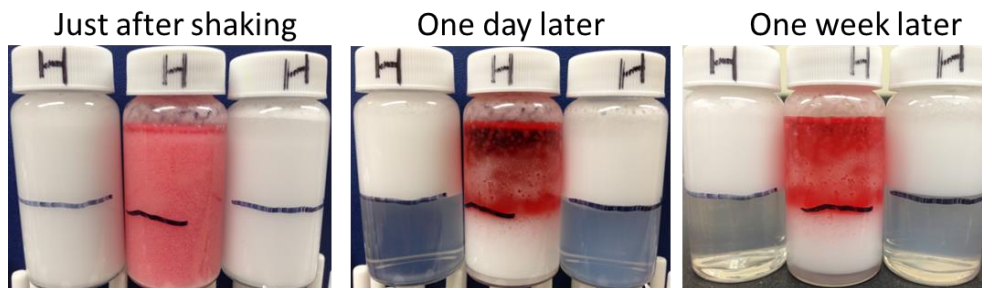
Figure 5.43 Photos of samples that were shaken by hand: just after shaking, one day later, and one week later. Photos of B/E, O/E, and D/E samples (left to right).

When the octane emulsion/brine sample and octane emulsion/nanoparticle dispersion sample were sonified there was an increase in the amount of emulsion. In Figure 5.44 the emulsion occupies more volume than before sonification, indicating that more emulsion was produced during sonification. More new emulsion was produced in the nanoparticle dispersion sample than the brine sample. It appeared that a small

amount of the emulsion coalesced when the octane emulsion/mineral oil was sonified because some excess nanoparticle dispersion was produced at the bottom of the vial. Majority of the emulsion stayed stable which was not the case when a mineral oil emulsion/mineral oil mixture was sonified in Setion 4.3.3.

Figure 5.44 Photos of samples that were shaken by hand: initially, just after sonification and one week later. Photos of B/E, O/E, and D/E samples (left to right).

Three samples were prepared where octane emulsion was added in equal parts by volume with octane (dyed red).   One sample was left undisturbed.   One was shaken by hand for one minute and one was sonified for three minutes.   Figure 5.45 shows the samples just after they were prepared.

Figure 5.45 The vials containing octane emulsion and octane in equal parts by volume just after they were prepared.   The black line indicates the original meniscus.

The emulsion in the sample that was left undisturbed remained stable. The meniscus was in approximately the same location and no nanoparticle dispersion was present at the bottom of the sample indicating that the emulsion remained stable. Figure 5.46 shows the sample that was left undisturbed for one week.

Figure 5.46 The octane emulsion and octane vial that was left undisturbed for a week.

There was no change to the emulsion that was shaken by hand for one minute because excess nanoparticle dispersion was not present indicating that none of the emulsion coalesced. Figure 5.47 shows the image of the vial with octane emulsion and octane just after it was shaken, one day later, and one week later.
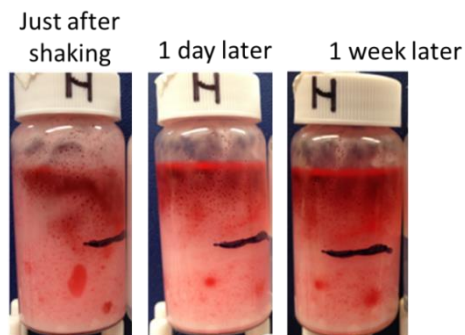
Figure 5.47 The octane emulsion and octane vial that was shaken by hand for one minute.

The third sample of octane and octane emulsion was sonified. Almost the entire emulsion coalesced. This was a similar result to the mineral oil and mineral emulsion

mixture that was sonified in Section 4.3.3. Catastrophic phase inversion most likely caused the coalescence of the emulsion. An interesting point is that when the octane emulsion and mineral oil were sonified, majority of the emulsion remained stable. This was not the case when the oil phase was the same as the internal oil of the emulsion. Figure 5.48 shows the octane emulsion and octane vial just after it was sonified, 1 day later, and 1 week later.
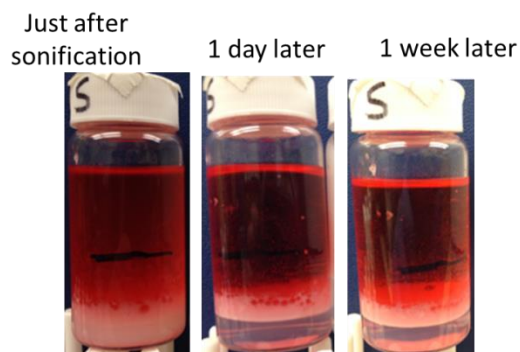
Figure 5.48 The octane emulsion and octane vial that was sonified for three minutes at 25% amplitude. The emulsion completely coalesced.

These experiments indicate that simply contacting a nanoparticle-stabilized emulsion with another phase – brine, nanoparticle dispersion, or oil (different from the oil phase of the emulsion) will not cause the emulsion to break. Under some conditions the addition of energy, sonification at 25% amplitude for three minutes, to the oil/emulsion mixture can cause the emulsion to break. This suggests that the forced movement of an emulsion through a porous medium is the cause of emulsion coalescence and/or breaking in the experiments reported in sections 5.5.1 through 5.5.3.

5.5.5 Effect of Diluting Emulsion Droplet Density

In this section experiments were performed to determine what effect diluting the emulsion droplet density had on the apparent viscosity. Droplet density is defined as the number of oil droplets per unit volume. This value was altered by injecting diluted emulsions with excess nanoparticle dispersion. If a diluted emulsion could give the same apparent viscosity as a pure emulsion it could reduce the amount of oil needed for a field application for mobility control, reducing overall costs. The experimental set-up that was used in this section is given in detail in Section 5.2.3.

5.5.5.1 Mineral oil-in-water emulsion

In the emulsion injection experiments performed in Section 5.5.1, 5.5.2, and 5.5.3 steps were taken to ensure that only 100% emulsion was injected into the core. Specifically, when emulsion and nanoparticle dispersion were added to the accumulator the contents were allowed to settle for 1 to 2 hours before starting emulsion injection, so that the excess nanoparticle dispersion would drain to the bottom of the accumulator. Here a Nyacol DP 9711 nanoparticle dispersion and mineral oil were co-injected at a 1:1 phase ratio through the 180 micron HiP beadpack to generate an emulsion. The total flow rate was 40 mL/min. A sample of the effluent was collected and allowed to settle so that the excess nanoparticle dispersion would drain from the emulsion enabling a determination that the generated emulsion was approximately 66% oil by volume.

In the first experiment in Core M, Figure 5.49, the effluent that was used to generate the emulsion as described in the previous paragraph was routed directly to the core. Because the excess nanoparticle dispersion and emulsion were routed directly into the core from the beadpack, the excess nanoparticle dispersion was diluting the emulsion

209

droplet density (density here refers to volume of droplets per volume of emulsion or the volume fraction of oil in the effluent emulsion) to a value of 0.5.   The pressure drop and apparent viscosity are shown in Figure 5.49.   The apparent viscosity of the diluted emulsion while flowing through the core was approximately 8.5 cP.   The apparent viscosity was small because the shear rate in the core was much higher for this experiment (4,842 s^{-1}) than any other coreflood experiment (typically less than 500 s^{-1}) and the emulsion is highly shear thinning, i.e. as shear rate increases the viscosity decreases.   The photos on the right of Figure 5.51 show the effluent from the beadpack and the core from the diluted emulsion injection.   The effluent from the core and beadpack appear very similar indicating that all of the oil remained as part of an emulsion, indicating the emulsion most likely completely coalesced and regenerated in the core. All of the oil was re-emulsified into a new emulsion because the emulsion was injected at such a high shear rate causing the effluents to appear similar.

Following the injection of the diluted emulsion, some of the emulsion generated from the beadpack was injected into the core. Like the other emulsion injection experiments, the emulsion was loaded into the accumulator and any excess nanoparticle dispersion settled to the bottom of the accumulator so that only 100% emulsion was injected into the core.   The emulsion that remained at the top of the accumulator was injected through the core at 40 mL/min.   The results are shown in Figure 5.50. The apparent viscosity of the emulsion as it flowed through the core was approximately 16.5 cP.   The apparent viscosity of the emulsion in Core M was very small due to the fact that a shear thinning emulsion was injected at a very high shear rate.   Only stable emulsion was produced in the effluent.   The droplet density for the emulsion injection

210

was simply the volume fraction of oil in the emulsion. This emulsion was approximately 66% oil by volume so the droplet density was 66%.

In the diluted emulsion injection experiment (Figure 5.49) it took approximately 2.5 PV for the apparent viscosity in the entire core to stabilize but in the first 2" of the core the apparent viscosity stabilized quickly (less than 0.5 PV). It is possible the coalescence and regeneration of the emulsion caused the pressure to build in the last 10" of the core while it was stable in the first 2" of the core. In previous experiments in Cores B-T, when emulsion was injected at lower rates the apparent viscosity would increase for the entire duration of the injection. This was attributed to the coalescence of injected droplets and the regeneration of new emulsion droplets which may have caused the increase in apparent viscosity in the last 10" of the core. In the 100 % emulsion injection (Figure 5.50) the pressure drop stabilized within 1 PV. This difference was most likely caused by the initial saturation of the core. When 100% emulsion was injected into the core there was already emulsion present in the core so the pressure drop stabilized within 1 PV. For the diluted emulsion injection experiment the core was saturated with brine so it may have taken longer to achieve steady state because emulsion droplets were not initially present in the core. The apparent viscosity in the first 2" was smaller than in the last 10" of the core for the 100% emulsion injection (Figure5.50). This may have been caused by a high amount of emulsion coalescence and regeneration in the first 2" of the core causing a smaller apparent viscosity compared to the last 10". The excess nanoparticle dispersion in the diluted emulsion injection accounted for approximately 25% of the effluent by volume but in the 100% emulsion injection this value was 0%. The injected and effluent volumes match in Figure 5.51 for the diluted

emulsion injection.   The droplet density or the volume fraction of oil injected for the diluted emulsion experiment was 50% because the mineral oil and emulsion were injected at a 1:1 phase ratio and all of the mineral oil remained in the effluent emulsion from the core.   A 16% reduction in droplet density, from 66% for 100% emulsion to 50% for the dilute emulsion, caused the emulsion viscosity to drop from 16.5 cP to 8.5 cP.

Core M-1 – Boise Core - Dilute Emulsion Injection					
k (mD)	ϕ	Pore Volume (mL)	Initial Saturation	Flow Rate (mL/min)	Shear Rate (s^{-1})
540	0.28	43	$S_w=1$	40	4842
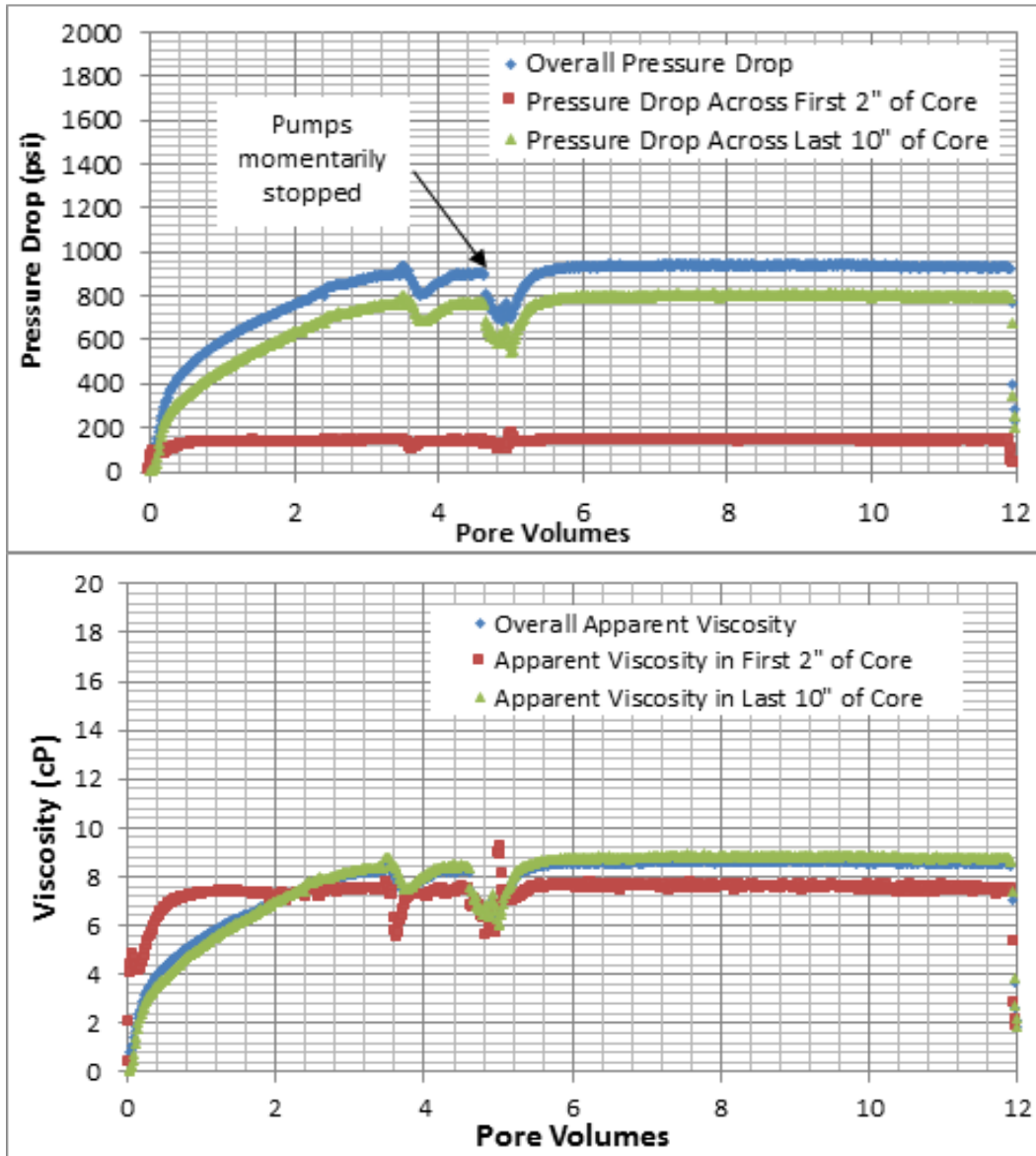
Figure 5.49 The experimental conditions, pressure drop, and apparent viscosity for the dilute emulsion injection in Core M.

213

Core M-2 - Boise Core - Pure Emulsion Injection					
k (mD)	ϕ	Pore Volume (mL)	Initial Saturation	Flow Rate (mL/min)	Shear Rate (s^{-1})
540	0.28	43	Emulsion	40	4842
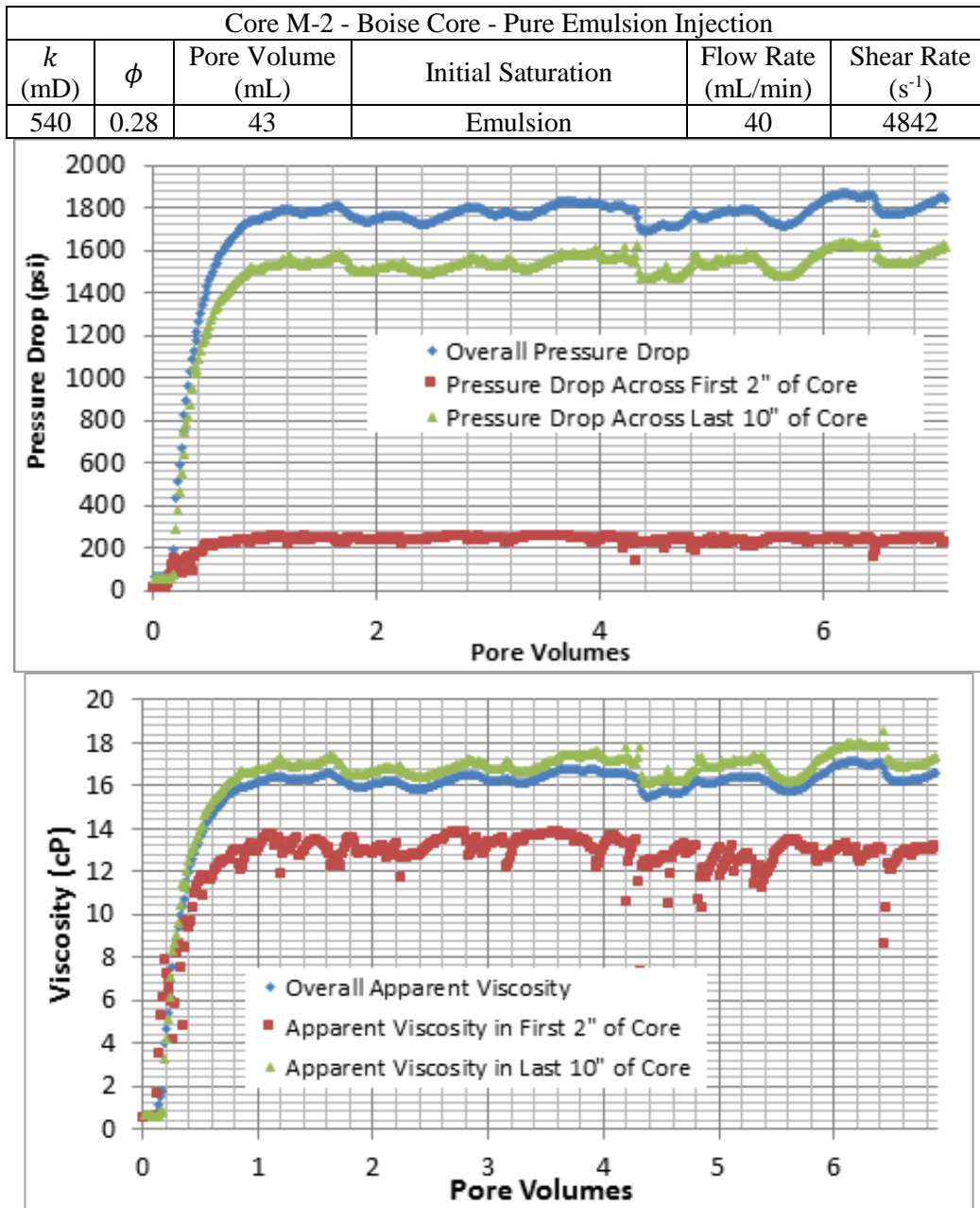
Figure 5.50 The experimental conditions, pressure drop, and apparent viscosity of the non-diluted emulsion injection in Core M following the injection of the diluted emulsion for 12 PV at 40 mL/min (cf Figure 5.49).
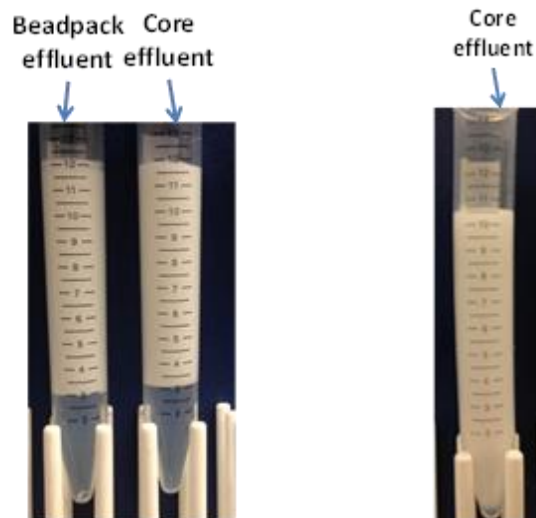
Figure 5.51 The effluent from the beadpack and core from the diluted emulsion (left). The effluent from the core for the emulsion injection (right).

5.5.5.2 Octane-in-water emulsion

Dilute emulsion experiments were performed in Core R with octane and Nyacol DP 9711 nanoparticle dispersion. To achieve a dilute emulsion, a 4:1 injection ratio of nanoparticle dispersion to octane was co-injected through the beadpack and routed through Core R. A highly dilute emulsion was created by co-injecting a 9:1 ratio of nanoparticle dispersion to octane. This emulsion effluent was routed directly into Core R after the first 4:1 injection. Finally a high droplet density emulsion was created by injecting a 2:3 ratio of nanoparticle dispersion to octane through the beadpack. This emulsion effluent was routed directly into Core R after the 9:1 injection. In each injection the effluent from the beadpack was collected for analysis first before routing it to Core R. The results are summarized in Figure 5.52. The droplet size of the emulsion leaving the beadpack and the emulsion from Core R were measured.

215

The steady state apparent viscosity of the 4:1 co-injection was approximately 7.9 cP. The average droplet diameter of the emulsion entering Core R was 32.6 microns. The average droplet diameter of the emulsion leaving Core R was 13.6 microns. The droplet density for this co-injection ratio was 20%.

When the ratio of nanoparticle dispersion was decreased to 9:1 the steady state apparent viscosity of was approximately 7.1 cP. The average droplet diameter of the emulsion entering Core R was approximately 14.8 microns. The average droplet diameter of the emulsion leaving Core R was approximately was 12.0 microns. The droplet density of this emulsion was 10%.

There was a large increase in the steady state apparent viscosity of the emulsion when the ratio of nanoparticle dispersion to octane was decreased to 2:3. The apparent viscosity of the emulsion was approximately 16.7 cP. The droplet density for this experiment was 60%. The average droplet diameter of the emulsion entering Core R was 31.8 microns. The average droplet diameter of the emulsion leaving Core R was 13.0 microns.

For each stage of injection the core produced an emulsion with a smaller droplet size than the beadpack. The reduction in emulsion droplet size was most likely from the smaller pores in the core than in the 180 micron beadpack. Core R was Boise sandstone and had a permeability of 720 mD. The porosity of Core R was 0.28 and the pore volume was 44 mL. The shear rate in Core R at 40 mL/min was 4,087 s^{-1}. The shear rate in the beadpack was 20,834 s^{-1}.

The injection pressure increased steadily for 2 PV during the 4:1 co-injection before reaching a plateau value, but jumped quickly to the plateau value for the 9:1 and

2:3 co-injections. This most likely occurred because for this injection the core was initially saturated with brine. In the other injections nanoparticle dispersion and some emulsion were already present in the core.

4:1 nanoparticle dispersion to octane (40 mL/min total)	
Beadpack Effluent	Core Effluent
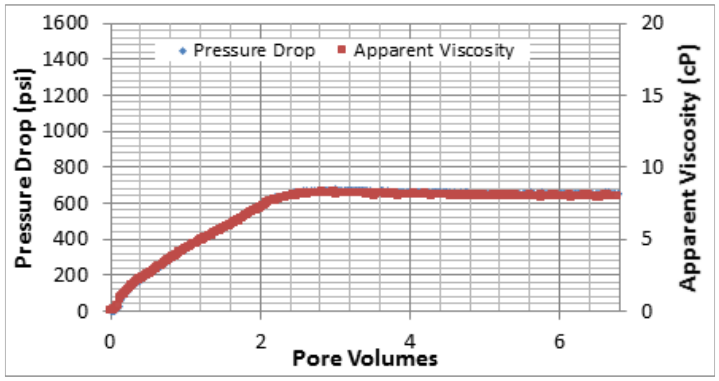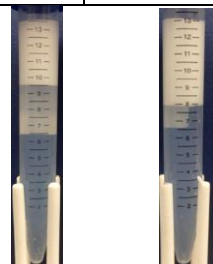
9:1 nanoparticle dispersion to octane (40 mL/min total)	
Beadpack Effluent	Core Effluent
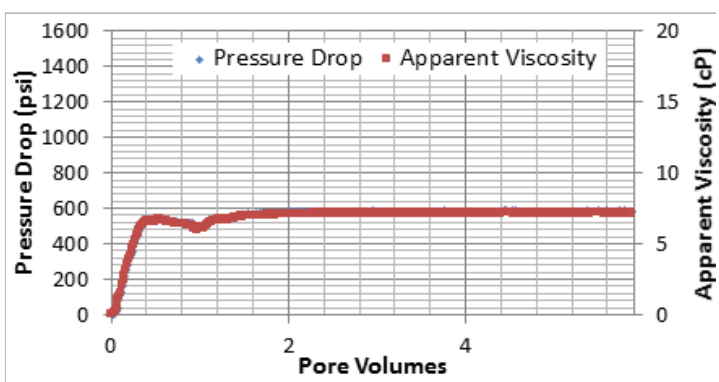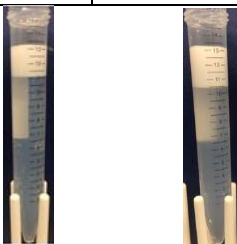
2:3 nanoparticle dispersion to octane (40 mL/min total)	
Beadpack Effluent	Core Effluent
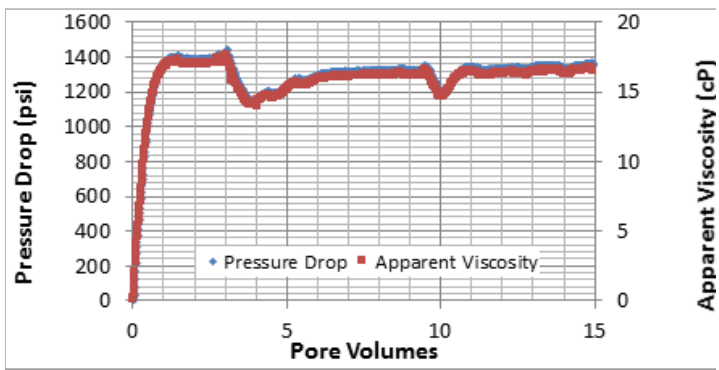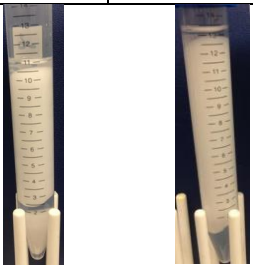
Figure 5.52 The pressure drop and apparent viscosity of the octane-in-water emulsion dilution experiments in Core R.   The effluent from the beadpack and core are shown.

Figure 5.53 summarizes the results from the dilution experiments performed with octane emulsion. The graph plots each emulsions apparent viscosity in the core as a function of droplet density. The average droplet diameter of the emulsion leaving the beadpack, which was injected into the core, is shown in red text. The average droplet diameter of the effluent emulsion from the core is shown in green text. Evidently the injected emulsion coalesces and is regenerated during flow through the core. This also suggests that dilute emulsions might let one droplet at a time go through a pore throat, and thereby survive; concentrated emulsions require multiple droplets to go through a throat so regardless of size they coalesce.
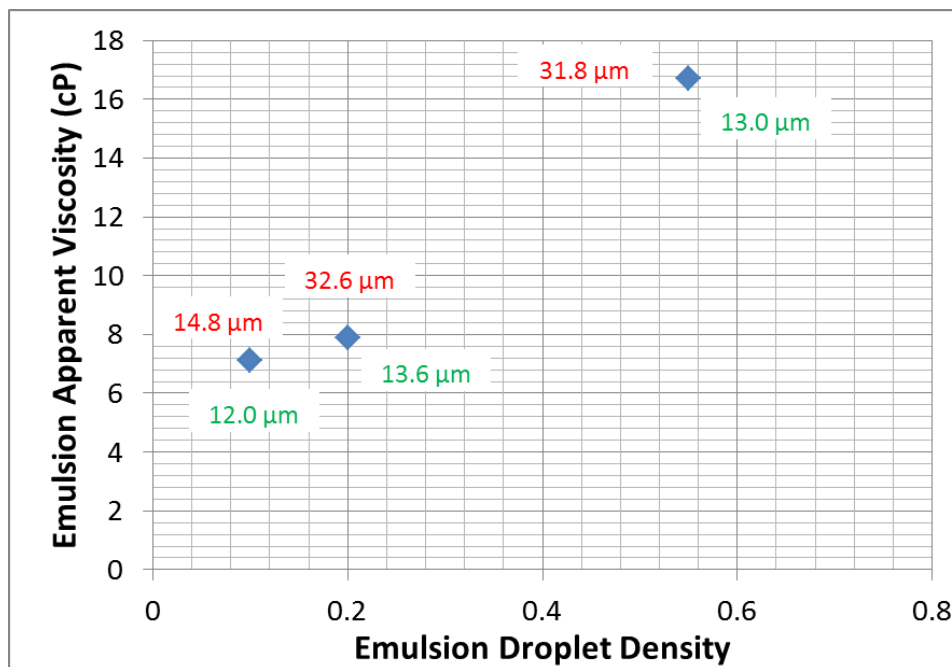
Figure 5.53 Octane emulsion apparent viscosity (through 720 mD Core R at a shear rate of 4,087 s^{-1}) increases as emulsion droplet density is increased. Green text is the average droplet diameter of the effluent emulsion from the core. The red text is the average droplet diameter of the emulsion entering the core.

5.5.6 Emulsion Generation by Nanoparticle Dispersion Imbibition

Coalescence of an injected emulsion can lead to regeneration of emulsion simply because the component phases become available after coalescence and flow together through the porous medium, which is a well-established method for generating emulsion. To determine if it was possible to generate stable emulsion in the core without two mobile phases the experiments in Core G and I (Figures 5.54 and 5.55) were conducted. Different nanoparticle dispersions were injected into Core G and I to displace the non-wetting oil phases. Chung (2013) found no evidence of emulsion generation during imbibition displacement of n-octane by nanoparticle dispersion but did find evidence of emulsion generation during drainage displacement of nanoparticle dispersion by n-octane (nanoparticle dispersion was 5 wt% Nyacol DP 9711 nanoparticles and 1 wt% NaCl) at shear rates of approximately 85 s^{-1}. The hypothesis for the emulsion generation proposed by Chung was Roof snap-off. In the experiments in Cores G and I emulsion was formed by imbibition displacement of mineral oil and dodecane with nanoparticle dispersions at shear rates greater than 1,700 s^{-1}, much greater shear rates than in Chung's work where emulsion did not form during imbibition (2013). In the imbibition experiments summarized in Figures 5.54 and 5.55 a different mechanism caused the stabilization of emulsion.

In the Core G experiment, Figure 5.54, nanoparticle dispersion was injected at different flow rates into a core that was at residual water saturation while the rest of the pore volume was occupied by mineral oil. The nanoparticle dispersion injected was 3 wt% nanoparticles and 2 wt% NaCl. The bulk nanoparticle dispersion that was diluted to make this dispersion was IPA-ST provided by Nissan Chemical. Initially the

220

nanoparticle dispersion was injected into the core at 3 mL/min. The flow rate was incrementally doubled making the three other flow rates: 6, 12, and 24 mL/min. When injecting at 3 mL/min an initial oil bank was displaced and no emulsion was produced in the effluent. As the flow rate was increased to 6 mL/min a very small amount of additional mineral oil was recovered but it was not in the form of an emulsion. When the flow rate was increased to 12 mL/min, a shear rate of 1784 s^{-1}, some additional oil was recovered in the form of stable emulsion. Then at 24 mL/min, 3568 s^{-1}, additional oil was displaced in the form of stable emulsion. The increase in capillary number at the larger flow rate causes some incremental oil to be mobilized; evidently the shear rates are large enough that this mobilized oil can be readily emulsified as it flows through pore throats along with the injected dispersion, presumably by the same mechanism that applies routinely during co-injection to generate emulsions. However the volume of oil recovered is substantially more than was recovered at the same rates when brine without nanoparticles was injected. At the highest rates (12 and 24 mL/min) simply flowing the nanoparticle dispersion past residual oil remaining in the core appears to entrain droplets of oil, which give the effluent a hazy appearance, and at 24 mL/min a substantial volume of emulsion is still being produced long after the change in flow rate. The incremental oil recovery is substantially larger than obtained when brine is injected at increasing rates, in Fig. 5.9. This indicates a novel mechanism of residual oil recovery; the affinity of the nanoparticles for the oil/water interface coupled with the large shear rate appears to enable residual oil to be mobilized, or perhaps to drag smaller droplets from residual oil blobs and entrain them into the flowing aqueous phase, stabilized by the nanoparticles and thus can be transported with the dispersion through the core.

221

In the Core I experiment, Figure 5.55, Nyacol DP 9711 dispersion was injected into a Boise sandstone core containing mobile dodecane and residual water. The nanoparticle dispersion is described in Section 5.1. The flow rate was incrementally increased to see if stable emulsion would form. The nanoparticle was dyed yellow to help distinguish it from the dodecane. In Figure 5.52 a small amount of stable emulsion was formed when the nanoparticle dispersion was injected at 24 mL/min, 2226 s^{-1}. This result is similar to the Experiment in Core G, indicating that incremental recovery above and beyond the yield from increasing the capillary number is possible if the brine phase contains suitable nanoparticles.

These experiments show that it is possible to generate stable emulsion in the core without two mobile phases but the injected nanoparticle dispersion must flow above the critical shear rate. For the Boise sandstone, the critical shear rate was between 1113 and 2226 s^{-1}. For the Berea sandstone, the critical shear rate was between 892 and 1784 s^{-1}.

Core G – Berea Core					
k (mD)	ϕ	Pore Volume (mL)	Initial Saturation	Flow Rate (mL/min)	Shear Rate (s^{-1})
408	0.24	37	$S_{w,irr}$=0.4 S_{oi}=0.6	3, 6, 12, 24	446, 892, 1784, 3568
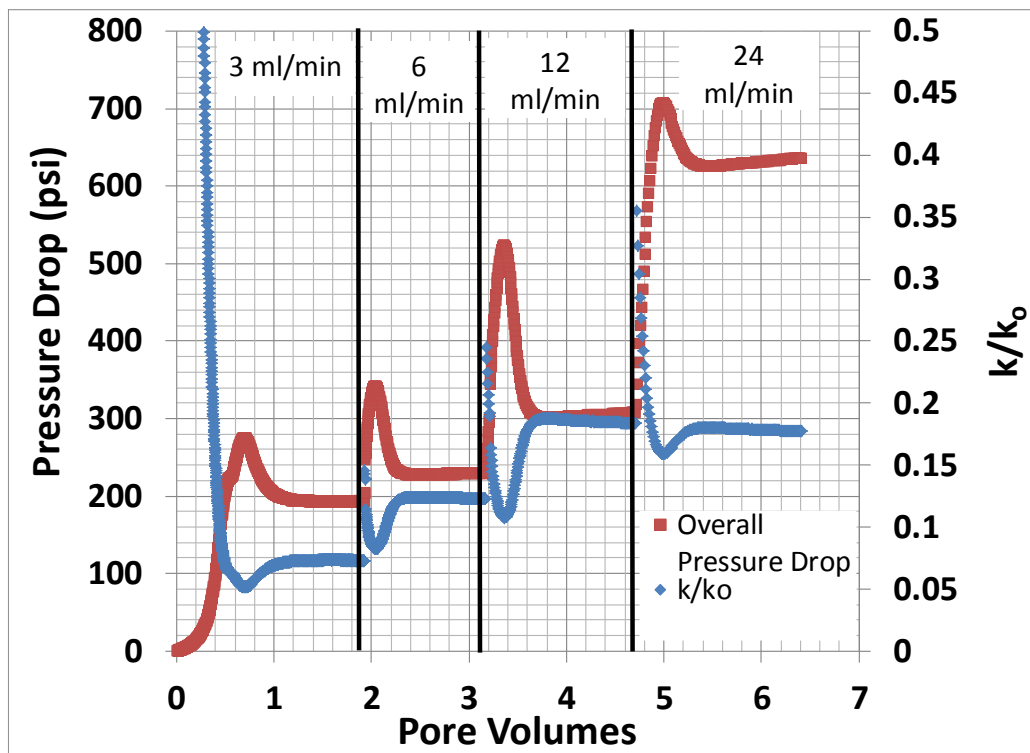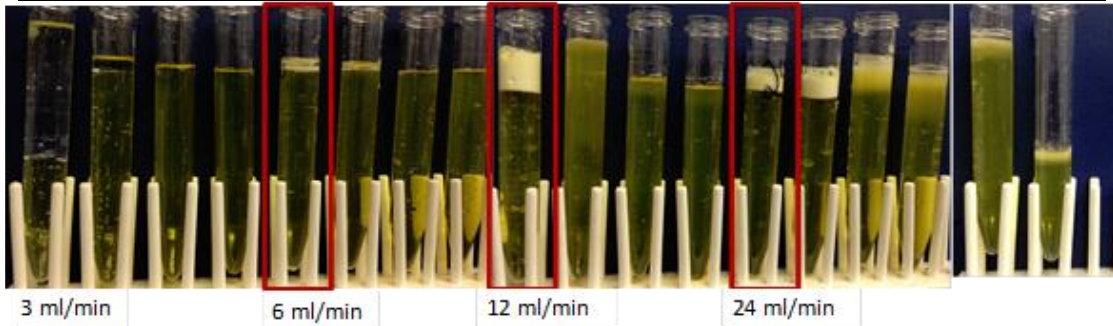
Figure 5.54 The experimental conditions, effluent, pressure data, and relative permeability of the nanoparticle dispersion (dyed yellow) injection in Core G initially containing mobile mineral oil saturation (S_{oi}=1-$S_{w,irr}$).

223

Core I – Boise Core					
k (mD)	ϕ	Pore Volume (mL)	Initial Saturation	Flow Rate (mL/min)	Shear Rate (s^{-1})
908	0.28	42	$S_{w,irr}=0.37$ $S_{oi}=0.63$	3, 6, 12, 24	278, 556, 1113, 2226
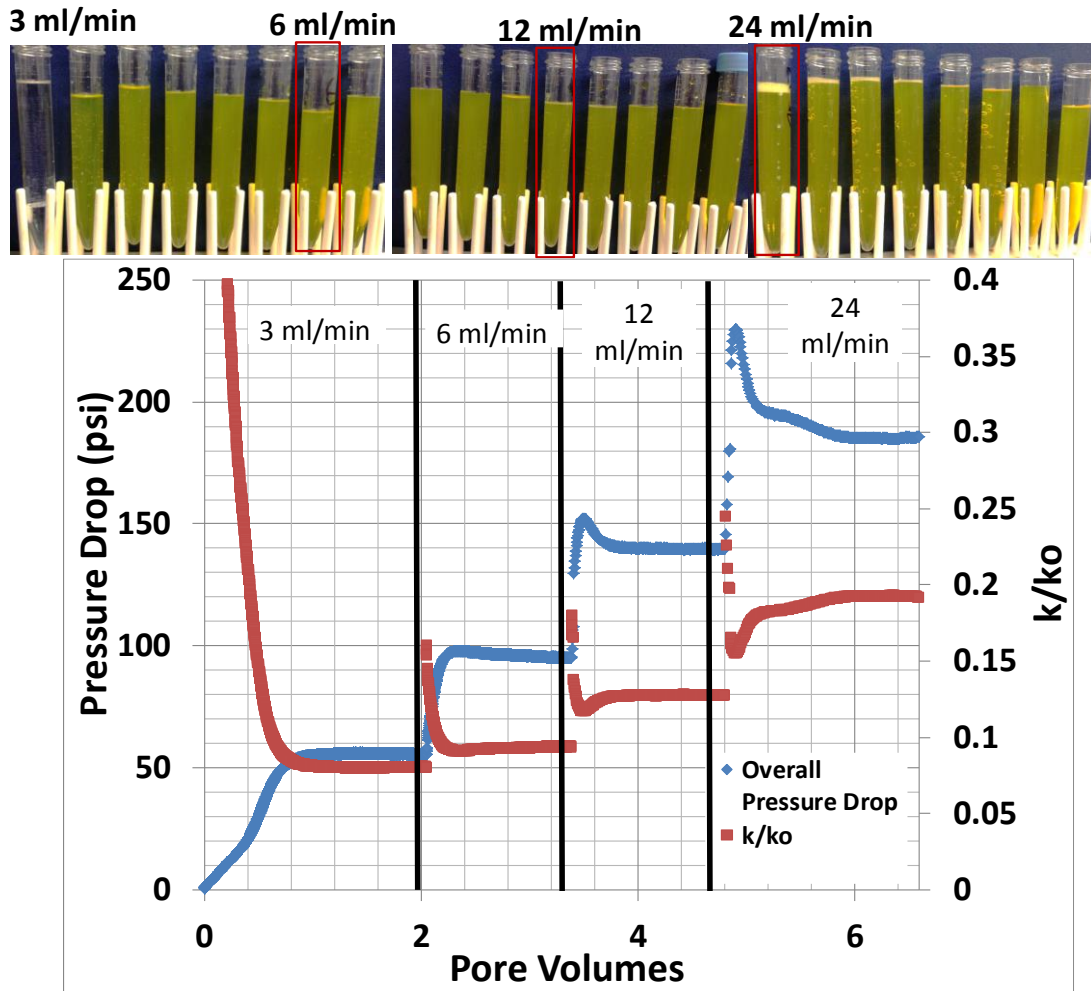
Figure 5.55 The experimental conditions, pressure drop, relative permeability, and effluent of the nanoparticle dispersion (dyed yellow) injection into Core I containing mobile dodecane (S_{oi}=1-$S_{w,irr}$). A little over 1 mL of stable emulsion was produced when the flow rate was increased (19th tube from left).

224

5.6 DISCUSSION

The experiment in Core E where a mineral oil emulsion was injected through a Berea core indicated there was critical shear rate required to maintain emulsion stability within the core. The mineral oil that was dispersed as droplets in the nanoparticle dispersion was produced as a separate phase in the effluent. This indicated that there was possibly a critical shear rate required to maintain stable emulsion in the core. The pressure drops across the entire core rose for the entire injection duration but the pressure drop across the taps stabilized. This indicated the possible movement of a front across the core. The high pressure drop was believed to be associated with the continued coalescence of droplets.

In Core B a mineral oil emulsion was injected through a Boise sandstone core. Stable emulsion was produced in the effluent while the rest of the injected emulsion coalesced to produce separate oil and aqueous phases in the effluent. The pressure drop across the core increased for the entire duration of the experiment. The effluent emulsion had a larger droplet size and was less viscous than the injected emulsion. This indicates that a significant amount of droplet coalescence takes place in the core. There are potentially two ways for the effluent emulsion droplets to become larger. One is that the injected emulsion completely coalesces into the two bulk phases within a short distance of the core inlet; the two phases then regenerate a new emulsion as the bulk phases pass through the pore space. The second is that the smaller droplets in the injected emulsion are coalescing into larger droplets but the process of coalescence stops when the droplets reach a characteristic larger size. The former possibility is consistent with the other observations in this Chapter and in Chapter 4. The apparent viscosity in

225

the core was between the viscosity of the injected emulsion and the viscosity of the effluent emulsion at the same shear rate measured with the rheometer. This suggests that three factors contribute to the pressure drop across the core: apparent viscosity of the injected emulsion, the resistance to flow arising from the process of droplet coalescence, and the apparent viscosity of the regenerated emulsion. At lower flow rates the resistance to droplet coalescence is relatively high causing large pressure drops. It is also possible that some of the droplets are trapped in pores, blocking pore space and decreasing the effective permeability of the core. This would cause a steady increase in the injection pressure

The several stages of emulsion injection in Core C further investigated whether there was a critical shear rate to maintain emulsion stability in the core. First, emulsion was injected at a very low flow rate. No stable emulsion was eluted at 11 s^{-1}. The pressure drop continued to rise for the entire duration of the experiment. Further inspection of the effluent indicated that the phase ratio of the injected emulsion was similar to the phase ratio in the effluent tubes. This supports the hypothesis of complete coalescence of injected emulsion and could also indicate droplets are not being trapped in the core, otherwise it is likely less oil would be present in the effluent. The increasing pressure gradient would instead be attributed to a growing region of larger viscosity fluid within the core, associated with a moving front between coalescence and regeneration regions. Very little emulsion was produced in the second stage of emulsion injection into Core C (Figure 5.15) at a shear rate of 106 s^{-1}. The pressure drop across the core increased for 2 PV then stabilized and the amount of stable emulsion in the effluent was constant, consistent with a moving front that arises in response to the change in boundary

226

conditions.   The belief is that at a higher flow rate the resistance to flow associated with droplet coalescence decreases and contributes less to the pressure drop.   The shear rate was just high enough to produce a small amount of stable emulsion but majority of it coalesced and was not regenerated because the shear rate was too low.   A steady balance of emulsion coalescence and regeneration contributed to the steady state pressure drop. This would be consistent with the moving front having reached the core outlet, so that only one regime of droplet coalescence/regeneration is active within the core.   In the next stage in Core C (Figure 5.16) the emulsion was injected at a higher shear rate.   The pressure drop steadily increased and then stabilized within 2 PV which is consistent with another front moving through the core after the change in boundary conditions, leading to a state with a light increase in stable emulsion produced in the effluent.   The experiments in Core C showed that there was a significant amount of emulsion coalescence and regeneration when injecting a statically stable emulsion through the core.

Mineral oil emulsion stabilized with the IPA-ST nanoparticle dispersion, with an average droplet diameter of 22 microns, was injected through Core D at different flow rates: 1, 2, 4, 8 mL/min. The critical shear rate for regenerating stable emulsion in this core was between 100 and 200 s^{-1}. Emulsion produced in the effluent at 2, 4, and 8 mL/min all had an average droplet diameter of approximately 12 microns, indicating the produced emulsion droplet size is independent of flow rate. When the emulsion was injected at 1 mL/min the pressure drop across the core steadily increased and no emulsion was produced in the effluent.   For the other injection rates the pressure drop across the core stabilized.   The hypothesis for this is that at lower flow rates the injected emulsion droplets resist coalescence and contribute to a large and increasing pressure drop.

227

When emulsion is injected at higher flow rates there is less resistance to coalescence and the newly formed droplets easily form at short distance from the core inlet. The newly generated droplets can then propagate through the core because the driving flow is sufficient enough to keep them from coalescing. The produced emulsions all had similar droplet sizes and apparent viscosities. At 2 mL/min the apparent viscosity was higher than the viscosity of the injected emulsion and the effluent emulsion. As the flow rate was increased to 4 and 8 mL/min the apparent viscosity was much closer to the effluent emulsion rheology. At the lower flow rate the resistance to droplet coalescence contributed to the increase in pressure drop and in turn the apparent viscosity. Then as the flow rate was increased the resistance to coalescence was less and key contribution to the pressure drop was the viscosity of the newly generated emulsion. Another possibility is that by the end of the 2 mL/min stage, the coalescence/regeneration regime was established throughout the core and the apparent viscosity contribution was from the shear thinning emulsion.

In the experiments performed in Section 5.5.2 the difference between injecting a premade emulsion with an average droplet diameter of 24 microns and co-injecting the two fluids at the same phase ratio as the emulsion was investigated. During the emulsion injection in Core M the apparent viscosity increased across the first 6" of core while it was steady in the last 6" of the core. During the emulsion injection in Core N the apparent viscosity in the first 2" of the core was stable while the apparent viscosity increased across the last 10" of the core. The hypothesis is that some type of front was propagating through the core and led to the increase in the apparent viscosity in certain sections of the core. In the Core N emulsion injection traveled through the first two

228

inches of the core rather quickly, leading to apparent viscosity stabilization in this section.   This front then traveled through the last 10" of the core exited the core around 5 pore volumes when the apparent viscosity in the entire core began to stabilize.   In the core M emulsion injection the front was traveling through the first 6" of the core contributing to the increase in apparent viscosity.   During the co-injection in Core M the front continued to travel through the core and the apparent viscosity began to stabilize in the last 6" of the core while the apparent viscosity increased in the last 6" of the core. The front is most likely a coalescence/regeneration front that moves slowly through the core and the apparent viscosity stabilizes when the emulsion exits the core.

In Core O the mineral oil and nanoparticle dispersion were co-injected into the core; then emulsion was injected into the core after the co-injection.   During the co-injection the apparent viscosity in sections and averaged across the core steadily increased throughout the co-injection.   This can be contributed to continual growth of a region in the core in which generation and coalescence of droplets occurs.   When the emulsion was injected the apparent viscosity increased throughout the entire core but stabilized in the first 2" of the core where the apparent viscosity was the highest.   The increase in apparent viscosity was attributed to the resistance associated with droplet coalescence.   The pressure drop in the last 10" of the core continued to increase throughout the injection consistent with an advancing front of droplets resisting coalescence and regeneration.

The experiments in Cores M, N and O showed that the effluent emulsion in terms of rheology and droplet size were similar for emulsion injection and co-injection nevertheless the processes that produce these emulsions are not similar because they

229

produce qualitatively different pressure responses. The emulsion produced during co-injection is from the two bulk fluids flowing through the pore space with oil droplets snapping off into the aqueous nanoparticle dispersion generating an emulsion. The effluent emulsion produced in the emulsion injection experiments most likely occurred from the coalescence of smaller droplets in the injected emulsion and from possible regeneration from the bulk phases from coalesced droplets. The droplets resistance to coalescence caused the pressure to increase in the core. It is hypothesized that the advancement of coalescence/regeneration front contributed to the pressure increase in certain sections of the core, although the exact mechanism still remains unclear.

The oil recovery experiment in Core P showed that the injection of an octane emulsion to recover mineral oil was more efficient than the waterflood, though because the emulsion was injected at a low flow rate the emulsion was expected to coalesce. The apparent viscosity was much higher in the first 2" of the core. This increase in pressure was associated with the droplets resistance to coalescence.

In Core Q an octane emulsion injected to recover residual mineral oil. The emulsion injection recovered more residual oil than when brine (with no nanoparticles) and octane were co-injected. The increase in recovery for the octane emulsion was attributed to its larger apparent viscosity which led to improved sweep efficiency. The improved sweep efficiency caused more coalesced octane to travel into the lower permeability regions recovering more residual oil.

The Core T experiment was similar to the Core Q except mineral oil was used instead of octane. Co-injecting mineral oil and brine recovered more residual oil than when a mineral oil emulsion was injected. The proposed mechanism is that the

230

emulsion coalesced and regenerated quickly in the core so stable droplets were flowing through the core. This did not allow the mineral oil from the emulsion to miscibly displace the residual oil because it was entrapped as stable droplets.

The results from the experiments in Core T and Q indicate that the most efficient recovery method of residual oil was an injection of octane emulsion at flow rate that caused the emulsion to coalesce. The coalescence of droplets increased the apparent viscosity compared to co-injecting the fluids at the same phase ratio and flow rate. This allowed some of the octane that was broken out of the emulsion to miscibly displace the residual oil in lower permeability sections. If the emulsion was injected at a higher flow rate the emulsion would most likely coalesce and regenerate quickly, not allowing the octane to miscibly displace the residual mineral oil because it would be trapped in droplets.

5.7 CONCLUSIONS

Whenever emulsion was injected into sandstone cores and emulsion was produced in the effluent, the effluent emulsion always had a different droplet size and rheology than the injected emulsion. Batch experiments with octane emulsion indicated that forcing the emulsion through a porous medium caused the emulsion to coalesce as opposed to the emulsion coming into contact with the other resident fluids in the core. This has important implications for design criteria in reservoir systems. The results from the corefloods indicate that if an emulsion with a certain viscosity and droplet size was designed to be injected through a reservoir to have certain mobility; it is highly likely that the emulsion properties would drastically change once the emulsion was injected into

the subsurface due to coalescence/regeneration based on the rock type, fluid type, and shear rate.

While injecting highly stable emulsions through sandstone cores sometimes only the constituent phases of the injected emulsion would be eluted, and other times a less viscous emulsion would be produced, apparently regenerated from the coalesced phases. Often all three fluids would be produced simultaneously, indicating that complete coalescence and partial regeneration (the extent depending on shear rate) is the general rule. The fractional flow of the three fluids in the effluent depended on flow rate and duration of injection. Whenever the emulsion was injected at low flow rates the pressure drop would typically increase for the entire duration of the emulsion injection. The increase in pressure was attributed to droplets resisting coalescence.

The pressure drop would increase then stabilize when emulsion was injected through cores at higher flow rates. Stabilization across the core typically coincided with the arrival of stable emulsion in the effluent after a period of only coalesced constituent phases being eluted. This suggests that a front between two regimes or states is moving through the core as emulsion is injected. The effluent emulsion had a smaller droplet size than the injected emulsion indicating that emulsion coalescence/regeneration still takes place at higher flow rates. It also suggests that the two regimes or states could involve different balance points in the competition between coalescence and regeneration of emulsion droplets. When emulsion was injected at three different flow rates (2, 4, 8 mL/min) through Core D, all of the effluents displayed similar rheology and droplet size indicating that the produced emulsion may be a function of pore size and shear rate which was consistent with the results in Chapter 3 from the critical shear rate experiments where

232

a different critical shear rate was found for different size beads (Section 3.3.2). Although the emulsions displayed similar properties in batch rheology measurements, the emulsion displayed higher apparent viscosities at lower flow rates. This was attributed to the droplets resisting coalescence at lower flow rates increasing the pressure drop and in turn the apparent viscosity. At higher flow rates there is less resistance to emulsion coalescence so the apparent viscosity is similar to the bulk effluent rheology at the same shear rate because the major contribution to the pressure drop is the coalesced/regenerated emulsion. The emulsions in the Core D experiments displayed same shear thinning behavior in porous media, similar to their bulk rheology.

The hypothesis that injected emulsions are completely coalesced when they flow through rock suggests that there should be no difference between injecting a premade emulsion and co-injecting nanoparticle dispersion and mineral oil at the same rate and at the same phase ratio. Supporting this suggestion, co-injection and emulsion injection typically produced emulsions with similar characteristics. On the other hand the pressure responses were typically different. Injecting emulsion caused the apparent viscosity to increase sequentially in sequential sections of the core and subsequently stabilize. The apparent viscosity was typically higher when injecting emulsion compared to co-injection because of the injected droplets resistance to coalescence.

Octane emulsion displaced more mineral oil than a water injection. The increase in recovery was attributed to the octane from the coalesced emulsion miscibly displacing the mineral oil providing strong support for the hypothesis that emulsions undergo complete coalescence when injected through rock. Octane emulsion was also more effective than co-injecting octane and brine to displace residual mineral oil. Because the

233

octane emulsion coalesced but still had a higher apparent viscosity than the co-injection, its improved sweep efficiency caused octane to miscibly displace mineral oil from the lower permeability sections. The higher apparent viscosity arises for the reasons discussed above. In contrast Co-injection of mineral oil and brine recovered more residual oil than a mineral oil emulsion injection. This is presumed to be the result of the quick coalescence/regeneration of stable emulsion did not allow the mineral oil from the emulsion to miscibly displace the residual oil. In contrast the regeneration of the octane emulsion in situ is presumed to be relatively slow; this is consistent with the higher critical shear rate needed to generate octane emulsions than mineral oil emulsions.

In the emulsion dilution experiments the diameter of the emulsion effluent from the beadpack that was routed into the core always had a larger average droplet diameter than the effluent emulsion from the core, indicating emulsion coalescence and regeneration. This was consistent with the other experiments at higher flow rates where the injected emulsion would coalesce and regenerate into smaller droplets. In the first stage of the emulsion dilution experiments, when the core was only saturated with brine, it would take 2 to 2.5 PV for the apparent viscosity in the core to stabilize, indicating the movement of an emulsion coalescence/regeneration front. Diluting a mineral oil emulsion droplet density from 66% to 50% reduced the apparent viscosity in the core by a factor of two. Similarly, diluting the octane emulsion droplet density from 60% to 10% and 20% reduced the apparent viscosity in the core by a factor of two for both cases.

Imbibition displacements in which nanoparticle dispersion displaced oil showed that it was possible to generate an emulsion by flowing past residual oil blobs at sufficiently large shear rate. This is evidence of a novel mechanism of residual oil

234

recovery; the affinity of the nanoparticles for the oil/water interface coupled with the large shear rate appears to enable residual oil to be mobilized, or for residual oil blobs to spawn smaller droplets into the flowing dispersion phase. The droplets become stabilized by the nanoparticles and thus can be transported with the dispersion through the core.

Chapter 6

Conclusions and Future Work

6.1 CONCLUSIONS

A schematic summary of the behavior observed in this work is shown in Figure 6.1. The general behavior of flowing nanoparticle-stabilized oil-in-water emulsions through porous media is broken down into four different categories.
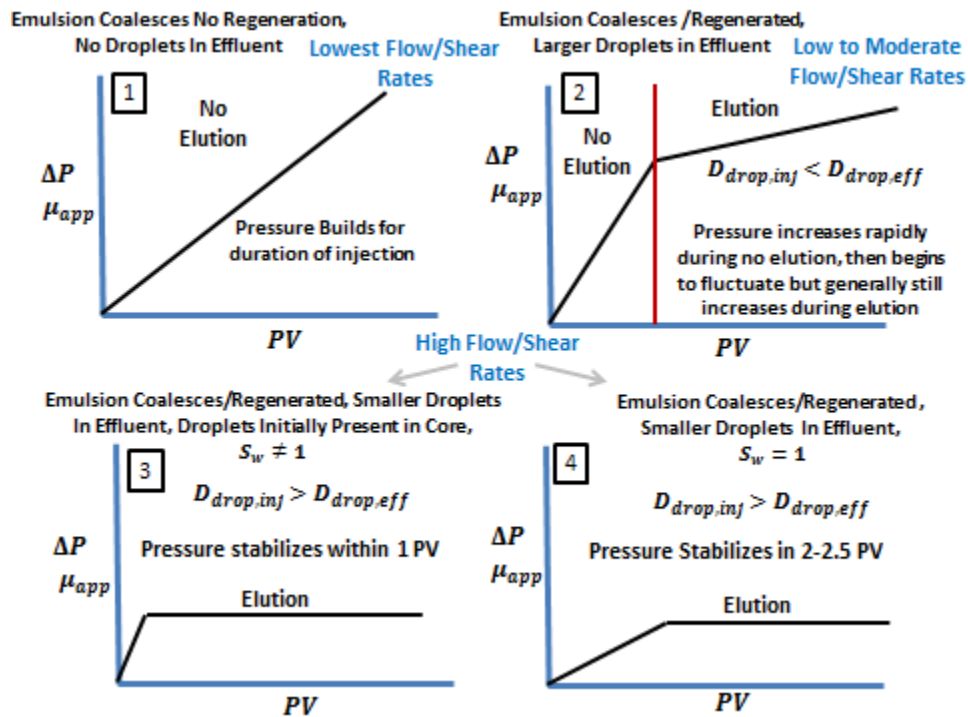
Figure 6.1 Schematic summary of emulsion flow through porous media. The observations in this thesis were classified into four different categories. The conclusions about effluent droplet size are only applicable to the corefloods in Chapter 5. The effluent emulsion droplet size was not measured in Chapter 4.

6.1.1 Emulsion Generation

Emulsions stabilized by suitable nanoparticles can be generated by co-injecting nanoparticle dispersion and oil through a beadpack. The droplet size of the generated emulsion was a function of shear rate and decreased with increasing shear rate. The droplet size of the emulsions was not correlated to the bead size. There exists a critical shear rate below which a stable emulsion will not be generated by co-injection through a beadpack. The critical shear rate was found for five different size beads and increased with decreasing bead size. All of the emulsions displayed highly shear thinning behavior. The emulsion viscosity was independent of the bulk viscosity of the oil dispersed as droplets but was highly dependent on the droplet size. Emulsions with smaller droplets were more viscous than emulsions with large droplets over the entire range of shear rates measured. The generation of emulsions with different oils showed that the critical shear rate to generate an emulsion was dependent on the viscosity of the oil phase. A higher shear rate was required to generate an emulsion with oil that was less viscous than the aqueous nanoparticle dispersion. When the oil was more viscous than the nanoparticle dispersion emulsions were generated at lower shear rates and the value of the threshold shear rate did not depend on the oil viscosity.

6.1.2 Emulsion Flow in Beadpacks

Nanoparticle-stabilized emulsions injected into beadpacks became unstable and coalesced into the bulk fluids in majority of the beadpack experiments. Injecting an emulsion with an average droplet diameter greater than the average pore throat size caused no emulsion to be produced from the beadpack. This flow behavior coincides with the 1st classification in Figure 6.1 and was associated with large pressure gradients.

237

Emulsions with larger droplets were inherently less stable than emulsions with smaller droplets when they were injected into beadpacks. Whether the fluids regenerated a new emulsion depended on several factors. If emulsion injection continued long enough, stable emulsions would eventually elute from the beadpack, and would continue to be eluted in a steady manner. This behavior corresponds with the 2nd classification in Figure 6.2. The time required for stable emulsions to arrive depended on whether the beadpack was initially saturated with mineral oil or water. It is hypothesized that catastrophic phase inversion caused the emulsion to become unstable when it encountered a bank of oil greatly delaying (or preventing) the arrival of stable emulsion in the effluent. Batch experiments showed that bringing an external fluid (mineral oil and water) into contact with the mineral oil emulsion did not cause the emulsion to coalesce, indicating that emulsion flow through porous media is the main cause of coalescence. Only when a large amount of energy was input into the oil and emulsion sample via sonification did the emulsion coalesce which is consistent with the resident mineral oil prolonging emulsion coalescence.

In several beadpack experiments the pressure gradient history shows a moving front transitioning from one flow regime where the emulsion completely coalesces to a second regime where the emulsion coalesces but some emulsion is regenerated. In the first regime the pressure steadily builds because of the flow resistance from the coalescence of droplets. Conversely, in the second flow regime the pressure gradient stabilizes but fluctuates due to the regeneration of emulsion from the coalesced bulk phases.

238

6.1.3 Emulsion Flow in Sandstone Cores

Coreflood experiments confirmed the mechanisms hypothesized for the beadpack emulsion injection experiments. When a nanoparticle-stabilized emulsion was injected the effluent emulsion rheology and droplet size were altered solely as a result of being forced through sandstone cores.   At lower flow rates no emulsion would be produced for the duration of injection, or an emulsion with larger droplets would be eluted, along with oil and aqueous phases from the coalesced injected emulsion (1st classification in Figure 6.1).   At higher flow rates the eluted emulsion had smaller droplets than the injected emulsion (3rd and 4th classification in Figure 6.1).   The pressure drop would continually increase for emulsion injections at low flow rates because of the injected emulsion resistance to droplet coalescence. The apparent viscosity in the first 2" of the core was higher compared to the rest of the core when emulsion was injected at low flow rates. This was attributed to majority of the droplets resisting coalescing/regenerating in the first 2" of the core. At higher flow rates the pressure drop would typically stabilize within a pore volume of injection because there was less resistance to droplet coalescence and the emulsion would coalesce into the new droplets within a short distance of entering the core inlet so the major contribution to the pressure drop was the apparent viscosity of the newly generated emulsion (3rd classification in Figure 6.1).   In both the beadpack and coreflood experiments when emulsion was injected at different shear rates the generated emulsion was less viscous at higher shear rates and more viscous at lower shear rates, consistent in behavior with their bulk rheology. At low flow rates where the resistance to droplet coalescence was the highest, contributing significantly to the overall pressure drop, the apparent viscosity of the emulsion in the core was higher than effluent emulsion

239

bulk viscosity at the same shear rate.   When the flow rate was increased, decreasing the droplets resistance to coalescence, the apparent viscosity was similar to the effluent emulsion rheology at the same shear rate.

The effluent emulsions from co-injection and emulsion injection at the same phase ratio and flow rates had similar droplet sizes and rheology.   However, the pressure drop across the core was different for both types of injection.   A slowly moving front associated with droplet resistance to coalescence/regeneration -- typically large apparent viscosity for the fluid upstream of the front and smaller apparent viscosity for the fluid downstream -- developed during the premade emulsion injections. This front was less evident in co-injection experiments because the newly generated droplets were less resistant to droplet coalescence than the smaller injected droplets.

In the emulsion dilution experiments the injected emulsion effluent from the beadpack had larger droplets than the effluent from the core indicating that emulsion coalesces and is regenerated in the core.   In the emulsion dilution experiments where the core was initially saturated with brine it took longer for the steady state apparent viscosity to stabilize (4th classification in Figure 6.1) than when droplets were already present in the core indicating the movement of a coalescence/regeneration front in the case of the brine saturated injections (3rd classification in Figure 6.1).   Diluting the droplet density of the emulsion lowered the apparent viscosity of the emulsion in the core.   Diluting a mineral oil emulsion droplet density from 66% to 50% reduced the apparent viscosity by a factor of two.   When an octane emulsions droplet density was diluted from 60% to 20% and 10% the apparent viscosity reduced by a factor of two for both cases.

6.1.4 Emulsion Injection for Displacing Oil from Cores

Oil recovery experiments showed that nanoparticle-stabilized oil-in-water emulsion could effectively increase the recovery of oil compared from a core compared to a waterflood. This was true for displacement of mobile (initial saturation = 1 - $S_{w,irr}$) and immobile (initial saturation = residual to waterflood) oil phase. The mechanism for recovery is the coalescence that universally accompanies flow of these emulsions through rocks: the coalesced oil droplets form a flowing phase that is miscible with oil present in the core and thus achieves a much more efficient displacement. Injecting nanoparticle-stabilized emulsion to recover residual oil was more efficient than co-injecting oil and brine (without nanoparticles), at the same phase ratio and flow rate, if no emulsion was eluted from the core during oil recovery. The coalesced octane emulsion was the most efficient recovery method because of the improved sweep efficiency, due to apparent viscosity that is larger than that for co-injection, and miscible displacement. Note that the larger apparent viscosity is not sufficient to account for the reduced residual oil saturation; it must act in concert with the release of an oil phase that miscibly displaces initially present oil. The hypothesis is that the octane emulsion injection produced unstable droplets in situ, increasing the apparent viscosity, while the octane from the coalesced droplets was still able to displace residual mineral oil. When the mineral oil emulsion remained stable in the core the mineral oil from the emulsion could not miscibly displace the residual oil because for most of its residence time in the core it remained dispersed as droplets, redispersed quickly whenever coalescence occurred.

A novel oil recovery mechanism was shown in imbibition experiments where nanoparticle dispersion was used to displace oil. The imbibition experiments showed

that it was possible to generate stable emulsion without two mobile phases in the core. The affinity of the nanoparticles for the oil/water interface coupled with the large shear rate appears to enable residual oil to be mobilized, or for residual oil blobs to spawn smaller droplets that are stabilized by the nanoparticles and thus can be transported with the dispersion through the core.

6.2 FUTURE WORKS

The following research objectives are proposed for the continuation and expansion of the research presented in this thesis:

- Nanoparticle-stabilized emulsion corefloods should be performed with heavy crude oils that are still mobile with viscosities ranging from 50 to 5,000 cP. The most viscous oil used in this thesis was mineral oil (40.5 cP). If nanoparticle stabilized emulsions are to be used in conformance control applications in the industry, further research is needed to determine their efficiency in recovering viscous oils.

- Corefloods should be performed with surfactant stabilized emulsions to determine if their behavior is similar to the nanoparticle stabilized emulsions investigated in this thesis. Specifically, the coalescence/ regeneration mechanism that was observed in both the beadpack and corefloods.

- Different nanoparticles with different cores and coatings should be used to stabilize emulsions. They should be injected into porous media to see if

their behavior is different than the coated silica nanoparticle stabilized emulsions in this thesis.

- Nanoparticle-stabilized emulsion corefloods with different cores should be performed to see how cores with different permeability and pore size affect emulsion flow.

- All of the emulsions in this thesis were stabilized by hydrophilic particles therefore they generated oil-in-water emulsions. Water-in-oil emulsions should be generated with hydrophobic nanoparticles. Corefloods should be performed with water-in-oil emulsions to compare their behavior to water-in-oil emulsions in porous media.

Appendices

A1 VISCOSITY MEASUREMENT

Viscosities of different emulsions, oils, and nanoparticle dispersions were measured using an AR-G2 magnetic bearing rheometer. Figure A.1 is a picture of the AR-G2 magnetic bearing rheometer. The procedure for measuring viscosity of a fluid is outlined below.

Figure A.1 Photo of AR-G2 magnetic bearing rheometer used to measure fluid viscosities.

Rheometer Procedure

1. Start airflow to instrument from the lab air supply. The regulator next to the air purifier/dryer (black dial) should read 30-32 psi.

2. Remove the bearing lock (black attachment at the bottom of the moving head) by holding the shaft and rotating the lock.

3. Start the Thermo-CUBE heat sink.

4. Start the main controller (located next to the heat sink).

5. Run the software for RHEOLOGY ADVANTAGE on the computer.

6. Attach the geometry, either Cone-plate or Couette.   If Couette geometry is used, the plate has to be replaced with the Couette holder.   Emulsions were measured with the Couette geometry while Newtonian fluids were measured with the cone and plate.
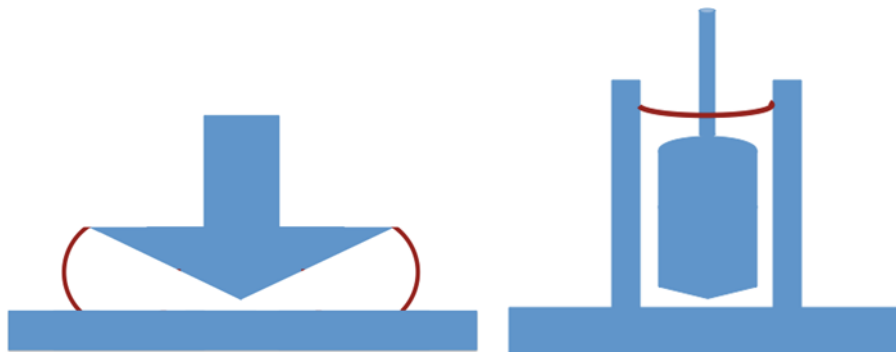

Figure A.2 Cone-plate geometry (left) and Couette geometry (right), where the red lines indicate the outer boundaries of samples.

7. If the smart-swap option is enabled in the software it will detect the fixture geometry.   To enable smart-swap click on "Geometry>>Smart-Swap enabled" (auto-swap should not be selected for pressure cell)

8. The software will ask to invalidate all current zero point setting > Click 'yes'.   It will ask to perform rotational mapping > Click 'yes' (select precision as bearing mapping type and 2 iterations; this would take 10 minutes).   Rotational mapping

is for the instrument (not the geometry), so you may do it only once before your set of experiments.

9. Chick on the zero-gap button to set the zero gap (manually lower the head until 5mm from the peltier plate, and then allow the software to set it).

10. Chick on the zero-gap button to set the zero gap (manually lower the head until 5mm from the peltier plate, and then allow the software to set it).
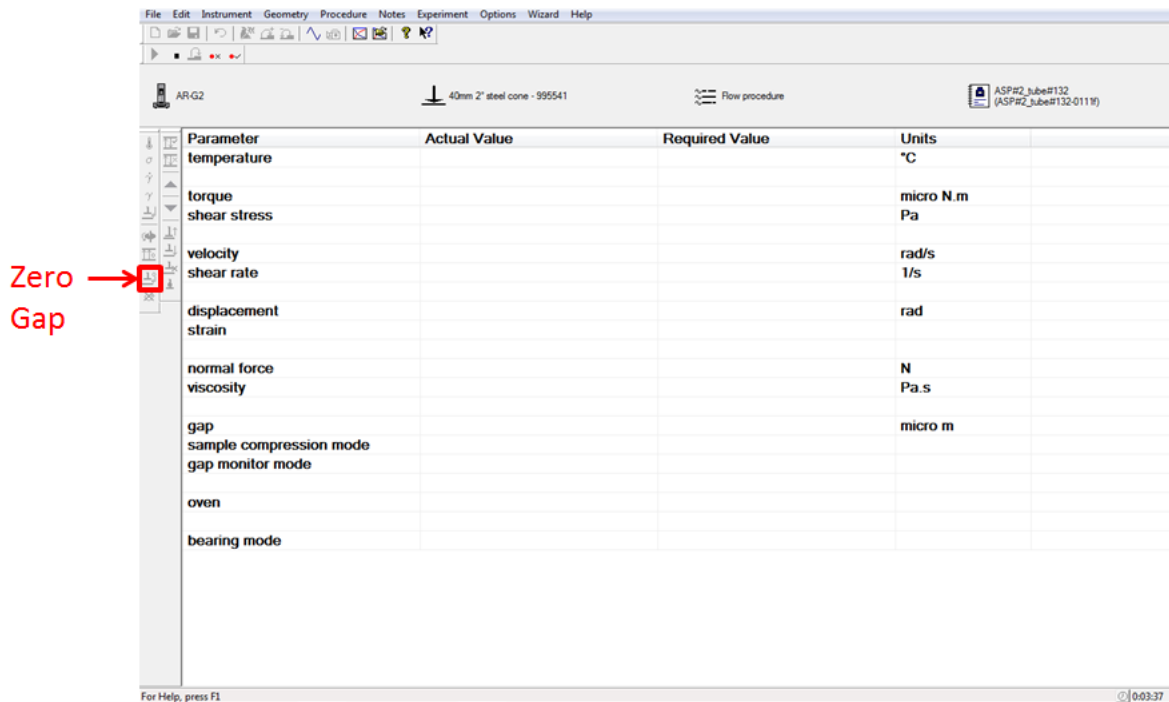

Figure A.3 Rheometer Zero Gap.

11. Adjust the flow procure to set the peltier plate temperature (temperature should be consistent in conditioning step, flow step, and post-experiment step), shear rate range, and data analysis conditions (points per decade, sample period, percentage tolerance, consecutive within tolerance, and maximum point time).
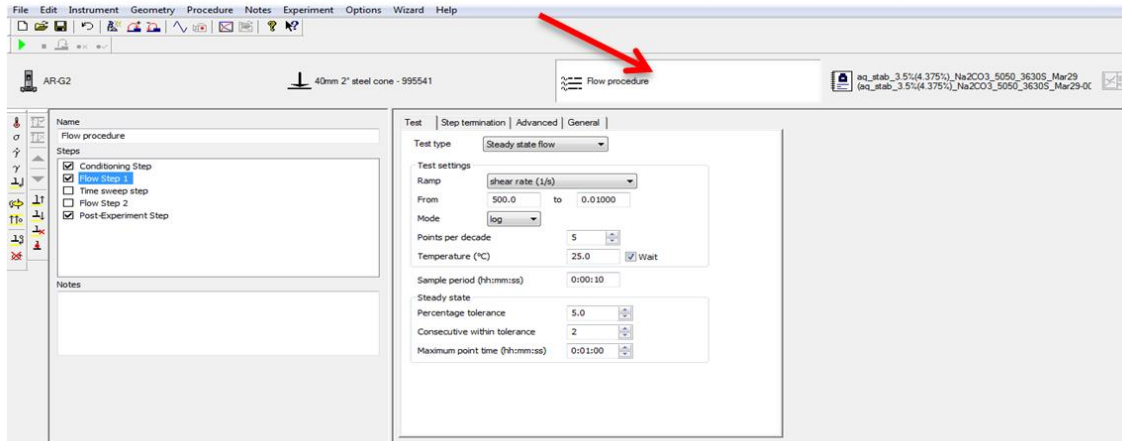
Figure A.4 Rheometer flow step setting.

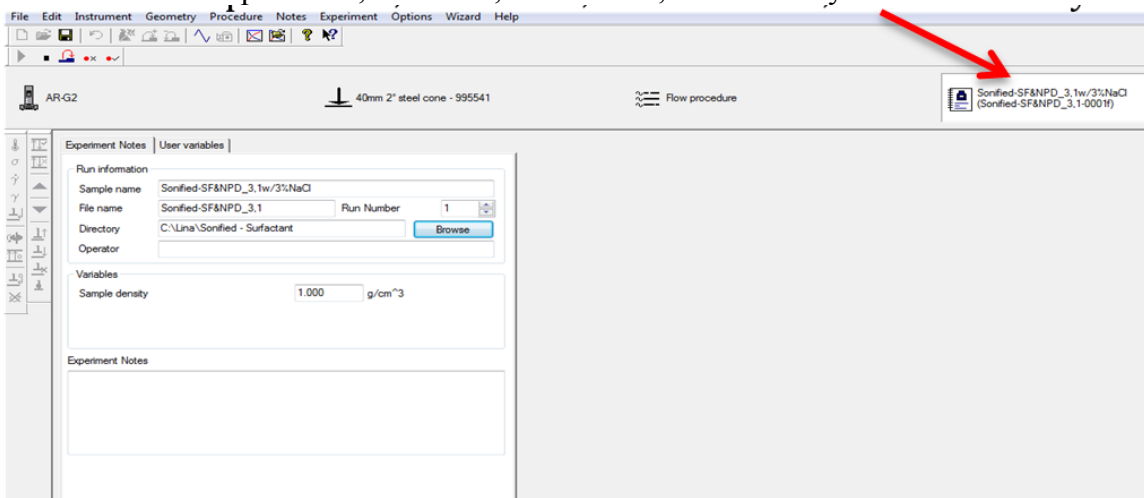12. Define sample name, file name, run number, and directory.

Figure A.5 Rheometer file setting.

13. Raise the head high enough to pour in the sample. Required sample size can be seen in the geometry tab under setting tab in geometry (0.59 mL for cone-plate / 19.9 mL for couette).

247

14. Lower the head until it is in contact with the top of the sample.   Lower the head slowly when closer to the sample to prevent a quick contact that would possibly create air bubbles in between the head and the sample.

15. Click run (green triangle on the top left corner) and a window will pop up asking to "Set the correct gap before proceeding?" Click yes.

16. After running all samples, raise the head and remove the fixture and the associated geometry and clean thoroughly.

17. Shut down the software, Thermo-CUBE, and main controller in the same order.

18. Put the black bearing lock on the shaft.

19. Turn off the air pressure knob.

A2 BEADPACK COMPONENTS AND LOADING PROCEDURE

Figure A.6 shows the components of the HiP beadpack.   The beads were loaded directly into and held in the beadpack (red square in Figure A.6).   The mesh end pieces were lodged in both end caps.   The connection fittings connect the end caps to the beadpack are also shown.

Figure A.6 The beadpack components including the connection fittings and end caps.

Mesh pieces were used to hold the beads in place and not allow them to flow through the effluent line.   The mesh end pieces were pushed into the end caps so that they completely covered the outlet of the beadpack.   Figure A.7 shows an image of the mesh pieces, the end cap without mesh, and the end cap with mesh.

Figure A.7 The mesh pieces (left), end cap without mesh (middle), end cap with mesh (right).

To load the beads into the HiP beadpack, one of the end caps with mesh was attached to the empty beadpack. The beadpack was then positioned in the vise grip with the end cap side facing down. A plastic disposable pipet, cut with scissors, was used to transfer beads into the open top side of the beadpack. Figure A.8 shows the beadpack filling procedure. Once the beadpack was filled with beads the top end cap with mesh was attached, completing the beadpack preparation procedure. The same procedure was used to load the larger beadpack.
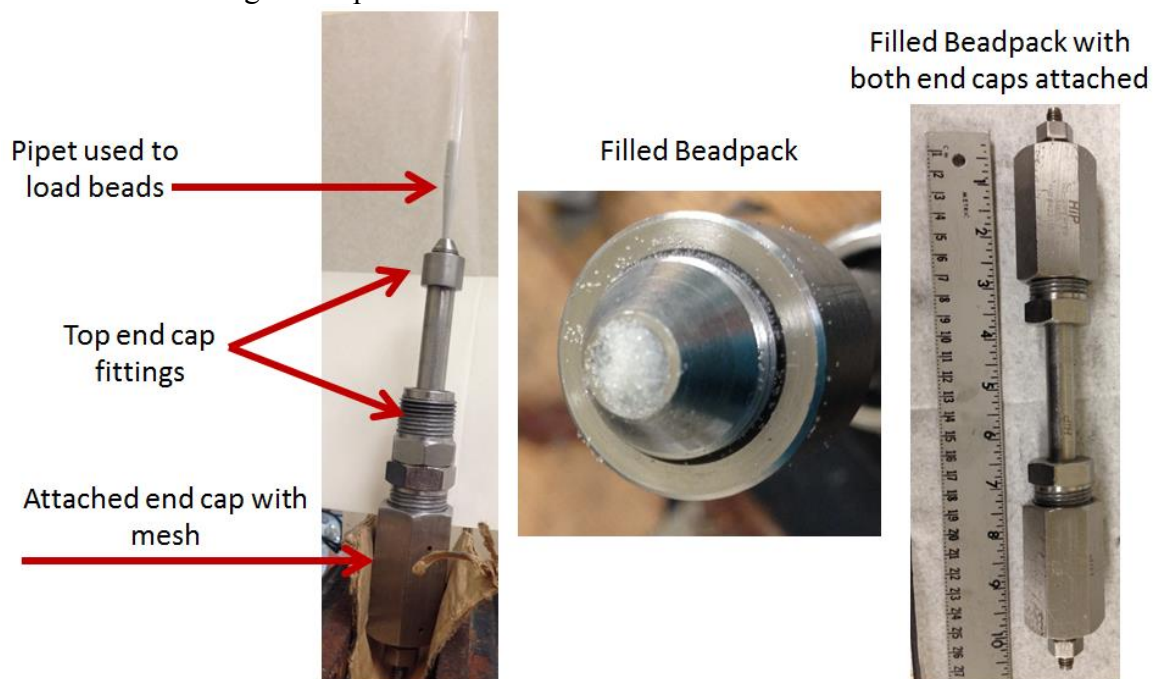

Figure A.8 The stages of the beadpack loading procedure. Loading the beads into the beadpack using the pipet and vise grip (left). The filled beadpack without top end cap (middle). The filled beadpack with both end caps attached (right).

A3 CORE HOLDER COMPONENTS

In this section the components of the coreflood experimental setups are shown. The core holder fittings, core holder, sandstone cores, and the rubber sleeve are all pictured in Figures A.9, A.10, and A.11.

Figure A.9 The core holder fittings including the top hand screw (left), top end piece (middle), and the bottom end piece (right).

Figure A.10 The core holder without fittings (left), top of the core holder with fittings (middle), and the bottom of the core holder with fittings.

Figure A.11 Example of the Boise and Berea sandstone cores used in this thesis (top). The cores were placed into the rubber sleeve pictured (bottom). The rubber sleeve with pressure taps was housed in the core holder.

References

Aveyard, R., Binks, B., Clint, J. Emulsions Stabilized Solely by Colloidal Particles. Advances in Colloid and Interface Science, 100-102, 503-546 (2003).

Binks, B., Rodrigues, J. Enhanced Stabilization of Emulsions Due to Surfactant-Induced Nanoparticle Flocculation. Langmuir, 23, 7436-7439, (2007).

Binks, B.P. Particles as Surfactants - Similarities and Differences. Current Opinion in Colloid and Interface Science, 7, 21-41 (2002).

Binks, B.P., Lumsdon, S.O. Catastrophic Phase Inversion of Water-in-Oil Emulsions Stabilized by Hydrophobic Silica, Langmuir, Volume 16, Issue 6, Pages 2539-2547, (2000).

Bragg, J.R. Solids-Stabilized Emulsion, U.S. Patent, 5910467 (1999).

Caldelas, F.M. Experimental Parameter Analysis of Nanoparticle Retention in Porous Media, M.S.E. Thesis, The University of Texas at Austin (2010).

Chung, D.H., Transport of Nanoparticles during Drainage and Imbibition Displacements in Porous Media, M.S.E. Thesis, The University of Texas at Austin (2013).

Davidson, A.M. Magnetic Induction Heating of Superparamagnetic Nanoparticles for Applications in the Energy Industry, M.S.E. Thesis, The University of Texas at Austin (2012).

Espinosa, D. Nanoparticle Stabilized Supercritical CO_2 Foams for Potential Mobility Control Applications, M.S.E. Thesis, The University of Texas at Austin (2011).

Fu, X., and Mamora, D. D. Enhanced Oil Recovery of Viscous Oil by Injection of Water-in-Oil Emulsions Made with Used Engine Oil, Presented at SPE Improved Oil Recovery Symposium, Tulsa, Oklahoma, SPE 129902 (2010).

Hariz, T.R. Nanoparticle-Stabilized CO_2 Foams for Potential Mobility Control Applications, M.S.E. Thesis, The University of Texas at Austin (2012).

Kaminsky, R. D., Wattenbarger, R. C., Lederhos, J., and Leonardi, S. A. Viscous Oil Recovery Using Solids-Stabilized Emulsions, Presented at SPE Technical Conference, Florence, Italy, SPE 135284 (2010).

Kwon, T.S., Yang, J.S., Baek, K., Lee, J.Y., Yang, J.W. (2006) Silicone emulsion-enhanced recovery of chlorinated solvents: batch and column studies . Journal of Hazardous Materials, 136, 3, 610-617, (2006).

Lake, L.W. Enhanced Oil Recovery. Englewood Cliffs, NJ: Prentice Hall (1989).

253

Lee, Y. C., Kwon, T. S., Yang, J. S., and Yang, J. W. Remediation of groundwater contaminated with DNAPLs by biodegradable oil emulsion. Journal of Hazardous Materials, 140, 1-2, 340-345, (2007).

McAuliffe, C. D. Oil-in-Water Emulsions and Their Flow Properties in Porous Media. Society of Petroleum Engineers, SPE 4369, (1973).

Moradi, M.M.. Kazempour, M.K., Alvarado, V.A. Crude Oil-in-water Emulsion Flooding for EOR, Presented at 74th European Association of Geoscientists and Engineers (EAGE) Conference and Exhibition, Copenhagen, Denmark, (2012).

Murphy, M.J. Experimental Analysis of Electrostatic and Hydrodynamic Forces Affecting Nanoparticle Retention in Porous Media, M.S.E. Thesis, The University of Texas at Austin (2012).

Otsubo Y., Prud'homme R.K., Effect of drop size distribution on the flow behavior of oil-in-water emulsions, Rheol. Acta 33, 303–306, (1994).

Pickering, S.U. Emulsions, CXCVI, J. Chem. Soc., 91, 2001 (1907).

Roberts, M.R. Shear-Induced Emulsions Stabilized with Surface-Modified Silica Nanoparticles, M.S.E. Thesis, The University of Texas at Austin (2011).

Rocha De Farias, M. L., Carvalho, M. da S., Souza, A. S. de, Hirasaki, G. J., and Miller, C. A. A Comparative Study of Emulsion Flooding and other IOR Methods for Heavy Oil Fields, Presented at the SPE Latin American and Caribbean Petroleum Engineering Conference, SPE 152290 (2012).

Romero, L., Ziritt, J. L., Marin, A., Rojas, F., Mogollon, J. L., and Paz, E. M. F. Plugging of High Permeability - Fractured Zones Using Emulsions, Presented at the SPE Symposium on Improved Oil Recovery, Tulsa, Oklahoma, SPE35461 (1996).

Stan, C.A., Tang, S.K.Y, Whitesides, G.M. Supporting Information. Independent Control of Drop Size and Velocity in Microfluidic Flow-Focusing Generators Using Variable Temperature and Flow Rate, Department of Chemistry and Chemical Biology, Harvard University (2009).

Tadros, T. F. Emulsion Formation, Stability, and Rheology, in Emulsion Formation and Stability Chapter 1 (ed T. F. Tadros), Wiley-VCH Verlag GmbH and Co. KGaA, Weinheim, Germany (2013).

Zeidani, K., Polikar, M., Huang, H., Application of Emulsion Flow for Sealing Leaky Gas Wells, Presented at the 7th Canadian International Petroleum Conference, Calgary, Alberta, Canada, (2006).

Zeidani, K., Polikar, M., Huang, H., Boyd, J. Heavy Oil-in-Water Emulsion as a Novel Sealant in the Near Well Bore Region, Presented at the 8th Canadian International Petroleum Conference, Calgary, Alberta, Canada, (2007).

Zhang, T. Emulsions Stabilized with Nanoparticles for Potential Conformance Control Applications, M.S.E. Thesis, The University of Texas at Austin (2009).

Zhang, T. Modeling of Nanoparticle Transport in Porous Media, Ph.D. Dissertation, The University of Texas at Austin (2012).

Zhang, T., M.R. Roberts, S.L. Bryant, and C. Huh, C. Foams and Emulsions Stabilized with Nanoparticles for Potential Conformance Control Applications, Presented at the SPE International Symposium on Oilfield Chemistry, Woodlands, TX, SPE 121744 (2009).

Zhang, W., Thompson, K.E., Reed, A.H., and Beenken, L. Relationship between packing structure and porosity in fixed beds of equilateral cylindrical particles. Chemical Engineering Science, 238, 24, 8060-8074, (2006).

Zhou, X., Han, M., Fuseni, A. B., and Yousef, A. A. Adsorption of an Amphoteric Surfactant onto Permeable Carbonate Rocks. Society of Petroleum Engineers. SPE 153988 (2012).